THE JOURNAL OF

PHYSICAL CHEMISTRY

Volume 74, Number 20 October 1, 1970

NOTES

AUTHOR INDEX

ANNOUNCEMENT

On the last page of this issue you will find reproduced the table of contents of the July 1970 issue of the *Journal of Chemical and Engineering Data*. In initiating this practice we hope to make our readers more aware of the large body of critically evaluated data appearing in the pages of that journal. We hope also that physical chemists searching for data on particular systems will find this service a convenience.

THE JOURNAL OF
PHYSICAL CHEMISTRY

VOLUME 74, NUMBER 20 OCTOBER 1, 1970

Substitution Effects on the Emissive Properties of *N*-Heteroaromatics. I. Substituted Quinolines

by C. M. O'Donnell,* G. A. Knesel, T. S. Spencer, and F. R. Stermitz

Department of Chemistry, Colorado State University, Fort Collins, Colorado 80521 *(Received December 30, 1969)*

Total emission spectra of 2-(2-hydroxyethyl)quinoline, 2-(2-deuterioxyethyl)quinoline, and the quinolinium ion were recorded. The effect of various solvents coupled with the phosphorescence lifetime data indicate that in nonpolar solvents a charge-transfer triplet intermediate is possible. The photochemistry of these 2-substituted compounds is understandable in light of the results presented and the generalization of these results to similar systems is discussed.

The effect of hydroxylic solvents on the luminescence of quinoline is well established.[1,2] A combination of orbital interchange and second-order vibronic spin–orbit interactions between (n,π^*) and (π,π^*) states is believed to be responsible for the changes observed in: (1) phosphorescence lifetimes, (2) the degree of polarization outside of the (0,0) phosphorescense band, and (3) the ratio of fluorescence to phosphorescence intensity.[3,4] An attempt to observe similar changes caused by intramolecular perturbation is important to the understanding of the emissive properties in simple *N*-heteroaromatic systems.

In our investigation of a number of substituted quinolines, we have found that 2-(2-hydroxyethyl)quinoline (HEQ) and 2-(2-deuterioxyethyl)quinoline (DEQ) behave quite differently from other 2-substituted derivatives. The quantum yield for the photoelimination reaction of these alcohols is higher in nonpolar than in polar solvents.[5] If the reactive intermediate is a singlet, a correlation between the quantum yield of photoelimination and the ratio of fluroescence to phosphorescence should be possible. Our results indicate that this is not the case and that unique effects are produced by a charge-transfer intermediate in nonpolar solvents.

Experimental Section

Emission and excitation spectra (77°K) were routinely recorded on a Perkin-Elmer Model MPF-2A fluorescence spectrophotometer. For higher resolution, the light from a 200-W xenon lamp was passed through a 0.25-m Jarrel–Ash monochromator for excitation while passing the emission through a 0.75-m Spex 1700-11 monochromator. The detection system consisted of an EMI 6256 S photomultiplier tube, a Keithley Model 414 picoammeter and a Moseley 7100 B strip chart recorder. Lifetimes were measured using an EG & GFX 12-0.25 flash lamp as excitation, monitoring a small band pass with a monochromator, and feeding the signal into a Textronic Type 531A oscilloscope to be recorded on Polaroid film using a C-12 oscilloscope camera. A least-squares analysis has been run on the lifetimes in addition to a semilog plot to determine if the decay contained any nonexponential segments.

HEQ was purchased from Aldrich Chemical Company. Subsequently, this compound was recrystallized twice from $CHCl_3$–ether and resublimed once to yield a

* To whom correspondence should be addressed.

(1) V. L. Ermolaev and I. P. Kotlyar, *Opt. Spectrosc.*, 9, 183 (1960).

(2) M. A. El-Sayed and M. Kasha, *Spectrochim. Acta*, 15, 758 (1960).

(3) M. A. El-Sayed, *J. Chem. Phys.*, 38, 2834 (1963).

(4) E. C. Lim and Jack M. H. Yu, *ibid.*, 47, 3270 (1967).

(5) F. R. Stermtiz, C. C. Wei, and C. M. O'Donnell, *J. Amer. Chem. Soc.*, 92, 2745 (1970).

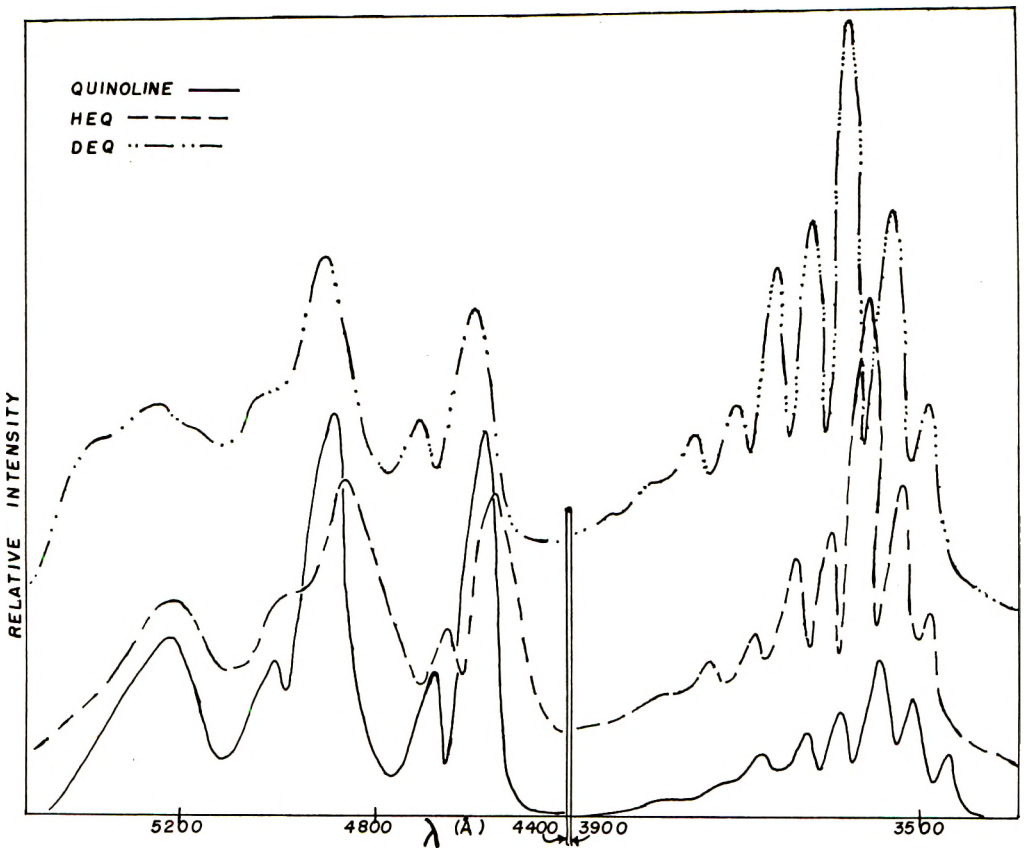

Figure 1. Total emission spectra of quinoline, HEQ, and DEQ in EPA at 77°K.

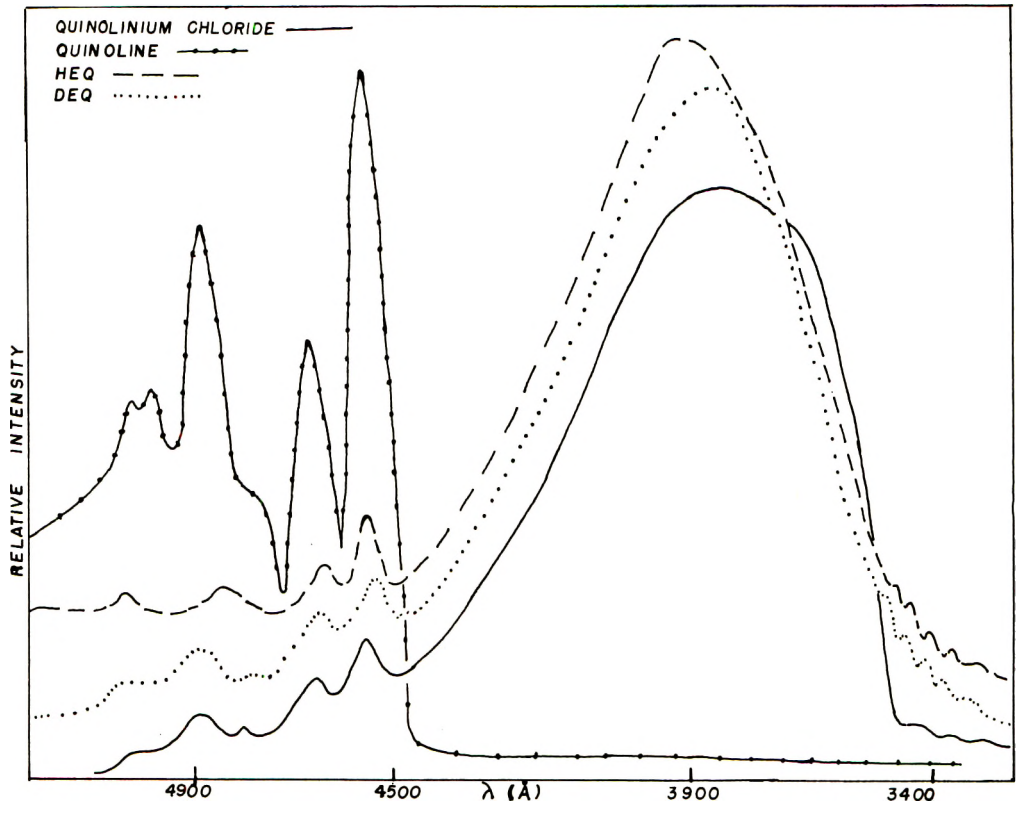

Figure 2. Total emission spectra of quinolinium chloride in EPA and quinoline, HEQ, and DEQ in 3-methylpentane at 77°K.

white crystalline material which melted at 102 to 104°. No changes in the emission spectra were evident when either the recrystallized or recrystallized and sublimed samples were used. A sample of the HEQ was warmed with D_2O and evaporated to dryness. This process was repeated three times and the resulting compound was shown to be completely the 2-(2-deuterioxyethyl)quinoline by nmr. Quinolinium chloride was prepared by the addition of hydrochloric acid to a solution of quinoline in methanol and evaporating the mixture to dryness. The resulting solid was recrystallized twice from 95% ethanol. 3-Methylpentane (Phillips Petroleum Company pure grade) was passed through a 90-cm column of alumina saturated with silver nitrate and checked for purity by absorption spectroscopy. EPA (5:5:2 by volume ether, isopentane, and ethanol) was used as obtained from Hartman-Leddon Co.

Results

The total emission spectra of quinoline, HEQ, and DEQ in EPA are presented in Figure 1, and the band maxima for their fluorescence and phosphorescence bands are given in Table I. A marked similarity between these spectra is evident except for an increase in the fluorescence yield in the 2-substituted compounds. However, in changing the solvent to 3-methylpentane, Figure 2, the quinoline emission reverts completely to phosphorescence as is expected, but the emission of HEQ and DEQ becomes rather broad and structureless. On either side of this broad emission several small bands occur at the same locations as the fluorescence and phosphorescence bands of HEQ and DEQ in EPA solvent. Small differences between these bands and the fluorescence and phosphorescence bands are found, but these differences can be attributed to the overlapping broad band luminescence. The emission spectrum of quinolinium chloride in EPA (it is not soluble in 3-methylpentane) was almost identical with those obtained for HEQ and DEQ except blue shifted. No noticeable differences are observed in the emission of HEQ and DEQ which indicates that the deuterium effect is indeed small.

Lifetimes of quinolinium chloride in EPA and quinoline, HEQ, and DEQ in both 3-methylpentane and EPA, are reported in Table II. As expected, the lifetimes observed in 3-methylpentane are shorter due to increased vibronic coupling between the $^3(n,\pi^*)$ and $^3(\pi,\pi^*)$ states in a hydrocarbon solvent.[6] In 3-methylpentane two long-lived species are observed. The first was the broad structureless band which had a measured lifetime of 0.05 seen at the 3800 Å maxima. A second long-lived species with a lifetime of approximately 1.3 sec at 4900 Å is presumably due to the emission from the same state observed in EPA. The measured lifetimes of the broad bands in HEQ, DEQ, and quinolinium chloride are virtually identical.

Table I: Solvent Effect on Luminescence[a]

Compd	Solvent	Fluorescence, Å	Charge transfer, Å	Phosphorescence, Å
Quinoline	3MP	None	None	4560
				4668
				4790 sh
				4870
				5000
	EPA	3137	None	4560
		3210		4670
		3268		4870
		3355		5000
		3420		5260
		3512		
		3578		
2-(2-Hydroxyethyl)quinoline	3MP[b]	3150	3880 max	4570
		3230		4670
		3290		4710 sh
		3380		
		3460		
	EPA	3180	None	4555
		3230		4660
		3295		4865
		3378		4980 sh
		3450		5010
		3540		
		3608		
		3700 sh		
2-(2-Deuterioxyethyl)-quinoline	3MP[b]	3170	3860 max	4584
		3245		4600
		3310		4700 sh
		3400		4890
		3480		5000 sh
	EPA	3180	None	4595
		3252		4705
		3335		4900
		3415		5010 sh
		3490		5260
		3575		
		3660		
		3730 sh		
Quinolinium chloride	EPA	3140 w	3820 max	4560
		3200 w		4660
		3260 w		4860
				5055

[a] w = weak, sh = shoulder. [b] These represented the fluorescence bands not completely covered by the charge-transfer luminescence.

Discussion

Vibronic spin-orbit interactions in quinoline[4] and related heteroaromatics have been shown to be responsible for much of the solvent dependency of the luminescence from these systems. If these processes were operative in HEQ and DEQ, they should manifest themselves as an increase in phosphorescence to fluorescence intensity in going from a hydroxylic to hydrocarbon

(6) G. A. Knesel and C. M. O'Donnell, unpublished results.

Table II: Solvent Effects on Phosphorescence Lifetimes

Compd	Solvent[d]	τ,[a] sec	λ,[a] Å	τ,[b] sec	λ,[b] Å
Quinoline	3MP	None		0.95 ± 0.05	4574
	EPA	None		1.35 ± 0.05	4560
Quinolinium chloride	EPA	0.05 ± 0.003	3800		
2-(2-Hydroxyethyl)quinoline	3MP	0.05 ± 0.003	3800	1.33 ± 0.1	4916[c]
	EPA	None		1.64 ± 0.05	4550
2-(2-Deuteriooxyethyl)-quinoline	3MP	0.05 ± 0.003	3800	1.28 ± 0.1	4900[c]
	EPA	None		1.72 ± 0.05	4571

[a] Mean lifetime of charge-transfer band at 3800 Å. [b] Mean lifetime of normal phosphorescence at wavelength indicated. [c] A longer wavelength band was used in these measurements to eliminate the overlap of the charge transfer band. Excitation spectra were run in 3MP observing at these wavelengths, and they were identical with that obtained for the parent compound in EPA. [d] All lifetimes were recorded at 77°K.

solvent. Alternately, if intramolecular hydrogen bonding were more effective in a hydrocarbon solvent, we might not observe any drastic change in this ratio. Certainly, there is nothing in this mechanism to account for a new band being formed with a location between the fluorescence and phosphorescence. If this was simply a red shift in the fluorescence of HEQ and DEQ, the same type of shift should be noticeable in quinoline. Since this emission is so similar to that observed from the quinolinium ion, it is reasonable to assume that the emission originates from some common state. A possible route which HEQ and DEQ might take to achieve this common state is *via* a transfer of charge in the excited state as depicted below. This ionization may take

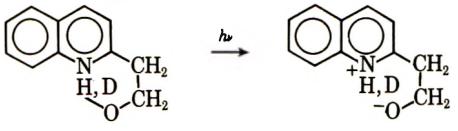

place in either a singlet or triplet state, but the luminescence from this ion is shown to be a triplet by our lifetime measurements.

In view of the lifetime data presented in Table II, we find convincing evidence for our assertions. The phosphorescence lifetimes of HEQ and DEQ are noticably longer than that observed for quinoline, but quite similar to that observed for 2-ethylquinoline.[5] We observe a decrease in the lifetime of quinoline in going from EPA to 3-methylpentane which agrees with previous literature values. A decrease in the lifetime of the 4900-Å bands of HEQ and DEQ with respect to that observed in EPA is also observed and based on the per cent change which occurs for 2-ethylquinoline when the solvent is changed from EPA to 3-methylpentane, which is expected. These lifetime measurements plus the close relationship between the location of the band maxima of these sidebands with the fluorescence and phosphorescence in EPA indicate that some of the un-ionized species is present. Excitation spectra for HEQ and DEQ with an emission wavelength of 4900 Å are identical with that observed for quinoline in 3-methylpentane or HEQ and DEQ in EPA. As shown in Table II, the lifetimes of all of the broad emissions are identical and this is rather convincing evidence of the identity of the lowest emitting state in all three compounds.

If a charge-transfer state is responsible for the photochemistry of these molecules, their photoelimination results become understandable. For both HEQ and DEQ, the quantum yield of photoelimination increased markedly on changing from a polar to a nonpolar solvent.[6] This result can be explained by proposing that the mechanism for photoelimination in these compounds in the nonpolar solvent is as follows.

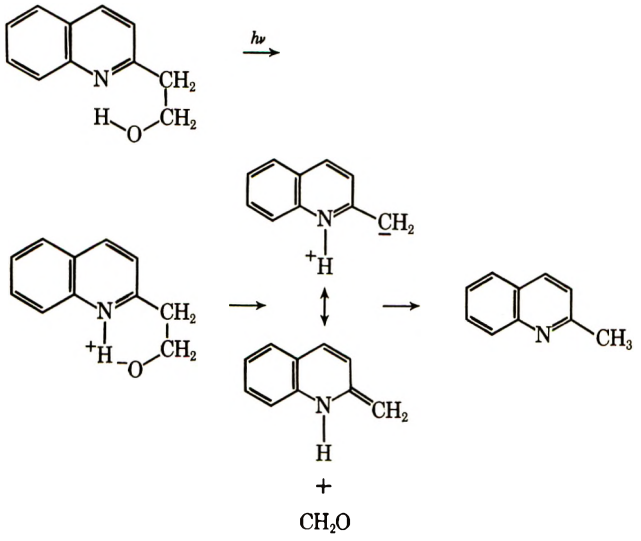

Since intramolecular hydrogen bonding would be greatly favored in a nonpolar solvent, this provides an explanation for the observed increase in quantum yields. The absence of this effect when quinoline is dissolved in

hydroxylic glass at 77°K also gives evidence to the necessity of the intramolecular bond in this photochemical reaction.

Conclusions

An unusual type of emission is observed for substituted quinoline in nonpolar solvents as a result of intramolecular hydrogen bonding. This charge-transfer state seems to be responsible for the photoelimination of these compounds and explains the effect of solvent on their quantum yields. A number of such systems can readily be conceived, including the related isoquinoline series which we shall report on in a future paper. The number of intramolecular hydrogen-bonded heterocycles found in biological systems is numerous. We suggest that this type of charge transfer state could occur whenever a similar acid group is present in such systems and might determine their photochemistry.

Acknowledgments. Acknowledgment is made to donors of the Petroleum Research Fund, administered by the American Chemical Society, for partial support of this research. Partial support was provided by grant GM-15425 from the U. S. Public Health Service and the Research Corporation. We wish to thank Professor S. J. Strickler for a number of helpful discussions.

Black Lipid Membranes (BLM) in Aqueous Media. Photoelectric Spectroscopy

by Nguyen Thuong Van and H. T. Tien

Department of Biophysics, Michigan State University, East Lansing, Michigan 48823 *(Received March 19, 1970)*

Black lipid membranes (BLM) of chloroplast extracts separating two aqueous solutions have been studied photoelectrometrically. The experimental arrangement and procedure for obtaining photoelectric spectra of the BLM are described in detail. The other salient points of this paper are as follows. (1) The photoelectric spectrum of the BLM obtained in the region of 350–800 nm is compared with its absorption spectrum of bulk solution. The two spectra, though obtained by two entirely different methods, are practically identical. (2) The origin of the photoelectric spectrum of the BLM is discussed in terms of various possible modes of interactions. Electrons and holes are produced in the BLM upon light excitation, which in turn give rise to the observed photovoltaic effect. (3) A comparative study is made between a silicon solar cell and a chloroplast BLM. The two systems exhibit striking similarities. (4) The photolysis of water by light mediated through chloroplast BLM is proposed. (5) The significance and general utility of BLM photoelectrometry, conceived and developed in the course of this investigation, are briefly indicated.

Introduction

In photosynthesis, the role of the thylakoid membrane of chloroplasts appears to be crucial in the primary photophysical and photochemical reactions. At present the structure of the thylakoid membrane is not sufficiently known but is thought to be a quasi-crystalline array of lipids, proteins, and pigments (for a recent review, see ref 1). These materials organized in ultrathin lamellae have been suggested earlier by Frey-Wyssling,[2] Menke,[3] and Frey-Wyssling and Steinmann[4] on the basis of birefringence and dichroism studies. Further evidence has been provided by X-ray diffraction data from chloroplasts gathered by Kreutz[5] and indirect monolayer experiments[6–8] as well as recent optical investigations.[9,10] The results of preceding work and of more recent electron microscopic studies and chemical analyses have led a number of investigators to propose detailed structural models.[11–14]

(1) D. Branton, *Ann. Rev. Plant Physiol.*, **20**, 209 (1969).
(2) A. Frey-Wyssling, *Protoplasma*, **29**, 279 (1937).
(3) W. Menke, *Biol. Zentr.* **63**, 326 (1943).
(4) A. Frey-Wyssling and E. Steinmann, *Biochim. Biophys. Acta*, **2**, 254 (1948).
(5) W. Kreutz and W. Menke, *Z. Naturforsch.*, **15b**, 483 (1960).
(6) E. E. Jocobs, A. S. Holt, R. Kromhout, and E. Rabinowitch, *Arch. Biochem. Biophys.*, **72**, 495 (1957).
(7) W. D. Bellamy, G. L. Gaines, and A. G. Tweet, *J. Chem. Phys.*, **39**, 2528 (1963).
(8) W. Sperling and B. Ke, *Photochem. Photobiol.*, **5**, 865 (1966).
(9) J. C. Goedheer, Ph.D. Thesis, University of Utrecht, 1957.
(10) K. Sauer, J. R. Smith, and A. J. Schultz, *J. Amer. Chem. Soc.*, **88**, 2681 (1966).
(11) W. Menke, *Brookhaven Symp. Biol.*, **19**, 328 (1967).

The essential feature of all these models assumes that the thylakoid or photosynthetic membrane consists of an ultrathin layer of lipid with sorbed protein. This feature to a large extent is consistent with the current view of the other types of biological membranes (*e.g.*, the cristae membrane of mitochondria and the visual receptor membrane of retina).

As is the case with the other types of biological membranes, direct experimentation with the thylakoid membrane has not been possible. Therefore in recent years several investigators, recognizing the importance of structural organization in photosynthetic processes, have initiated studies with deposited layers of chlorophylls and their related compounds on solid supports as model systems and have demonstrated the existence of a number of interesting phenomena.[15-17]

More recently, the search for a better model system for studying photosynthesis *in vitro* has led to the discovery of the photoelectric effects in thin and black lipid membranes.[18] A black lipid membrane (BLM) is an ultrathin membrane (40–140 Å thick) formed by two monolayers of lipid molecules with the hydrophilic end oriented toward the aqueous phase. The photoactive BLM containing chloroplast pigments or other light-sensitive materials is usually formed on a hydrophobic support separating two aqueous solutions. At present, a photoactive BLM, in spite of its simplicity, serves a more realistic model for the photosynthetic (thylakoid) membrane.

The present study is an extension of previous work[18] in that it has shown the wavelength dependence of photoelectric effects in the chloroplast BLM (Chl–BLM for short). The aim of this work is twofold: (a) to develop a simple setup so that photoelectric spectra of the BLM can be obtained reproducibly, and (b) to demonstrate that a Chl–BLM is similar to a semiconductor device capable of converting light energy into electrical energy. Because of the novel approach involved, a portion of this paper is devoted to the experimental setup and its relationship to other spectroscopic techniques.

Experimental Section

Materials. All reagents were CP grade and were used without further purification. Diphosphopyridine nucleotide (DPN) and triphosphopyridine nucleotide (TPN) were obtained from Sigma Chemical Co. Quinhydrone, phthalocyanine, and various carotenoid pigments were supplied by Eastman Kodak Co. Hydrocarbon solvents used in this study were purchased from Phillips Petroleum Co. Fresh spinach leaves were obtained from local food markets.

Preparation of BLM-Forming Solution. The following steps are a modified version of a detailed procedure described elsewhere:[18] (a) fresh spinach leaves are washed thoroughly with ordinary distilled water and the midribs removed; (b) they are finely chopped in an electric mixer for 3 min in a solution of sucrose 0.5 *M* in 0.05 *M* $KHCO_3$; (c) the filtrate is extracted 3 times with petroleum ether–methanol solution (2:1, v/v); (d) the soluble portion is evaporated in a flash evaporator (Buchler Instruments Co.) to dryness; (e) the residue is taken up in a small volume of *n*-dodecane–butanol solution (3:1, v/v).

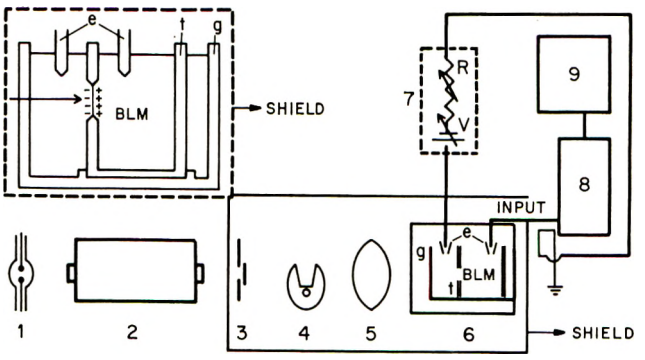

Figure 1. Schematic diagram of experimental setup for measurement of electrical changes in the Chl–BLM (details see text).

Other BLM-forming solutions were simply prepared by dissolving various amount of pigments (phthalocyanine, retinal, etc.) in oxidized cholesterol solution.[19b]

Methods of Black Lipid Membrane (BLM) Formation. The BLM were formed either by the brush technique[19] or by injection of a small amount (2 μl) of the lipid solution in the aperture with a microsyringe (Model PB-600-1, Hamilton Co., Whittier, Calif.). Further details on the BLM techniques have been given elsewhere.[20]

Apparatus. The major parts of experimental setup are illustrated in Figure 1. The function of this experimental setup is to provide radiations of known intensity and wavelength to excite the BLM (the optical part) and secondly to provide electrical contact with the BLM in order to measure or detect any electrical changes in the latter (the electrical part). The listing of parts is identified by a number in parentheses in Figure 1 and described below.

(12) T. E. Weier and A. A. Benson, *Am. J. Bot.* **54**, 389 (1967).

(13) K. Muehlethaler in "Biochemistry of Chloroplasts," Vol. 1, T. W. Goodwin, Ed., Academic Press, New York, N. Y. 1966, pp 49–64.

(14) R. C. Park and N. G. Pon, *J. Mol. Biol.*, **3**, 1 (1961).

(15) R. C. Nelson, *J. Chem. Phys.*, **27**, 864 (1957).

(16) W. Arnold and H. K. Maclay, *Brookhaven Symp. Biol.*, No. 11, 1 (1959).

(17) G. Tollin, D. R. Kearns, and M. Calvin, *J. Chem. Phys.*, **32**, 1013 (1960).

(18) H. T. Tien, *J. Phys. Chem.*, **72**, 4512 (1968).

(19) (a) P. Mueller, D. O. Rudin, H. T. Tien, and W. C. Wescott, *ibid.*, **67**, 534 (1963); (b) for a recent review, see H. T. Tien in "Surface Chemistry of Biological Systems," M. Blank, Ed., Plenum Press, New York, N. Y., 1970, pp 135–154.

(20) H. T. Tien and R. E. Howard in "Techniques of Surface Chemistry and Physics," Vol. 1, Marcel Dekker, New York, N. Y., to be published.

A. The Optical Section (1–5, Figure 1). (1) Source: dc xenon compart arc lamp (Hanovia, Type 976C, 1000 W) (Schoeffel Instruments Co., Model LH151N); lamp power supply (Schoeffel Instruments Co., Model LPS255). (2) Monochromator: visible grating, high-intensity monochromator (Bausch & Lomb, Model 5) and Littrov quartz prism compact monochromator (Schoeffel Model QPM30). (3) Shutter and diaphragm: variable speed $^1/_{100}$ sec–1 sec, T, B (Alphax, Wollensak, Rochester). (4) Rotating sector: variable rotating sector is made from a piece of thin tin plate driven by a small electric motor (Synchron, 60 rpm). (5) Collimating lens: ordinary convergent lens (Edmund Scientific Co.).

B. The Electrical Section (6–9, Figure 1). (6) BLM forming chamber: electrodes (calomel electrodes: Beckman fiber junction Type 39270 or Beckman platinum electrodes Type 39281). (7) Variable current and voltage box: similar to Heath pH Test Box Model EUA-20-12. (8) Electrometer: (a) high-speed picoammeter (Keithley Instruments Inc., Model 417); (b) multirange electrometer (Keithley Instruments Inc., Model 610B); (c) vibrating reed electrometer (Cary Instruments Model 31). (9) Recorder Keithley Instruments Inc. Model 370.

Other instruments and components used for calibration and comparison are the following: (a) factory calibrated thermopile (Eppley Laboratory Inc., Bi–Ag, linear 12 junction, lamp black coated); (b) dc indicating amplifier (Leeds & Northrup Model 9835A) is used to monitor the thermopile; (c) silicon solar cell (Edmund Scientific Co.); (d) spectrophotometer, Cary Model 14 (Applied Physics Corp.); (e) spectrofluorimeter, (Aminco-Bowman); (f) neutral filters, Grau-filter (Carl Zeiss).

To obtain accurate results, shielding against electrical noises and stray light is necessary. For this purpose, the whole BLM-forming chamber and electrodes were contained in a metal box. In the wall of the latter, an aperture is provided for light excitation and BLM formation. A large box made of copper wire mesh is used to enclose parts 3–6 of Figure 1. The two shields are properly grounded to a tap.

Procedure

A. Calibration of Light Source. The main experimental setup was used. The BLM-forming chamber and the two electrodes were replaced by the thermopile. External resistance and voltage were set to zero and the dc indicating amplifier was used to measure the voltage from the thermopile. Care was taken to ensure that the conditions of illumination of the thermopile, especially the optical alignment and the size and the angle of incidence of the light beam, were identical with the excitation of the BLM. The thermopile was factory-calibrated against two tungsten light bulbs of the National Bureau of Standard. The linearity to intensity of incident radiation and the spectral flatness were quite satisfactory (*i.e.*, photocurrent/radiant power = constant at any wavelength of the visible). The readings of the meter (in μV) are converted into ergs/sec and shown in Figure 2. It should be mentioned that the calibration was very sensitive to optical alignment.

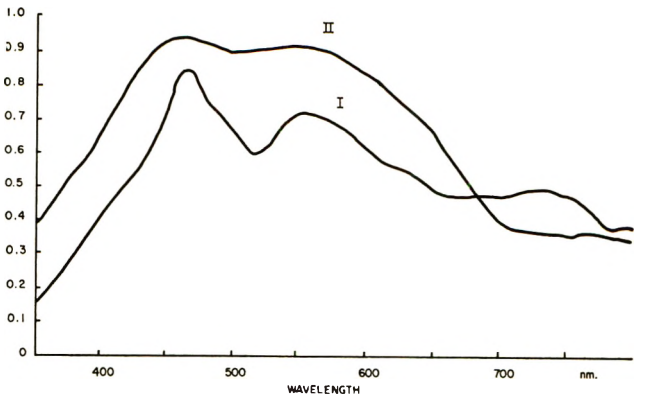

Figure 2. Spectral energy distribution of the incident light. Curve I: measured by a spectrally flat thermopile, scale: $\times 10^{-4}$ V; 0.059 V = W/cm^2; curve II; spectral response of a silicon solar cell measured with the same source (arbitrary units).

B. Measurement of Photocurrent. The BLM-forming chamber (g and t, Figure 1) was thoroughly washed with acetone, tap water, double-distilled water, and then dried with hot air. Both chambers were filled with the aqueous solution with a pipet. Care was taken not to wet the upper border of the inner Teflon chamber. When monochromatic light was used, filters or monochromator were placed in position (marked no. 2 in Figure 1). The wavelength scale could be checked with the blue (436 nm), green (546 nm), and yellow (580 nm) lines of the mercury xenon arc but most of the excitation of the Chl–BLM was done with a xenon arc lamp. The light beam was aligned to give maximum power. This was done by adjusting the chamber by hand until the light beam covered the hole entirely and was normal to it. For quantitative work, the area covered by the light beam was identical with the area of the thermopile illuminated during the calibration process.

The measurement of the photocurrent was made with the electrometer which had been previously calibrated with the box (marked no. 7 in Figure 1). This was done as follows. The dark current was first measured by moving the range knob from the less sensitive range to higher sensitivity ranges until the meter read in the middle of the scale. For a stable membrane, the meter moved little from this position with time; when recorded, this was taken as the base line of the photocurrent. When the diaphragm was open, an increase in current was noted; the latter was the photocurrent. When the dark current was particularly high, *e.g.*, when an external voltage was applied across the BLM or when some chemical was introduced into one aque-

ous phase, the small photocurrent could usually be detected by bucking out the dark current on the meter (this can be easily done with Keithley 417 which has a calibrated current source).

In measuring the photocurrent of a BLM, several factors were taken into account to decide the time of exposure of the BLM to light and darkness. These were the saturation time of the BLM (*i.e.*, the time it takes for the photocurrent to level off), the lifetime of the BLM, and the number of observations required per BLM. When only a few observations were needed, the diaphragm was open in full and waited for the photocurrent to rise and level off and an average photocurrent could be calculated for the period of illumination. When several observations were necessary (*e.g.*, the whole photoelectric spectrum), some arbitrary time of exposure was chosen so that all required observations could be obtained from the same membrane and no damage could be done to the BLM due to long exposure to light. The choice of exposure time may affect the final form of the photoelectric spectrum. Fortunately, when the time of exposure was small (<5 sec), the relative spectral response did not change very much when this time was varied within the range 2–5 sec, as will be shown later. The exposure times used were 2.5 sec to light, 3.5 sec to darkness or 4 sec to light and 6 sec to darkness. When only the photovoltaic effect was measured, the open circuit procedure was adopted. In this manner, the membrane was directly connected to the electrometer *via* electrodes and solutions.

C. Photoelectric Spectrum. Generally, photocurrents of BLM were measured by two different procedures. The continuous procedure consisted of moving the wavelength cam with a synchronous electric motor (Hurst synchronous motor, Model AR-DA, $^1/_3$ rpm) and the output current recorded. Since the scanning of the whole spectrum, from 350 to 800 nm, would require 3 min during which time the membrane was continuously exposed to light, it is sometimes necessary to correct for the base line shift due to long exposure. A solution to this problem consisted of having a rotating sector in front of the exit slit of the monochromator. Fortunately, some of the continuous spectra were good enough to make this correction unnecessary.

The second point-by-point procedure was preferred for more accurate work. In this method, the photocurrent was measured at 10-nm intervals, starting from 350 nm. The wavelength setting was made without disturbing the optical alignment of the monochromator by the use of the same synchronous motor and a switch. Three readings were taken for each wavelength and the mean calculated. When conditions allowed, *e.g.*, for long-lived BLM, the whole procedure was repeated in the reverse direction (800 to 350 nm). If the spectrum changed appreciably, this was an indication that the time of exposure was not correct or the BLM had become irreversible with illumination.

When a chemical agent was studied, it was either dissolved in the electrolyte solution (generally 0.1 *M* KCl) or added by a dispenser, in solution form, to the chambers. If addition to only one side of the BLM was required, care was taken to add an equivalent amount of the electrolyte solution to the other side to restore the BLM to its earlier configuration. A small magnetic stirrer was used to stir the solution.

D. Photoelectric Spectrum of the Silicon Cell. Photoelectric spectra were obtained by the same setup described in Figure 1 with the difference that the photocell had replaced the BLM forming chamber 6. The positive pole of the photocell was connected to the input of the electrometer and the negative to the ground *via* the voltage and resistance box (7). Use of rotating sectors was not necessary since the base line did not shift. For the calculation of the quantum efficiency, the illumination of the solar cell was identical with the illumination of the thermopile during the calibration process.

E. Absorption and Fluorescence Spectrum of the BLM-Forming Solution, and Fluorescence Spectrum of a Thin Lipid Membrane in Aqueous Media. Absorption spectra were obtained with a known dilution (generally $^1/_{50}$ to $^1/_{100}$) of the stock solution. Measurement was made with a Cary 14, in a 0.1-cm path length cell. Results, corrected for baseline shift, were converted to the initial concentration.

Fluorescence spectra were obtained in the usual way with the Aminco Bowman spectrofluorimeter at room temperature. Phosphorescence spectra were made at 77°K (liquid nitrogen).

Fluorescence spectra for the thin membrane (thickness $< 1\ \mu$) were obtained in the following manner. The thin membrane was formed by immersing a large Teflon ring (1 cm diameter) in a cuvette with 4 quartz walls (Figure 3). The cuvette contained one aqueous phase (KCl 0.1 *M*) occupying most of the volume of the cuvette and a thin lipid phase (1 mm of BLM forming solution) on top of the aqueous phase. The Teflon ring, which was held by a wire, was lowered to the same level where the excitation beam traverses the cuvette, the plane of the Teflon ring was orientated with a diagonal plane of the cuvette (Figure 3), and the measurement was made normally, at room temperature, with the spectrofluorimeter.

Results and Discussion

Interactions of Photons and the Chl–BLM. The models of interactions of photons and matter can be extended to the BLM.[21] These interactions can be broadly divided into two types: (i) interactions without energy transfer from the photons to the Chl–BLM and (ii) interactions involving energy transfer.

(21) E. E. Loebner in "Photoelectronic Materials and Devices," Van Nostrand, Princeton, N. J., 1965, p 281.

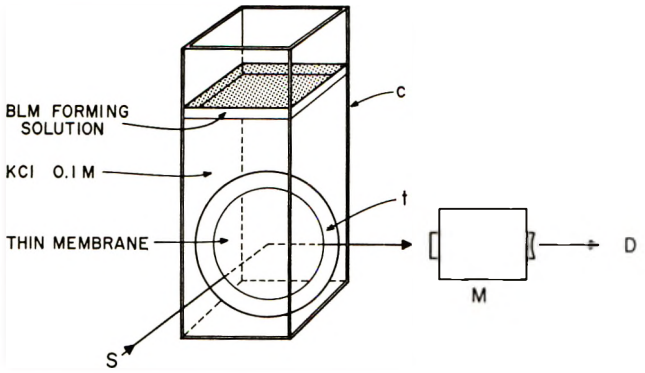

Figure 3. Schematic diagram of experimental setup to obtain fluorescence spectrum for a thin lipid membrane: c, four quartz wall cuvette; t, Teflon ring (1 cm diameter); S, excitation source; M, monochromator; D, detector.

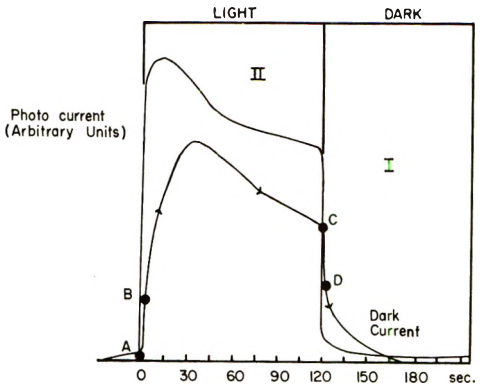

Figure 4. Light response under prolonged illumination. Curve I, BLM; curve II, silicon solar cell; AB, CD are the fast components of the BLM light response.

Only the latter interactions are relevant to the photoelectric effects.

In an experimental setup such as the one described in Figure 1, the spectral distribution of the energy incident upon the photon convertor (*i.e.*, BLM) is

$$W_\lambda = \int_{\lambda_1}^{\lambda_2} I_\lambda M_\lambda d\lambda \qquad (1)$$

where I, M, and W denote source intensity, monochromator transmittance, and incident radiant power, respectively. Subscript λ refers to wavelength and the integral sign is used to denote that W is not usually a scalar but certain function of the wavelength. For a monochromator, W_λ is generally gaussian with most of its energy concentrated at the wavelength where the monochromator is set.

Since the photocurrent and the radiant power are proportional to the number of electrons and of quantum of light, respectively, then i_λ (photocurrent) and W_λ (radiant power) are expressed in absolute units, the following relation holds

$$\frac{i_\lambda \text{ (A)}}{W_\lambda \text{ (erg/sec)}} = \frac{n}{n'} = \text{quantum yield} \qquad (2)$$

Equation 2 is similar to a relation derived by Hein.[22]

Dark Conductivity of the Chl–BLM. The dark resistance of the BLM measured directly with a multirange electrometer (Keithley 610B) is 1–2 × 10^5 ohms-cm^2 for a thickness of 70–100 Å. The specific conductivity is therefore about 1–2 × 10^{-11} mho/cm. The last figure is considered as the lower limit for a semiconductor (about 10^{-12} mho/cm). Compared to other phospholipids and oxidized cholesterol, the conductivity of the Chl–BLM is, however, 1 to 4 orders higher. This relatively higher conductance is due to the presence of chlorophylls in the membrane since the phospholipids contained in the BLM-forming solution are not different from the other lipids, and when chlorophylls are incorporated in low conductivity lipids, the latter become more and more conductive with the concentration of chlorophylls.

The dark conductivity increased by one order when the temperature increased from 15 to 40°. It also increased with the ionic strength of the bathing solution. The shape and sign of the light response to long illumination (>20 sec) (Figure 4) shows light response to time of illumination of a Chl–BLM and a silicon cell. It shows that the silicon cell is a hard-type response cell and the Chl–BLM is a soft-type response cell since in the latter, it takes several seconds for the photocurrent to reach the maximum value. The softness of the Chl–BLM may be due to several factors; the large resistance and capacitance of the BLM can also increase the response time. However, it is possible to change drastically the shape of the light response by varying experimental conditions such as the applied field, the light intensity, and especially the nature and concentration of the solute in the bathing solution. The sign of the light response can also be reversed by varying these parameters.

When the Chl–BLM is in contact with two identical solutions, the direction of the photocurrent indicates that the illuminated face is *negative* with regard to the dark interface. However, this behavior is not constant and reversal of the polarity is observed for 10% of the BLM. When the *dark* side of the BLM contains an electron acceptor such as DPN, TPN, or $FeCl_3$, the polarity is always the same, being negative with respect to the illuminated interface, when no external field is applied.

A silicon cell with known polarity is used to establish the polarity of the BLM. When the former replaces the BLM in the experimental setup (Figure 1), with its positive pole connected to the input of the electrometer, the photocurrent observed moves the meter in the same direction as the photocurrent produced by the Chl–BLM when the latter is connected as in Figure 1.

(22) C. C. Hein, *J. Opt. Soc. Amer.*, **25**, 203 (1935).

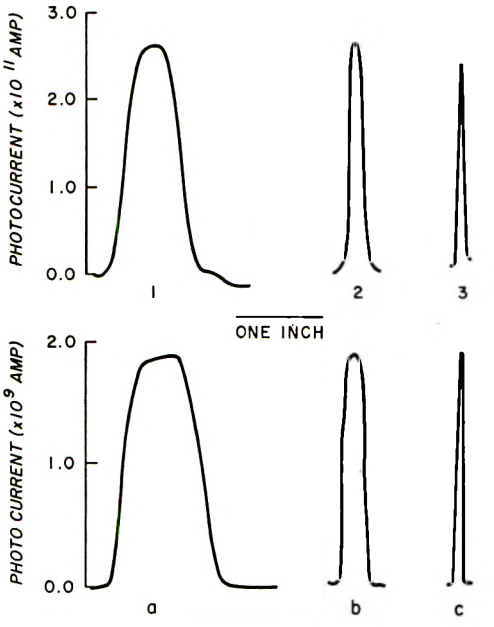

Figure 5. Light response and short illumination (2.5 sec light/3.5 sec dark). Fast components of the BLM light response recorded at various chart speeds (1, 20 in./min; 2, 5 in./min; 3: 1 in./min). a, b, c are corresponding responses of a silicon solar cell.

Light Response to Short Illumination (5 sec). Figure 5 shows light response to short periods of illumination (2.5 sec of light followed by 3.5 sec of darkness). Similarity of the silicon cell and the Chl–BLM is remarkable. In short periods of illumination, only the fast components of the light response are measured and the slow components which are made of ionic currents and secondary electronic currents are neglected. For periods under 5 sec, the photocurrent is almost linear with time and the photoelectric spectrum (see later), is not distorted if the time of illumination is smaller than 5 sec. Table I shows that the relative response does not change when the illumination time passes from 2.5 to 4 sec although the absolute response does.

Table I: Relative Light Response and Duration of Illumination

Duration of illumination (sec) followed by darkness given in parentheses	Photocurrent (×10¹⁰ amp) at wavelength 425	550	660 (nm)
A. 2.5 (3.5)	0.82	0.29	0.60
B. 4.0 (8.0)	1.35	0.46	1.00
Ratio: A/B	0.61	0.63	0.60

The light response generally does not change appreciably for the whole life of the BLM, and in one occasion, light response is observed unaltered for one Chl–BLM for 1 hr and 25 min. However, important changes do happen with time, especially when drastic

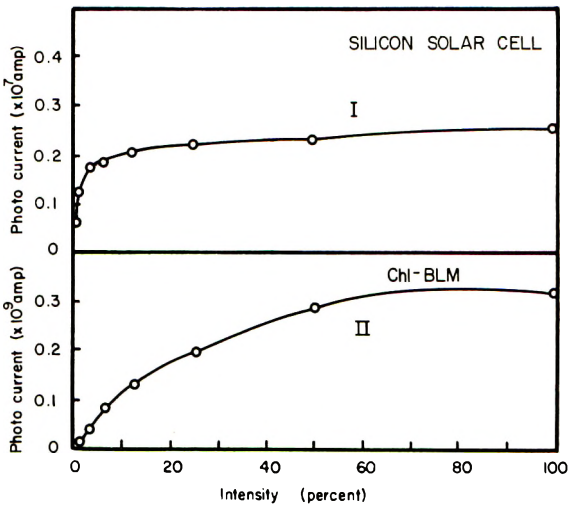

Figure 6. Light response as a function of light intensity. Attenuation of initial intensity (100%) achieved with neutral filters of known transmittance.

physico-chemical conditions such as high temperature and low pH are imposed upon the Chl–BLM.

Photocurrent and Light Intensity. Figure 6 shows the variation of photocurrent with the intensity of the incident light beam for a silicon cell and a Chl–BLM. The photocurrent is not linear for both photon detectors but the saturation point is reached much earlier for the silicon cell.

This behavior may be due to the fact that most of the incident light is absorbed by the silicon cell and only a very small fraction is absorbed by the BLM. This experiment is carried out with white light and the attenuation of light intensity is achieved by the use of neutral filters.

Photocurrent and Applied Voltage. Figure 7 shows the variation of photocurrent with applied voltage for the silicon cell and a Chl–BLM. At zero applied field, the photocurrent is still observable, even when the small electrode potential is balanced out. The photocurrent varies exponentially with the applied voltage. The latter increases the photocurrent when its direction is the same as the photocurrent (*i.e.*, same polarity as the BLM) and decreases the photocurrent when it opposes the BLM. It is possible to find an applied voltage which can balance out completely the emf of the BLM. When this happens, the number (also mobility and life time) of the electrons moving in one direction is exactly equal to the number of holes moving in the opposite direction and the photoelectric effect is not observable. However, when the applied voltage exceeds this critical value, the photocurrent is reversed. For a Chl–BLM in contact with electron acceptors at its dark side, this critical voltage can exceed 100 mV.

Photocurrent and the Nature of the Chemicals in Solution. There is not a clear difference of light response between KCl and NaCl. When the latter is used, the

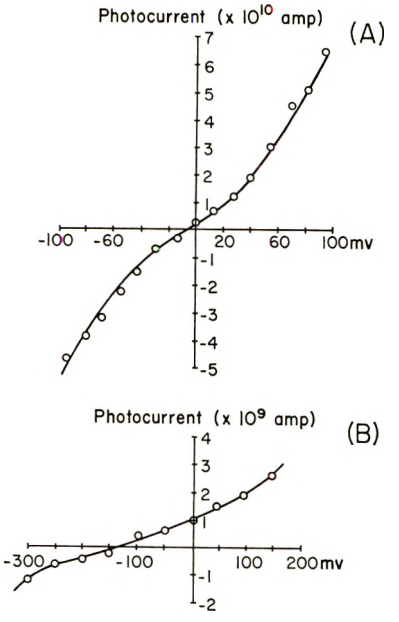

Figure 7. Light response as a function of applied electric field. Curve a, solutions on both sides are identical; curve b, the dark side contains a small amount of electron acceptor.

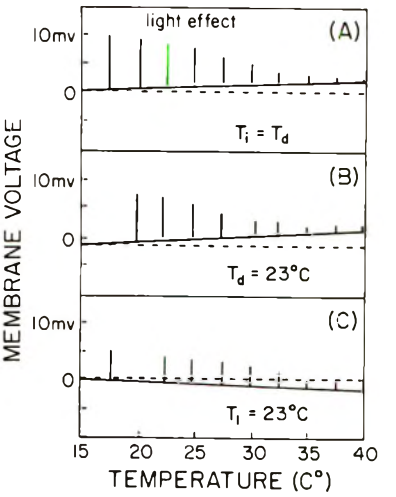

Figure 8. Light response as a function of temperature: solid lines refer to open circuit membrane voltages, vertical lines to light response for short illumination (2 sec). Curve a, $T_i = T_d$ where T_i and T_d are the temperature of the light, and the dark compartments, respectively. Curve b, only T_i varies, T_d is kept constant and serves as reference. Curve c, T_d varies, T_i is kept constant.

concentration effect is important and the light response decreases in this order, 0.01, 0.1, 1, 2 *M*. Distilled water gives quite satisfactory light response. When buffered solutions are used (*e.g.*, phosphate buffer), light response is almost completely abolished (<5%) when the concentration of the buffer is high (0.1 or higher). The pH of the buffer studied varies from 5 to 8. Each buffer system had a different effect on the light response, but in general, an acid pH increased the light response and *vice versa*. The ionic effect was similar to the temperature effect, *i.e.*, an increase in ionic strength decreased the membrane resistance and the photoelectric effect.

To be efficient, there must be some asymmetry in the concentration of the chemical in the two compartments (*i.e.*, illuminated and dark sides of the BLM). DPN and TPN are found to increase considerably the photoelectric effect even at a low concentration (0.001%). $FeCl_3$ and quinhydrone also increase the response to light at concentrations as low as 10^{-3} *M*. The effect is particularly dramatic when the BLM gives very small response at the start and in one occasion, 2 drops of 0.025% DPN, increased the photocurrent by three orders of magnitude.

As a general rule, oxidants (*i.e.*, electron acceptor) increase the light response. They may act as a sink to attract electrons released by the BLM.

Thin Colored Membranes. The colored membrane (1000–8000 Å) produced appreciably less photoeffect than the black membrane since the light response measured in open circuit, *i.e.*, independently of the resistance change in the membrane, increased with the black area during the thinning process. The Plateau–Gibbs border appeared also capable of photoelectric effects but generally, for a given total area, a membrane with large Plateau–Gibbs border gave less light response than a membrane with small Plateau–Gibbs border. No quantitative study was made on this interesting observation, however.

Temperature Effect (Figure 8). The temperature decreased the resistance of the membrane by one order when the temperature of the bathing solution increased from 15 to 40°. The open circuit membrane potential changed by a few millivolts. The same behavior was observed when the temperature of only one compartment was varied. The light response decreased with temperature and became extinct at 40°. All these effects were partially reversible; that is, when the temperature was decreased, the membrane potential changed in the opposite direction and the light response increased, although they did not necessarily reach their former magnitude.

Quantum Efficiency of the Chl–BLM. Since photosynthesis is a highly efficient process, the quantum efficiency of the Chl–BLM should also be large if it is to be a good model for the thylakoid membrane. We have therefore estimated the quantum yield of the Chl–BLM from eq 2.

When the photoelectric spectrum is given as amperes per watt, it is possible to obtain directly the quantum efficiency[22] since 100% efficiency which corresponds to the release of 1 electron by the absorption of 1 quantum is given by the curve $y = 10^7\ e/h\nu$ (or $e/h\nu$ if the spectrum is given as A/erg sec).

Figure 9 shows 4 photoelectric spectra in A/W of incident light. Since most of the light is lost by trans-

Table II: Quantum Efficiency of a Chl-BLM

Wavelength, nm (1)	Absorbance, E^a (2)	Absorbance, $E'^b \times 10^6$ (3)	Fraction of light absorbed by BLM (100 Å) $1 - 10^{-E}$ (4)	Radiant power incident on BLM erg/sec[c] (5)	Radiant power absorbed by BLM erg/sec (4) × (5) (6)	Photocurrent,[d] A × 10^{10} (7)	Photocurrent per absorbed erg/sec amp/erg/sec × 10^{10} (7)(7)/(6) (8)	$e/h\nu$, amp/erg sec × 10^{10} (9)	Quantum efficiency,[e] % (8)/(9) (10)
420	50	50	0.001151	146.6	0.1687	1.35	8.00	336	2.38
550	2.84	2.84	0.00006539	211.8	0.01385	0.462	33.36	440	7.58
660	21	21	0.0004835	148.33	0.07171	1.00	13.94	529	2.63

[a] The absorbance is obtained from a 100 dilution of the stock solution (Cary 14, 0.1-cm cell). The arithmetic means of three independent determinations are 420 nm = 0.50; 550 nm = 0.00284; 660 nm = 0.21 [b] Calculated for a 100-Å layer. [c] Corrected for BLM area and reflection loss. Area of BLM = 1 (1 mm²). [d] Arithmetic mean of three determinations (4 sec exposure to light, 6 sec to dark). [e] This quantum efficiency does not take into account the slow components of the photoresponse (Figure 5), the overall efficiency can be twice or 3 times as much. The quantum efficiency for 550 nm is ±50%. The quantum efficiencies at 420 nm and 660 nm are ±1 and 3%, respectively. These percentages are the coefficient of variation of the absorbance readings.

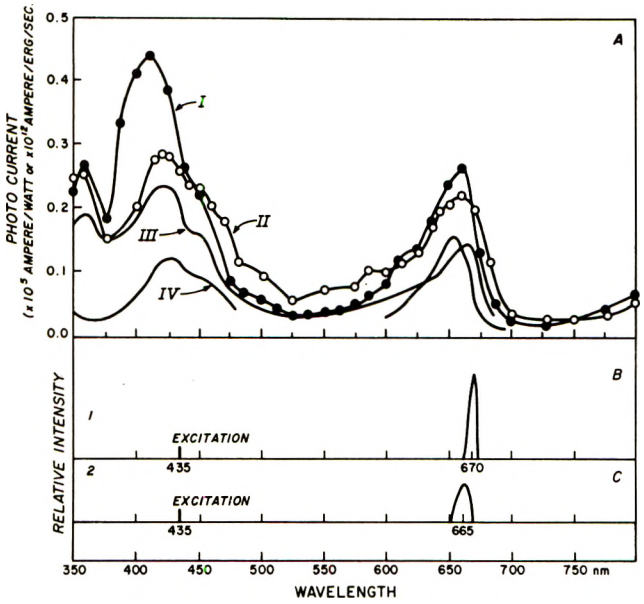

Figure 9. Photoelectric spectrum of the Chl-BLM. Curve I, uncorrected curve; curve II, curve I corrected with curve I of Figure 2, curve III, absorption curve of a 100 dilution of the stock solution in a 0.1-cm path length cell (first left-hand side scale); curve IV, $(I-T)$ curve; T, the transmittance is calculated from curve III; T, 10^{-A} where A is the absorbance.

mission, the quantum yield is very small, about 1–5 × 10^{-6} A/W, rather less than 0.005%.

The quantum yield for absorbed light can only be calculated if the absorption of the BLM is known. Since the BLM is extremely thin (100 Å) and absorbs very little light, no known spectrophotometer is sensitive enough to measure its absorption spectrum. If it could be assumed that the concentration of chlorophyll in the BLM is the same as the concentration in the BLM-forming solution (lower limit), it is possible to calculate the absorbance for a 100 Å layer of this solution.

Table II gives the details of the quantum efficiency calculation for a Chl-BLM. The efficiency of blue and red light is not very different (2.4 and 2.6%, respectively), but the efficiency of green light is unusually high (7.5%). However, this last figure is given with much uncertainty (±50%) since the absorbance of the solution measured at this wavelength is less than 0.003.

For comparison, the quantum yields of a silicon cell and of a thermopile are also calculated (Table III and IV). The quantum yield is about 30% for the silicon cell in most of the range. The quantum yield for the thermopile is about 5%. These two figures are in very

Table III: Quantum Efficiency of a Silicon (Solar) Cell

Wavelength, nm	Radiant Power incident on solar cell, erg/sec	Photocurrent, A × 10^6	Photocurrent per erg, A/erg/sec × 10^6	$e/h\nu$, A/erg/sec	Quantum efficiency,[a] %
420	3927	4.93	1.255	3.36	37.35
550	5668	6.64	1.171	4.40	26.61
660	3972	1.35	0.3223	5.29	24.95

[a] For incident light. For the solar cell, no light is transmitted and reflection loss is small with antireflection coating.

Table IV: Quantum Efficiency of a Thermopile

Wavelength, nm	Radiant power incident on thermopile,[a] erg/sec	Photocurrent,[b] A × 10^8	Photocurrent per erg, A/erg/sec × 10^8	$e/h\nu$[c]	Quantum efficiency,[d] %
420	2200	0.47	0.213	3.36	6.35
550	3178	0.68	0.213	4.40	4.86
660	225	0.475	0.213	5.29	4.03

[a] Calculated from calibration data and readjusted to area illuminated. [b] Calculated from calibration data $i = V/R$, R = 11.5 ohms. [c] The spectral response photocurrent/radiant power is flat. [d] For incident radiation.

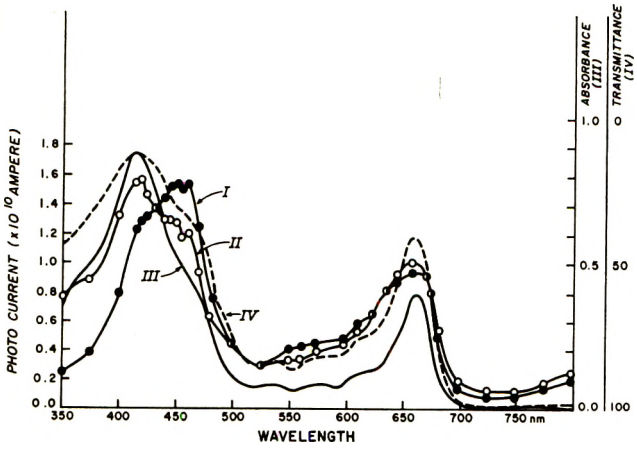

Figure 10. Modification of photoelectric spectra by chemical agents. Curve I, quinhydrone ($10^{-3}M$) in the dark side of BLM; curve II, DPN (0.01%); curve III, TPN (0.01%); curve IV, ferricyanide (10^{-3} M).

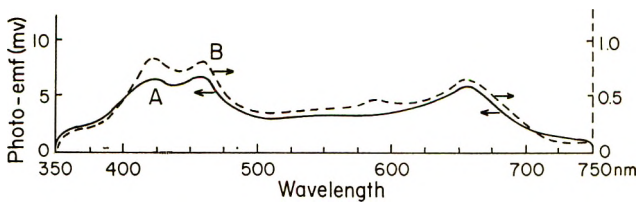

Figure 11. Variation of spectrum with light intensity. Curve A refers to 100% output of the monochromator, curve B to 6% of the output (neutral filter).

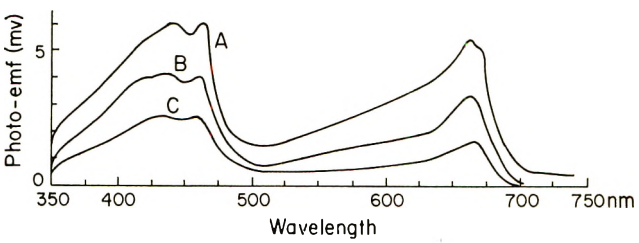

Figure 12. Variation of the spectrum with applied voltage. Curves A, B, and C refer to applied electric field of 100, 75, and 40 mV, respectively.

good agreement with published data. This also shows that the figures for the Chl–BLM are reliable if the assumption regarding the concentration is granted.

Photoelectric Spectrum. Figure 10 shows a photoelectric spectrum. Curve I is the uncorrected spectrum; curve II is curve I corrected with the calibration curve (curve I, Figure 2). Curve 3 is the absorption curve of the BLM-forming solution and curve IV is the (I–T) curve (*i.e.*, the transmittance curve plotted upside down). The resemblance between II and IV is striking, and would remove any doubt that the photoelectric effect is not due to the photosynthetic pigments.

The resolution of the photoelectric spectrum is as good as the resolution of an absorption spectrum obtained with a good spectrophotometer. Not only the two peaks at 420 and 660 nm correspond but also the shoulders at 450, 620 nm are clearly visible.

For some spectra, although the wavelengths for the maximum remain the same, the relative height of the peaks changes considerably (curve IV, Figure 10) and the photoelectric spectrum only remotely resembles the (I–T) spectrum. This may be due to fluorescence. Light absorbed at 375–475 nm region is reemitted as red light (fluorescence spectra of Figure 9B). When this happens, fewer electrons are produced in the blue and more are released in the red since most of the fluorescent light would be absorbed in the red, then reconverted into electrons similar to the incident light. A careful study of the photoelectric spectrum and the (I–T) spectrum would allow one to calculate directly the amount of fluorescent light absorbed by the sample. This important piece of information can not be obtainable by classical spectrofluorimetry.

Variation of Spectra with Light Intensity and Applied Field. Figures 11 and 12 show, respectively, some continuous spectra obtained with different light intensities and applied fields. It is evident that the shape of the spectrum is not altered appreciably with light intensity but noticeably with the electric field. However, the magnitude of the light response is not proportional to the light intensity but is almost linear to the applied field. This is in good agreement with the study with white light.

Conclusion

This investigation demonstrates conclusively that a simple black lipid membrane formed from chloroplast extract in an aqueous environment behaves like a photovoltaic cell in several respects. The most unique feature of this membrane is that it is capable of converting light energy into electronic energy with high efficiency. Since the electronic reaction is the most rapid of all reactions, it seems very probable that the generation of charge carriers and their subsequent separation are the first reactions in photosynthesis. Whether the photolysis of water is also accomplished in this Chl–BLM is uncertain at the present time, although there are some evidences that H^+ is formed during the illumination.

The method termed "BLM photoelectrometry" developed in the course of this investigation is not only relevant for understanding photosynthesis but is of general utility. The only requirements for a compound to be studied by this method are: (i) it should be soluble in a BLM-forming solution, and (ii) it should be capable of absorbing incident radiation. Such simple requirements are met by a vast number of compounds. In our preliminary experiments we have examined two other pigments. These were all-*trans* retinal and phthalocyanine. The BLM-forming solution used in both cases was oxidized cholesterol in *n*-octane. These

compounds exhibited photoelectric effects similar to the Chl–BLM.

It should be mentioned that although our present investigation has been limited to the use of visible light in the electromagnetic spectrum, the BLM photoelectrometry can be easily extended to other regions as well with proper equipment. The use of readily available commercial instruments is anticipated.

Acknowledgment. This work was supported by a National Institutes of Health grant (GM-14971).

Aggregation of Alkylammonium Tetrahaloferrates in Benzene

by A. S. Kertes, O. Levy, and G. Markovits

Department of Inorganic Chemistry, The Hebrew University, Jerusalem, Israel *(Received December 17, 1969)*

Osmometric, vapor pressure lowering measurements on 0.005–0.1 *M* benzene solutions of trilaurylammonium tetrahaloferrates, $(C_{12}H_{25})_3NHFeCl_4$ (TLAHFeCl$_4$) and $(C_{12}H_{25})_3NHFeBr_4$ (TLAHFeBr$_4$), and tetraheptylammonium halides, $(C_7H_{15})_4NCl$ (TeHpACl) and $(C_7H_{15})_4NBr$ (TeHpABr), and tetrahaloferrates, $(C_7H_{15})_4NFeCl_4$(TeHpFeCl$_4$) and $(C_7H_{15})_4NFeBr_4$ (TeHpAFeBr$_4$), indicate that the deviation of these solutions from an ideal behavior is due to a dipole–dipole-type molecular association leading to the formation of oligomers as high as the 24-mer. The deviation has also been interpreted in terms of changes in the activity coefficients of the solutes *via* the Gibbs–Duhem relationship. The theory of the osmometric technique has been modified and extended to show that a nonlinear relationship of osmometric calibration curves is an intrinsic property of the method.

Reporting recently on the nonideal behavior of solutions of tridodecylammonium salts in nonpolar solvents,[1] we have shown that both the extent (number) and the degree (size) of molecular association of these solutes is markedly affected by the anionic part of the ion pairs. Such an effect, observed in the past by Kraus and coworkers[2] in systems containing short-chain (five carbon atoms per chain, or less), lead to the generalization that for salts having a small and a large ion, the association number reaches very high values. Since this dipole–dipole aggregation is also affected by the amine class from which the salts are derived,[3] it occurred to us that an extension of the earlier work to include both large anions and different amine classes may be desirable before further generalizations on the behavior of these and similar electrolytes in nonpolar solvents could be justified. We have prepared[4] salts of tetrachloro- and tetrabromoferric acid (having a radius of the anion about 2.65 Å[5]) of tridodecylamine (trilaurylamine, TLA) and tetraheptylammonium (TeHpA) hydroxide and measured the vapor pressure lowering of their benzenic solutions. For comparison, we have also studied the behavior of the corresponding simple alkylammonium halides, not investigated previously.[1]

In this report, as in the previous one,[1] the osmometric data are analyzed in two ways: (i) in terms of nonspecific nonideality in the system expressed through the activity coefficients of the solutes *via* the Gibbs–Duhem relationship, and (ii) in terms of specific nonideality, assuming that the observed nonideality is entirely due to association of the solutes into molecular aggregates, oligomers, of different size in a mass action law equilibrium with each other.

Experimental Section

Materials. The preparation and purification of tri-*n*-dodecylammonium and tetra-*n*-heptylammonium chlorides, bromides, and tetrahaloferrates has been described previously, along with some of their physical properties.[4] Benzene was an anhydrous AR purity Mallinckrodt product.

Osmometry. The equipment and the procedure for measurements in the solute concentration range 0.005–0.1 *M* were earlier reported.[1] Due to the properties of the matched thermistors, reproducibility of readings is frequently poor (>1%) at concentrations below the lower limit, whereas the upper limit is dictated by one or both of the following factors. The rate of heat exchange through the vapor phase[6] becomes slow above

(1) A. S. Kertes and G. Markovits, *J. Phys. Chem.*, **72**, 4202 (1968).

(2) C. A. Kraus, *ibid.*, **60**, 129 (1956), and references therein.

(3) Y. Marcus and A. S. Kertes, "Ion Exchange and Solvent Extraction of Metal Complexes," Wiley-Interscience, New York, N. Y., 1969, Chapter 10.

(4) O. Levy and A. S. Kertes, *J. Inorg. Nucl. Chem.*, **31**, 888 (1969).

(5) A. S. Kertes, H. Gutmann, O. Levy, and G. Markovits, *Israel J. Chem.*, **6**, 421 (1968).

0.1 M, due mainly to the formation of a liquid film at the drop surface[7] attributed to the surface-active properties of the solutes under consideration, and the possibility of some heat loss due to the high temperature differences between the solution drop and its environment.

If reproducibility of experimental readings is satisfactory, the accuracy of molecular weights and/or activities determination will depend primarily on the calibration curves obtained by the calibration standards. Theoretically, using benzene solutions of nonassociated calibration standards such as triphenylmethane, triphenylamine, benzil, and biphenyl, resistance change is a linear function of the mole fraction of the solutes. It has been pointed out, however, that a slight deviation from ideal behavior has been observed, especially at higher solute concentrations. While the deviation may still be due to a small but finite lack of ideality of the calibrating solutes, we have now analyzed the theory of the method which may explain the lack of an ideally linear dependence of resistance changes with solute concentration, except perhaps in the dilute region.

In a way similar to the van't Hoff–Planck limiting law for freezing point depression,[8] the temperature difference, ΔT, between the pure solvent and a given solution of molar concentration c, is given[9] by the simplified expression

$$\Delta T = \frac{RT^2}{\Delta H_v}\left[\frac{Mc}{1000\varphi} - (1/2 + \beta)\left(\frac{Mc}{1000\varphi}\right)^2\right] \quad (1)$$

where β is a constant expressing the interaction (solute–solute or solute–solvent), M and φ the molecular weight and density of the solvent, respectively, and ΔH_v its molar heat of vaporization. Over a temperature range of a few degrees and a small resistance range, the temperature dependence of the thermistor resistance, r, of a pair of matched thermistors can be approximated[10] as

$$\Delta T = -T^2\Delta r/Br_0 \quad (2)$$

where B is the so-called thermistor material constant depending on the nature of the semiconductor, and its value is determined from the experimental polynome $\log r = -2.015 + 1727/T$, when $r_0 = 6700\ \Omega$ for the Hewlett-Packard No. 4115 thermistor after more than a year in use (for 36–38°, B is 3973°K).

Combining now eq 1 and 2 results in

$$\Delta r = \frac{Br_0R}{\Delta H_v}\left[\frac{Mc}{1000\varphi} - (1/2 + \beta)\left(\frac{Mc}{1000\varphi}\right)^2\right] \quad (3)$$

to show that a plot Δr *vs.* c should not necessarily yield a perfectly straight line, but with increasing c a decreasing slope can be expected, the initial value of the slope being defined as

$$tg\alpha = Br_0RM/1000\varphi\Delta H_v \quad (4)$$

Following the known[11] theoretical considerations and calculations concerning the heat balance, one can evaluate the maximum value of $tg\alpha$ in eq 4 which depends on a constant, termed the thermodynamic yield, η, and which at 37°, using the equipment with physical and thermal characteristics as given by the manufacturer and those of benzene as used by the authors,[11] has a value of $\eta = 0.811$, and the calculated value for $\eta tg\alpha = 489$ (on a molar basis), as compared to the observed $\eta tg\alpha = 492$ for the lowest concentration of the standards measured. It is thus apparent that the difference between the observed and calculated slope is not significant and that the change in slope with the solute concentration is an intrinsic property of the method.

For all osmometric measurements the anhydrous salts were dissolved in dry benzene. Triplicate Δr readings at equilibrium (5–20 min, depending on the temperature) show agreement to within 1% or better.

The LETAGROP ALGOL program for treatment of osmometric data developed by Sillén[12] and translated to FORTRAN by Mango,[13] used in this work (CDC-6400 computer), requires a constant slope for the input. We have now modified the program to use as input the

Table I: Values of the Coefficients a, b, c, d in Eq 5

Solute	t, °C	a	b	c	d
TLAHCl[a]	25	0.00205	0.7916	−1.945	8.46
TLAHCl[b]	37	−0.0015	1.114	−10.14	41.31
TLAHBr[b]	25	−0.0002	0.917	−6.839	36.23
TLAHBr[b]	37	0.0003	0.928	−9.522	122.01
TLAHFeCl$_4$	25	0.806	−16.14	168.09	−630.80
TLAHFeCl$_4$	37	0.840	−15.62	158.57	−576.91
TLAHFeCl$_4$	50	0.740	−17.33	201.97	−823.69
TLAHFeBr$_4$	37	0.525	−17.91	277.67	−1485.77
TeHpACl	37	0.505	−13.27	154.56	−614.5
TeHpACl	50	0.412	−14.85	232.61	−1233.17
TeHpABr	37	0.448	−14.24	199.94	−934.06
TeHpABr	50	0.418	−11.19	139.06	−602.34
TeHpAFeCl$_4$	50	0.381	−10.51	125.14	−512.32
TeHpAFeBr$_4$	50	1.060	−13.10	176.25	−812.49

[a] According to polynome ($S = a + bB + cB^2 + dB^3$). [b] From ref 1 ($S = a + bB + cB^2 + dB^3$).

(6) P. P. Brady, H. Huff, and J. W. McBain, *J. Phys. Colloid Chem.*, 55, 304 (1951).

(7) W. I. Higuchi, M. A. Schwartz, E. G. Rippie, and T. Higuchi, *J. Phys. Chem.*, 63, 996 (1959).

(8) R. Haase, "Thermodynamic der Mischphasen," Springer-Verlag, West Berlin and Heidelberg, 1956, p 364.

(9) R. V. Bonnar, M. Dimbat, and F. H. Stross, "Number Average Molecular Weight," Interscience, New York, N. Y., 1958, p 116.

(10) J. A. Becker, C. B. Green, and G. L. Pearson, *Elec. Eng. Trans.*, 65, 713 (1946); R. H. Muller and H. J. Stolten, *Anal. Chem.*, 25, 1103 (1953).

(11) C. T. Tomlinson, S. H. Chylewski, and W. Simon, *Tetrahedron*, 19, 949 (1963).

(12) L. G. Sillén, *Acta Chem. Scand.*, 18, 1085 (1964); N. Ingri and L. G. Sillén, *Ark. Kemi*, 23, 97 (1964).

(13) L. Mango, Italian Report RT (FIMA) CNEN (67) 1 (1967).

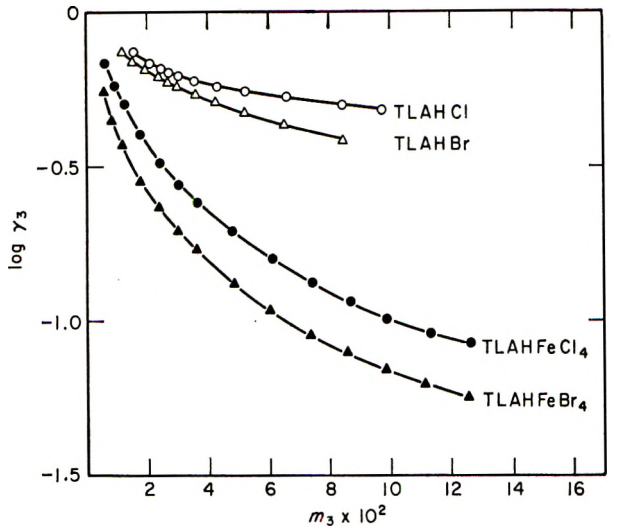

Figure 1. Activity coefficients of trilaurylammonium salts in benzene at 37°.

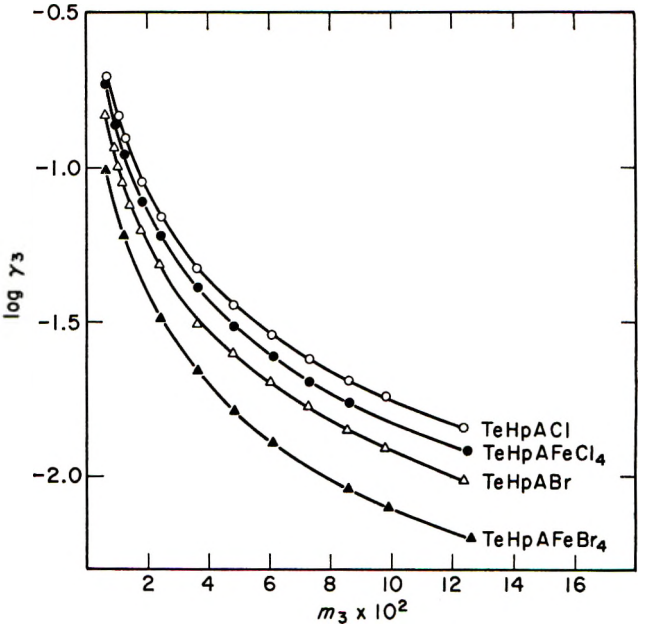

Figure 2. Activity coefficients of tetraheptylammonium salts in benzene at 50°.

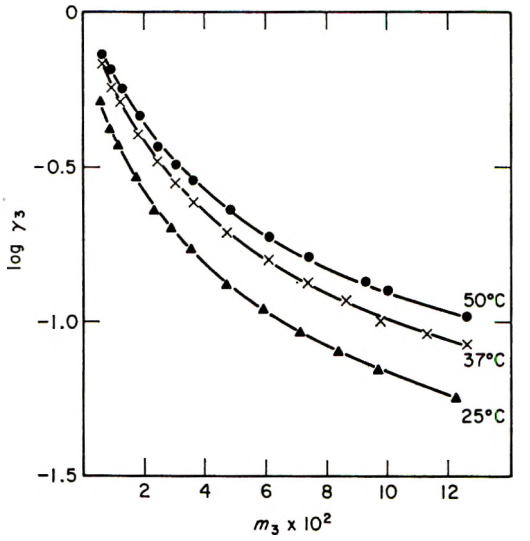

Figure 3. Activity coefficients of trilaurylammonium tetrachloroferrate in benzene at different temperatures.

osmometric concentrations calculated for each sample by means of the calibration curve, having thus $\Delta r/c = 1$.

Results

The osmometric concentrations, S, were calculated from the experimental readings of Δr *via* the calibration curves and the analytical solute concentrations, B, fitted into the polynome

$$S = aB + bB^2 + cB^3 + dB^4 \qquad (5)$$

The constants of eq 5 calculated by a nonlinear least-squares computer program are compiled in Table I for benzene as the solvent.

Activity Coefficients. Similarly to our previous treatment[1] of the experimental data *via* the Gibbs–Duhem equation (where the equations and their deductions are given in full), the activity coefficients of the solutes, (γ_3), in benzene were evaluated by a computer program. Figures 1 and 2 represent the variation of the activity coefficients with the molal solute concentration for the tertiary and quaternary ammonium salts, respectively. Figure 3 shows the effect of temperature upon the activity coefficient of trilaurylammonium tetrachloroferrate.

Molecular Association. Using again the theoretical approach described in detail earlier[1] and assuming an activity coefficient of unity for the solute aggregates formed in benzenic solution, we have evaluated by a linear least-squares program the overall stability constant, β_n of the aggregates. Over 100 models were tested, the choice having been dictated by (i) the lowest value of the error square sum, and (ii) the restriction that in the temperature range of 25–50° no change of the model is likely to take place, meaning that the same oligomers persist for a given solute regardless of the temperature changes. The aggregation models for the solutes investigated and the appropriate β values are compiled in Table II. Some thermodynamic functions were calculated[1] for systems where measurements were made at more than one temperature. Values for $\Delta H_n°$ and $\Delta S_n°$ are compiled in Table III, and Table IV shows the standard free energy change in the $TLAHFeCl_4$–benzene system, along with the β's evaluated independently by a nonlinear least-squares program. The values for log β at all three temperatures shown in Tables II and IV, calculated by two different methods, are in good agreement.

Discussion

Though the shape of the curves representing the con-

Table II: Log β_n for the Various Salts

Salt	t, °C	Model a–b–c	Log β_a	Log β_b	Log β_c
$TLAHFeCl_4$	25	2–8–22	2.14 ± 0.05	14.94 ± 0.05	44.55 ± 0.06
$TLAHFeCl_4$	37	2–8–22	1.95 ± 0.03	14.32 ± 0.01	42.06 ± 0.06
$TLAHFeCl_4$	50	2–8–22	1.81 ± 0.06	13.45 ± 0.03	39.39 ± 0.10
$TLAHFeBr_4$	37	2–8–10	2.21 ± 0.09	15.32 ± 0.27	20.04 ± 0.04
TeHpACl	37	3–18	4.96 ± 0.06	43.34 ± 0.16	
TeHpACl	50	3–18	4.74 ± 0.08	41.91 ± 0.18	
TeHpABr	37	3–18	5.25 ± 0.19	46.15 ± 0.06	
TeHpABr	50	3–18	4.99 ± 0.18	43.60 ± 0.29	
$TeHpAFeCl_4$	50	3–24	5.73 ± 0.05	63.14 ± 0.21	

Table III: The Thermodynamic Functions for $TLAHFeCl_4$, TeHpACl, and TeHpABr

System	n	$\Delta H_n°$, kcal mol^{-1}	$\Delta S_n°$, cal mol^{-1} deg^{-1}
$TLAHFeCl_4$	2	−4.4	−4.9
	8	−27.7	−23.1
	22	−100.0	−132.0
TeHpACl	3	−7.7	−1.9
	18	−50.6	+36.2
TeHpABr	3	−9.2	−5.6
	18	−90.6	−80.0

Table IV: The Standard Free Energy Changes and Formation Constants as Recalculated from the Thermodynamic Functions for $TLAHFeCl_4$

	25°		37°		50°	
n	$\Delta G°$, kcal	log β_n	$\Delta G°$, kcal	log β_n	$\Delta G°$, kcal	log β_n
2	−2.92	2.13	−2.86	2.00	−2.79	1.88
8	−20.78	15.15	−20.50	14.37	−20.19	13.59
22	−60.70	44.25	−59.08	41.43	−57.36	38.61

centration dependence of the activity coefficients does not indicate formation of micellar aggregates of constant activity, as it is usually assumed to be the case,[14] still this dependence suggests a more pronounced nonideality of the metal-bearing salts, as was expected from our earlier results.[1] In the same line, aggregation of the quaternary ammonium salts is stronger than that of the tertiary salts with the same anion and approximately the same molecular weight, at any given solute concentration in the range investigated.

Trilaurylammonium salts, regardless of the anion, associate invariably through the dimer, which is apparently the basic aggregated unit in solution in equilibrium with the monomer and higher oligomers. Dielectric constant measurements on such solutions[15] indeed suggest that these dimers have a considerable dipole moment μ_2 = 7.8 D for TLAHCl and 10.7 D for $TLAHFeCl_4$, implying a bent structure or a possible parallel position of the monomeric units in the dimer, rather than an antiparallel configuration which should lead to low or zero dipole moment of the dimer. For the dimers of the simple trilaurylammonium salts, the chloride and the bromide, the calculated[1] bond energy has a value of $\Delta H_2°$ = 3.3 kcal/mol, as compared to the value of 4.4 kcal/mol in the case of the tetrachloroferrate.

The process of aggregation of the quaternary ammonium salts is apparently more complicated as reflected by the drastic changes in the γ_3 values with increasing solute concentrations. As a consequence, the choice for a model is more difficult, and for the most aggregated system, $TeHpAFeBr_4$–benzene, no appropriate model to fit the experimental data could have been chosen. The basic unit is apparently the trimer for both simple halides and the tetrachloroferrate, with a bond energy in a linear trimer of 3.9–4.6 kcal/mol. Earlier[15] and more recent[16] evaluations of the dipole moments of these salts from dielectric constant measurements in benzene suggest that no dimers but indeed trimers are formed in solution, with a dipole moment of ~13 D for the simple halides and ~20 D for the tetrahaloferrates.

(14) K. Shinoda in "Solvent Properties of Surfactant Solutions," K. Shinoda, Ed., Marcel Dekker, New York, N. Y., 1967, p 5.

(15) A. S. Kertes, O. Levy, and G. Markovits in "Solvent Extraction Research," A. S. Kertes and Y. Marcus, Ed., Wiley-Interscience, New York, N. Y., 1969, p 177.

(16) O. Levy, Ph.D. Thesis, The Hebrew University, Jersusalem, 1969.

Temperature Dependences of Chlorine and Bromine Nuclear Quadrupole Resonances in Hexahalometallates[1]

by Theodore L. Brown* and L. G. Kent[2]

Materials Research Laboratory and Noyes Chemical Laboratory, University of Illinois, Urbana, Illinois 61801
(Received March 9, 1970)

The ^{35}Cl and ^{81}Br nuclear quadrupole resonance frequencies are reported for a number of A_2MX_6 compounds, where A = K^+, Rb^+, or Cs^+; M = W, Re, Os, Pt, Sn, Te, or Mo; for AMX_6, where M = Nb, Ta, or W; and for WX_6. The temperature dependences of the resonance frequencies are reported for the compounds over varying ranges of temperature in the interval 100–300°K. The variations in resonance frequencies with temperature at constant pressure, $(d\nu/dT)_P$, are evaluated at 300°K, and the resonance frequencies at 300°K are compared. Comparisons of the ^{35}Cl and ^{81}Br resonance frequencies for compounds of the same M and A suggest that the lattice charge distribution does not operate through a large Sternheimer antishielding term to produce a large contribution to the quadrupole coupling constant at the halogen. The systematics of the temperature dependences as a function of metal T_{2g} orbital occupancies suggest that a positive contribution to $d\nu/dT$ arises from metal-halogen π bonding. The mechanism by which the π bonding leads to a positive $d\nu/dT$ is not clear, but it is proposed that metal-halogen stretching modes rather than the bending modes may be responsible for the observed effects.

Since the beginnings of nuclear quadrupole resonance spectroscopy there has been an interest in the temperature dependences of the resonance frequencies. The Hamiltonian which describes the interaction of the nuclear quadrupole moment with the local electric field gradient is of the form[3,4]

$$H_Q = \sum_{\mu=-2}^{2} Q_\mu \nabla E_\mu \qquad (1)$$

where the Q_μ are the components of the quadrupole moment and ∇E_μ are the components of the electric field gradient, ∇E. In a crystalline solid the field gradient can be expanded in terms of displacements of the nuclei from their equilibrium positions as

$$\nabla E_\mu = A_{0\mu} + \sum_i A_{1\mu} r_i + \sum_{i,j} A_{2\mu} r_i r_j \qquad (2)$$

The first term, a constant, determines the pure nuclear quadrupole resonance energy levels in the absence of lattice motions. The higher, time-dependent terms are responsible for the temperature dependence of the resonance frequency and for quadrupolar spin-lattice relaxational effects.

Nuclear quadrupole resonance frequencies are usually observed to decrease with increasing temperature. Most studies have been carried out in the temperature range from 77°K to perhaps 350°K. The lower frequency torsional modes of vibration are generally thought to be of major importance in affecting the electric field gradient in this temperature range. Bayer[5,6] has developed a model for the simple case in which a quadrupolar nucleus is involved in torsional motion about an axis coincident with the single bond which connects the atom to another atom. The resonant nucleus is assumed to experience an axially symmetric field gradient tensor which follows the nuclear motion. The temperature dependence of the resonance frequency is described by the equation[3]

$$\nu(T) = \nu_0[1 - (3h^2/4Ik\theta_t) \coth(\theta_t/2T)] \qquad (3)$$

where ν_0 is the limiting value of the resonance frequency, I is the moment of inertia of the torsional oscillator, θ_t is the torsional frequency ω expressed as $hc\omega/k$, and T is the absolute temperature.

The halogen nqr frequencies of the metal hexahalometallates have been of considerable interest, and have provided useful data in assessing the nature of metal–halogen bonds as a function of electronic configuration at the metal, oxidation state, ionic radius, etc.[7] In addition to comparative values of the resonance frequencies among different compounds, the temperature dependences of the nqr frequencies have occasioned considerable interest. This interest has arisen in part because many of the resonance frequencies exhibit

* To whom correspondence should be addressed at Department of Chemistry and Chemical Engineering, University of Illinois, Urbana, Ill. 61801.

(1) This research was sponsored in part by the Advanced Projects Research Agency of the Department of Defense, through contract SD-131, and in part by the National Science Foundation, under grant GP 6396X.

(2) National Science Foundation cooperative Fellow, 1966–1969.

(3) K. R. Jeffrey and R. L. Armstrong, *Phys. Rev.*, 174, 359 (1969).

(4) T. P. Das and E. L. Hahn in "Solid State Physics," F. Seitz and D. Turnbull, Ed., Academic Press, New York, N. Y., 1958, Supplement 1.

(5) H. Bayer, *Z. Physik.*, 130, 227 (1951).

(6) Reference 4, page 41.

(7) M. Kubo and D. Nakamura, *Advan. Inorg. Chem. Radiochem.*, 6, 257 (1966).

positive temperature coefficients. Kubo, Nakamura, and coworkers[8] recognized a systematic trend in the temperature dependences among the heavy metal MCl_6^{2-} species, where M varies from W through Pt. A positive contribution to the temperature dependence was associated with halogen–metal π-bonding, since $(d\nu/dt)_P$ was observed to be more positive as the number of vacancies in the d_π orbital set of the metal increased. This idea has been more quantitatively developed by Haas and Marram.[9] As an additional or alternative explanation, a positive $(d\nu/dt)_P$ might be associated with an increase in q on volume expansion.[10] Most recently, O'Leary has suggested,[11] on the basis of a very thorough study of K_2ReCl_6, that a positive temperature coefficient in MCl_6^{2-} systems is due to the existence of a soft-mode phase transition at low temperature.

As part of a study of metal hexachloro and hexabromo complexes of transition metals in various oxidation states we have observed the temperature dependences of the resonances insofar as our experimental techniques permit. Our data, while considerably more extensive than any which have previously appeared, in terms of the number and variety of compounds studied and in terms of the number of temperature data taken for some of the compounds studied, are less complete than those reported for K_2PtCl_6 and K_2PdCl_6 by Jeffrey and Armstrong,[3] and for K_2ReCl_6 by O'Leary.[11] They do provide a firm basis for determining whether there is a systematic pattern to the temperature dependences in the vicinity of 300°K and for comparing temperature coefficients for chlorine and bromine compounds.

The quadrupole coupling constants for the halogens in compounds of the form A_mMX_6, $(m = 0,1...)$ have been generally interpreted in terms of covalency effects in the M–Cl bond.[7,12] In general, the halogens in these structures are not situated at a center of symmetry. There is on this account some question regarding the possible magnitude of Sternheimer antishielding effects arising from the charge distribution surrounding the halogen. The total effective quadrupole moment is very much larger than the nuclear quadrupole moment because of a large induced nuclear moment

$$Q_{\text{total}} = Q + Q_{\text{induced}} = Q(1 - \gamma_\infty) \qquad (4)$$

Since γ_∞ is very large for free ions,[13] (about 55 for Cl^- and 120 for Br^-),[14] charge distributions outside the radius of the halogen might make an important contribution to the electric field gradient at the halogen.[15] Chemists have generally ignored the Sternheimer factor in dealing with halogen bound to metals in the A_mMX_6 systems and have treated the quadrupole coupling constant in terms of metal–halogen covalency and π-bonding effects.

We have employed this approach in our work[16] and present here an argument for its validity based on comparison of chlorine and bromine resonances in equivalent compounds.

Experimental Section

The samples studied were, for the most part, sealed under vacuum in 15-mm diameter glass vials. The compounds were prepared and characterized as described elsewhere.[16]

The quadrupole resonance spectrometers employed were superregenerative oscillator-detectors, with Zeeman modulation; phase-sensitive detection (Princeton Applied Research model HR-8) was employed. Frequency determinations were made by employing a Drake Model 2-B receiver, very loosely coupled to the oscillator. The first conversion oscillator of the receiver was replaced by a stable oscillator controlled by one of a bank of crystals.[17] A broadly tuned, crystal-controlled converter was used in the input to permit reception of signals in the range 30–300 MHz. This arrangement permits measurement of frequencies to an accuracy of about 1 kHz in the range 3–30 MHz, and to about 1 kHz + 0.005% of the carrier frequency in the range 30–300 MHz. Because of difficulties with multiple side bands attendant upon use of a superregenerative system, the frequency of a resonance can often not be determined to better than about 50 kHz, although usually about 10 kHz accuracy is easily possible. In most cases, however, it is possible to follow the temperature dependences of the resonance frequencies with an accuracy of 2–3 kHz or better, since the overall appearance of the resonance multiplet changes only gradually with variation in temperature.

Signal to noise level was found, in most instances, to decrease with decrease in temperature. In many cases the temperature dependences could be studied over only a limited temperature range because of loss of signal.

Temperature variation was effected by passage of nitrogen gas, obtained from boil-off of liquid nitrogen, over the sample in a jacketed assembly.[18] By careful attention to the rate of boil-off, constant temperature to within ±1°K could be maintained for a few hours.

(8) R. Ikeda, D. Nakamura, and M. Kubo, *J. Phys. Chem.*, **69**, 2101 (1965).

(9) T. E. Haas and E. P. Marram, *J. Chem. Phys.*, **43**, 3985 (1965).

(10) T. Kushida, G. B. Benedek, and N. Bloembergen, *Phys. Rev.*, **104**, 1364 (1956).

(11) (a) G. P. O'Leary, *Phys. Rev. Lett.*, **23**, 782 (1969); (b) G. P. O'Leary and R. G. Wheeler, to be published in *Phys. Rev.*

(12) R. Bersohn and R. G. Shulman, *J. Chem. Phys.*, **45**, 2298 (1966).

(13) E. A. C. Lucken, "Nuclear Quadrupole Coupling Constants," Academic Press, New York, 1969, Chapter 5.

(14) R. M. Sternheimer, *Phys. Rev.*, **146**, 140 (1966).

(15) P. W. Smith and R. Stoessiger, *Molec. Physics*, **17**, 503 (1969).

(16) W. G. McDugle, Jr., L. G. Kent, and T. L. Brown, *J. Amer. Chem. Soc.*, **92**, 3645 (1970).

(17) L. G. Kent, Ph.D. Thesis, University of Illinois, 1969.

(18) T. L. Brown, P. A. Edwards, C. B. Harris, and J. L. Kirsch, *Inorg. Chem.*, **8**, 763 (1968).

Table I: Temperature Dependences of ^{35}Cl and ^{81}Br Nuclear Quadrupole Resonance

°K	ν(MHz)	S/N
WCl_6		
340	10.620	(12)
325	10.590	(30)
304	10.547	(28)
298	10.535	(28)
289	10.520	(10)
$CsNbCl_6$		
358	8.319	(10)
	8.644	(10)
345	8.299	(10)
	8.630	(10)
335	8.289	(15)
	8.623	(10)
326	8.277	(15)
	8.613	(15)
319	8.269	(10)
	8.608	(15)
315	8.262	(10)
	8.604	(10)
310	8.257	(5)
	8.600	(5)
305	8.251	(3)
	8.593	(5)
$CsWCl_6$		
343	11.306	(15)
	11.632	(15)
	11.788	(12)
304	11.295	(12)
	11.610	(10)
	11.751	(15)
284	11.271	(10)
	11.593	(5)
	11.736	(10)
226	11.240	(5)
	11.677	(5)
169	11.22	(5)
	11.54	(5)
123	11.20	(5)
	11.55	(5)

°K	ν(MHz)	S/N
WBr_6		
318	72.45	(500)
306	72.27	(400)
294	72.04	(250)
262	71.66	(70)
225	71.23	(50)
209	70.84	(40)
180	70.57	(20)
163	70.36	(30)
140	70.06	(30)
$CsTaCl_6$		
358	8.838	(6)
	9.144	(12)
339	8.829	(6)
	9.141	(12)
322	8.815	(5)
	9.132	(12)
312	8.810	(3)
$RbWCl_6$		
348	11.343	(5)
	11.572	(5)
305	11.323	(5)
	11.557	(10)
297	11.321	(10)
	11.546	(15)
262	11.305	(5)
	11.529	(10)
232	11.291	(5)
	11.513	(10)
$KWCl_6$		
339	11.353	(5)
	11.485	(5)
319	11.343	(5)
	11.470	(5)
306	11.338	(10)
	11.460	(5)

°K	ν(MHz)	S/N
Cs_2WCl_6		
344	10.928	(15)
304	10.911	(20)
269	10.902	(15)
254	10.897	(15)
232	10.892	(11)
211	10.882	(10)
K_2WCl_6		
348	10.245	(100)
305	10.200	(50)
284	10.182	(20)
259	10.164	(5)
227	10.15	(2)
Mo_2Cl_{10}		
305	14.085	(10)
296	14.092	(5)
286	14.108	(5)
272	14.127	(5)
259	14.148	(5)
189	14.213	(10)
176	14.228	(10)
134	14.252	(20)
117	14.262	(30)
105	14.268	(30)
Cs_2ReCl_6		
316	14.592	(10)
284	14.590	(20)
226	14.593	(20)
171	14.593	(20)
136	14.590	(20)
117	14.591	(20)

°K	ν(MHz)	S/N
Rb_2WCl_6		
367	10.609	(15)
354	10.602	(15)
335	10.594	(15)
322	10.587	(20)
307	10.580	(20)
238	10.570	(20)
259	10.545	(15)
237	10.525	(15)
205	10.518	(10)
Cs_2MoCl_6		
342	10.764	(20)
306	10.736	(25)
298	10.731	(20)
270	10.715	(20)
233	10.681	(10)
K_3MoCl_6		
343	9.536	(5)
	9.806	(5)
	9.841	(5)
305	9.540	(5)
	9.793	(5)
	9.876	(5)
293	9.543	(5)
	9.795	(5)
	9.864	(5)
262	9.546	(3)
	9.79	(5)
222	9.55	(3)
181	9.55	(5)
	9.78	(3)
146	9.56	(2)
	9.78	(3)
K_2ReCl_6		
307	13.879	(50)
287	13.874	(50)
263	13.874	(50)
238	13.871	(50)
200	13.865	(40)
160	13.863	(50)
138	13.858	(50)
120	13.853	(50)
107	13.852	(30)

°K	ν(MHz)	S/N
K_2OsCl_6		
370	16.800	(50)
348	16.807	(40)
325	16.815	(25)
312	16.820	(20)
306	16.821	(20)
281	16.825	(15)
264	16.833	(15)
247	16.841	(25)
222	16.844	(15)
209	16.847	(20)
143	16.854	(30)
110	16.860	(40)
100	16.864	(40)
Cs_2PtCl_6		
303	26.545	(10)
296	26.554	(20)
265	26.582	(5)
253	26.594	(10)
217	26.610	(5)
210	26.639	(10)
147	26.637	(15)
120	26.692	(15)
Cs_2SnBr_6		
333	109.94	(1000)
321	109.97	(600)
299	110.01	(300)
237	110.15	(300)
138	110.23	(250)
134	110.36	(250)

°K	ν(MHz)	S/N
K_2PtCl_6		
307	25.769	(80)
267	25.309	(60)
231	25.866	(50)
204	25.900	(50)
155	25.928	(65)
127	25.955	(85)
113	25.968	(120)
Cs_2PbCl_6		
362	17.673	(30)
327	17.690	(25)
304	17.701	(32)
284	17.713	(30)
257	17.736	(20)
211	17.748	(20)
167	17.770	(25)
$K_2ReBr_6(^{79}Br)$		
323	112.74	(100)
315	112.72	(100)
301	112.69	(100)
292	112.66	(100)
284	112.64	(65)
270	112.60	(40)
Cs_2SnCl_6		
305	16.055	(10)
282	16.066	(10)
253	16.076	(5)
140	16.107	(10)

°K	ν(MHz)	S/N
K_2OsBr_6		
329	111.78	(500)
318	111.78	(300)
296	111.78	(200)
282	111.77	(300)
263	111.77	(300)
253	111.76	(200)
232	111.73	(200)
222	111.73	(110)
217	111.71	(50)
Cs_2OsBr_6		
321	116.83	(50)
319	116.83	(50)
296	116.82	(50)
242	116.87	(40)
209	116.86	(40)
192	116.87	(30)
175	116.87	(30)
151	116.88	(30)
Cs_2WBr_6		
308	75.31	(90)
288	75.28	(60)
294	75.28	(60)
273	75.22	(50)
253	75.15	(40)
243	75.13	(40)
211	75.05	(30)
194	75.03	(20)
184	75.00	(15)
163	74.97	(10)

°K	ν(MHz)	S/N
Cs_2PtBr_6		
333	173.04	(10)
299	173.18	(10)
270	173.32	(10)
217	173.54	(10)
146	173.83	(10)
K_2PtBr_6		
320	167.15	(100)
295	167.27	(100)
268	167.42	(50)
240	167.52	(50)
225	167.58	(40)
192	167.68	(100)
160	167.89	(20)
Cs_2TeCl_6		
308	15.566	(10)
288	15.560	(10)
261	15.572	(5)
233	15.580	(3)
198	15.588	(2)
152	15.593	(2)
120	15.594	(2)

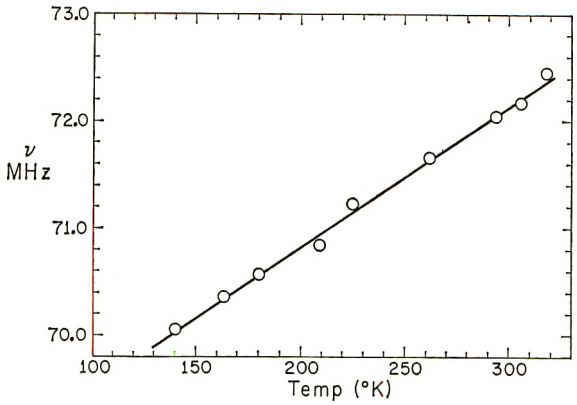

Figure 1. Temperature dependence of the ^{81}Br nqr signal in WBr_6.

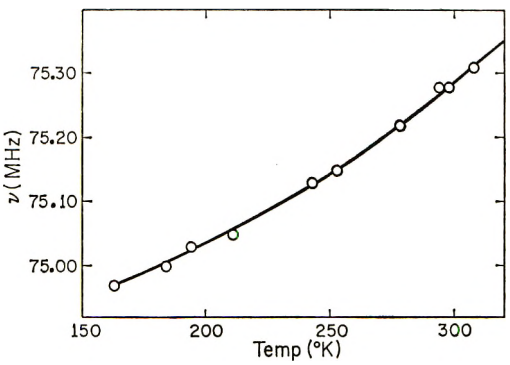

Figure 2. Temperature dependence of the ^{81}Br nqr signal in Cs_2WBr_6.

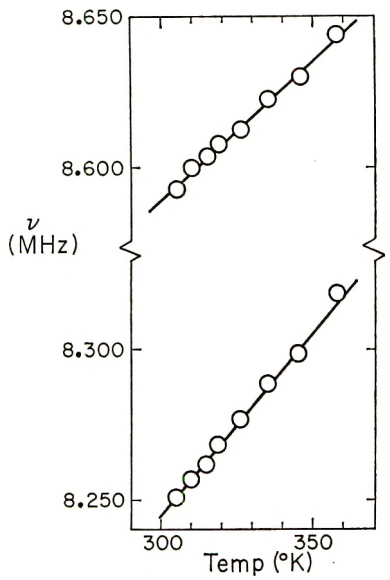

Figure 3. Temperature dependence of the ^{35}Cl nqr signal in $CsNbCl_6$.

Temperatures to about 100°K could be obtained in this manner. Temperatures higher than room temperature were obtained by passing nitrogen gas through a heater and then over the sample and coil assembly. Temperatures were measured with a copper–constantan or chromel–alumel thermocouple mounted against the sample vial. The system was allowed to equilibrate at each temperature for an extended time before measurements were taken.

Results

The nuclear quadrupole resonances obtained at various temperatures are given in Table I. Data for a few of the systems are depicted in Figures 1–3. These serve to indicate the general character of the data. For the most part the curvature in the frequency *vs.* tem-

Table II: ^{35}Cl and ^{81}Br Nuclear Quadrupole Resonance Data

Compd[a]	ν (MHz), 300°K	$\left(\frac{d\nu}{dt}\right)$ (kHz/°K), 300°K
WCl_6[b]	10.538	1.80
WBr_6	72.12	13.0
$CsNbCl_6$	8.589	0.92
	9.245	1.20
$CsTaCl_6$	9.127	0.3
	8.803	0.62
$CsWCl_6$	11.748	0.94
	11.605	0.60
	11.281	0.56
$RbWCl_6$	11.546	0.54
	11.320	0.48
$KWCl_6$	11.455	0.78
	11.335	0.46
Cs_2WCl_6	10.913	0.35
Cs_2WBr_6	75.28	3.04
K_2WCl_6[c]	10.195	0.84
Rb_2WCl_6	10.575	0.49
Cs_2ReCl_6[d]	14.592	0.00
K_2ReCl_6[e]	13.879	0.11
K_2ReBr_6[f]	94.13	2.19
K_2OsCl_6[g]	16.823	−0.27
K_2OsBr_6	111.78	0.29
Cs_2OsBr_6	116.83	−0.42
K_2PtCl_6[h]	25.774	−1.04
K_2PtBr_6[i]	167.25	−5.1
Cs_2PtCl_6[j]	26.552	−0.83
Cs_2PtBr_6[k]	173.18	−4.3
Cs_2SnCl_6	16.057	−0.43
Cs_2SnBr_6	110.01	−2.2
Cs_2MoCl_6	10.732	0.76
K_2MoCl_6	9.541	0.12
	9.795	−0.15
	9.876	
Mo_2Cl_{10}	14.085	−1.44
Cs_2TeCl_6	15.566	−0.21
Cs_2PbCl_6	17.705	−0.50

[a] The footnotes refer to prior literature on the same compound. The first item gives the resonance frequency, at 300°K unless a different temperature is indicated. The second item gives $d\nu/dt$, in kHz/°K, where sufficient data are available, at or near 300°K. Data reported for ^{79}Br resonances are scaled to ^{81}Br by dividing by 1.197. [b] 10.536; +2.00 (19). [c] 10.22 (293°); +0.44 (8). [d] 14.611 (293°); +0.06 (20). [e] 13.887 (293°); +0.13 (20). [f] 94.12 (293°); +2.34 (20). [g] 16.839 (21); −0.22 (20). [h] 25.816 (20); −1.00 (8). [i] 167.24 (22). [j] 26.60; −0.6 (22). [k] 173.07; −5.9 (22).

perature graphs is not noticable or very slight, but in a few cases there is significant nonlinearity in the graphs, *e.g.*, for K_2OsCl_6, and Cs_2WBr_6. There might, however, be one or more phase transitions in these systems, leading to slight frequency displacements, which would escape detection, with the number and accuracy of the data taken in this study.

In Table II[19-22] are listed the frequencies of all the resonances detected at 300°K, obtained from smoothed plots of frequency *vs.* temperature. The slopes of these graphs at 300°K, are also given for each resonance. Many of the data duplicate those reported in previous studies from other laboratories, and appropriate footnotes are provided. For the most part the data are in excellent agreement with those reported by the Japanese workers. The only exception of note is K_2WCl_6, for which their results were fragmentary and covered a limited temperature range.

Every compound of composition A_2MX_6 exhibited only one resonance at 300°K. By contrast, the $AMCl_6$ salts all exhibit multiple resonances, as expected from the reported powder data.[23]

Discussion

Lattice Effects. The data in Table II provide comparisons which are relevant to the question of the lattice contribution to the halogen quadrupole coupling constant. The lattice contributions to the chlorine nqr frequencies in K_2PtCl_6 and Cs_2PtCl_6 have been calculated[15] assuming that the Sternheimer antishielding factor, γ_∞, is 28. (In another, more recent calculation on K_2PtCl_6 and K_2ReCl_6 a value of 10 was chosen.[24]) The results indicate that the lattice contribution in K_2PtCl_6 is on the order of 3 MHz, and about 0.5 MHz smaller than this for Cs_2PtCl_6. Thus, assuming that the intraionic contribution to the coupling constant is the same in the two salts, the difference in lattice contributions in the two salts is of the order of magnitude of the experimentally observed difference, about 0.8 MHz at 300°K. It is not likely, however, that this approach can account for the entire body of comparative data in Table II. For example, the differences between K^+ and Cs^+ salts of the bromides, when scaled by 5.859, the ratio of $^{81}Br/^{35}Cl$ quadrupole moments, is about the same as that for the chlorides, although γ_∞ for Br^- is more than twice as large as for Cl^-.

If the lattice contribution to the quadrupole coupling constant were as large as indicated by such a calculation, the effects of changing partial covalency in the MX_6^{2-} species would be expected to affect the bromides differently than the chlorides. Furthermore, the molecular solids WCl_6 and WBr_6 should experience very much smaller lattice effects. Figure 4 shows a graph of the ^{81}Br resonance frequencies *vs.* the ^{35}Cl frequencies for all equivalent pairs listed in Table II. The dotted line in the figure passes through the origin and has a slope of 5.859, the ratio of nuclear quadrupole moments. The

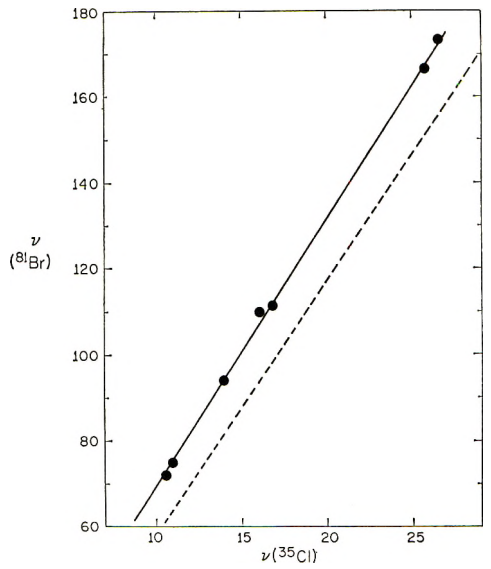

Figure 4. ^{35}Cl *vs.* ^{81}Br nqr frequencies at 300°K in WCl_6–WBr_6 and various A_2MCl_6–A_2MBr_6 pairs. The dotted line passes through the origin with slope 5.86, the ratio of ^{81}Br–^{35}Cl quadrupole moments. The compounds represented on the figure are, from left to right, WCl_6, Cs_2WC_6, K_2ReCl_6, Cs_2SnCl_6, K_2OsCl_6, K_2PtCl_6, Cs_2PtCl_6 and the corresponding bromides.

observed data fall on a line slightly displaced from this line, but of about the same slope. It is remarkable that the data all fall on this line, since they include the molecular solids WCl_6–WBr_6 and compounds of the form A_2MX_6 with widely differing coupling constants. This empirical evidence indicates, in our opinion, that the electric field gradient due to lattice charge distribution does not make a significant contribution to the halogen quadrupole coupling constant. This does not mean, however, that lattice *effects* do not contribute to the coupling constant. Interactions between cations and the halogens of the MX_6^{2-} species can be expected to affect the intraionic charge distribution to some extent. In addition, repulsive interactions between the lattice units, which determine the equilibrium lattice distance parameters, have the effect of quenching the polarizations which give rise to the large antishielding terms in the free ions.[25] Thus it is unrealistic to employ a value for γ_∞ which is characteristic of the free ion. It would appear, therefore, that the variations in quadrupole resonance frequency with cation in A_nMX_6 lattices is probably due mainly to covalency

(19) R. P. Hamlen and W. S. Koski, *J. Chem. Phys.*, **25**, 360 (1956).
(20) R. Ikeda, A. Sasane, D. Nakamura, and M. Kubo, *J. Phys. Chem.*, **70**, 2926 (1966).
(21) K. Ito, D. Nakamura, K. Ito, and M. Kubo, *Inorg. Chem.*, **2**, 690 (1963).
(22) D. Nakamura and M. Kubo, *J. Phys. Chem.*, **68**, 2986 (1964).
(23) (a) K. W. Bagnall and D. Brown, *J. Chem. Soc.*, **9**, 3021 (1964); (b) K. W. Bagnall, D. Brown, and J. G. H. DuPreez, *ibid.*, 2603 (1964).
(24) T. B. Brill, Z Z. Hugus, Jr., and A. F. Schreiner, *J. Phys. Chem.*, **74**, 469 (1970).
(25) H. W. de Wijn, *J. Chem. Phys.*, **44**, 810 (1966).

changes within the MX_6^{-n} species, with a relatively minor contribution from variations in electric field gradient generated in the lattice. This means that comparisons of parameters derived from a model for bonding in the MX_6^{n} species, *e.g.*, the Townes and Dailey model,[26,27] or a molecular orbital population analysis,[28] should be internally consistent so long as isostructural species involving a common cation are compared, *e.g.*, K_2MCl_6 or $CsMBr_6$. Comparison of species involving differing charge types, *e.g.*, K_2WCl_6, $KWCl_6$, WCl_6, must be expected to be less quantitatively significant.

Temperature Dependences. The temperature dependences of the halogen nqr frequencies, as expressed in the slopes $(d\nu/dt)_P$ at 300°K show a number of remarkable regularities. Perhaps the most notable general effect is that the slopes are most positive for the cases in which the number of vacancies in T_{2g} orbitals consisting mainly of metal 5d orbitals is largest. This is true for both the chlorides and bromides and for various charge types. The slopes for the bromides are, in general, quite similar to those for the equivalent chlorides after scaling by the ratio of resonance frequencies. In the A_2MX_6 systems, the slopes vary in a regular way with the number of 5d metal electrons, for a given halogen and cation. In Figure 5 are shown the results for the K_2MBr_6 and Cs_2MBr_6 compounds; in Figure 6, the analogous results for the chlorides. After scaling to account for the relative frequencies the chloride and bromide data are remarkably similar, even to the point of showing the same change upon variation of cation from K^+ to Cs^+.

It is not possible to say on the basis of these results that the presence or absence of a phase transition involving a soft librational mode[11] does not account for all of these results. However, the regularities observed in Figures 5 and 6, coupled with the large positive temperature coefficients observed in the molecular solids WCl_6 and WBr_6, and the $AMCl_6$ systems, place a severe burden of credibility on this model as a general explanation. The positive slopes, and regular diminution in slope with increasing $5d_\pi$ metal orbital occupancy, can be accommodated very satisfactorily by the hypothesis that the presence of chlorine–metal π bonding is responsible for a positive component in the temperature dependence. This positive contribution must be added to a negative contribution to the temperature coefficient arising from the low-frequency lattice modes as in K_2PtCl_6.[3] The notion that π bonding from halogen to metal is responsible for the positive temperature coefficient does not account in an obvious way for the fact, reported by O'Leary and Wheeler,[11] that the temperature coefficients below the 110°K phase transition in K_2ReCl_6 are all negative. On the other hand, to suggest that the positive temperature coefficients in the resonance frequencies are due to halogen–metal π bonding is not to hypothesize a mechanism for

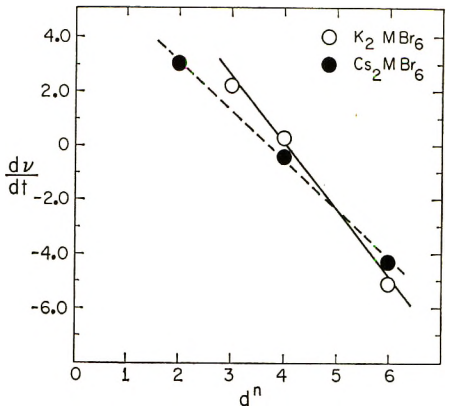

Figure 5. Temperature dependence of the ^{81}Br nqr signal, $(d\nu/dt)$ 300° *vs.* the number of electrons occupying the metal 5d (T_{2g}) orbitals in bromo complexes.

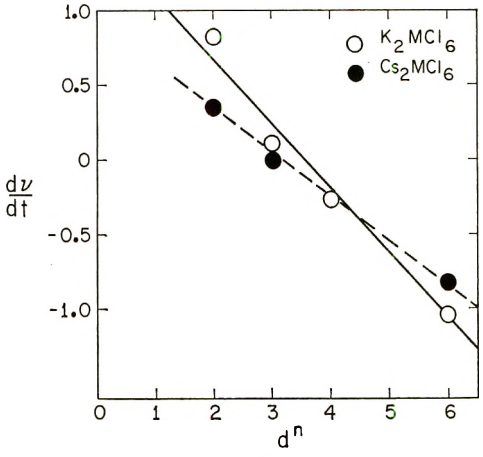

Figure 6. Temperature dependence of the ^{35}Cl nqr signal, $(d\nu/dt)$ 300° *vs.* the number of electrons occupying the metal 5d (T_{2g}) orbitals in chloro complexes.

how the existence of the π bonding operates to effect the observed results. That is, the association of the temperature coefficients with metal d orbital occupancies, and hence with the extent of halogen–metal π bonding, is an empirical generalization supported by a large body of data. There remains the question of a model which will satisfactorily account for the result.

Haas and Marram have developed a model[9] in which they purport to show that activation of metal–halogen bending modes can account for the way in which the π bonding produces the positive contributions to the temperature dependence. They argue that the overlap of a metal d_π orbital with a chlorine p_π orbital is diminished by bending, so that the π bonding, proportional to the extent of orbital overlap, is diminished. The argument is, however, erroneous insofar as it depends on the supposed variation in π overlap. In the equilib-

(26) C. H. Townes and B. P. Dailey, *J. Chem. Phys.*, **17**, 782 (1949).
(27) Reference 13, Chapter 7.
(28) F. A. Cotton and C. B. Harris, *Inorg. Chem.*, **6**, 376 (1967).

rium configuration, the metal d orbitals form t_{2g} and e_g representations within the O_h point group. The chlorine p_π orbitals mix to form ligand symmetry orbitals which interact with the t_{2g} set of metal d orbitals. In the distorted configurations formed in the bending motions, the metal d orbitals are no longer separated as in the O_h symmetry. A molecular orbital description of the bonding in the distorted form would, therefore, involve some new interaction of a given chlorine p_π orbital with metal d orbitals to which it was orthogonal in the equilibrium configuration. At the same time, overlap with the single metal d orbital with which it was previously nonorthogonal is diminished. It is evident, however, that motion of a given chlorine on the surface of a sphere about the metal cannot change the total overlap of the halogen p_π orbital with the complete set of metal d orbitals. The bending motions simply result in some mixing of the metal d orbitals in the distorted configurations. If the departure from the equilibrium octahedral symmetry is not large, however, it may be assumed that the *total* amount of π bonding from the halogens, as seen at the metal, is not changed by the bending motion. In a given symmetry mode it may happen that, because of changes in hybridization, etc., certain of the halogens will have more, and others less, π bonding in a given symmetry displacement. Since, however, the modes in question are degenerate, the effects of these changes should average to zero for a given metal–halogen bond. Nor does it matter for this argument to what extent the d_π orbitals are partially filled. Regardless of the symmetry mode of bending distortion, after rehybridization to form metal orbitals directed toward the ligands, there is always the equivalent of a full three metal d orbitals available for occupancy by the metal nonbonding electrons, and for π bonding with the halogens. Averaged over the various degenerate bending modes, therefore, the situation is really no different than in the equilibrium configuration. Thus, the bending modes are not obviously accountable for the positive temperature coefficients.

Haas and Marram ruled out the metal–halogen stretching modes as responsible for the temperature dependences. They argue that in an expansion of the electric field gradient $q(r)$, in a power series in Δr about the equilibrium distance, second-order terms in the expansion, and deviations from pure harmonic character, tend to cancel each other. For a harmonic oscillator, the expectation value for the metal–halogen distance does not change with vibrational excitation. In this connection, however, it should be noted that the expectation value for the electric field gradient operator evaluated at a nucleus involved in vibrational motion will in general not be invariant, when averaged over the vibrational motion, even for a harmonic oscillator. Secondly, and perhaps more importantly, the metal–halogen stretching modes are not harmonic oscillators. Thus it can be expected that the metal–halogen distances will increase upon vibrational excitation. Although the increase may not be large, there is ample evidence that in polar metal–halogen bonds, vibrational excitation can lead to large changes in electric field gradient at the halogen. For example, the electric field gradient at ^{35}Cl in LiCl increases by 0.4 MHz with each quantum of vibrational excitation from $v = 0$ to $v = 3$.[29] Numerous other cases of large increases and a few large decreases in coupling constant in diatomic chlorides and bromides are known.[30] This is not to say that the origin of the coupling constant increase in the MX_6^n species is due to the same changes in bonding character as in the diatomic halides. It is, however, very plausible, in light of these results, that changes in coupling constant of similar magnitude might accompany vibrational excitation in the MX_6^n systems. Since, as a result of the anharmonic character of the metal–halogen bond, there is some lengthening of the bond on vibrational excitation, the positive contribution of the π bonding to the temperature coefficient possibly arises from the effect of slight changes in metal–halogen bond distance on the relative σ and π bonding. We have shown in earlier work[16] that π bonding in MX_6^n systems is in a sense sacrificial, in that an increase in π bonding is accompanied by a decreased σ covalency, such that the total covalency is constant. Thus, if there is a greater decrease in metal–halogen orbital overlaps in the π system than in the σ system upon lengthening of the M–X bond, the relative loss in π bond order is amplified, as it were, by concomitant increase in σ covalency. Thus, the coupling constant at halogen, which depends on the difference in σ and π orbital populations, might increase markedly with vibrational excitation of stretching modes. Furthermore, the effect should increase roughly linearly with the extent of π bonding, which is in turn related to the number of metal T_{2g} orbital vacancies. The slightly greater slope of the temperature dependence with d orbital occupancy for the potassium than for the cesium salts may result from the slightly higher frequencies of the vibrational modes for salts involving the larger cation.

One can estimate the magnitude of change required in the coupling constant upon vibrational excitation which is required to produce the observed temperature dependences. Assume that an M–Cl bond possesses a fundamental stretching frequency of 300 cm^{-1}, with an effective degeneracy of one.[31] Then the rate at which vibrational quanta are added as a function of tempera-

(29) D. T. F. Marple and J. W. Trischka, *Phys. Rev.*, **103**, 597 (1956).

(30) Reference 13, Chapter 12.

(31) The vibrational frequencies for a number of MCl_6^n systems are given in ref 16. There are three vibrational stretching modes, of A_{1g}, E_g, and T_{1u} representations. The normal modes involved are clustered at about 300 cm^{-1}. Therefore, considering a single M–Cl stretch mode approximates the total contribution to a given M–Cl bond from all the normal modes involving bond stretching.

ture, on a per-molecule basis, is simply the coefficient of $Nh\nu$ in the expression for $C_v = dE_v/dt$[32]

$$\frac{dE}{dt} = (Nh\nu)\left[\frac{h\nu}{kT^2}\frac{e^{h\nu/kT}}{(e^{h\nu/kT}-1)^2}\right] \quad (5)$$

At 300°K the quantity in brackets has the value 0.00197°K^{-1}. Its value at 150°K is 0.00123°K^{-1}. If the contribution to the temperature dependence of the coupling constant from vibrational excitation is to be on the order of say +1.5 kHz/°K for a metal–chlorine system, the change in coupling constant upon unit increase in the vibrational quantum number must be on the order of $1.5 \times 10^3/2.0 \times 10^{-3} \approx 1$ MHz. While this is fairly large, it is well within the range of plausibility.

The assumption of a single effective vibrational frequency leads to the prediction of a nonlinear temperature coefficient, with increasing slope as temperature increases. This is the sort of behavior occasionally observed, *e.g.*, Figure 2. In general, however, this concave-upward behavior is not observed. Although there are other factors involved in the temperature dependence which might produce an oppositely directed effect, it seems unlikely that they would be as large as the nonlinearity predicted by eq 5. In this respect therefore, the simple model does not appear to be entirely adequate.

In what we have said we seek only to account for the *variation* in temperature dependence of the quadrupole resonance frequency with metal 5d orbital occupancy. It is not possible at this point to assess the relative importance of the stretching modes *vs.* the bending modes in contributing to the temperature dependence of the coupling constant in a salt such as K_2PtCl_6. Jeffrey and Armstrong have fitted the temperature dependence quite well with a single-term Bayer-type expression,[3] corresponding to a lattice mode of about 38 cm^{-1}. On the other hand, the internal bending modes make a significant contribution to the temperature dependence in this case.[33]

In light of Wheeler and O'Leary's work, it may be incorrect to assume that the lattice dynamics among the A_2MCl_6 species are similar, and that the lattice and internal bending mode contributions to the temperature dependences for M other than Pt can be obtained by multiplying the temperature coefficient for the Pt salt by the ratio of nqr resonance frequencies ν_M/ν_{Pt}. There is no straightforward way at present, therefore, to separate out the parts of the temperature dependences due to various mechanisms. The present work shows that, in an empirical sense, a positive contribution to the temperature dependence of the nqr frequencies can be associated with the extent of metal–halogen π bonding.

(32) W. Kauzmann, "Kinetic Theory of Gases," W. A. Benjamin, New York, N. Y., 1966, p 113.

(33) R. L. Armstrong, G. L. Baker, and K. R. Jeffrey, *Phys. Rev.*, B1,2847 (1970).

Nuclear Magnetic Resonance Studies of Hindered Internal Rotation in Higher *N,N*-Dialkylamides and -thionamides[1]

by T. H. Siddall, III, W. E. Stewart, and F. D. Knight

Savannah River Laboratory, E. I. du Pont de Nemours & Company, Aiken, South Carolina 29801
(Received June 1, 1970)

Barrier heights are reported for rotation around the C(X)–N bond of fifteen amides and thionamides of the type $RC(X)N(R')_2$ where R = H or CH_3 and R′ = methyl, ethyl, isopropyl, or isobutyl. The barriers were determined by signal shape analysis using the principle of superimposition of coalescing doublets.

Introduction

Numerous measurements of the barriers to rotation around the C(X)–N (amide) bond in *N,N*-dimethylamides and -thionamides have been made in recent years. The various approximate methods of analysis in the earlier measurements have been replaced by more sophisticated methods, such as total signal shape analysis[2-6] and the spin–echo method.[7,8] As a result, accurate and reproducible barrier height measurements have recently been reported for a variety of *N,N*-dimethylamides and -thionamides. These results have shown that the barriers are consistently higher in thionamides than in the corresponding amides,[9-11] and that the barrier heights depend strongly upon the steric and electronic characteristics of the substituent attached to the carbonyl carbon.[4,12]

Only a few approximate measurements have been reported for *N,N*-dialkylamides in which the *N*-alkyl substituent is larger than the methyl substituent.[13-16] In these amides, the spin–echo method cannot be used unless the alkyl substituents are partially deuterated and the signal shape analysis method becomes much more difficult because of the signal multiplicities. The purpose of the present paper is to report the results of barrier measurements of twelve higher amides and thionamides.

Experimental Section

The amides which were not commercially available were prepared and purified as described previously.[17] The thionamides were prepared by treating the corresponding amide in boiling xylene with a 100% excess of P_2S_5.[18] The thionamides were purified by vacuum distillation or by fractional crystallization in methylcyclohexane or both.

Samples were prepared by dissolving 100 mg of amide in 500 μl of dry o-dichlorobenzene, purging with nitrogen, and then sealing in nmr tubes under nitrogen. All spectra were obtained with a Varian A-60 spectrometer equipped with the variable temperature accessory. Temperatures were measured with methanol and ethylene glycol "thermometers" at the lower temperatures. At the higher temperatures, the ethylene glycol appeared to undergo partial decomposition or polymerization which led to high temperature readings. Consequently, the higher temperatures were determined with a copper–constantan thermocouple inserted into an open tube of ethylene glycol. All normal precautions to avoid signal saturation were taken.

o-Dichlorobenzene was chosen as the solvent because of its high boiling point, comparatively low viscosity and freezing point, and good solvent characteristics. In particular, a high-boiling solvent was necessary in order to reach the temperature range of intermediate exchange for the thionformamides.

(1) The information contained in this article was developed during the course of work under Contract AT(07-2)-1 with the U. S. Atomic Energy Commission.

(2) (a) A. Allerhand, H. S. Gutowsky, J. Jonas, and R. A. Meinzer, *J. Amer. Chem. Soc.*, **88**, 3185 (1966); (b) R. C. Neuman, Jr., W. R. Woolfenden, and V. Jonas, *J. Phys. Chem.*, **73**, 3177 (1969).

(3) A. Pines and M. Rabinovitz, *Tetrahedron Lett.*, 3529 (1968).

(4) R. C. Neuman, Jr., and V. Jonas, *J. Amer. Chem. Soc.*, **90**, 1970 (1968).

(5) H. S. Gutowsky, J. Jonas, and T. H. Siddall, III, *ibid.*, **89**, 4300 (1967).

(6) R. C. Neuman, Jr., D. N. Roark, and V. Jonas, *ibid.*, **89**, 3412 (1967).

(7) A. Allerhand and H. S. Gutowsky, *J. Chem. Phys.*, **41**, 2115 (1964).

(8) K. H. Abramson, P. T. Inglefield, E. Krakower, and L. W. Reeves, *Can. J. Chem.*, **44**, 1685 (1966).

(9) Reference 6 and references therein.

(10) G. Schwenker and H. Rosswag, *Tetrahedron Lett.*, 4237 (1967).

(11) J. Sandström, *J. Phys. Chem.*, **71**, 2318 (1967).

(12) L. L. Graham and R. E. Diel, *ibid.*, **73**, 2696 (1969).

(13) R. M. Hammaker and B. A. Gugler, *J. Mol. Spectrosc.*, **17**, 356 (1965).

(14) A. G. Whittaker and S. Siegel, *J. Chem. Phys.*, **43**, 1575 (1965).

(15) C. E. Holloway and M. H. Gitlitz, *Can. J. Chem.*, **45**, 2659 (1967).

(16) A. Loewenstein, A. Melera, P. Rigny, and W. Walter, *J. Phys. Chem.*, **68**, 1597 (1964).

(17) T. H. Siddall, III, and W. E. Stewart, *J. Chem. Phys.*, **48**, 2928 (1968).

(18) R. B. Wagner and H. D. Zook, "Synthetic Organic Chemistry," John Wiley & Sons, New York, N. Y., 1953.

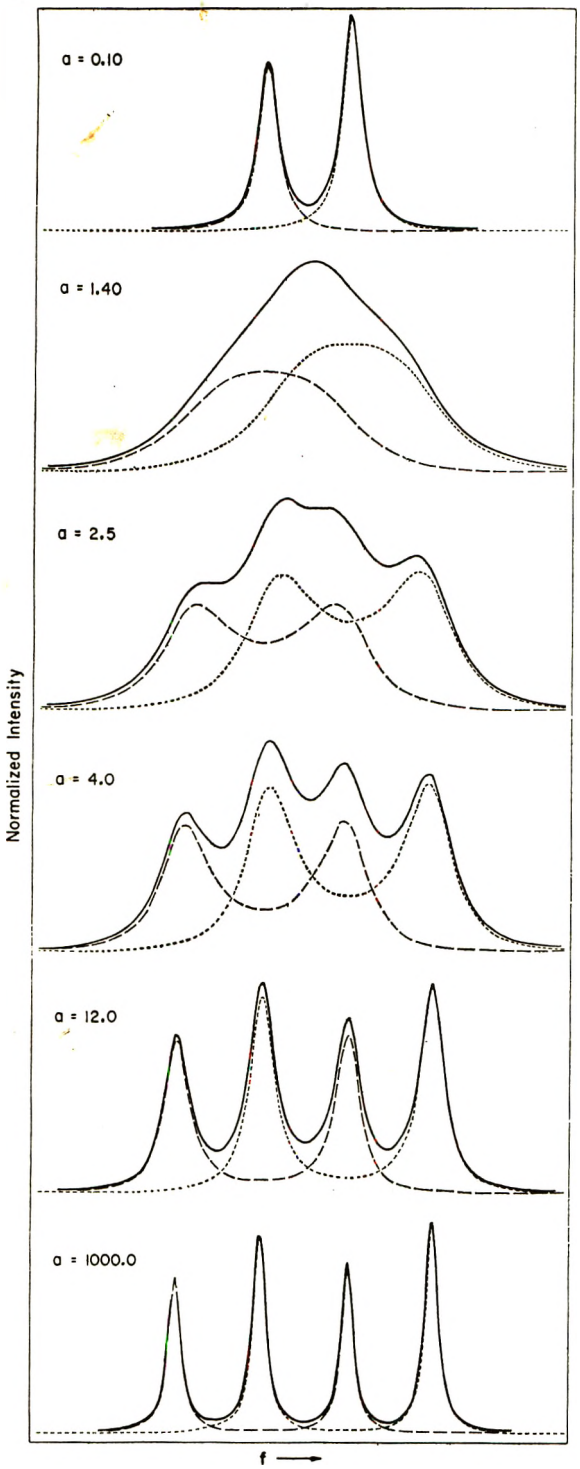

Figure 1. Computer simulation of coalescence of cis and trans doublets of α protons of N,N-diisobutylformamide.

Signal Shape Analysis

The signal shape curves for the coalescing multiplets were computed by the method of superimposition of coalescing doublets. In cis and trans multiplets, the low-field components of each multiplet arise from those molecules in which the protons coupled to the proton being observed have the maximum I_z, *i.e.*, $I_z = I$ where I is the total spin of the coupled protons. The other components can be similarly paired, *i.e.*, the second lowest components arise from adjacent protons with $I_z = I - 1$, etc. If the lifetimes of the spin states are long compared to the transition time for rotation, the multiplet coalescence can thus be treated as a superimposition of coalescing doublets, as shown in Figure 1. (Similar procedures have already been reported.[19] Details of our computer program are available on request.)

The signal shapes of the coalescing doublets were generated by Nakagawa's formulation [20] of the equation for exchange of two uncoupled groups.[21]

$$v = Cx[\{(1 + ar_A/2 + ar_B/2)K + a(f - {}^1/_2)L\}/(K^2 + L^2)]$$

where v describes the transverse component of the resultant magnetic moment and is proportional to the absorption intensity and

$$K = {}^1/_2(r_A + r_B) + a\{r_Ar_B - f(f - 1)\}$$

$$L = f(1 + ar_A + ar_B) - (ar_A + {}^1/_2)$$

$$C = -\gamma H_1 Mo/2\pi|\nu_A - \nu_B|$$

$$a = 2\pi\tau|\nu_A - \nu_B|$$

$$r_A = {}^1/_2\pi T_{2A}|\nu_A - \nu_B| = w_A/|\nu_A - \nu_B|$$

$$r_B = {}^1/_2\pi T_{2B}|\nu_A - \nu_B| = w_B/|\nu_A - \nu_B|$$

$$f = (\nu - \nu_A)/(\nu B - \nu_A)$$

$$w_A = \text{(half-width of A component)}/2$$

The quantities $|\nu_A - \nu_B|$, w_A, and w_B are measured over as wide a temperature range as possible below the onset of exchange broadening and extrapolated to the temperature of measurement. The lowest frequency signal shape is generated for given values of r_A, r_B, $|\nu_A - \nu_B|$, and a and is the base shape. The frequency positions of the other components are calculated for increments of J, the coupling coefficient, where $J = J_{HH}/|\nu_A - \nu_B|$ (J_{HH} is the spacing between the components of the multiplets). The lowest frequency component is assigned unit intensity, and the intensities of the other components are fixed by the relative intensities obtained from the experimental spectra. Superimposed spectra are then calculated for a series of a values and compared to the experimental spectra to obtain a value for τ from which $\Delta F^*(T)$ is calculated

$$\Delta F^*(T) = 2.303RT \log \frac{2\tau kT}{h}$$

where the transmission coefficient is assumed to be unity.

(19) R. Munday and I. O. Sutherland, *J. Chem. Soc., B*, 80 (1968).
(20) T. Nakagawa, *Bull. Chem. Soc. Jap.*, **39**, 1006 (1966).
(21) M. T. Rogers and J. C. Woodbrey, *J. Phys. Chem.*, **66**, 540 (1962).

Results and Discussion

The observed rotational barriers are given in Table I, and in Table II the results of some previous measurements are tabulated. The use of the free energy of activation, rather than the Arrhenius energy of activation, as a measure of the barrier heights may be questioned. However, values of the energy of activation, E_a, for a given amide measured in different laboratories usually show very wide variations because of unavoidable systematic errors. (The problems associated with E_a measurements have been discussed.[2a]) On the other hand, ΔF^* measurements do not have the limitations of E_a measurements, and the values obtained by different laboratories usually agree remarkably well. Furthermore, changes in ΔF^* more accurately measure the internal changes produced by structural variations, such as these being reported here.[22]

Table I: Barriers to Rotation Around the Amide Bond in $RC(X)N(R')_2$

R	R′	Signals studied	ΔF^*(T), kcal/mol X = O	ΔF^*(T), kcal/mol X = S	Δ[a]
H	Methyl			24.1 (160)	
H	Ethyl	α	20.9 (116)	24.5 (172)	3.6
H	2-Propyl	α	20.6 (120)		4.0
		α	20.6 (140)		
		β	20.7 (105)	24.6 (154)	
H	Isobutyl	α	21.0 (114)		3.5
		α	20.9 (119)		
		γ	21.0 (100)	24.6 (171)	
Me	Methyl		18.5 (45)	21.8 (136)	3.3
Me	Ethyl	α	17.7 (57)	20.6 (124)	2.9
		β	17.8 (40)	20.7 (111)	2.9
Me	2-Propyl	α	16.2 (49)	19.2 (114)	3.0
		β	16.3 (40)		
Me	Isobutyl	α	17.6 (60)	20.3 (111)	2.7

[a] $\Delta = \Delta F^*(X = S) - \Delta F^*(X = O)$.

Table II: Previously Reported Values for Barriers to Rotation in Various Amides $RCON(R')_2$ and Thionamides

R	R′	Solvent	Method[a]	ΔF^*(T), kcal/mol	Reference
		Amides			
H	Me	Neat	S.S.	20.9 (119)	3
H	Me	0.04 mol fraction $CHCl_2CHCl_2$	A.S.S.	20.9 (115)	29
Me	Me	Neat	S.S.	18.1 (75)	4
Me	Me	In $CD_3S(O)CD_3$	S.S.	18.3 (75)	4
H	Et	Neat	A.S.S.	20.4 (100)	13
Me	Et	Neat	A.S.S.	16.9 (25)	13
Me	2-Pr	Neat	A.S.S.	15.7 (25)	13
		Thionamides			
H	Me	40% o-$C_6H_4Cl_2$	A.S.S.	24.1 (160)	16
H	2-Pr	40% o-$C_6H_4Cl_2$	A.S.S.	24.6 (161)	16
Me	Me	In o-$C_6H_4Cl_2$	A.S.S.	21.6 (141)	11

[a] S.S. = Complete signal shape analysis. A.S.S. = Approximate signal shape analysis.

The most accurate ΔF^* values are those obtained just below the coalescence temperature;[2a] however, the wide range of the coalescence temperatures of different amides and thionamides precludes comparison at one temperature. Fortunately for the comparison, however, recent accurate measurements have shown that the entropy of activation for rotation around the C–N bond is very small,[3-5,23-28] and thus the error introduced by comparisons at different temperatures will also be very small.

In the present work, ΔF^* was measured where possible just below the coalescence temperature, but the high coalescence temperatures of the thionformamides made it necessary to measure ΔF^* at the beginning of coalescence. Therefore, the thionformamide values are probably less accurate than the others.

In several cases, the coalescences of two different groups of signals were used to obtain ΔF^*; in all cases, the values obtained agreed within experimental error even though the two groups of signals coalesced at different temperatures. In a few cases, measurements were obtained for a single group of signals at two temperatures, and over the maximum temperature range (20°) studied, good agreement was obtained. We were unable to obtain ΔF^* for *N*,*N*-dimethylformamide because of accidental degeneracy of the *N*-methyl resonances in *o*-dichlorobenzene.

The barriers in the formamides and thionformamides showed no appreciable changes as the size of the *N*-substituent was varied. The barriers are about 3.6 kcal/mol higher in the thionamides (taking $\Delta F^* = 20.9$ for *N*,*N*-dimethylformamide[3]) which agrees with previous comparisons of amides and thionamides.

In the acetamide series, replacement of methyl by ethyl decreases the barrier from 18.5 to 17.7 kcal/mol; isopropyl substitution causes a further decrease to 16.2 kcal/mol; and isobutyl substitution increases the barrier to 17.6 kcal/mol. In the thionacetamides, the ethyl, 2-propyl, and isobutyl groups decrease the barrier by slightly larger amounts than in the corresponding amides.

The barrier heights in amides depend upon electronic and steric effects. Any effect which increases the delocalization of the nitrogen lone-pair electrons into the

(22) See, for instance, A. Streitwieser, Jr., "Molecular Orbital Theory for Organic Chemists," Wiley, New York, N. Y., 1961, p 311.

(23) J. A. Weil, A. Blum, A. H. Heiss, and J. K. Kinnaird, *J. Chem. Phys.*, **46**, 3132 (1967).

(24) A. Mannschreck, A. Mattheus, and G. Rissmann, *J. Mol. Spectrosc.*, **23**, 15 (1967).

(25) J. C. Chupp and J. F. Olin, *J. Org. Chem.*, **32**, 2297 (1967).

(26) P. Hampson and A. Mathias, *Mol. Phys.*, **11**, 541 (1966).

(27) P. Hampson and A. Mathias, *J. Chem. Soc., B*, 673 (1968).

(28) D. Herbison-Evans and R. E. Richards, *Mol. Phys.*, **8**, 19 (1964).

amide bond should increase the barrier. However, when bulky *N*-alkyl groups are present, especially when the carbonyl substituent is larger than hydrogen, considerable steric repulsion between the alkyl groups is present, the energy of the ground state is increased, and the activation energy should decrease.

The results of this study enable us to test the prediction that the amide barrier will increase as the size of the *N*-alkyl substituent is increased.[26] This prediction was made on the basis of ^{14}N chemical shift studies of a variety of primary, secondary, and tertiary alkylamides, in which it was found that *N*-substituents larger than methyl caused large downfield ^{14}N shifts.[26-28] Downfield shifts in amides are believed to indicate increased delocalization of the nitrogen lone-pair electrons, and thus an N-substituent which causes a downfield shift might be expected to increase the amide barrier. The causes of the downfield shifts with increased size are not understood, but the effect is presumably electronic in origin.

Our results show that the predicted trend is not observed. In the formamides and thionformamides, the barrier heights do not change as the size of the *N*-substituent is increased; in the acetamides and thionacetamides, the barriers *decrease* as the size of the *N*-substituent is increased. It is further seen that the Δ value is smaller between acetamides and thionacetamides (average Δ = 3.0 kcal/mol) than between the formamides and thionformamides (average Δ = 3.6 kcal/mol). Thus, if electron delocalization is increased by increasing the size of the *N*-alkyl substituent, the steric effect is equal and opposite in the formamides and thionformamides, and dominant in the acetamides and thionacetamides.

Our results can be explained by assuming that there is substantially more delocalization in thionamides than in amides, but that variations within the amides as a class on the one hand and variations within thionamides as a class on the other are entirely due to steric effects. The smaller value of Δ for acetamides and thionacetamides is consistent with this viewpoint. The larger sulfur atom makes substitution of the methyl group for the formyl proton even more effective in reducing barriers than is the case with the smaller oxygen atom in amides.

(29) B. Sunners, L. H. Piette, and W. G. Schneider, *Can. J. Chem.*, **38**, 681 (1960).

Effect of Phase on the Radiolysis of Solid Isobutane as Studied by Electron Spin Resonance Spectroscopy and Product Analysis

by Terunobu Wakayama, Tetsuo Miyazaki,* Kenji Fueki, and Zen-ichiro Kuri

Department of Synthetic Chemistry, Faculty of Engineering, Nagoya University, Chikusa-ku, Nagoya, Japan
(Received February 12, 1970)

The effect of phase on the radiolysis of solid isobutane at 77°K has been studied by esr spectroscopy and product analysis. Though only the isobutyl radical is formed in the polycrystalline state by γ irradiation of pure isobutane or of isobutane containing a small amount of 3-methylpentane or methylcyclohexane (MCH), the tertiary butyl radical is mainly formed in the glassy state. Since the isobutyl radical does not isomerize to the *tert*-butyl radical on standing at 77°K for 40 hr in an *i*-C_4H_{10}–MCH (4 mol/100 mol of *i*-C_4H_{10}) matrix and it does not isomerize by warming the γ-irradiated sample above 77°K, it has been concluded that the *tert*-butyl radical is formed in the glass as a primary product and not through thermal isomerization at 77°K. The phase effect has not been observed on the decomposition of the excited isobutyl radical formed by illumination of the isobutyl radical with uv light at 77°K. The phase effect on the formation of butyl radicals is discussed from the viewpoints of cage effect and/or efficiency of energy transfer. It has also been found that the yields of CH_4 and C_3H_6 in the radiolysis of solid isobutane at 77°K are much higher in the polycrystalline state than in the glassy state.

Introduction

Since product analysis and the observation of reaction intermediates reveal different aspects of mechanisms of radiolysis, we have studied the reaction of nitrous oxide with electrons in organic glass,[1] the radiolysis of phenyl acetate,[2] and the radiolysis of isobutane[3] at 77°K using both methods.

It was found in previous studies that while the fragmentation of excited ions plays an important role in the radiolysis of isobutane in the gas[4] and liquid[5] phases, the fragmentation of excited molecules is an important process in the solid state at 77°K.[3] We reported in a previous communication[6] that quite different radicals are formed in the radiolysis of solid isobutane at 77°K depending on whether it is in the glassy or crystalline state. Although the isobutyl radical is formed in the crystalline state, the *tert*-C_4H_9 radical is the main radical produced by radiolysis in the glassy state. Since such a phase effect has not been reported previously in the radiolysis of solid hydrocarbons, although it was observed for the case of alkyl halides,[7] we have studied in more detail the effect of phase on the radiolysis of solid isobutane by esr spectroscopy and product analysis.

Experimental Section

Isobutane, 3-methylpentane (3MP), methylcyclohexane (MCH), and isopentane (*i*-P) were more than 99.9% pure. Gas chromatographic analysis did not show any detectable impurity. They were purified by distillation on a vacuum line and dried over a sodium mirror. Nitrous oxide was of high purity and was used without further purification.

Pure isobutane forms a polycrystalline solid at 77°K. When a sample of isobutane containing a small amount of 3MP, MCH, or *i*-P is plunged into liquid nitrogen, it forms a clear glass. The sample is annealed by immersing it in liquid nitrogen and then warming it up to a higher temperature than 77°K. When this procedure is repeated several times, the material becomes polycrystalline.

The samples were irradiated with γ rays from ^{60}Co at a dose rate of 4.2×10^5 rads/hr. The illumination was carried out at 77°K with uv light from a medium-pressure mercury lamp.

Esr measurements were made on a JES-3BX ESR spectrometer. Gaseous products not condensable at liquid nitrogen temperature were analyzed by a gas buret connected to a Toepler pump and a cupric oxide furnace kept at 240°. Hydrocarbon products were analyzed by a gas buret connected to a Toepler pump and a cupric oxide furnace kept at 240°. Hydrocarbon products were analyzed by a Hitachi K53 gas chromatograph equipped with a flame ionization detector (activated alumina column, 2 m, 100°).

The G value is expressed here by the number of product molecules per 100 eV absorbed in isobutane.

* To whom correspondence should be addressed.

(1) T. Wakayama, T. Kimura, T. Miyazaki, K. Fueki, and Z. Kuri, *Bull. Chem. Soc. Jap.*, **42**, 266 (1969).

(2) Y. Noro, M. Ochiai, T. Miyazaki, A. Torikai, K. Fueki, and Z. Kuri, *J. Phys. Chem.*, **74**, 63 (1970).

(3) T. Wakayama, T. Kimura, T. Miyazaki, K. Fueki, and Z. Kuri, *Bull. Chem. Soc. Jap.*, **43**, 1017 (1970).

(4) T. Miyazaki, *J. Phys. Chem.*, **71**, 4282 (1967).

(5) K. Tanno, S. Shida, and T. Miyazaki, *ibid.*, **72**, 3496 (1968).

(6) T. Miyazaki, T. Wakayama, K. Fueki, and Z. Kuri, *Bull. Chem. Soc. Jap.*, **42**, 2086 (1969).

(7) H. W. Fenrick, S. V. Filseth, A. L. Hanson, and J. E. Willard, *J. Amer. Chem. Soc.*, **85**, 3731 (1963).

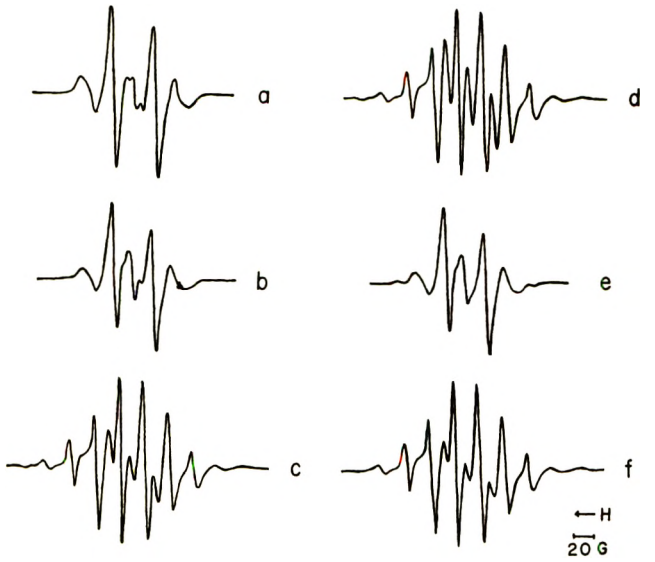

Figure 1. (a) Esr spectrum of γ-irradiated i-C_4H_{10} at 77°K; (b) esr spectrum of γ-irradiated i-C_4H_{10}–3MP (8.7 mol/100 mol of i-C_4H_{10}) system in the polycrystalline state at 77°K; (c) esr spectrum of γ-irradiated i-C_4H_{10}–3MP(8.7 mol/100 mol of i-C_4H_{10}) system in the glassy state at 77°K; (d) esr spectrum of γ-irradiated i-C_4H_{10}–MCH (4 mol/100 mol of i-C_4H_{10}) system in the glassy state at 77°K; (e) esr spectrum of γ-irradiated i-C_4H_{10}–MCH (4 mol/100 mol of i-C_4H_{10}) system in the polycrystalline state at 77°K; (f) esr spectrum of γ-irradiated i-C_4H_{10}–i-P (14 mol/100 mol of i-C_4H_{10}) system in the glassy state at 77°K. Irradiation dose: 1.4×10^5 rads. Spectrometer gain settings of figures a–f are approximately the same.

Results and Discussion

Effect of Phase on Solvent Radical Formation in the Radiolysis of Solid Isobutane. The esr spectrum of γ-irradiated pure isobutane, which is polycrystalline at 77°K, is shown in Figure 1a. The spectrum can be assigned to isobutyl radical.[8] When isobutane containing a small amount of 3MP or MCH is γ-irradiated in the polycrystalline state, the spectra shown in Figures 1b and e are obtained; they are the same as the spectrum obtained in the radiolysis of pure isobutane at 77°K. Quite different esr spectra, however, are obtained by γ-irradiation of the mixtures in the glassy state (Figures 1c, d, and f). The spectra consist of ten equally spaced lines with a coupling constant of 22.3 G, which is consistent with the reported value of 22.5 G for the *tert*-C_4H_9 radical.[9] The spectrum coincides with that of *tert*-C_4H_9 radicals produced by dissociative electron attachment to *tert*-C_4H_9Br in the radiolysis of 3-methylpentane containing 5 mol % *tert*-C_4H_9Br at 77°K.

It was concluded in a previous study[3] that the solvent radicals in the radiolysis of solid isobutane are formed by the fragmentation of excited molecules produced directly by γ irradiation. This conclusion is based on the following observations. Firstly, the yields of solvent radicals are not changed by the presence of conventional electron scavengers, such as phenyl iodide, ethyl iodide, nitrous oxide, and sulfur hexafluoride. Secondly, the yields of solvent radicals do not increase upon the photobleaching of toluene anions in the γ-irradiated isobutane–toluene (5 mol %) system. Thirdly, the yields decrease upon the addition of excitation quenchers, such as CCl_4 or toluene.

Therefore, the phase effect on the formation of solvent radicals may be depicted as

$$i\text{-}C_4H_{10} \rightsquigarrow i\text{-}C_4H_9 + H \text{ (crystal)} \quad (1)$$

$$i\text{-}C_4H_{10} \rightsquigarrow tert\text{-}C_4H_9 + H \text{ (glass)} \quad (2)$$

The phase effect can be discussed from the following two viewpoints: (i) whether the phase change affects the secondary reaction of butyl radicals, which are produced by γ irradiation; and (ii) whether the phase change affects the primary process such as fragmentation of excited molecules in the radiolysis of solid isobutane.

Effect of Phase on Final Products in the Radiolysis of Solid Isobutane. Products from the radiolysis of isobutane at 77°K are mainly hydrogen, methane, propane, and propylene. The effect of phase on their yields is shown in Table I. It is notable that the yields of methane and propylene in the radiolysis of crystalline isobutane are higher than those in the glassy isobutane—MCH (or 3MP) system. Similar phase effect on the products was also observed in the radiolysis of methanol[10] and phenyl acetate[2] in the solid state. Since methyl and propyl radical are not observed by esr in the radiolysis of solid isobutane, methane and propylene are probably produced by nonradical processes. As was discussed in the previous report,[3] the possibility that propylene is produced directly from the fragmentation of excited isobutane ions will be small in the solid state. Propylene may be produced by the fragmentation of excited molecules.

$$i\text{-}C_4H_{10} \rightsquigarrow C_4H_{10}^* \quad (3)$$

$$C_4H_{10}^* \longrightarrow CH_4 + C_3H_6 \quad (4)$$

It seems that reaction 4 occurs more easily in the crystalline state than in the glassy state.

The fact that the yield of hydrogen in the glass is higher than that in the crystal is partly because hydrogen can also be produced from MCH and 3MP in the radiolysis of mixtures. It is interesting that the yields of hydrogen, which are not affected by the addition of N_2O in the solid state and correspond to the yields from the nonionic process, are much higher than those in the radiolysis of i-C_4H_{10}–SF_6 (5 mol/100 mol of i-C_4H_{10}) system in the liquid state.

(8) J. Lin and F. Williams, *J. Phys. Chem.*, **72**, 3707 (1968).

(9) P. B. Ayscough and C. Thomson, *Trans. Faraday Soc.*, **58**, 1477 (1962).

(10) S. B. Milliken and R. H. Johnsen, *J. Phys. Chem.*, **71**, 2116 (1967).

Table I: Effect of Phase on the Radiolysis of Isobutane[a]

Experimental conditions			G Values			
	Phase	Temp, °K	H_2	CH_4	C_3H_8	C_6H_6
i-C_4H_{10}	Crystal	77	3.89	1.23	0.30	0.89
	Crystal	77	3.79	1.23	0.29	0.86
i-C_4H_{10}–N_2O(3[b])	Crystal	77	3.61	[c]	0.31	0.77
	Crystal	77	3.56	[c]	0.30	0.72
i-C_4H_{10}–MCH(10[b])	Glass	77	4.60	1.09	0.32	0.58
	Glass	77	4.60	1.01	0.32	0.49
i-C_4H_{10}–MCH(10[b])–N_2O(3[b])	Glass	77	4.56	[d]	0.31	0.34
	Glass	77	4.77	[d]	0.31	0.41
i-C_4H_{10}–3MP(14[b])	Glass	77	4.52	1.09	0.37	0.71
	Glass	77	4.51	1.02	0.35	0.63
i-C_4H_{10}[e]	Liquid	293	4.16	1.98	0.68	1.62
i-C_4H_{10}–SF_6(5[b])[e]	Liquid	293	2.08	1.90	1.41	0.82

[a] Irradiation dose: 4.3×10^6 rads. [b] Unit, mol/100 mol of i-C_4H_{10}. [c] The sum of $G(N_2)$ and $G(CH_4)$ is about 1.68. [d] The sum of $G(N_2)$ and $G(CH_4)$ is about 2.80. [e] Reference 5.

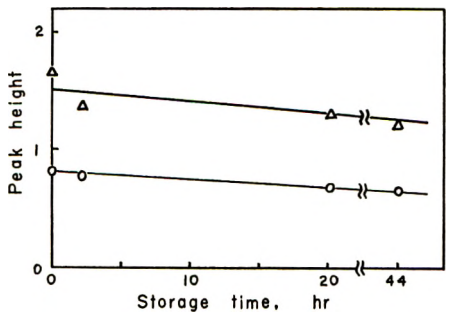

Figure 2. Effect of storage time on the amounts of butyl radicals produced in γ-irradiated i-C_4H_{10}–MCH (4 mol/100 mol of i-C_4H_{10}) system in the glassy state at 77°K. Irradiation dose: 1.4×10^5 rads; Δ—Δ, $tert$-C_4H_9 radical; O—O, i-C_4H_9 radical.

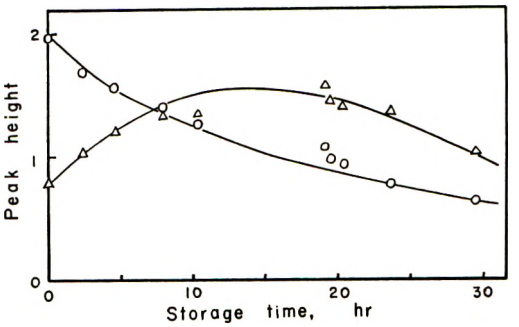

Figure 3. Effect of storage time on the amounts of butyl radicals produced in γ-irradiated i-C_4H_{10}–MCH (4 mol/100 mol of i-C_4H_{10})–i-C_4H_9Cl (1 mol/100 mol of i-C_4H_{10}) system in the glassy state at 77°K. Irradiation dose: 1.4×10^5 rads; Δ—Δ, $tert$-C_4H_9 radical; O—O, i-C_4H_9 radical.

Possibility of Thermal Isomerization of the Isobutyl Radical to the Tertiary Butyl Radical. Ayscough and Evans[11] reported previously that i-C_4H_9 radicals produced in γ-irradiated alkyl halides isomerize on standing at 77°K to $tert$-C_4H_9 radicals. When the i-C_4H_{10}–MCH (4 mol/100 mol of l-C_4H_{10}) system is γ-irradiated in the glassy state, the isobutyl radical is produced in addition to the $tert$-C_4H_9 radical as shown in Figure 1d. When the γ-irradiated sample was stored in the dark at 77°K for about 40 hr, the isomerization of isobutyl radicals could not be observed at all (Figure 2). When the isobutyl radical was produced from dissociative electron attachment to i-C_4H_9Cl in the γ-irradiated i-C_4H_{10}–MCH (4 mol/100 mol of i-C_4H_{10})–i-C_4H_9Cl (1 mol/100 mol of i-C_4H_{10}) system, the isomerization could be observed (Figure 3). Therefore, the isomerization of isobutyl radicals cannot be ascribed to the physical state of the system (the glassy state), but to the phenomenon characteristic of alkyl halides.

When the i-C_4H_{10}–MCH (4 mol/100 mol of i-C_4H_{10}) system is γ-irradiated in the crystalline state, the i-C_4H_9 radical is the main radical observed. Warming the γ-irradiated sample from 77°K to a temperature slightly below the melting point (113°K) and cooling it again to 77°K does not cause the isomerization of i-C_4H_9 radicals to $tert$-C_4H_9 radicals, but only the decrease in the amount of i-C_4H_9 radicals.

Decomposition of the Excited Isobutyl Radical. When the γ-irradiated pure isobutane was illuminated with uv light at 77°K, it was found that the illumination causes the transformation of radicals. The esr spectrum of isobutyl radicals changes by the uv illumination into a complex spectrum, which represents the formation of new radicals (Figure 4). The new spectrum consists of four peaks and the peak-to-peak separations are 19, 14, and 20 G; the values are approximately consistent with

(11) P. B. Ayscough and H. E. Evans, *J. Phys. Chem.*, **68**, 3066 (1964).

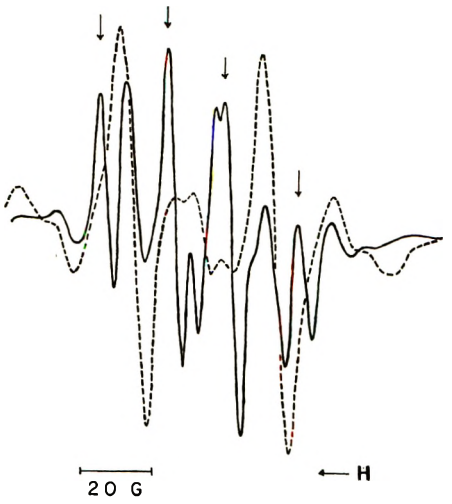

Figure 4. Change in esr spectrum upon uv illumination of γ-irradiated i-C_4H_{10} at 77°K. Irradiation dose: 1.4×10^5 rads: ———, before uv illumination; ———, after uv illumination for 4 hr. The arrows indicate the signals of new radicals.

the values of 18, 14, and 18 G for the allenyl radical (C_3H_3).[12] The new spectrum coincides with the spectrum of allenyl radicals produced by uv illumination of allyl chloride at 77°K. The effect of illumination time on the esr spectra is shown in Figure 5. The i-C_4H_9 radical decreases in intensity with increasing illumination time, while allenyl radical increases complementally. The yields of fragment products, such as H_2, CH_4, and C_3H_6, also increase with increasing illumination time (Figures 6 and 7). The uv illumination of the isobutane at 77°K without γ irradiation did not produce any products and radicals. Therefore, the effect of uv illumination may be interpreted in terms of the decomposition of excited isobutyl radicals produced by the absorption of uv light.

$$i\text{-}C_4H_9 \xrightarrow{uv} C_4H_9^* \quad (5)$$

$$C_4H_9^* \longrightarrow CH_4 + C_3H_5 \quad (6)$$

$$\searrow H_2 + C_4H_7 \quad (7)$$

$$C_3H_5 \xrightarrow{uv} C_3H_5^* \quad (8)$$

$$C_3H_5^* + i\text{-}C_4H_{10} \longrightarrow C_3H_6 + C_4H_9 \quad (9)$$

$$C_3H_5^* \longrightarrow H_2 + C_3H_3 \quad (10)$$

$$C_4H_7 \xrightarrow{uv} C_4H_7^* \quad (11)$$

$$C_4H_7^* + i\text{-}C_4H_{10} \longrightarrow C_4H_8 + C_4H_9 \quad (12)$$

$$C_4H_7^* \longrightarrow CH_4 + C_3H_3 \quad (13)$$

where $C_4H_9^*$, $C_3H_5^*$, and $C_4H_7^*$ are excited radicals. The yields of hydrogen by uv illumination of γ-irradiated isobutane for 30 hr become four times as large as those without uv illumination (Figure 6). This is because i-C_4H_9 radicals, which are produced in reactions 9 and 12, decompose again by reactions 5, 6, and 7. Allylic radicals, such as C_3H_5 and C_4H_7, could not be observed by esr spectroscopy upon uv illumination (Figure 4). This may be because allylic radicals absorb uv light and disappear by way of reactions 8–13.

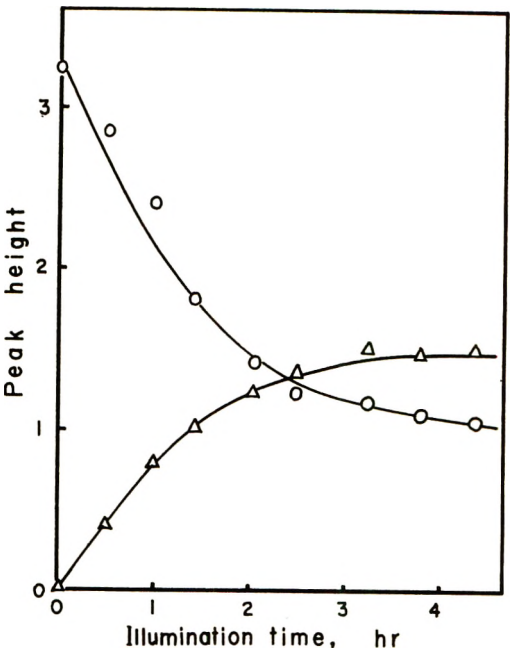

Figure 5. Effect of uv illumination time on the esr spectra of γ-irradiated i-C_4H_{10} at 77°K. Irradiation dose: 1.4×10^5 rads: O—O, isobutyl radical; Δ—Δ, allenyl radical.

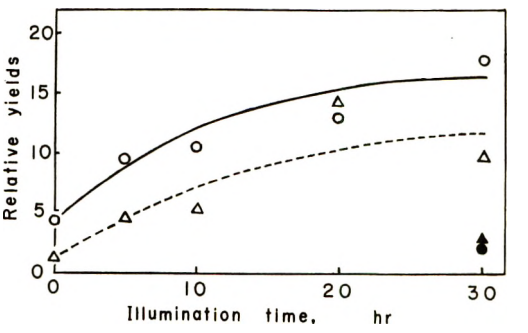

Figure 6. Effect of uv illumination time on the yields of H_2 and CH_4 from γ-irradiated i-C_4H_{10}. Irradiation dose: 1.4×10^6 rads: O—O, H_2 from γ-irradiated i-C_4H_{10}; Δ---Δ, CH_4 from γ-irradiated i-C_4H_{10}; ●, H_2 from i-C_4H_{10} without γ-irradiation; ▲, CH_4 from i-C_4H_{10} without γ-irradiation.

When the γ-irradiated glassy sample of i-C_4H_{10}–MCH (4 mol/100 mol of i-C_4H_{10}) is illuminated with uv light, the t-C_4H_9 radical is converted to the i-C_4H_9 radical, as reported by Iwasaki and Toriyama.[13] The i-C_4H_9 radical is further converted by continuing illumination to the radical which is the same as that produced by the uv illumination of γ-irradiated isobutane in the crystalline state.

(12) D. H. Volman, K. A. Maas, and J. Wolstenholme, *J. Amer. Chem. Soc.*, **87**, 3041 (1965).

(13) M. Iwasaki and K. Toriyama, *J. Chem. Phys.*, **46**, 2852 (1967).

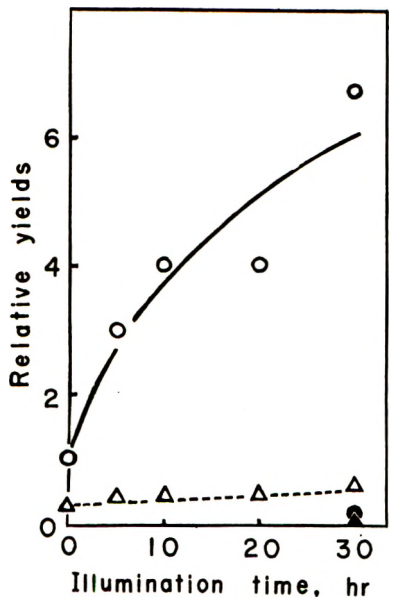

Figure 7. Effect of uv illumination time on the yields of C_3H_6 and C_3H_8 from the γ-irradiated i-C_4H_{10}. Irradiation dose: 1.4×10^6 rads: O—O, C_3H_6 from γ-irradiated i-C_4H_{10}; Δ---Δ, C_3H_8 from γ-irradiated i-C_4H_{10}; ●, C_3H_6 from i-C_4H_{10} without γ irradiation; ▲, C_3H_8 from i-C_4H_{10} without γ irradiation.

Therefore, we cannot attribute the phase effect in the radiolysis of solid isobutane to reactions 14, 15, and 16 for the following reasons.

$$i\text{-}C_4H_{10} \rightsquigarrow C_4H_9^* + H \quad (14)$$

$$C_4H_9^* \xrightarrow[\text{crystal}]{} i\text{-}C_4H_9,\ CH_4,\ C_3H_6,\ C_3H_3 \quad (15)$$

$$C_4H_9^* \xrightarrow{\text{glass}} tert\text{-}C_4H_9 \quad (16)$$

Firstly, there was no difference in the decomposition of excited butyl radicals in the glassy state from that in the crystalline state. Secondly, the allenyl radicals were not observed in the radiolysis of isobutane in the crystalline state, and these radicals would have been formed in the decomposition of excited butyl radicals if reactions 14, 15, and 16 were responsible for the allenyl radicals.

Cause of Phase Effect. It can be concluded from the present results that the formation of different types of butyl radicals in the glass and in the crystal is not ascribed to the secondary reaction of butyl radicals. Then, the phase change may affect the primary process of the formation of butyl radical. As was discussed in the previous reports,[3,14] the C_4H_9 radical may be formed in the radiolysis of solid isobutane by the following mechanism

$$C_4H_{10} \rightsquigarrow C_4H_{10}^* \quad (17)$$

$$C_4H_{10}^* \longrightarrow C_4H_9 + H \quad (18)$$

$$H + C_4H_{10} \longrightarrow C_4H_9 + H_2 \quad (19)$$

where H atoms produced in reaction 18 represent hot atoms. It will be discussed below how the phase change affects the reactions 18 and 19.

One of plausible explanations is given by the cage effect, which is discussed by Willard,[15] in the radiolysis of solid hydrocarbons. Since the C–C bond of *tert*-C_4H_9 radical is formed by sp^2-hybrid orbitals, three methyl groups construct a planar structure. Therefore, the structural rearrangement of the C–C bonds would be necessary for the formation of *tert*-C_4H_9 radical from the isobutane molecule, while such a change would not be unnecessary for the formation of i-C_4H_9 radical. In the radiolysis of isobutane in the polycrystalline state, the formation of *tert*-C_4H_9 radical accompanied by the structural rearrangement of the C–C bonds may be suppressed in the rigid crystal and only the primary C–H bond, which is stronger than the tertiary C–H bond, is ruptured. The effect of rigidity of the matrix was also observed in the abstraction of hydrogen atoms by hot hydrogen atoms produced from the photolysis of HI in the isobutane matrix by a mercury lamp.[16] The hot H atom abstracts mainly the primary hydrogen atom from isobutane in the polycrystalline state at 77°K, while it abstracts mainly the tertiary hydrogen atom in the glassy state.

Another attractive explanation about the phase effect is given by the difference between the efficiency of energy transfer in the glass and that in the polycrystal. It was suggested in the previous report[14] that excitation transfer in the radiolysis of isobutane in the glass is more efficient than that in the polycrystal, if it does occur at all. In other words, the excitation energy may spread over many more molecules in the glass and the fragmentation of the isobutane molecule may become more mild in the glass than in the polycrystal. In fact, the C–H bond rupture in the glass depends mainly upon the strength of C–H bonds and the tertiary C–H bond is ruptured favorably, while the C–H bond rupture in the polycrystal is not affected by the bond strength. If the excitation energy of $C_4H_{10}^*$ (*cf.* reaction 18) in the polycrystal is higher than that in the glass, it may be expected that the energy of hot hydrogen atoms in the polycrystal is higher than that in the glass. It was found that the H-abstraction reaction by hot hydrogen atoms depends upon the energy of hot hydrogen atoms.[16] The hot hydrogen atom, which is produced by the illumination of HI by the light of 2537 Å and has an energy of 20 or 41 kcal/mol depending on the electronic state of the iodine atom produced,[17] abstracts the primary hydrogen atom from polycrystalline isobutane

(14) T. Miyazaki, T. Yamada, T. Wakayama, K. Fueki, and Z. Kuri, *J. Phys. Chem.*, submitted for publication.

(15) J. E. Willard, "Fundamental Process in Radiation Chemistry," P. Ausloos, Ed., Interscience, New York, N. Y., 1968, p 599.

(16) T. Wakayama, T. Miyazaki, K. Fueki, and Z. Kuri, unpublished results.

(17) S. Aditya and J. E. Willard, *J. Amer. Chem. Soc.*, **88**, 229 (1966).

at 77°K. The hot hydrogen atom, which is produced by the dissociative electron attachment to HI and may have an energy about 5–6 kcal/mol, however, abstracts the tertiary hydrogen atom from isobutane in the polycrystal. The result that the yields of CH_4 and C_3H_6 in the radiolysis of crystalline isobutane are higher than those of glassy isobutane is also explained by taking into account the difference between the efficiency of energy transfer in the glass and that in the polycrystal, if it is assumed that the excitation energy of C_4H_{10}* (*cf.* reaction 4) in the polycrystal is higher than that in the glass.

The Oxidation of Thioglycolic Acid by Molybdenum(V) and Molybdenum(VI)

by J. F. Martin[1] and J. T. Spence*

Chemistry Department, Utah State University, Logan, Utah 84321 *(Received May 22, 1970)*

The oxidation of thioglycolic acid (TGA) by Mo^{V} and Mo^{VI} in phosphate buffer in the pH range 4.60–7.50 has been investigated. The reaction of Mo^{VI} with TGA proceeds in two steps, the Mo^{VI} first being reduced to a dimeric Mo^{V}–TGA complex and then to a stable Mo^{IV} species of unknown structure. In both steps TGA is oxidized to dithiodiglycolic acid (DTDGA). At pH 6.00, Mo^{VI} forms a complex with TGA in which the ratio of Mo^{VI} to TGA is 1:2. The oxidation at pH 6.00 proceeds *via* this complex and its rate was found to be second order, first order in complex and first order in TGA. From pH 4.60–5.50, the rate of reaction is independent of pH but decreases rapidly as the pH is raised above 5.50. At pH 7.50, the reaction is third order, second order in TGA and first order in Mo^{VI}. At pH 6.00, Mo^{V} forms a strong dimeric complex with TGA in which the ratio of Mo^{V} to TGA is 1:2. The Mo^{V} complex was obtained as a solid and its formula determined to be $Na_4[Mo^{V}_2O_3(TGA)_4]$. This complex reacts further with excess TGA to produce an Mo^{IV} species. The reaction of the Mo^{V} complex with TGA was found to be third order, second order in Mo^{V} complex and first order in TGA. It was also found to be essentially pH independent over the range 4.60–7.50. At pH 7.50, no spectral evidence for complex formation between Mo^{VI} and TGA was found, but Mo^{V} appears to form a weak complex. Rate constants and activation parameters have been obtained for both reactions and mechanisms have been postulated. Implications for Mo-containing enzymes have been discussed.

It is now reasonably well established that molybdenum is involved in the electron transfer process of a number of redox enzymes.[2-4] Various recent studies,[5,6] using different experimental approaches, have indicated that molybdenum is most probably bound to a thiol group (cysteine) at the active site of the enzyme, and that it alternates between +5 and +6 oxidation states during the catalytic process, although lower oxidation states cannot be completely excluded.[7] It is well known that thiols are readily oxidized to the corresponding disulfide compounds, and reactions between thiols and Mo^{VI} compounds are therefore of interest as possible models for such redox processes in the enzymes. The oxidation of a simple thiol ligand, thioglycolic acid (mercaptoacetic acid), by both Mo^{VI} and Mo^{V} species in solution has been investigated in detail and the results are reported here. A previous paper dealt with similar oxidations of cysteine and glutathione.[8]

Numerous studies of the oxidation of thiols involving metal ions have been made,[9-11] but no investigations

* To whom correspondence should be addressed.

(1) Abstracted from the Ph.D. Dissertation of J. F. Martin, Utah State University, 1969.

(2) R. C. Bray, P. F. Knowles, and L. S. Meriwether, "Magnetic Resonance in Biological Systems," A. Ehrenberg, B. G. Malmstrom, and T. Vanngard, Ed., Pergamon Press, Oxford, England, 1967, p 249.

(3) A. Nason, "The Enzymes," Vol. 7, P. D. Boyer, H. Lardy, and K. Myrback, Ed., Academic Press, New York, N. Y., 1963, p 587.

(4) K. B. Taylor, *J. Biol. Chem.*, **244**, 171 (1969)

(5) M. P. Coughlan, K. V. Rajagopalan, and P. Handler, *J. Biol. Chem.*, **244**, 2658 (1969).

(6) L. S. Meriwether, W. F. Marzluff, and W. G. Hodgson, *Nature*, **212**, 465 (1966).

(7) G. Palmer and V. Massey, *J. Biol. Chem.*, **244**, 2614 (1969).

(8) J. F. Martin and J. T. Spence, *J. Phys. Chem.*, **74**, 2863 (1970).

(9) T. J. Wallace, A. Schriesheim, H. Hurwitz, and M. B. Blaser, *Ind. Eng. Chem., Process Des. Develop.*, **3**, 237 (1964).

(10) R. C. Kapoor, O. P. Kachwaha, and B. P. Sinha, *J. Phys. Chem.*, **73**, 1627 (1969).

of redox reactions of these compounds with molybdenum species have been published. A number of complexes of Mo^{V} and Mo^{VI} with various thiol ligands of biological importance have been reported in the literature[12,13] and thioglycolic acid has been used in the analytical determination of both oxidation states of the metal.[14] A preliminary study of an esr active Mo^{V}–TGA species with a g value and hyperfine splitting constants similar to those observed with the enzymes has been published,[6] but few details were given.

Complexes. Both Mo^{V} and Mo^{VI} have been reported to form complexes with thioglycolic acid in which the metal ion to ligand ratio is 1:2.[14] In phosphate buffer at pH 6.00, these results were verified by continuous variation and molar ratio studies, and the reported absorption maxima and molar absorptivities confirmed [λ_{max} 365 nm, ϵ 4.40 $\times$ 10^{-3} for the Mo^{VI} complex; λ_{max} 355 nm, ϵ 2.50 $\times$ 10^{-3} for the Mo^{V} complex]. Esr analysis at both room temperature and $-195°$ of samples from the Mo^{V}–TGA solution indicated only a small amount (<0.1%) of the total Mo^{V} is present as monomer. The Mo^{V} complex was precipitated from solution and an elemental analysis obtained for the solid. The results are in agreement with the formula $[MoO(SCH_2COO)_2]_2ONa_4$. The ir spectrum of the solid showed peaks at 920 and 760 cm^{-1}, corresponding to Mo=O and Mo–O–Mo stretches, as assigned in previous work.[15] When the solid was redissolved in the buffer the electronic absorption spectrum was found to be identical with the spectrum obtained before its precipitation. Based on these data, and by analogy to similar complexes previously investigated,[13] the following reasonable structures for the two complexes are proposed

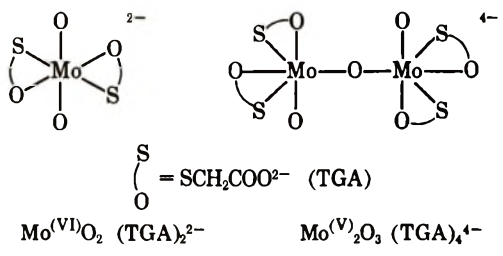

No spectral evidence for complex formation between Mo^{VI} and TGA was found at pH 7.50 in phosphate buffer. When $(NH_4)_2$ $MoOCl_5$ (Mo^{V}) was added to a solution of TGA in the buffer at pH 7.50, some increase in the absorbance at 355 nm was observed, but no maximum in the absorption spectrum was found. Attempts to determine the composition of the Mo^{V} complex present using the molar ratio method were unsuccessful, with the absorbance at 355 nm becoming constant only at ratios of TGA:Mo^{V} of greater than 20:1; thus only a rather weak complex can be present at pH 7.50.

Stoichiometry. When Mo^{VI} was added to a deaerated solution containing excess TGA in phosphate buffer in the pH region 4.50–6.00, $Mo^{V}_2O_3(TGA)_4^{4-}$ was first formed. The concentration of the Mo^{V} complex, however, reached a maximum and then decreased, suggesting further reduction of the Mo^{V} complex by TGA (Figure 1). Furthermore, at pH 6.00 the initial absorbance of the Mo^{VI} complex at 365 nm changed first to that of the Mo^{V} complex (λ_{max} 355 nm); this was followed by a change to a second species with λ_{max} at 365 nm and a shoulder at about 510 nm. The second change corresponded in time to the disappearance of the Mo^{V} complex. When $(NH_4)_2MoOCl_5$ was added to excess TGA under the same conditions, the initial peak at 355 nm due to $Mo^{V}_2O_3(TGA)_4^{4-}$ changed to a peak at 365 nm with a shoulder at 510 nm and the Mo^{V} complex disappeared (Figure 2). The Mo^{V} complex is easily oxidized by atmospheric oxygen, changing rapidly to the Mo^{VI} complex; the reduction product of the Mo^{V} complex, in contrast, is quite stable and the spectrum of a solution exposed to the air does not change appreciably over a period of 24 hr.

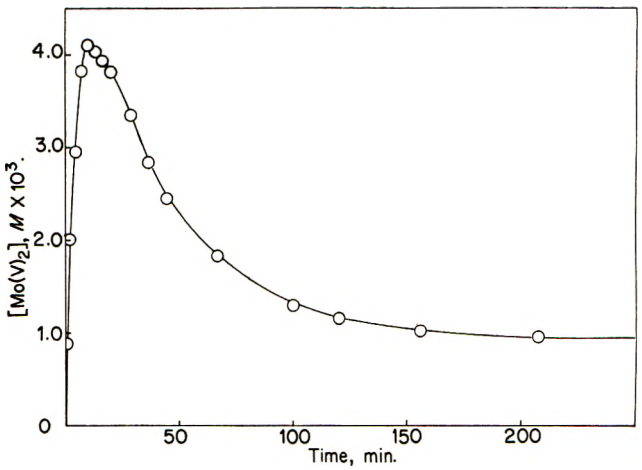

Figure 1. Change of concentration of Mo^{V}_2 with time during the oxidation of TGA by Mo^{VI} and Mo^{V}_2: $[Mo^{VI}]_0 = 1.00 \times 10^{-2}$ M; $[TGA]_0 = 5.20 \times 10^{-1}$ M; pH 6.00, 1.00 M phosphate buffer, 60°.

The expected oxidation product of TGA is dithiodiglycolic acid, DTDGA. Because of the difficulty of determining small amounts of DTDGA in the presence of excess TGA and various Mo species by the usual titrimetric procedures, an nmr method was used to detect and measure DTDGA. This method depends on the fact that the nmr absorbance of the methylene protons of DTDGA occurs at a different resonance than those of TGA. The results showed that one DTDGA

(11) F. P. Dwyer and D. P. Mellor, "Chelating Agents and Metal Chelates," Academic Press, New York, N. Y., 1952, p 374.

(12) A. Kay and P. C. H. Mitchell, *Nature*, 219, 267 (1968).

(13) L. R. Melby, *Inorg. Chem.*, 8, 349 (1969).

(14) A. I. Busev, "Analytical Chemistry of Molybdenum," Daniel Davy and Co., Inc., New York, N. Y., 1964, p 52.

(15) P. C. H. Mitchell, *Quart. Rev.* (*London*), 20, 103 (1966).

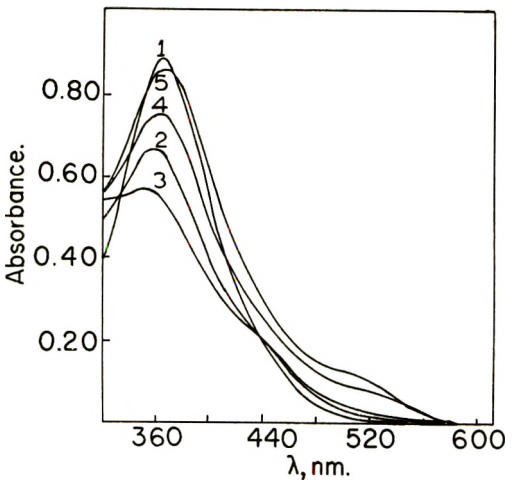

Figure 2. Changes in absorption spectrum with time during the oxidation of TGA by Mo^{VI} and Mo^{V}_2. $[Mo^{VI}]_0 = 2.00 \times 10^{-3}$ *M*; $[TGA]_0 = 4.40 \times 10^{-2}$ *M*; pH 6.00, 1.00 *M* phosphate buffer, 60°; 0.1000-cm cells. 1, 60.0 sec; 2, 91.2 sec; 3, 234 sec; 4, 1176 sec; 5, 27,220 sec.

is formed for each Mo^{VI} used in the complete reaction, indicating an overall two electron reduction for Mo^{VI}. In the oxidation of TGA by Mo^{V}, similar analysis showed one DTDGA is formed for each two Mo^{V} reacted. Thus, the reaction at pH 6.00 proceeds in two steps

$$2Mo^{VI}O_2(TGA)_2^{2-} + 2TGA \longrightarrow Mo^{V}_2O_3(TGA)_4^{4-} + DTDGA$$

$$Mo^{V}_2O_3(TGA)_4^{4-} + 2TGA \longrightarrow 2Mo^{IV} + DTDGA$$

Attempts were made to isolate the Mo^{IV} species as a solid, but only tarry, intractable substances were obtained which could not be purified. The ir spectrum of this substance in KBr showed the absence of Mo=O and Mo–O–Mo peaks. Since most Mo^{IV} compounds are very unstable in H_2O, disproportionating into Mo^{III} and Mo^{V} species, the formation of a compound in the IV oxidation state is unusual. It was attempted to obtain the Mo^{IV} product by the addition of $MoCl_4$ to TGA in buffer, but the expected disproportionation occurred rapidly. Thus the formulation of the product is presently not possible and only the formal oxidation state is indicated in the stoichiometric equation.

An esr study of the second reaction was made by withdrawing samples at various reaction times and freezing them in liquid nitrogen. As can be seen in Figure 3, the initial signal obtained with Mo^{V} and TGA are mixed is quite asymmetric, with $g_\perp = 1.955$, $g_{||} = 2.009$, $\bar{g} = 1.973$, and $A = 63.5$ G. After about 7 hr, when the reaction is essentially complete, the signal is considerably smaller and has become quite symmetrical ($g = 1.984$).

Kinetics of the Oxidation of TGA by Mo^{V}. The overall reaction clearly consists of the reduction of Mo^{VI} in two steps, with the second step being considerably

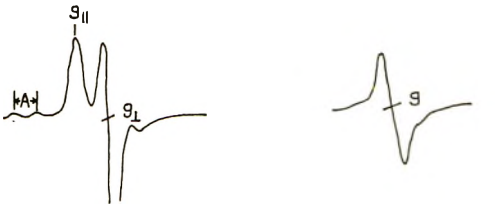

Figure 3. Changes in esr spectrum during oxidation of TGA by Mo^{V}_2; $[Mo^{V}_2]_0 = 2.00 \times 10^{-2}$ *M*; $[TGA]_0 = 5.40 \times 10^{-1}$ *M*; pH 6.00, 1.00 *M* phosphate, 60°. First signal, after 30.0 sec. Second signal, after 26,770 sec. Second signal, twice the signal level of first signal. Recorded at −195°; $A = 63.5$ *G*, $g_\perp = 1.955$; $g_{||}$ 2.009, $\bar{g} = 1.973$; $g = 1.984$.

slower than the first at pH 6.00. The oxidation of TGA by Mo^{V} was treated first, since it could be studied without interference by a subsequent reaction. The kinetics were investigated by following the disappearance of Mo^{V} with time. The Mo^{V} was obtained by dissolving $(NH_4)_2$ $MoOCl_5$ in buffer, by reducing Mo^{VI} over Hg in 3 *M* HCl, or by reducing Mo^{VI} with dithionite in the buffer; the rate of its reaction with TGA was the same in all cases and agreed with the rate of disappearance of Mo^{V} in the overall reaction. Thus, ligand exchange of Cl^- or phosphate groups with TGA is much faster than the oxidation of TGA. Because of the slowness of the reaction, all rates were measured with a large excess of TGA present. Preliminary investigation indicated the rate varied with both Mo^{V} and TGA concentrations. The rate was therefore expressed as

$$-d[Mo^{V}_2]/dt = k\,[Mo^{V}_2]^n[TGA]^m$$

$$(Mo^{V}_2 = Mo^{V}_2O_3(TGA)_4^{4-})$$

This expression was easily integrated, since the TGA concentration was always in excess. For values of n greater than 1, the half-life of the reaction is given by[16]

$$t_{1/2} = \frac{2^{n-1}}{k\,[TGA]^m A_0^{n-1}(n-1)}$$

where A_0 = initial $Mo^{V}_2O_3(TGA)_4^{4-}$ concentration. When log $t_{1/2}$ was plotted *vs.* log [TGA] at constant initial $Mo^{V}_2O_3(TGA)_4^{4-}$ concentration, a straight line was obtained with slope = -1.09 ± 0.10, thus indicating an order of 1 with respect to TGA. A plot of log $t_{1/2}$ *vs.* initial $Mo^{V}_2O_3(TGA)_4^{4-}$ concentration at known values of TGA concentration gave a straight line with slope -0.95 ± 0.10, which indicated that the order with respect to $Mo^{V}_2O_3(TGA)_4^{4-}$ is 2 (slope = $1 - n$). Second-order kinetic plots in Mo^{V}_2 were found to fit the data, and these plots gave straight lines to 80–85% reaction with consistent rate constants. The reaction is thus pseudo-second order. Using these

(16) S. W. Benson, "The Foundation of Chemical Kinetics," McGraw-Hill, New York, N. Y., 1960.

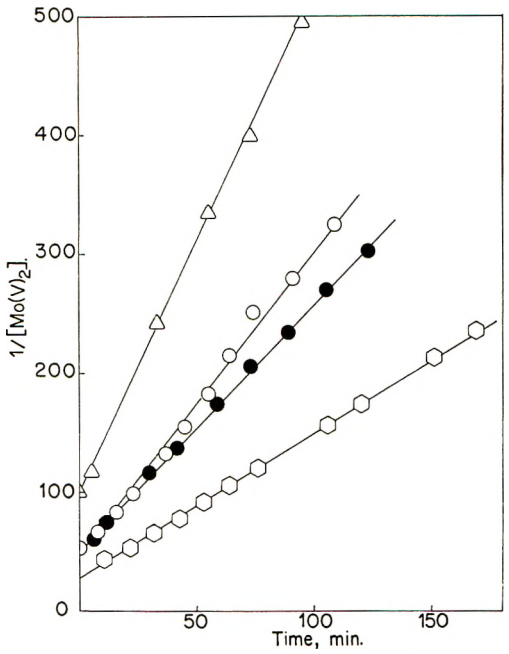

Figure 4. Pseudo-second-order plots for the oxidation of TGA by Mo^{V}_2: △, $[Mo^{V}_2]_0 = 5.00 \times 10^{-3}$ *M*, $[TGA]_0 = 10.00 \times 10^{-1}$ *M*; pH 6.00; ○, $[Mo^{V}_2]_0 = 1.25 \times 10^{-2}$ *M*, $[TGA]_0 = 4.50 \times 10^{-1}$ *M*; pH 6.00; ○, $[Mo^{V}_2]_0 = 1.00 \times 10^{-2}$ *M*, $[TGA]_0 = 5.20 \times 10^{-1}$ *M*; pH 4.60; ●, $[Mo^{V}_2]_0 = 1.00 \times 10^{-2}$ *M*, $[TGA]_0 = 5.20 \times 10^{-1}$ *M*; pH 7.50; 1.00 *M* phosphate, 60°; $\mu = 1.71$.

values of n and m, the rate expression gives upon integration

$$\frac{1}{[Mo^{V}_2]} = \frac{1}{[Mo^{V}_2]_0} = k_3 t[TGA] = kt$$

The experimental psuedo-second-order rate constants were obtained from the plots of $1/[Mo^{V}_2]$ *vs.* t. The third-order rate constants, k_3, were obtained from the experimental rate constants by the expression, $k = k_3[TGA]$. Typical plots of the data are shown in Figure 4 and the rate constants are collected in Table I.

In order to determine the effect of pH, the rate of reaction was determined at a number of pH values between 4.60 and 7.50. As can be seen from Table I, there is a very small pH dependence in the region pH 4.60–5.28, but the rate is independent of pH from 5.28–7.00. An increase of ionic strength was found to increase the rate (run 11, Table I), while the addition of the oxidized product, DTDGA, had no effect on the rate (run 10, Table I). Activation parameters were obtained by measuring the rate at various temperatures and plotting $1/T$ *vs.* log k_3 in the usual way.

Kinetics of the Oxidation of TGA by Mo^{VI}. At pH 6.00, the oxidation of TGA by $Mo^{VI}O_2(TGA)_2^{2-}$ is considerably faster than its oxidation by $Mo^{V}_2O_3(TGA)_4^{4-}$ (Figure 1). Therefore, there appeared to be a good possibility that the oxidation by Mo^{VI} might be treated independently and the subsequent oxidation by Mo^{V} ignored for a good part of the reaction.

Table I: Rate Constants for the Oxidation of TGA by Mo^{V}_2[a]

Run	$[Mo^{V}_2]_0$, $M \times 10^3$	$[TGA]_0$, $M \times 10$	pH	T, °C	k_3, M^{-2} sec$^{-1} \times 10$
1	5.00	2.50	6.00	60	1.45
2	5.00	3.20	6.00	60	1.38
3	5.00	6.70	6.00	60	1.36
4	5.00	8.20	6.00	60	1.43
5	5.00	9.20	6.00	60	1.34
6	5.00	10.00	6.00	60	1.37
7	7.50	6.00	6.00	60	1.34
8	10.00	4.60	6.00	60	1.33
9	12.50	4.50	6.00	60	1.30
10	5.00	8.20	6.00	60	1.36[b]
11	10.00	5.20	6.00	60	2.98[c]
12	5.00	5.20	4.60	60	1.72
13	5.00	5.20	4.85	60	1.65
14	5.00	5.20	5.30	60	1.45
15	5.00	5.20	6.50	60	1.43
16	5.00	5.20	7.00	60	1.45
17	5.00	5.20	7.50	60	1.42
18	10.00	4.20	6.00	30	0.44
19	10.00	5.20	6.00	40	0.68
20	10.00	5.20	6.00	50	1.00

[a] Average with standard deviation (runs 1–10), $k_3 = (1.35 \pm 0.05) \times 10^{-1}$ M^{-2} sec^{-1}. $Ea = 8.0 \pm 0.1$ kcal, $\Delta G^{\pm} = 13.7 \pm 0.2$ kcal, $\Delta S^{\pm} = -17 \pm 1$ eu 60°, pH 6.00. [b] 1.00 *M* DTDGA added. [c] 1.00 *M* Na_2SO_4 added, $\mu = 4.71$.

In order to test this, the rate of the reaction was measured at different concentrations of reactants. Again, because of the relatively slow rate, TGA was generally in excess. Trial and error plots at constant TGA concentration were found to fit a first-order expression to about 75% reaction, and consistent values of the rate constants were obtained from the slopes of the straight lines. Furthermore, the half-life of the reaction was found to be independent of initial Mo^{VI} complex concentration, confirming the order of 1 with respect to Mo^{VI} complex. To determine the order with respect to TGA, the reaction was followed at different initial TGA concentrations and the rate data plotted as first order in Mo^{VI} complex. When the log of the experimental rate constant, k, was plotted *vs.* log of TGA concentration, a straight line was obtained with a slope of 1.01 ± 0.10 which indicates the reaction is first order in TGA, and overall second order. When the ratio of TGA : Mo^{VI} used was lower than 10 : 1, the data could not be treated as a psuedo-first-order reaction, but gave straight lines when treated as second order, first order in each reactant. The rate of the reaction can thus be expressed as

$$-d[Mo^{VI}]/dt = k_2[Mo^{VI}][TGA]$$

$$(Mo^{VI} = Mo^{VI}O_2(TGA)_2^{2-})$$

Upon integration, this expression gives the standard first- and second-order equations, respectively, depending on TGA concentration. The experimental con-

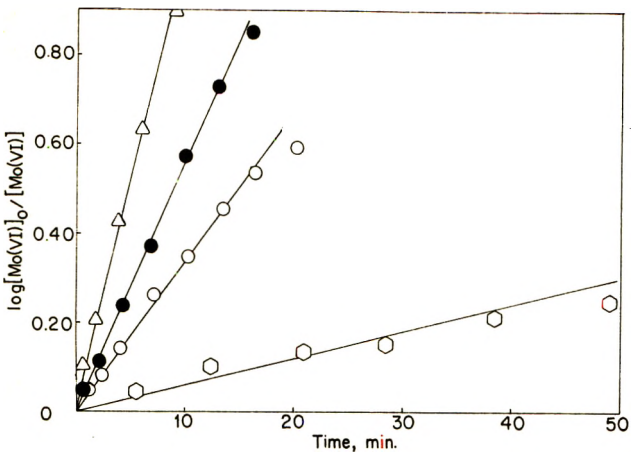

Figure 5. Pseudo-first-order plots for the oxidation of TGA by Mo^{VI}: ●, $[Mo^{VI}]_0 = 1.00 \times 10^{-2}$ *M*, $[TGA]_0 = 3.30 \times 10^{-1}$ *M*; pH 6.00; △, $[Mo^{VI}]_0 = 1.00 \times 10^{-2}$ *M*, $[TGA]_0 = 3.30 \times 10^{-1}$ *M*; pH 4.50; ○, $[Mo^{VI}]_0 = 1.00 \times 10^{-2}$ *M*, $[TGA]_0 = 3.50 \times 10^{-1}$ *M*; pH 6.50; ○, $[Mo^{VI}]_0 = 1.00 \times 10^{-2}$ *M*, $[TGA]_0 = 5.20 \times 10^{-1}$ *M*; pH 7.50; 1.00 *M* phosphate, 60°.

stants, k, obtained from the pseudo-first-order plots, were used to obtain the second-order constants, k_2, by the expression, $k = k_2[TGA]$. The rate constants are found in Table II, and typical plots are shown in Figure 5.

In the rate determinations at pH <6.00, it was assumed that essentially all the Mo^{VI} is present as the complex, $Mo^{VI}O_2(TGA)_2^{2-}$, in agreement with the formula of the complex, and all TGA concentrations were corrected for the amount bound to the metal ion. When the total TGA concentration was lowered to values less than three times the total Mo^{VI} concentration, little reaction occurred, as expected if the reactive species is the complex $Mo^{VI}O_2(TGA)_4^{2-}$.

The departure from second-order kinetics at about 75% reaction is most readily explained by the subsequent reaction of $Mo_2^{V}O_3(TGA)_4^{4-}$ with TGA discussed above. The complete rate expression, with respect to $Mo^{V}_2O_3(TGA)_4^{4-}$ is

$$d[Mo^{V}_2]/dt = k_2/2\ [Mo^{VI}][TGA] - k_3[Mo^{V}_2]^2[TGA]$$

Unfortunately, this is a nonlinear differential equation, for which an exact solution is not available.[16] A consideration of the rate constants, however, indicates that in the concentration range of Mo^{VI} used, the second reaction should become significant at about 70–80%, in agreement with the results.

The reaction rate was found to increase with an increase in ionic strength (run 14, Table II) and the addition of the oxidized product, DTDGA, had no effect on the rate (run 13, Table II).

The effect of pH was determined by measuring the rate at seven pH values between pH 4.50 and 7.50. Essentially no effect of pH in the region pH 4.50–5.50 was found, as seen in Table II. Above pH 5.50, however, the rate decreased rapidly with increasing pH, in contrast to the rate of the subsequent reaction of the Mo^{V} complex with TGA. The result is that as the pH is raised, the second reaction becomes significant at a much lower per cent reduction of Mo^{VI} (at pH 7.50, this occurs at about 30–35% reaction, as estimated by departure from a pseudo-first-order plot). When the rate data for different TGA concentrations at pH 7.50 were plotted as a pseudo-first-order reaction it was apparent that the order of the reaction with respect to TGA concentration is greater than 1. A plot of log k *vs.* log [TGA] at pH 7.50 gave a straight line with slope of 2.10 ± 0.10, indicating the reaction changes from second to third order in going from pH 6.00 to 7.50, providing the use of only the first 30–35% of the reaction to obtain rate constants is meaningful. Because of this apparent change, direct comparison of rate constants in this pH region is not particularly useful; a comparison of half-lives, however, as seen in Table III, indicates a strong pH dependence of the rate. When the experimental pseudo-first-order constants were converted to third-order constants by use of the relation-

Table II: Rate Constants for the Oxidation of TGA by Mo^{VI}

Run	$[Mo^{VI}]_0$, $M \times 10^2$	$[TGA]_0$, $M \times 10$	pH	T, °C	k_2,[a,b] M^{-1} sec^{-1} $\times 10^2$	k_3, M^{-2} sec^{-1} $\times 10^4$
1	1.00	1.20	6.00	60	6.60	
2	1.00	1.40	6.00	60	6.96	
3	1.00	2.20	6.00	60	6.65	
4	1.00	3.30	6.00	60	6.88	
5	1.00	4.20	6.00	60	6.88	
6	1.00	4.50	6.00	60	6.81	
7	1.00	5.20	6.00	60	6.76	
8	1.50	3.30	6.00	60	6.76	
9	2.00	3.40	6.00	60	6.78	
10	1.00	0.300	6.00	60	6.98	
11	1.00	0.410	6.00	60	6.75	
12	1.00	0.550	6.00	60	6.83	
13	1.00	2.20	6.00	60	6.85[c]	
14	1.00	1.00	6.00	60	10.67[d]	
15	1.00	3.30	4.50	60	12.53	
16	1.00	3.20	5.00	60	12.58	
17	1.00	3.20	5.50	60	11.08	
18	1.00	5.20	7.50	60		7.08
19	1.00	5.00	7.50	60		6.36
20	1.00	3.50	7.50	60		7.99
21	1.00	2.20	7.50	60		6.50
22	2.00	3.60	6.00	30	1.11	
23	2.00	3.20	6.00	40	2.16	
24	2.00	3.30	6.00	50	3.65	

[a] Average with standard deviation (runs 1–13) $k_2 = (6.81 \pm 0.12) \times 10^{-3} M^{-1}$ sec^{-1} 1.00 *M* phosphate, $\mu = 1.71$. [b] Average with standard deviation (runs 18–21) $k_3 = (6.98 \pm 0.42) \times 10^{-4}$ M^{-2} sec^{-1} 1.00 *M* phosphate, $\mu = 1.71$. $Ea = 11.3 \pm 0.15$ kcal; $\Delta G^{\ddagger} = 16.6 \pm 0.2$ kcal; $\Delta S^{\ddagger} = -16 \pm 1$ eu, at pH 6.00, 60°. [c] 5.00×10^{-3} *M* DTDGA added. [d] 1.0 *M* Na_2SO_4 added, $\mu = 4.71$.

Table III: Half-life as a Function of pH in the Oxidation of TGA by Mo^{VI}[a]

pH	$t_{1/2}$, sec
4.50	228
5.00	240
5.50	240
6.00	342
6.50	618
7.00	4100
7.50	7680

[a] $[Mo^{VI}]_0 = 1.00 \times 10^{-2}\ M$, $[TGA]_0 = 3.20 \times 10^{-1}\ M$, μ = 1.71, 60°.

ship, $k = k_3[TGA]^2$, consistent values of k_3 were obtained (Table II).

Discussion

The reduction of Mo^{VI} to a Mo^{IV} species by TGA was unexpected. There has been one recent report in the literature of the apparent formation of an Mo^{IV} species with cysteine,[17] although few details were given. The Mo^{IV} species produced in the reaction with TGA is probably complexed with TGA and may be similar to the Mo^{IV}–cysteine complex reported above.

Taking into account the various complexes present and the results of the kinetic investigations, the following mechanism is proposed for the oxidation of TGA by Mo^{VI} at pH < 6.00.

$$Mo^{VI}O_2(TGA)_2^{2-} + TGA \longrightarrow Mo^{V}O_2(TGA)_2^{3-} + TGA\cdot \quad (1)$$

$$2Mo^{V}O_2(TGA)_2^{3-} \rightleftarrows Mo^{V}_2O_3(TGA)_4^{4-} \quad (2)$$

$$2TGA\cdot \longrightarrow DTDGA \quad (3)$$

In this mechanism, reaction 1 is rate determining. At pH 6.00, as shown by the molar ratio studies, essentially all the Mo^{VI} is present as the complex $Mo^{VI}O_2(TGA)_2^{2-}$, and this complex is the reactive species. This mechanism leads directly to the rate equation

$$-d[Mo^{VI}]/dt = k_1[Mo^{VI}][TGA] \qquad (Mo^{VI} = Mo^{VI}O_2(TGA)_2^{2-})$$

This equation is identical with the experimental rate expression.

At pH 7.50, since there is no apparent Mo^{VI}–TGA complex present, the Mo^{VI} is present as MoO_4^{2-}. Experimentally, however, the reaction is second order in TGA. A reasonable assumption is that the reactive species is a 1:1 complex, $Mo^{VI}TGA$, present in a very small amount

$$Mo^{VI} + TGA \rightleftarrows Mo^{VI}TGA \quad (1)$$

$$Mo^{VI}TGA + TGA \longrightarrow Mo^{V}TGA + TGA\cdot \quad (2)$$

$$2Mo^{V}TGA \longrightarrow Mo^{V}_2TGA_2 \quad (3)$$

$$2TGA\cdot \longrightarrow DTDGA \quad (4)$$

Applying the steady-state assumption to the concentration of this Mo^{VI} complex, the following rate law is easily derived

$$-d[Mo^{VI}]/dt = \frac{k_1k_2[Mo^{VI}][TGA]^2}{k_{-1} + k_2[TGA]} \qquad (Mo^{VI} = MoO_4^{2-})$$

If $k_{-1} \gg k_2[TGA]$, which is a reasonable assumption, this reduces to

$$-d[Mo^{VI}]/dt = \frac{k_1k_2[Mo^{VI}][TGA]^2}{k_{-1}}$$

This equation is identical with the experimental rate expression at pH 7.50.

At pH 7.50, the formulas of both the Mo^{V} and Mo^{VI} TGA complexes are not known, and they are represented simply as $Mo^{V}TGA$ and $Mo^{VI}TGA$; since all runs were made in a large excess of TGA, however, their formulas do not effect the kinetics.

At pH values between 6.00 and 7.50, the reaction is most likely mixed second and third order, and no attempt has been made to analyze the data in this intermediate pH region.

At both pH 6.00 and 7.50 a positive salt effect on the rate was observed, which suggests the rate-controlling step is a reaction between like charged species. This suggestion agrees with the proposed structure of the Mo^{VI}–TGA complex, which is doubly negatively charged and with the fact that in the pH region used, TGA exists predominately as the monoanion, $HSCH_2COO^-$ ($K_1 = 2.10 \times 10^{-4}$, $K_2 = 2.10 \times 10^{-11}$).

For the oxidation of TGA by Mo^{V} it is more difficult to propose a reasonable mechanism, since the reaction is experimentally second order in Mo^{V} complex and first order in TGA. Some type of reactive intermediate complex involving the addition of an additional TGA ligand to the $Mo^{V}_2O_3(TGA)_4^{4-}$ present, followed by reaction of this intermediate species with a second molecule of the original complex would lead to the observed rate law, but such a formulation is rather arbitrary. It therefore seems best to simply indicate that the net activation process at pH ≤ 6.00 is

$$2Mo^{V}_2O_3(TGA)_4^{4-} + TGA \longrightarrow \text{products } [2Mo^{IV} + DTDGA]$$

The structure of the Mo^{IV} species formed as a product is unknown, although it is probably a TGA complex. Work to determine its nature is currently underway.

Again, as with the oxidation by Mo^{VI}, the evidence indicates the reaction species are negatively charged, in agreement with the observed positive salt effect on the rate.

The esr data show the $Mo^{V}_2O_3(TGA)_4^{4-}$ (dimer) exists in equilibrium with a small amount of monomer, and as previously reported,[6] the electron is consider-

(17) E. Bayer and P. Krauss, *Z. Naturforsch., B*, **24**, 776 (1969).

ably delocalized (high g value). The final signal, although considerably smaller than the original signal, indicates a different esr active species is present, also in small amounts. Again, the g value is high, indicating electron delocalization. It is difficult to postulate a structure for an esr active Mo^{IV} complex, since only one possible species has been reported[17] ($g = 1.995$) and the only well characterized stable Mo^{IV} complex, $Mo(CN)_8^{4-}$, is diamagnetic. Since Mo^{IV} is a d^2 ion, two unpaired electrons would be expected in an octahedral field. In the case of the d^3 ion $MoCl_6^{3-}$ no esr signal is seen in solution due to severe line broadening. Whether such line broadening would occur with an octahedral Mo^{IV} complex is unknown.

The results have some interesting implications. First, the reduction of Mo^{VI} to a stable Mo^{IV}–TGA complex suggests that Mo^{IV} compounds might not be so unstable in water as previously thought and invites an investigation of their properties. Second, the formation of this Mo^{IV} species supports the suggestion of Palmer and Massey[7] that in the enzyme xanthine oxidase the Mo might be reduced to the IV oxidation state. Finally, although there is at present no evidence that the cysteine–cystine groups are directly involved in the electron transfer processes of the molybdenum enzymes, the results reported here indicate such involvement is a possibility.

Experimental Section

Materials. Molybdenum(VI) solutions were prepared from B and A. $Na_2MoO_4 \cdot 2H_2O$, determined by the α-benzoinoxime method[18] to be 99.8% pure. Molybdenum(V) solutions were prepared by the quantitative reduction of Mo^{VI} solutions over Hg in 3 M HCl, or from $(NH_4)_2MoOCl_5$.

Ammonium oxopentachloromolybdate(V) ($(NH_4)_2MoOCl_5$) was synthesized according to the method of Klason.[19] Its purity (99.0%) was determined by measuring its extinction coefficient in 3 M HCl[20] and by the α-benzoinoxime method after oxidation to Mo^{VI} with Ce^{4+}.

Thioglycolic acid (TGA) was purchased from Aldrich Chemical Company and its purity, which varied somewhat from lot to lot, was determined by iodine titration. Dithiodiglycolic acid (DTDGA) was obtained from Aldrich Chemical Co. and was used without further purification. All buffers were prepared from reagent grade chemicals.

$Na_4O[MoO(SCH_2COO)_2]_2$. $(NH_4)_2MoOCl_5$ (10 mmol) 3.255 g, was dissolved in 25 ml of 3 N HCl and the solution cooled to 0°. $NaOOCCH_2SH$, 40 mmol, 4.564 g, was added, followed by enough cold 8 M NaOH to bring the solution to pH 6.00. The solution was allowed to stand for 4 days at 0° after which the deep red precipitate was collected by suction filtration. The precipitate was redissolved in a minimum of water and reprecipitated by the addition of ethanol. It was then dried *in vacuo* over P_2O_5. Elemental analysis gave the results: Calcd: Mo, 27.8; C, 13.86; H, 1.16; S, 18.53. Found: Mo, 27.7; C, 13.92; H, 1.95; S, 18.06. The ir spectrum of the solid in KBr gave peaks at 920 cm^{-1} (Mo–O) and 760 cm^{-1} (Mo–O–Mo), in agreement with literature assignments for similar Mo^V complexes.[15] The uv visible absorption spectrum in phosphate buffer at pH 6.00 was identical with that of a solution of Mo^V and TGA at the same pH.

A similar procedure was followed in an attempt to obtain a solid Mo^{VI} product. The precipitated solids were tarry materials, for which no consistent elemental analysis could be obtained, even after repeated reprecipitation. The ir spectrum in KBr of the solid, however, indicated Mo = 0 and Mo–O–Mo bands were absent.

Analytical Methods. The total concentration of Mo^V was measured by withdrawing samples of the reaction solution (deaerated with He, 99.95% pure) with a gas-tight syringe and addition of the sample to a deaerated solution of 8-hydroxyquinoline in ethanol. The solution was allowed to stand for 5 min, after which no further increase in the deep red color, due to the 8-hydroxyquinoline–Mo^V complex, occurred. It was then centrifuged for 3 min to remove insouble Mo^{VI} and phosphate species. The absorbance at 540 nm was read in a Beckman DU spectrophotometer. The method was calibrated using $(NH_4)_2MoOCl_5$ of known purity (measured by titration with standard Ce^{IV}). The 8-hydroxyquinoline–Mo^V complex was found to obey Beer's law over the concentration range used.

The concentration of DTDGA was measured using an nmr method. DTDGA has a peak at 215 Hz due to the absorbance of the methylene protons. The methylene protons of TGA adsorb at 195 Hz, allowing the determination of DTDGA in the presence of an excess of TGA. The peak height for the DTDGA was calibrated using known concentrations of DTDGA in the presence of TGA. The presence of both Mo^{VI} and Mo^V had no effect on the nmr spectrum.

Kinetics. The kinetics were determined by following the total concentration of Mo^V with time. The reactions were run in vessels that could be deaerated with He before the reactants were mixed. Samples were withdrawn through a rubber diaphragm, using a gas-tight syringe, and subjected to analysis.

Rate constants and activation parameters were obtained from the proper plots, using the method of least squares to obtain the best values.

Esr Analysis. Samples for esr analysis were removed with a gas-tight syringe and frozen immediately in deaerated quartz esr tubes in liquid N_2. For use as a standard, a solution of $K_3Mo(CN)_8$ was prepared by the

(18) H. B. Knowles, *J. Res. Nat. Bur. Stand.*, 9, 1 (1932).

(19) W. G. Palmer, "Experimental Inorganic Chemistry," Cambridge University Press, Cambridge, England, 1954, p 406.

(20) J. Frank, Ph.D. Dissertation, Utah State University, 1964.

method of Furman and Miller.[21] The area under the esr absorption curve of a standard $K_3Mo(CN)_8$ solution was obtained by double integration and compared with the area of the esr signal obtained from the sample, allowing the number of spins in the sample to be estimated. The error of the method is estimated to be ±15–20%.

The g values for the esr signals were determined by comparison with the g value of 1,1-diphenyl-2-picrylhydrazyl, either as an internal or external standard. All esr spectra were obtained on a Varian V-4500-10 X-band spectrometer equipped with 100-KHz field modulation.

Acknowledgment. This work was supported by the U. S. Public Health Service, Grant GM 08347, National Institute of General Medical Sciences, and by Research Career Development Award 5-K3-GM-22,643 to J. T. S.

(21) N. H. Furman and C. O. Miller, *Inorg. Syn.*, **3**, 160 (1950).

Kinetics of Redox Reactions of Oxidized *p*-Phenylenediamine Derivatives. II

by R. C. Baetzold

Research Laboratories, Eastman Kodak Company, Rochester, New York 14650 *(Received June 8, 1970)*

The kinetics and mechanisms of the reactions of a quinonediimine derivative (QDI), produced by photolysis of *p*-azido-*N*,*N*-diethylaniline in water, with hydroquinone (H_2Q), tin(II) ion, and azomethine leuco dye (LD) are reported. The QDI reacts with H_2Q or tin(II) producing a semiquinone species which reacts more slowly with the reducing agent to form *p*-phenylenediamine derivative. These reactions proceed by a mechanism involving hydrogen atom transfer. The reaction of LD with QDI does not produce any detectable SQ and may proceed by a hydride transfer mechanism. The LD ionizes with $pK_a \sim 9.9$; the basic form of LD is almost twenty times as reactive with QDI as the acid form.

I. Introduction

It has recently been shown[1] that a quinonediimine derivative (QDI) is produced when *p*-azido-*N*,*N*-diethylaniline is photolyzed in water. This method of forming QDI permitted a study of the kinetics and mechanism of the Michaelis reaction[2] (eq 2) between QDI and substituted *p*-phenylenediamine derivatives (designated PPD).

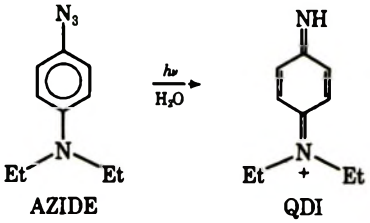

(1)

The product of this redox reaction is semiquinone (SQ), which is a one-electron intermediate oxidation state between PPD and QDI.

A technique for photolyzing azides containing *p*-dialkylamino groups was used to produce QDI. The reactions of the latter with a variety of reducing agents

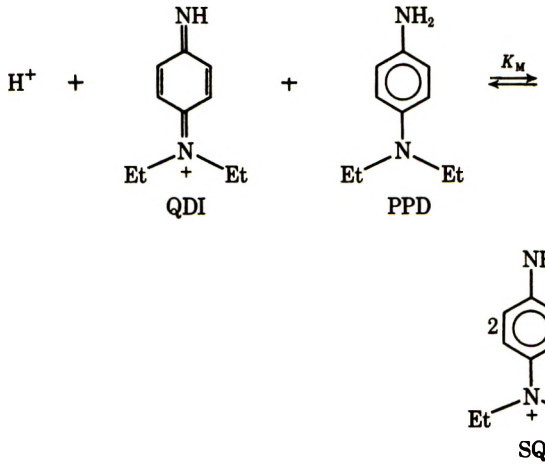

(2)

are the major concerns of this report. First, we were interested in determining whether QDI could be reduced to PPD without going through the SQ form; Michaelis[3]

(1) R. C. Baetzold and L. K. J. Tong, submitted for publication in *J. Amer. Chem. Soc.*

(2) L. Michaelis, M. P. Schubert, and S. Granick, *ibid.*, **61**, 1981 (1939).

(3) L. Michaelis, *Trans. Electrochem. Soc.*, 71, 107 (1937).

has stated that no simultaneous two-electron transfers occur in the PPD system. We were also interested in determining the origin of the proton which is present on SQ or PPD when QDI is reduced. The evidence reported here is that an electron and proton can be transferred simultaneously when QDI is reduced.

In this report reduction of QDI by hydroquinone (H_2Q), by tin(II) ion and by leuco dye is examined. Each of these reducing agents can lose two electrons forming a stable oxidation state. Hydroquinone is the only species in this study known to have a stable one-electron oxidation state.[4]

II. Experimental Section

The experimental procedure and apparatus have been described.[1] Runs are carried out with an excess of reducing agent relative to QDI to obtain pseudo-first-order kinetics whenever possible. The initial azide concentration is 2×10^{-5} *M*, of which roughly 25% is photolyzed by the Pyrex-filtered radiation of a 200-J xenon flash. These runs were carried out at 25° ± 0.5° with phosphate buffers of ionic strength 0.188.

The materials used in this work were Eastman Reagent Grade or highest purity available. Azide was prepared as described.[1]

Leuco dye is produced by reducing a pure sample of the dye with sodium borohydride. Borohydride is added until the solution becomes colorless; a slight molar excess is then added. There is no reaction of QDI with excess borohydride, because QDI reacts almost three orders of magnitude faster with leuco dye. The leuco dye solution is prepared just before photolysis and is kept deaerated by bubbling in nitrogen in order to prevent autoxidation of the leuco dye. The SQ and dyes that are formed as reaction products were identified by comparison of their absorption spectra with known spectra, as before.

Table I: Reduction of QDI by H_2Q

H_2Q concn, *M*	pH 6.78 Pseudo-first-order rate constant, sec^{-1}	Bimolecular rate constant, l./mol sec
6.12×10^{-5}	13.2	2.16×10^5
1.22×10^{-4}	27.7	2.27×10^5
2.45×10^{-4}	55.5	2.26×10^5
4.90×10^{-4}	113.5	2.32×10^5
		$2.25 \pm 0.05 \times 10^5$

Reduction of SQ by H_2Q

H_2Q concn, *M*	pH 6.78 Pseudo-first-order rate constant, sec^{-1}	Bimolecular rate constant, l./mol sec
3.06×10^{-5}	0.20	6.54×10^3
6.12×10^{-5}	0.403	6.58×10^3
1.22×10^{-4}	0.792	6.49×10^3
2.45×10^{-4}	1.35	5.50×10^3
		$6.22 \pm 0.42 \times 10^3$

The SQ extinction coefficient (ϵ), expressed as molar absorptivity, is determined by completely oxidizing a known amount of PPD with ferricyanide to the SQ state. Optical density of SQ is measured within milliseconds of mixing in a flow machine. At 526 mμ, $\epsilon = 7.6 \times 10^3$ l./mol cm for the *N*,*N*-diethyl derivative.

III. Hydroquinone

Hydroquinone reduces QDI to SQ and further reduces SQ to PPD. When excess H_2Q is present, the formation of SQ follows first-order kinetics according to eq 3.

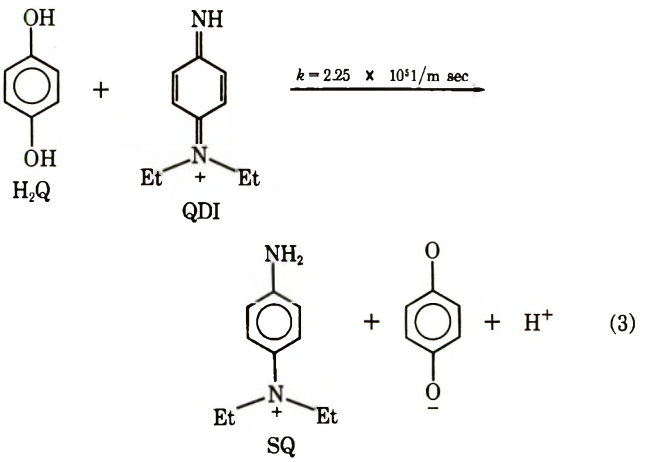

(3)

Variation of H_2Q concentration shows that the reaction is also first order in H_2Q (Table I). Measurement of the reaction at various pH's (Figure 1) shows that nonionized H_2Q is the reactive form of the reducing agent since H_2Q has $pK_{1a} = 9.85$.

We write the anion radical of hydroquinone as a product of eq 3 since the hydroquinone radical ionizes[5] with $pK_a = 5.9$. Equilibrium measurements[4] show that the anion radical disproportionates almost completely in the pH range used in these experiments, making the back reaction in eq 3 negligible.

Reduction of SQ to PPD is a first-order reaction in SQ. The data in Table I indicate that this reaction is also first order in H_2Q concentration, although at the higher concentrations of H_2Q there may be some deviation from this behavior. Figure 1 shows the dependence of the rate constant on pH and indicates that the monoanionic and the nonionized forms of H_2Q are reactive. The rate constants for the hydroquinone monoanion and the nonionized form are determined using pK_{1a}, as mentioned before. Any involvement of hydroquinone dianion in the reduction could not be evaluated since at the higher pH's required for its formation, SQ is unstable because of disproportionation.[1] The observed reactions are written in eq 4a and 4b.

(4) C. A. Bishop and L. K. J. Tong, *J. Amer. Chem. Soc.*, **87**, 501 (1965).

(5) N. K. Bridge and G. Porter, *Proc. Roy. Soc. (London)*, **244**, 259, 276 (1958).

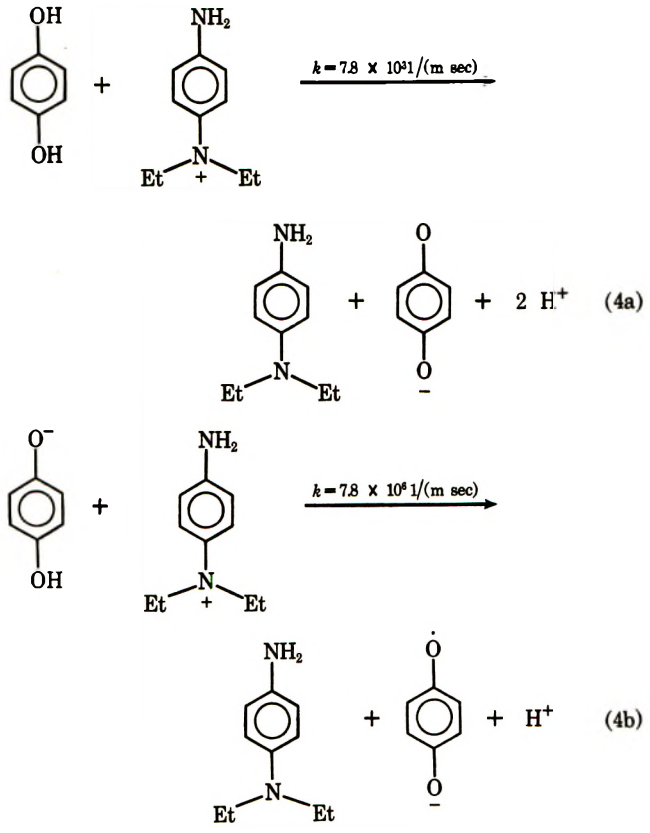

A kinetic isotope effect is observed for reaction 3 when rates are compared in normal and heavy water. The ratio $k_{H_2O}/k_{D_2O} = 2.83 \pm 0.10$ at pH 6.90 indicates that a bond involving hydrogen isotope is broken in the rate-determining step of this reaction. This effect is consistent with the transfer of a hydrogen atom from H_2Q to QDI, as shown in transition state I.

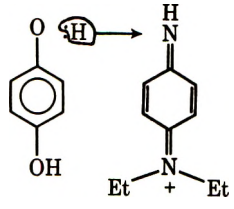

Recently it was shown that hydroquinone can transfer a hydrogen atom to $MnOH^{2+}$ upon reduction of the latter.[6] Since QDI is also capable of accepting a hydrogen atom, we expect that the two mechanisms are similar. The activation energy, measured by an Arrhenius-type plot, is 6.4 kcal/mol for reaction 3. This value is low and nearly the same as the activation energy[1] for reduction of QDI by ferrocyanide. This reaction was also believed to proceed by a hydrogen atom transfer.

IV. Tin(II) Ion

Tin(II) ion is described as a two-electron reducing agent in standard textbooks.[7] When it reacts with QDI, however, one-electron paths are favored, probably because a stable oxidation state (SQ) can be formed.

SQ is formed by first-order kinetics when azide is photolyzed in the presence of excess tin(II) ion. The pseudo-first-order rate constant of this reaction is proportional to tin(II) ion concentration (Table II). Since the rate-determining step of the reaction is first order in QDI and Sn^{2+}, we believe that a trivalent oxidation state of tin is produced in the reaction. Other kinetic studies[8,9] indicate that tin(III) can be formed, although it is unstable.

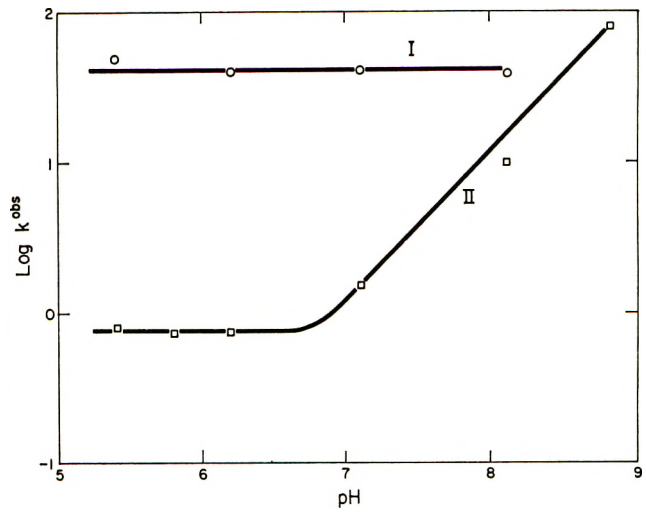

Figure 1. Dependence on pH of the rate of SQ formation (curve I) and decay (curve II) at 8.90×10^{-5} M hydroquinone.

Table II: Reduction of QDI to SQ by Tin(II) Ion

pH = 6.10	
$SnCl_2$ concn, M	$k^{obsd}(SnCl_2)$, l./mol. sec
5.02×10^{-5}	4370
1.26×10^{-4}	3720
4.39×10^{-4}	4380
1.16×10^{-3}	5430
2.32×10^{-3}	4750
2.90×10^{-3}	4980

Tin(II) ion is present as the trihydrated ion[10] at the nearly neutral pH and low chloride ion concentration of these experiments. The trihydrated species ionizes with $pK_a = 9.55$ according to the equilibrium

$$Sn(H_2O)_3^{2+} \overset{K_a}{=} H^+ + Sn(H_2O)_2OH^+ \qquad (5)$$

This result is correlated with the pH dependence of the SQ formation rate shown in Figure 2. The pH-independent reaction is attributed to

(6) G. Davies and K. Kustin, *Trans. Faraday Soc.*, **65**, 1630 (1969).

(7) E. S. Gould, "Inorganic Reactions and Structure," 1st ed, Holt, New York, N. Y., 1962.

(8) T. R. Ball, W. Wulfkuehler, and R. E. Wingard, *J. Amer. Chem. Soc.*, **57**, 1729 (1935).

(9) J. Weiss, *J. Chem. Soc.*, 309 (1944).

(10) Stability Constants, Special Publication No. 17, The Chemical Society, London, 1964, p 68.

$$Sn(H_2O)_3^{2+} + QDI \xrightarrow{k_1} SQ + Sn(H_2O)_2OH^{2+} \quad (6)$$

The increase in rate with pH is attributed to

$$Sn(H_2O)_2OH^{+} + QDI \xrightarrow{k_2} SQ + Sn(H_2O)(OH)_2^{+} \quad (7)$$

When all of the hydrated complex is ionized, the rate should become pH independent. From the data in Figure 2 and $pK_a = 9.55$, we can evaluate $k_1 = 5.0 \times 10^3$ l./mol sec and $k_2 = 1.9 \times 10^6$ l./mol sec.

Equation 8, involving the simultaneous transfer of two electrons from tin(II) to QDI, can be ruled out as accounting for SQ formation.

$$\text{tin(II)} + QDI \xrightarrow{k_1} PPD + \text{tin(IV)} \quad (8a)$$

$$PPD + QDI + H^+ \xrightarrow{k_2} 2SQ \quad (8b)$$

This mechanism predicts the observed dependence of rate on tin(II) concentration only if step 8a is rate limiting. The rate data of reference 1, however, indicate that SQ could not be formed fast enough by path 8b to account for the observed rates (Table II).

The rate of SQ formation decreases when D_2O is substituted for H_2O as the reaction medium. The rates are

$$k_{H_2O}/k_{D_2O} = 2.28 \pm 0.20 \text{ at pH } 7.00$$
$$k_{H_2O}/k_{D_2O} = 1.98 \pm 0.06 \text{ at pH } 8.15 \quad (9)$$

This effect is consistent with breakage of an oxygen–hydrogen bond required for the transfer of a hydrogen atom from hydrated tin(II) to QDI in the rate-determining step of the reaction at low pH. The effect of D_2O at high pH would be to increase the pK_a for ionization of the complex (eq 5). This effect alone predicts that $k_{H_2O}/k_{D_2O} > 1$. It is much more likely that electron transfer, not hydrogen atom transfer, is involved in this reaction at high pH. The low-pH isotope effect, together with the effect of heavy water on pK_a, suggests that the ratio k_{H_2O}/k_{D_2O} should be greater at high pH than at low pH if hydrogen atom transfer were taking place.

The activation energy of this reaction in the pH-independent region is measured by plotting log k^{obs} *vs.* reciprocal temperature. The observed activation energy at pH 6.10 is 16.0 kcal/mol. This value is considerably higher than that observed for reduction of QDI by H_2Q, PPD[1] or ferrocyanide.[1] A high activation energy is expected when an unstable product (such as tin(III)) is formed.[11]

Semiquinone that is formed by reactions 6 and 7 is not stable. The rate of decay is increased by increasing pH or concentration of tin(II) (Table III). The decay does not follow first-order kinetics, but when PPD is added, SQ decays by second-order kinetics. The bimolecular rate constant is determined from the product of SQ extinction coefficient and the slope of Figure 3; it varies inversely with PPD concentration according to Figure 4. These observations are consistent with

Table III: Decay of SQ in Tin(II) System

Tin(II)[a] concn, *M*	$k^{bimolecular}$, l./mol sec
4.81×10^{-5}	9.65×10^3
1.45×10^{-4}	2.85×10^4
2.41×10^{-4}	4.95×10^4
3.61×10^{-4}	7.90×10^4
4.81×10^{-4}	1.02×10^5
PPD concn, *M*[b]	**$k^{bimolecular}$, l./mol sec**
6.55×10^{-5}	6.34×10^4
8.24×10^{-5}	4.95×10^4
1.23×10^{-4}	3.30×10^4
2.46×10^{-4}	2.32×10^4
4.12×10^{-4}	6.24×10^3

[a] pH 8.17, PPD concn = 8.24×10^{-5} *M*. [b] pH 7.86, Tin(II) concn = 2.41×10^{-4} *M*.

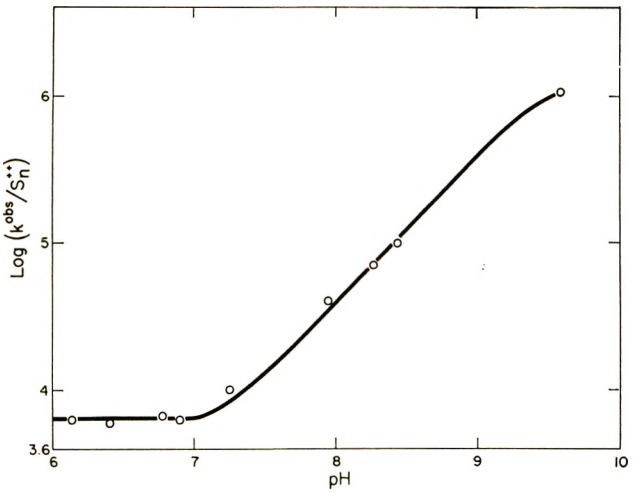

Figure 2. Dependence on pH of the bimolecular rate of SQ formation by reaction of QDI with tin(II).

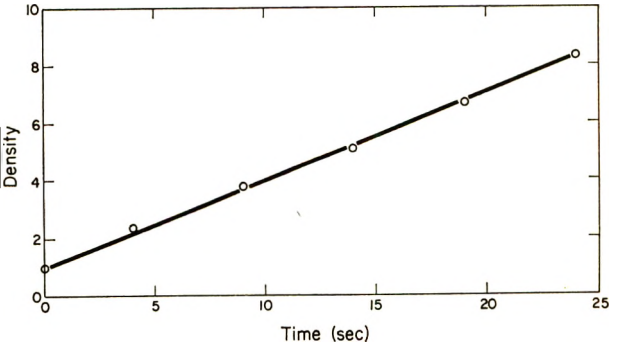

Figure 3. Plot of reciprocal SQ optical density *vs.* time for decay of SQ at pH 7.86, PPD = 2.46×10^{-4} *M*, stannous ion = 2.41×10^{-4} *M*.

(11) J. Halpern, *Can. J. Chem.*, **37**, 148 (1959).

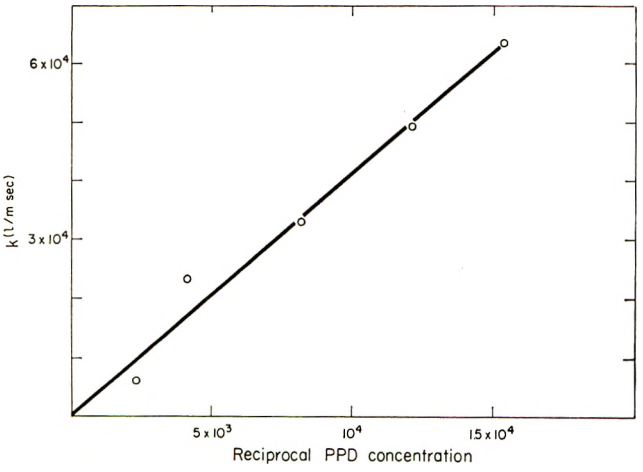

Figure 4. Plot of bimolecular rate constant *vs.* reciprocal PPD concentration for SQ decay; pH 7.86, stannous ion concentration = 2.41×10^{-4} *M*.

the decay of SQ by eq 10a and 10b which involves reactions already known.

$$QDI + Sn(H_2O)_2OH^+ \xrightarrow{k_1} SQ + Sn(H_2O)(OH)_2^+ \quad (10a)$$

$$2SQ \underset{k_3}{\overset{k_2}{\rightleftharpoons}} PPD + QDI + H^+ \quad (10b)$$

A solution for the decay of SQ by mechanism 10 is possible by applying the steady-state assumption to QDI.

$$\frac{d(T)}{dt} = 0 = -k_1(T)(A) + k_2(SQ)^2 - k_3(R)(T)(H^+) \quad (11)$$

where (T) = concentration of QDI, (A) = concentration of hydrated tin(II), and (R) = concentration of PPD not protonated.

The differential equation for SQ formation (eq 12) is solved

$$\frac{d(SQ)}{dt} = -2k_2(SQ)^2 + 2k_3(R)(T)(H^+) + k_1(T)(A) \quad (12)$$

by substituting eq 11 and is

$$\frac{d(SQ)}{dt} = -k_1(T)(A) = \frac{-k_1k_2(SQ)^2(A)}{k_3(R)(H^+) + k_1(A)} \quad (13)$$

This equation predicts the second-order decay kinetics observed for SQ (Figure 3) as well as the dependence of the rate constant on pH, the concentration of PPD, and the concentration of tin(II) ion, as mentioned previously.

Equation 13 predicts the behavior of Figure 4 where R equals $k_1k_2(A)/[k_3(R)(H^+) + k_1(A)]$. We use the value of k_1 from Figure 2 and the equilibrium constant for PPD protonation ($K_R = 1.0 \times 10^8$) to calculate $k_3/k_2 = 3.0 \times 10^8$ from this slope when $k_3(R)(H^+) \gg k_1(A)$. The published[12] value $k_3/k_2 = 2.9 \times 10^8$ supports this mechanism.

We conclude that the reduction of QDI by hydrated tin(II) ion proceeds by the formation of the unstable oxidation state, tin(III). This results in a high activation energy; the reaction may proceed by a hydrogen atom transfer. A concerted mechanism whereby the proton comes to QDI from water while the electron comes from tin(II) ion, however, cannot be ruled out. Tin(II) ion does not react directly with SQ because mechanism 10 results in a more rapid removal of SQ from the system. We can say that at pH 6 and Sn^{2+} at 10^{-3} *M*, the possible direct reaction of SQ with tin(II) ion must have $k \leq 10^2$ l./mol sec since the observed SQ decay required several seconds.

V. Leuco Dye

Leuco dyes (designated LD) are intermediates in the oxidative coupling of QDI and phenols.[13,14] In all of

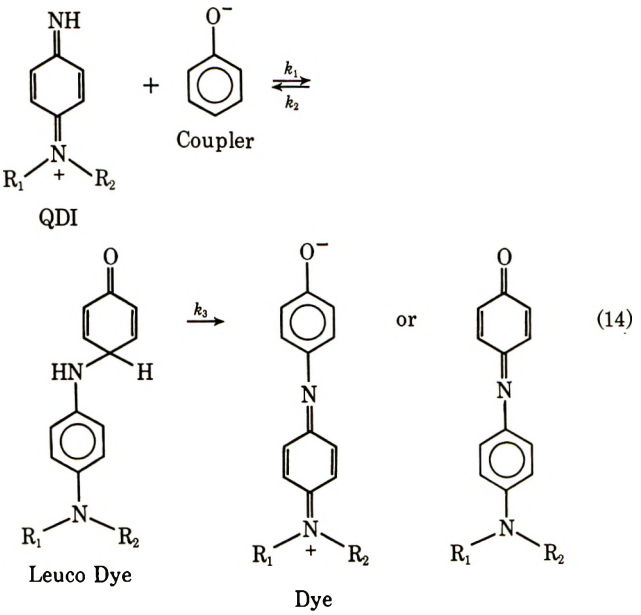

R_1, R_2 = alkyl groups

the systems currently reported where the phenolic compound is unsubstituted para to hydroxyl, the rate of dye formation in the above reaction is determined by coupling. Leuco dye is oxidized to dye more rapidly than it is formed and is present only in steady-state amounts. Thus, the rate of the oxidation of LD to dye cannot be studied by measurement of dye formation.

We have studied oxidation of the LD (produced by borohydride reduction of dye as in eq 15) to dye by

(12) L. K. J. Tong and M. C. Glesmann, *Photogr. Sci. Eng.*, **8**, 319 (1964).

(13) L. K. J. Tong and M. C. Glesmann, *J. Amer. Chem. Soc.*, **90**, 5164 (1968).

(14) L. K. J. Tong and M. C. Glesmann, *ibid.*, **79**, 583 (1957).

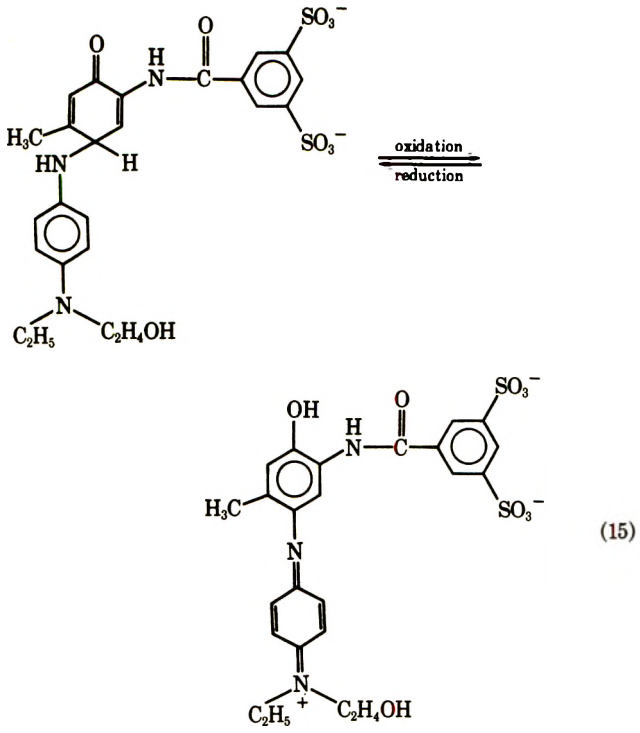

(15)

photolysis of azide in the presence of LD; formation of dye is monitored *vs.* time for kinetic analysis. Coupling rates for this dye were reported earlier.[14] The reaction is studied with an excess concentration of LD compared to QDI concentration. Under these conditions dye appears by first-order kinetics with a rate constant proportional to LD concentration (Table IV).

Table IV: Oxidation of Leuco Dye by QDI at pH 6.96

Concn of LD, *M*	k^{obs}, sec^{-1}	k^{obs}/(concn of LD), l./mol sec
3.48×10^{-5}	173	4.97×10^{6}
6.96×10^{-5}	308	4.43×10^{6}
1.05×10^{-4}	468	4.49×10^{6}
1.74×10^{-4}	815	4.69×10^{6}
		$4.65 \pm 0.19 \times 10^{6}$

The dependence on pH of the dye formation rate constant (at constant concentration of LD = 3.22×10^{-5} *M*) is shown in Figure 5. These data show that two species of LD react with QDI, an acid form at low pH and a base form at high pH. Attempts to measure spectroscopically the ionization of LD were unsuccessful since spectral dependence on pH was small. Analysis of rate data for the above model gives

$$k^{obs} = \frac{C_0}{K_a + (H^+)}\{k_c K_a + k_{HC}(H^+)\} \qquad (16)$$

where C_0 is the total concentration of LD, K_a is its dissociation constant, and k_c and k_{HC} are rate constants for the basic and acid forms of LD, respectively. Rate data at low pH determine $k_{HC} = 4.7 \times 10^6$ l./mol sec.

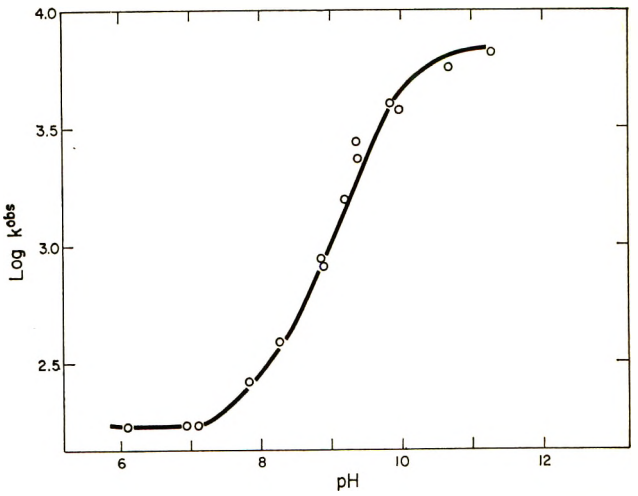

Figure 5. Dependence on pH of dye formation rate constant for 3.22×10^{-5} *M* LD concentration.

Rate data at high pH determine $k_c = 2.1 \times 10^8$ l./mol sec, and allow evaluation of $K_a = 1.52 \times 10^{-10}$ *M*.

When QDI reacts with LD we do not detect SQ as a reaction intermediate. If SQ is involved in the mechanism, it must react more rapidly than it is formed; otherwise its presence would be detected. Alternatively, QDI may react with LD by a direct two-electron transfer. Such a reaction could involve hydride transfer.

The question of whether SQ can oxidize LD to dye has been investigated by photolyzing azide in the presence of PPD and LD. In this experiment, use is made of the Michaelis reaction[1] (eq 2) to convert QDI to SQ. The concentrations of LD and PPD are adjusted in order to convert practically all QDI to SQ (eq 17b) before any dye is formed (eq 17a).

$$QDI + LD \longrightarrow dye + PPD \qquad (17a)$$

$$QDI + PPD + H^+ \longrightarrow 2SQ \qquad (17b)$$

Upon flashing azide in the presence of LD and a high concentration of PPD, we observe formation of SQ. SQ decays while dye forms; both processes have the same first-order rate. When the PPD concentration is decreased, no SQ forms, but dye forms with the same rate as in the absence of PPD. Data supporting these conclusions appear in Table V.

The rate of dye formation from SQ and LD is proportional to the LD concentration. This observation suggests the mechanism in eq 18 to account for this reaction where I is the one-electron oxidation product

$$SQ + LD \xrightarrow{k_1} I + PPD \qquad (18a)$$

$$SQ + I \xrightarrow{k_2} dye + PPD \qquad (18b)$$

of LD. The dependence of rate constant on LD concentration requires that step 18a be rate limiting with $k_1 = 2.3 \times 10^6$ l./mol sec.

Table V: Dye Formation Rates in the Presence of PPD

a. Effect of PPD Concn

pH	Concn of LD, M	Concn of PPD, M	Reaction observed	k^{obs}, sec^{-1}
6.19	2.11×10^{-5}	0	dye formation	92
6.19	2.11×10^{-5}	9.8×10^{-5}	dye formation	100
6.19	2.11×10^{-5}	4.04×10^{-3}	dye formation	90
6.19	2.11×10^{-5}	4.04×10^{-3}	SQ decay	87

b. Effect of LD Concn

6.42	2.11×10^{-5}	5.16×10^{-3}	dye formation	103
6.42	4.22×10^{-5}	5.16×10^{-3}	dye formation	215
6.42	6.33×10^{-5}	5.16×10^{-3}	dye formation	289

A small isotope effect has been observed for reaction 17a by comparing rates of dye formation in normal and heavy water. The ratio is $k_{H_2O}/k_{D_2O} = 1.4$ at pH 6.19, in the pH-independent region of Figure 5. While this effect is much smaller than isotope effects for other reactions of QDI,[1] it cannot be used to rule out the hydride transfer mechanism. There are reports[15] in the literature of hydride transfer mechanisms with isotope effects as low as this. The other possible mechanism for dye formation from LD and QDI is written in eq 19.

$$\text{QDI} + \text{LD} \xrightarrow{k_1} \text{I} + \text{SQ} \qquad (19a)$$

$$\text{SQ} + \text{I} \xrightarrow{k_2} \text{dye} + \text{PPD} \qquad (19b)$$

(I has been defined in eq 18.) Step 19a must be rate determining to account for the observed kinetics (Table IV).

The activation energy for reaction of QDI with LD to form dye has been measured for the pH-independent region of Figure 5. Arrhenius plots give the value 6.7 kcal/mol. This parameter is nearly the same as for QDI reactions with H_2Q, PPD and ferrocyanide, as mentioned earlier, all of which involve some form of hydrogen transfer. A higher activation energy might be expected if hydride transfer were involved in this mechanism since this would require extensive electronic reorganization.

VI. Conclusions

1. Hydroquinone and tin(II) ion reduce QDI to PPD by proceeding through the SQ state. Leuco dye may react with QDI by a hydride transfer mechanism; no evidence for one-electron steps is obtained, although they cannot be ruled out.

2. Leuco dye is the only reducing agent examined for QDI which does not produce any detectable SQ upon reaction.

3. The high activation energy observed for reducing QDI by tin(II) ion may be due to the formation of the unstable tin(III) oxidation state.

4. A high-pH form of LD is oxidized twenty times as rapidly to dye by QDI than is the low-pH form of LD. The pK_a for this LD ionization is 9.9.

Acknowledgment. The author gratefully acknowledges Dr. L. K. J. Tong for advice during this work.

(15) C. G. Swain, R. A. Wiles, and R. F. W. Bader, *J. Amer. Chem. Soc.*, **83**, 1945 (1961).

Radical Reactions of Highly Polar Molecules. Relative Reactivity of Halogenated Olefins in Haloalkyl Radical Additions

by Leonard O. Moore

Research and Development Department, Chemicals and Plastics, Union Carbide Corporation, South Charleston, West Virginia 25303 *(Received April 17, 1970)*

Reactivities of various chlorinated olefins in radical addition reactions in the presence of tetrafluoroethylene have been determined. These reactivities have been related to the electron densities, resonance stabilizations, and steric interactions of both the various chlorinated olefins and the radicals which are adding to them. An example is given of unusual steric control in the elimination or transfer of a chlorine atom from a chloroalkyl radical to form an olefin.

Various halogenated olefins are known to undergo three types of reactions under radical conditions. Vinyl chloride and vinylidene chloride polymerize readily;[1] 1,2-dichloroethylene and trichloroethylene are converted to dimers;[2-9] and trichloroethylene and tetrachloroethylene act as telogens with ethylene and vinyl ethers in the formation of telomers.[10-12] We have now examined the reactivities of the chlorinated ethylenes in the presence of tetrafluoroethylene (TFE) and report some results on relative reactivities to haloalkyl radical additions.

Experimental Section[13]

Reaction of Tetrachloroethylene with Tetrafluoroethylene. An 80-g portion of tetrachloroethylene[14] and 1.6 g of benzoyl peroxide were placed in a 300-cm^3 Parr Magnedash autoclave made of 316 stainless steel. The autoclave was cooled to *ca.* −70° in a Dry Ice–acetone cooled bath, evacuated, and 20 g of TFE was charged. The reactor was heated to 125° for 1 hr while stirring at 300 oscillations/min. After the reactor was cooled, 7 g of unreacted TFE was bled into a Dry Ice-cooled trap. The liquid products were poured from the reactor and the last was rinsed out with methylene chloride. After the methylene chloride and the tetrachloroethylene were distilled from the products, the 8 g of residue was extracted with acetone for 48 hr. The 3 g of insoluble residue melted at 204–208° and contained 11.16% of chlorine. This represents a composition with an average of 11.06 molecules of TFE per molecule of tetrachloroethylene.[15]

The acetone was distilled to leave 5 g of residue, melting at 70–76° and containing 18.08% of chlorine. The ratio of TFE to tetrachloroethylene in the product was 6.19. An infrared spectrum of this material showed the presence of unsaturation and carbon–chlorine and carbon–fluorine bonding.

A chain transfer constant was calculated by the general method described by Walling,[16] $C = [C_2F_4]/(n[C_2Cl_4])$, where the concentrations are those in solution. The concentrations were estimated from the pressure and the known volume of the reactor. The chain transfer constant was calculated to be 0.030.

Reaction of Trichloroethylene with Tetrafluoroethylene. This reaction was carried out as described just above but using trichloroethylene in place of the tetrachloroethylene. During discharge of the autoclave, 15 g of unreacted TFE was recovered. Distillation of the liquid product separated 16 g, 20% of 1,1,3,3,4,4-hexachlorobutene-1 (I),[7] bp 105° (7 mm), n^{20}D 1.5467, and left 4 g of a black tarry residue which was shown to contain some fluorine but was not further characterized. The butene was identical with that prepared from 160 g of trichloroethylene and 1.6 g of benzoyl peroxide without

(1) C. Walling, "Free Radicals in Solution," Wiley, New York, N. Y., 1957, p 62.

(2) A. L. Henne, *J. Amer. Chem. Soc.*, **69**, 279 (1947).

(3) M. Mugden and J. Wimmer (to Consortium fur Electrochemische Industrie, Gmbh), U. S. Patent 2,161,078 (June 6, 1939).

(4) W. Bauer, U. S. Patent 2,267,712 (Dec 30, 1941).

(5) L. Schmerling and J. P. West, *J. Amer. Chem. Soc.*, **71**, 2015 (1949).

(6) C. E. Frank and A. U. Blackham, *ibid.*, **72**, 3283 (1950).

(7) N. Inamoto, *Yuki Gosei Kagaku Kyokai Shi*, **16**, 454 (1958); *Chem. Abstr.*, **52**, 19909f (1958).

(8) O. Simamura and N. Inamoto, *Bull. Chem. Soc. Jap.*, **27**, 152 (1954).

(9) A. J. Blardinelli and W. H. Yanko (to Monsanto Chemical Co.), U. S. Patent 3,085,953 (April 16, 1963).

(10) D. T. Clark, J. N. Murrell, and J. M. Tedder, *J. Chem. Soc.*, 1250 (1963).

(11) J. R. Roland (to E. I. du Pont de Nemours and Co.), U. S. Patent 2,438,021 (March 16, 1948); E. I. du Pont de Nemours and Co., British Patent 589,065 (June 10, 1947).

(12) E. I. du Pont de Nemours and Co., British Patent 599,762 (March 19, 1948).

(13) Boiling and melting points are uncorrected.

(14) The haloethylenes used in this study were fractionated just prior to use. They were of greater than 99.8% purity by gas chromatography.

(15) The composition was calculated from the elemental analyses by the formula $n = (142 - 1.66\,(\%\ \mathrm{Cl}))/(\%\ \mathrm{Cl})$ to give the ratio of TFE to tetrachloroethylene in the product.

(16) See ref 1, pp 150–153.

TFE. In this case the yield was 27 g, 17%, of I and a 3-g tarry residue was left. The minimum value of 6.0 as a measure of the relative reactivities of trichloroethylene and TFE was determined assuming that this residue was a TFE telomer.

The structure of I was confirmed by an nmr spectrum using a Varian A-60 spectrometer. There were singlets at 6.6 and 6.1 ppm for the hydrogens at positions 2 and 4, respectively.

Reaction of cis-1,2-Dichloroethylene with Tetrafluoroethylene. The procedure described above was used for this reaction but with *cis*-1,2-dichloroethylene in place of tetrachloroethylene. Eleven of the 20 g of TFE fed was recovered after the reaction. Two fractions were separated by distillation. The first, 15 g, 18.7%, was a 50:50 mixture of *cis*- and *trans*-1,3,4,4-tetrachlorobutene-1 (III), bp 70–75° (8 mm), n^{20}D 1.5108. The second was 5 g, 4.1%, of *trans*-1,5,6,6-tetrachloro-3,3,4,4 tetrafluorohexene-1 (V), bp 90–100° (8 mm), n^{20}D 1.4652.

Anal. Calcd for $C_6H_4Cl_4F_4$: Cl, 48.25. Found: Cl, 48.24.

The ir spectrum showed unsaturation, carbon–hydrogen, carbon–chlorine, and carbon–fluorine bonding. The nmr spectra for both the hydrogens and the fluorines confirm the structure assigned, as indicated in the discussion.

Reaction of trans-1,2-Dichloroethylene with Tetrafluoroethylene. The same procedure was used with *trans*-1,2-dichloroethylene. There was recovered 12 g of TFE and the products were 13 g of III and 1 g of V.

Reaction of Vinylidene Chloride with Tetrafluoroethylene. The same procedure as described above was used for vinylidene chloride. There was recovered 18 g of TFE, 90% of that fed, and 75 g of dry polymer. No vinylidene chloride was recovered. The polymer contained 1.2% of fluorine which represented incorporation of 1.6% of TFE.

Calculations of Relative Reactivities. The relative reactivities of the various chlorinated olefins were computed from the concentrations of the reactants and the total incorporation of each reactant into product. The concentrations were estimated from (a) the liquid densities and the vapor pressures of the chlorinated olefins extrapolated to reaction temperature, (b) the pressure in excess of that vapor pressure was taken as an inverse measure of the solubility of tetrafluoroethylene in the chlorinated olefins at temperature. The incorporation of the reactants into products was based on the isolation and analysis of the products.

The relative reactivities were then simply

$$\text{reactivity} = \frac{(\text{chloroolefin in product} \times \text{TFE in solution})}{(\text{TFE in product} \times \text{chloroolefin in solution})}$$

Results and Discussion

Tetrachloroethylene was already known to form telomers with TFE,[17] but the mode of chain transfer has not been considered. At least two mechanisms for chain transfer are possible. One involves chlorine abstraction by the growing telomer chain radical from tetrachloroethylene, eq 1 and 2, and the other involves addition of the growing chain radical to tetrachloroethylene followed by loss of a chlorine atom which would then start a new chain, eq 3–5.

$$CCl_2{:}CCl_2 + R_f\cdot \longrightarrow CCl_2{:}CCl\cdot + R_fCl \quad (1)$$

$$CCl_2{:}CCl\cdot + nCF_2{:}CF_2 \longrightarrow CCl_2{:}CCl(CF_2CF_2)n\cdot \quad (R_f\cdot) \quad (2)$$

$$CCl_2{:}CCl_2 + R_f\cdot \longrightarrow R_fCCl_2CCl_2\cdot \quad (3)$$

$$R_fCCl_2CCl_2\cdot \longrightarrow R_fCCl{:}CCl_2 + Cl\cdot \quad (4)$$

$$Cl\cdot + nCF_2{:}CF_2 \longrightarrow Cl(CF_2CF_2)_n\cdot \quad (R_f\cdot) \quad (5)$$

If the first mechanism is correct, reactivity to chlorine transfer can be compared to that of carbon tetrachloride. A brief study of the reaction showed that tetrachloroethylene has a chain transfer constant of 0.030, larger than that for carbon tetrachloride, 0.019, under the same conditions.[18]

The greater reactivity of tetrachloroethylene could be related to charge distribution in the transition state which is more favorable than that of carbon tetrachloride in chlorine abstraction by trifluoromethyl radicals.[19] However, the bond dissociation energy of the C–Cl bond in vinyl chloride, 86 kcal/mol, is much larger than that of a C–Cl bond of methyl chloride, 80.6 kcal/mol.[20,21]

If the second mechanism is correct, the results obtained for tetrachloroethylene could not be compared with those for carbon tetrachloride since there is no similarity. This mechanism is closely related to that proposed for the dimerization of trichloroethylene and of 1,2-dichloroethylene. On the basis of bond energies and the similarity to other chloroolefins, this seems to be the most likely mode of chain transfer.

Consideration of this mechanism coupled with the degree of incorporation of the two olefins into the products provides evidence that the growing fluoroalkyl radical adds to tetrachloroethylene at a rate only 0.1 of that at which it adds to tetrafluoroethylene.

In the radical reaction of trichloroethylene and TFE the isolated products are I and a small amount of a residue. The residue contains fluorine and appears to be a telomer product. This result was somewhat un-

(17) G. C. Jeffrey (The Dow Chemical Co.), U. S. Patent 3,235,611, (Feb 15, 1966).

(18) L. O. Moore, unpublished results.

(19) W. G. Alcock and E. Whittle, *Trans. Faraday Soc.*, **62**, 134 (1966).

(20) M. Szwarc, *Chem. Rev.*, **47**, 75 (1950).

(21) The increase in bond order for chlorine conjugated to unsaturation, *i.e.*, $CH_2{=}CHCl$ or C_6H_5Cl, is discussed by J. R. Hoyland and L. Goodman, *J. Phys. Chem.*, **64**, 1816 (1960).

expected since telomers are the main products from trichloroethylene with ethylene.[7-9,22]

The reactive radical intermediate formed in this reaction apparently is $CHCl_2CCl_2\cdot$, which then can add to either trichloroethylene or TFE. If it is assumed that the residue product is all telomer, then a relative reactivity can be calculated. The addition of the tetrachloroethyl radical to trichloroethylene is at least six times as fast as to TFE.

The dimer I formed in the presence of TFE is the same as that formed when it is not present. Its identity was confirmed by comparison to properties reported earlier[7-9] and by nmr spectra of samples prepared under the two conditions.

The radical reaction of 1,2-dichloroethylene and TFE provided two products, 1,3,4,4-tetrachlorobutene-1 (III) (Scheme I) and 1,5,6,6-tetrachloro-3,3,4,4-tetrafluorohexene-1 (V) (Scheme II). It appears that the first radical formed is $CHCl_2CHCl\cdot$ which then adds to either 1,2-dichloroethylene or to TFE followed by an

Scheme I

$$CHCl{:}CHCl + Cl\cdot \longrightarrow CHCl_2CHCl\cdot$$

$$CHCl_2CHCl\cdot \xrightarrow{CHCl{:}CHCl} CHCl_2CHClCHClCHCl\cdot \longrightarrow$$

II

$$CHCl_2CHClCH{:}CHCl + Cl\cdot$$

III 50:50 (cis:trans)

Scheme II

$$CHCl{:}CHCl \longrightarrow CHCl_2CHCl\cdot \xrightarrow{CF_2{:}CF_2} CHCl_2CHClCF_2CF_2\cdot \xrightarrow{CHCl{:}CHCl} CHCl_2CHClCF_2CF_2CHClCHCl\cdot$$

IV

$$\xrightarrow{-Cl\cdot} CHCl_2CHClCF_2CF_2CH{:}CHCl$$

trans-V

addition to 1,2-dichloroethylene. Since no other products were isolated, the yields of III and V are the result of a competitive reaction of the two olefins for the radical $CHCl_2CHCl\cdot$.

Vinylidene chloride is in a somewhat different category than the chloroethylenes discussed above, since it it known to polymerize. In the presence of TFE it still polymerized, but incorporated only a small part of the TFE which was present. The growing polyvinylidene chloride chain radical adds to vinylidene chloride 12 times as readily as to TFE.

It is evident that there is a striking difference in reactivity of the various chloroethylenes and TFE to the addition of haloalkyl radicals. Using TFE as a point of reference, the following values of reactivity have been found (Table I).

Table I: Radical Addition Reactions, Relative Reactivities

Competitive olefins	Attacking radical	Relative reactivity, TFE = 1.0
$CCl_2{:}CCl_2$/TFE	$-CF_2CF_2\cdot$	0.1
CHCl:CCl_2/TFE	$CHCl_2CCl_2\cdot$	6.0 (minimum)
cis-CHCl:CHCl/TFE	$CHCl_2CHCl\cdot$	1.0
trans-CHCl:CHCl/TFE	$CHCl_2CHCl\cdot$	3.0
$CH_2{:}CCl_2$/TFE	$-CH_2CCl_2\cdot$	12.0

The differences of reactivity are apparently due primarily to the differences of electron density in the olefinic bond,[23] but with the electrophilic nature of the attacking radical also of importance.

Tetrachloroethylene has a low electron density in the double bond and is quite unreactive to radical addition, particularly by a perfluoroalkyl radical, which is more electrophilic than are the chlorinated radicals.

Trichloroethylene is compared most readily with vinylidene chloride because of the similarity of the attacking radicals, both having a $-CCl_2\cdot$ group ($CHCl_2CCl_2\cdot$ for trichloroethylene and $-(CH_2CCl_2)_nCH_2CCl_2\cdot$ for vinylidene chloride). The trichloroethylene is less reactive as would be expected since the electron density in the double bond of trichloroethylene is less than that in vinylidene chloride. Both are much more reactive than is TFE. The overall olefinic electron density in 1,2-dichloroethylene is about the same as that of vinylidene chloride; however, the carbon being approached is different, CHCl: *vs.* CH_2:, and the radicals which add to these two systems are quite different, $CHCl_2CHCl\cdot$ for 1,2-dichloroethylene and $-(CH_2CCl_2)_nCH_2CCl_2\cdot$ for vinylidene chloride. The more electrophilic radical, that from vinylidene chloride with two chlorine atoms on the carbon with the free electron, is more stabilized by resonance interactions and appears to be less reactive than is the radical with the single chlorine. This greater reactivity of *trans*-1,2-dichloroethylene over that of the cis isomer agrees with other studies on the radical reactions of these isomers.[24]

Undoubtedly steric inhibition plays a role in the failure of tetrachloroethylene to dimerize and in its very low reactivity to attack by fluoroalkyl radicals. It is also a factor in the failure of both trichloroethylene and 1,2-dichloroethylene to form high molecular weight polymers.

(22) The difference between ethylene and TFE for the addition of trichloromethyl radicals was examined by J. M. Tedder and J. C. Walton, *Trans. Faraday Soc.*, 62, 1859 (1966). For ethylene the energy of activation was 3.2 and that for TFE was 6.1 kcal. The values for log A were 5.6 for ethylene and 7.1 for TFE.

(23) M. Szwarc, in discussions at the Union Carbide South Charleston Technical Center, Feb 10, 1967, indicated that the electron density in the olefinic bond is the important controlling factor in the addition of trifluoromethyl radicals to olefins.

(24) See ref 1, pp 128–129.

Stereochemistry

The products isolated during the radical reaction of a mixture of 1,2-dichloroethylene and TFE provide an interesting example of control of stereochemistry in a radical reaction. The product V is found to be entirely in the trans configuration, contrasting sharply with III which is a 50:50 mixture of the cis and trans isomers. To aid in understanding this situation, Newman projections of the four conformations of the intermediate radicals from which a chlorine atom would be lost are shown in Scheme III. The major difference

Scheme III

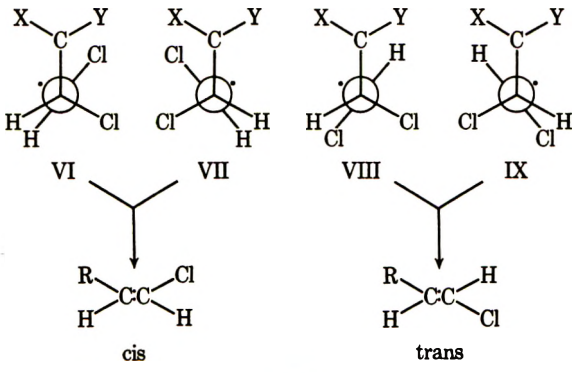

II, X = Cl; Y = H
or X = H; Y = Cl
IV, X = Y = F
III, R = $CHCl_2CHCl-$
V, R = $CHCl_2CHClCF_2CF_2-$

between the two intermediate radicals, II and IV is that X and Y in Scheme III are hydrogen and chlorine in II and are both fluorine in IV.

Chlorine loss from II apparently involves all conformations, as there is no indication of selectivity. Chlorine loss from IV, however, must involve only conformations VIII and IX.

The expected steric influence in this reaction should favor conformations VIII and IX over VI and VII. The difference of size between a $-CF_2-$ and a $-CHCl-$ group[25] is of secondary importance. It therefore appears that dipole interactions, and/or hydrogen bonding[26]

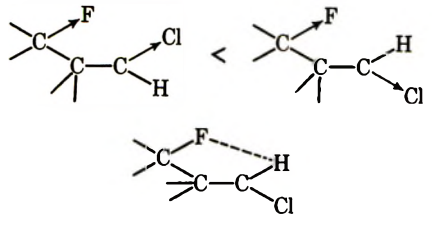

as well as the steric interactions of the groups have a significant role in controlling relative stabilities of the conformations of IV. (See also Tables II and III.)

Nmr Spectra

Several characteristics of the nmr spectra of these products deserve mention. The coupling constant J_{5-6}

Table II: Nmr of 1,3,4,4-Tetrachlorobutene-1

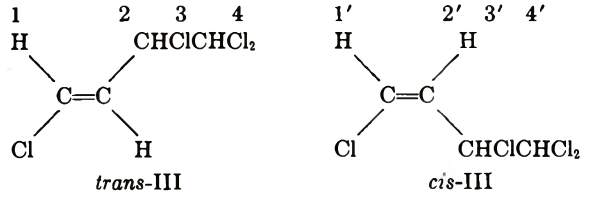

	Atom	Chemical shifts[a] Ppm, δ	Type
trans-III	1	6.51	Doublet
	2	6.12	Doublet of doublets
	3	4.70	Doublet of doublets
	4	5.83	Doublet
cis-III	1′	6.42	Doublet
	2′	6.08	Doublet of doublets
	3′	5.26	Doublet of doublets
	4′	5.89	Doublet

Coupling constants, cps

trans-III	$J_{1-2} = 13$
	$J_{2-3} = 8$
	$J_{3-4} = 4$
cis-III	$J_{1'-2'} = 7$
	$J_{2'-3'} = 9$
	$J_{3'-4'} = 4$

[a] Chemical shifts are relative to tetramethylsilane.

Table III: Nmr of 1,5,6,6-Tetrachloro-3,3,4,4-tetrafluorohexene-1

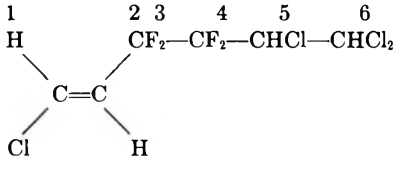

Atom	Hydrogen chemical shifts[a] Ppm, δ	Type
H_1	6.81	Doublet (split to triplets)
H_2	6.08	2 Triplets
H_5	4.78	Triplet (broad)
H_6	6.33	Doublet

Coupling constants, cps

$J_{1-2} = 13.5$
$J_{2-F3} = 12.0$
$J_{5-F4} = 10.5$
$J_{5-6} = 1.6$
$J_{1-F3} = 2.0$

Atom	Fluorine chemical shifts Ppm relative to CCl_3F	Type
F_3	104.5	Doublet
F_4	109.6	Triplet

Coupling constants, cps

$J_{F3-H2} = 12.0$
$J_{F3-F4} = 1.6-1.9$
$J_{F4-H5} = 9.4$
$J_{F3-H1} = 2$

[a] Chemical shifts are relative to tetramethylsilane.

in compound V is only 1.6 cps. This value is low for coupling of vicinal hydrogens and can only be explained if the dihedral angle is close to 60°, in which case the value is predicted by Karplus' theory.[27] Examples of other compounds with low coupling constants, although not as low, include *cis*- and *trans*-III where J_{3-4} = 4 cps (see Table I); $CHCl_2CHClCH_3$ where J_{1-2} is 3.8 cps;[28] and $CHCl_2CHO$ where J_{1-2} = 2.9 cps.[29] The fluorine nmr spectrum signal for F_4 in compound V appears as a triplet, which may be due to nonequivalence because of the asymmetry of carbon 5.[30] The small coupling for J_{F3-F4}, = 1.6–1.9, is not unusual.[31]

The nmr spectrum of the mixture of *cis*- and *trans*-III was quite complex. The cis and trans isomers were not purified but each was concentrated in separate distillation cuts and the nmr bands for each isomer identified by the changes of intensities. The assignment of bands was then made on these groups and found to be those expected for the cis and trans isomers of III.

Acknowledgment. Appreciation is due to W. T. Pace and C. B. Strow, Jr., for running the nmr spectra.

(25) A. Bondi, *J. Phys. Chem.*, **68**, 441 (1964).

(26) A CH bond adjacent to halogen is polar and interacts with fluorine in other molecules. The high solubility of partially fluorinated alkanes in hydrogen fluoride is an example of this. See W. H. Pearlson in "Fluorine Chemistry," Vol. I, J. H. Simons, Ed., Academic Press, New York, N. Y., 1950, p 466.

(27) J. W. Emsley, J. Feeney, and L. H. Sutcliffe, "High Resolution Nuclear Magnetic Resonance Spectroscopy," Vol. 1, Pergamon Press, New York, N. Y., 1966, pp 166–170.

(28) H. F. White, *Anal. Chem.*, **36**, 1291 (1964).

(29) Y. Yukawa, Ed., "Handbook of Organic Structural Analysis," W. A. Benjamin, New York, N. Y., 1965, p 485.

(30) E. I. Snyder, *J. Amer. Chem. Soc.*, **85**, 2624 (1963); G. M. Whitesides, D. Holtz, and J. D. Roberts, *ibid.*, **86**, 2628 (1964).

(31) D. D. Elleman, L. C. Brown, and D. Williams, *J. Mol. Spectrosc.*, **7**, 322 (1961).

The Effects of Pressure on the Sedimentation Equilibrium of Chemically Reacting Systems

by G. J. Howlett, P. D. Jeffrey, and L. W. Nichol*

Russell Grimwade School of Biochemistry, University of Melbourne, Parkville (Melbourne), Victoria 3052, Australia, and Division of Protein Chemistry, CSIRO, Parkville (Melbourne), Victoria 3052, Australia *(Received April 17, 1970)*

A chemically interacting system in which there is a volume change on polymerization of a monomer to form a single higher polymer is discussed. Equations are derived which allow the individual concentration distributions of monomer and polymer at sedimentation equilibrium to be calculated. From these distributions, graphs of weight average molecular weight *vs.* concentration are computed for a model system and it is shown that nonsuperposition of such graphs can arise from the effect of pressure in experiments performed at different angular velocities. A method of treating the experimental data from a system of the type discussed so as to obtain both the volume change and the equilibrium constant is suggested. The way in which the equations can be generalized to include chemically interacting systems of the type $mA + nB \rightleftharpoons C$ is indicated.

Introduction

Available theories[1-4] describing the sedimentation equilibrium distribution of chemically interacting systems of the types $mA \rightleftharpoons C$ (polymerization) and $mA + nB \rightleftharpoons C$ (heterogeneous association) have assumed no volume change on chemical reaction and thus neglect effects due to the pressure dependence of the equilibrium constants for the reactions. Other workers have examined such effects in relation to sedimentation velocity[5-7] and density gradient equilibrium experiments,[8] but made only qualitative comment on the operation, magnitude, and consequences of pressure effects on chemically reacting systems subjected to sedimentation equilibrium in the absence of a density gradient. It is the purpose of this work to examine these questions further by presenting the equations

* To whom correspondence should be directed at the former address.

(1) E. T. Adams, Jr., and H. Fujita in "Ultracentrifugal Analysis in Theory and Experiment," J. W. Williams, Ed., Academic Press, New York, N. Y., 1963, p 119.

(2) E. T. Adams, Jr., *Proc. Nat. Acad. Sci. U. S.*, **51**, 509 (1964).

(3) L. W. Nichol and A. G. Ogston, *J. Phys. Chem.*, **69**, 4365 (1965).

(4) E. T. Adams, Jr., *Ann. N. Y. Acad. Sci.*, **164**, 226 (1969).

(5) R. Josephs and W. F. Harrington, *Proc. Nat. Acad. Sci. U. S.*, **58**, 1587 (1967).

(6) G. Kegeles, L. Rhodes, and J. L. Bethune, *ibid.*, **58**, 45 (1967).

(7) G. Kegeles, *Biopolymers*, **7**, 83 (1969).

(8) L. F. Ten Eyck and W. Kauzmann, *Proc. Nat. Acad. Sci. U. S.*, **58**, 888 (1967).

required to construct numerical examples simulating the sedimentation equilibrium of a system comprising monomer and a single higher polymer and involving a volume change on polymerization. It will also be shown that the approach may be readily extended to systems of the type $mA + nB \rightleftarrows C$.

Theory

Consider first a system comprising monomer A in chemical equilibrium with a polymer C, where it is assumed that the activity coefficient of each solute species i (i denotes A or C), equals unity. It will be assumed further that the density of the solution, ρ, and the density increment for each solute species, $\partial\rho/\partial c_i$, are not functions of pressure.[9] As Casassa and Eisenberg[10] have noted, it is convenient in practice to replace the conventional $(1 - \bar{v}_i\rho)$ term with $\partial\rho/\partial c_i$, even though the substitution is strictly valid only in the limit $c_i \to 0$. It follows that the molar volume of reaction, ΔV, is given by

$$\Delta V = \frac{mM_A(\partial\rho/\partial c_A) - M_C(\partial\rho/\partial c_C)}{\rho} \quad (1)$$

where M_A is the molecular weight of monomer and $M_C = mM_A$. It is clear from eq 1 that ΔV is a constant independent of pressure provided the above assumptions (pressure independence of ρ and $\partial\rho/\partial c_i$) are fulfilled and that $\Delta V = 0$ only when $\partial\rho/\partial c_i$ is identical for each solute species. In the ultracentrifuge, the pressure, P, varies with the radial distance from the center of rotation, r, according to $dP = r\omega^2\rho dr$ and thus the pressure dependence of the equilibrium constant, $(\partial \ln K/\partial P)_T = -\Delta V/RT$, may be expressed in integrated form[5,6,8] as

$$K(r_1) = K(r_2)e^{-\{\Delta V\omega^2\rho(r_1^2 - r_2^2)\}/2RT} \quad (2)$$

where ω is the constant angular velocity, R the gas constant, T the absolute temperature, and r_1 and r_2 are any radial distances between or at r_m and r_b, the positions of the meniscus and base of the cell, respectively.

For each solute species, the condition for sedimentation equilibrium is given by[1-4]

$$c_i(r_1) = c_i(r_2)e^{\phi_i M_i(r_1^2 - r_2^2)} \quad (3a)$$

$$\phi_i = \frac{\omega^2(\partial\rho/\partial c_i)}{2RT} \quad (3b)$$

where $c_i(r_1)$ is the concentration in grams per unit volume at any radial distance r_1, with a similar definition applying to $c_i(r_2)$. Adams and Fujita[1] and Nichol and Ogston[3] have shown for situations where $\partial\rho/\partial c_i$ (and hence ϕ_i) is assumed identical for each solute species that the use of eq 3 to describe the sedimentation equilibrium distribution of each solute species separately is not inconsistent with the requirement that chemical equilibrium also be maintained throughout the cell. Indeed in their treatments it was shown that in the absence of pressure effects $c_C(r_1)/c_A^m(r_1) = c_C(r_2)/c_A^m(r_2) = K$ and thus a single value of K pertained throughout the cell equal to that describing the undisturbed equilibrium mixture in the absence of a centrifugal field. However, it cannot be assumed *a priori* that eq 3 written for each solute species describes the situation when values of ϕ_i are not identical. The latter point may be established by rearranging eq 3 as

$$\frac{c_C(r_1)}{c_A^m(r_1)} = \frac{c_C(r_2)}{c_A^m(r_2)}e^{(M_C\phi_C - mM_A\phi_A)(r_1^2 - r_2^2)} = \frac{c_C(r_2)}{c_A^m(r_2)}e^{\omega^2(r_1^2 - r_2^2)(M_C\partial\rho/\partial c_C - mM_A\partial\rho/\partial c_A)/2RT} \quad (4)$$

whereupon it is clear that eq 4 is consistent with the description of chemical equilbrium expressed in eq 1 and 2. It is therefore possible to utilize eq 3 in constructing plots of c_i *vs.* r (or r^2) for a chosen set of the defined parameters, provided c_i may be determined at any r position between or at r_m and r_b.

The amount in grams of any solute species *in the cell*, $(Q_i)_{cell}$, is given by

$$(Q_i)_{cell} = b\theta\int_{r_m}^{r_b} rc_i(r)dr \quad (5)$$

where θ is the cell sector angle in radians and b is the cell thickness. Combination of eq 3 and 5 gives on integration between the limits r_m and r_b

$$(Q_i)_{cell} = \frac{c_i(r_b)\theta b(1 - e^{\phi_i M_i(r_m^2 - r_b^2)})}{2\phi_i M_i} \quad (6)$$

Although this amount is contained in the volume, $V_{cell} = 2\theta b/(r_b^2 - r_m^2)$, the ratio $(Q_i)_{cell}/V_{cell}$ does not equal the concentration of the ith species in the undisturbed mixture in the absence of the centrifugal field.[2] However, a statement of conservation of mass may be written as

$$(Q)_{total} = \bar{c}_p V_{cell} = (Q_A)_{cell} + (Q_C)_{cell} \quad (7)$$

where $\bar{c}_p$ is the total weight concentration of all forms of solute in the original mixture. The required simultaneous equations have now been written, which permit construction of a distribution for any specified values of M_A, m, $\partial\rho/\partial c_A$, $\partial\rho/\partial c_C$, ω, T, V_{cell}, θ, b, r_b, $\bar{c}_p$, and $K(r_m)$, where the latter equilibrium constant is that at the meniscus ($P = 1$ atm) and equal to that characterizing the undisturbed equilibrium mixture. First, eq 6 is written as

$$\frac{(Q_C)_{cell}}{(Q_A)_{cell}^m} = \frac{c_C(r_b)(1 - e^{\phi_C M_C(r_m^2 - r_b^2)})\ (\theta b)^{1-m}(2\phi_A M_A)^m}{c_A^m(r_b)(1 - e^{\phi_A M_A(r_m^2 - r_b^2)})^m(2\phi_C M_C)} = Z \quad (8)$$

(9) P. F. Fahey, D. W. Kupke, and J. W. Beams, *Proc. Nat. Acad. Sci. U. S.*, **63**, 548 (1969).

(10) E. F. Casassa and H. Eisenberg, *Advan. Protein Chem.*, **19**, 287 (1964).

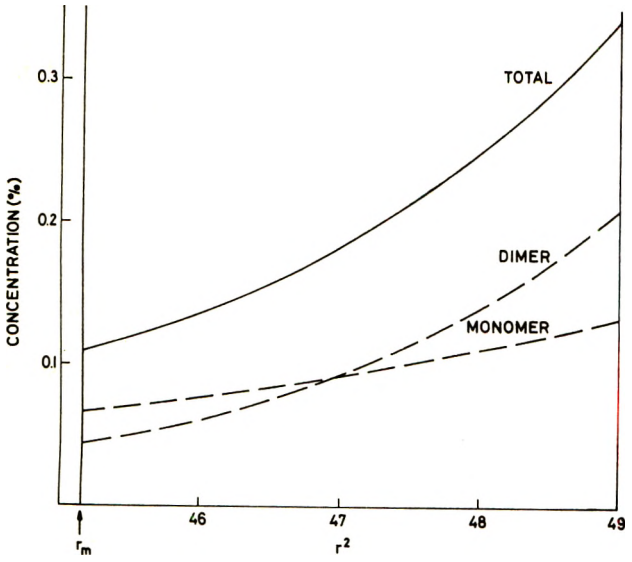

Figure 1. Numerical examples of sedimentation equilibrium distributions (plots of concentration *vs.* r^2) for a dimerizing system involving a volume change on reaction. Values selected for relevant parameters (see text) were M_A = 15,000, m = 2, $\partial\rho/\partial c_A$ = 0.27, $\partial\rho/\partial c_C$ = 0.30, T = 293°K, V_{cell} = 0.1 ml, θ = 0.0436 radian, b = 1.2 cm, r_b = 7.0 cm, $\bar{c}_\rho$ = 0.2%, $K(r_m)$ = 1000 ml/g, and ω = 1500 radians/sec.

The ratio $c_C(r_b)/c_A{}^m(r_b)$ may be evaluated using eq 4 with $r_1 = r_m$ and $r_2 = r_b$, on noting that $c_C(r_m)/c_A{}^m(r_m) = K(r_m)$. The value of Z follows directly from eq 8. Secondly, combination of eq 7 and 8 yields

$$Z(Q_A)_{cell}{}^m + (Q_A)_{cell} - (Q)_{total} = 0 \qquad (9)$$

The positive real root of this equation provides the value of $(Q_A)_{cell}$ and hence from eq 7 the value of $(Q_C)_{cell}$. These values may now be used in eq 6 to give values of $c_A(r_b)$ and $c_C(r_b)$, which may be employed in eq 3 to evaluate the complete sedimentation equilibrium distribution of each solute species.

An example of the above calculation performed with the aid of an IBM 7044 computer is presented in Figure 1 where individual distributions of A and C are shown as broken curves (- - -) and their sum, $\bar{c}(r)$, as a solid curve (——), both as a function of r^2. The choice of parameters specified in Figure 1 was essentially arbitrary, but the molar volume change on dimerization of −450 ml per mol of monomer selected seems not unrealistic, at least for certain associating protein systems in an aqueous environment.[5,8] Using the individual solute distributions, it is a simple matter to calculate ln $K(r)$ as a function of $r^2/2$ and to confirm that a plot of these variables yields a straight line of slope $(-\omega^2\rho\Delta V/RT)$ and ordinate intercept ln $K(r_m)$ at the $r_m{}^2/2$ position as demanded by eq 2. This suggests an iterative procedure by which estimates of $K(r_m)$ and ΔV could be obtained in practice from plots of total concentration, $\bar{c}(r)$, as a function of r recorded either in terms of optical density (absorption optics) or refractive index (Rayleigh interference optics). Provided it was assumed that the extinction coefficients or specific refractive increments of each polymeric species were identical, a set of results such as those in Figure 1 (——) could be analyzed as follows.

$$\bar{c}(r_1) = c_A(r_1) + c_C(r_1) \qquad (10a)$$

$$\bar{c}(r_2) = c_A(r_1)e^{\phi_A M_A(r_2{}^2 - r_1{}^2)} + c_C(r_1)e^{\phi_C M_C(r_2{}^2 - r_1{}^2)} \qquad (10b)$$

If $\partial\rho/\partial c_C$ (or $\partial\rho/\partial c_A$) could be measured in a concentration range where the relative amount of other polymer were negligible, then a first estimate of the unknown density increment could be made and eq 10a and 10b could be solved simultaneously to provide apparent values of $c_A(r_1)$ and $c_C(r_1)$ and hence an apparent value of $K(r_1)$. Similar solutions of apparent equilibrium constants $K(r)_{app}$ could be obtained using any paired values of the points $(\bar{c}(r),r^2)$ and a plot made of ln $K(r)_{app}$ *vs.* $r^2/2$. Treatment of the data as linear would provide an estimate of ΔV from the slope which could be used in eq 1 to give a revised estimate of $\partial\rho/\partial c_A$ (or $\partial\rho/\partial c_C$). Reiteration of the procedure until the plot of ln $K(r)_{app}$ *vs.* $r^2/2$ assumed linearity would give values of both ΔV and $K(r_m) = K(1\text{ atm})$

The differential form of eq 3 is frequently used to interpret sedimentation equilibrium results in terms of point weight-average molecular weights, $M_w(r)$, according to

$$\frac{\mathrm{d}\ln\sum_i c_i}{\mathrm{d}r^2} = \frac{\mathrm{d}\ln\bar{c}(r)}{\mathrm{d}r^2} = \phi M_w(r) \qquad (11)$$

and on the assumption that all $\partial\rho/\partial c_i$ are constant and identical (*i.e.*, that $\Delta V = 0$ and a single value of ϕ pertains). If this were the case, a smooth continuous plot of $M_w(r)$ *vs.* $\bar{c}(r)$ would result regardless of the value of ω selected as illutrated by the curve (- - -) in Figure 2. In contrast, the present approach permits exact numerical illustration of the behavior of this type of plot in situations where $\Delta V \neq 0$. For example, the curve (——) of Figure 2 was calculated on the basis of the individual distributions shown in Figure 1 and therefore refers to ω = 1500 radians/sec; while curve (-·-) of Figure 2 refers to the same system with ω = 2500 radians/sec. It is clear when $\Delta V \neq 0$, that M_w at a fixed $\bar{c}(r)$ assumes different values at different angular velocities. In practice, this would be manifested in plots of $M_w(r)$ *vs.* $\bar{c}(r)$ found with the same solution at different ω in that they would not overlap. The same type of effect would also be observed in a series of experiments conducted at constant ω, but varying $\bar{c}_\rho$. It is of interest that a variety of qualitative explanations,[11-14] including postulated heterogeneity of the sample and experimental error in measurement, have

(11) P. G. Squire and C. H. Li, *J. Amer. Chem. Soc.*, **83**, 3521 (1961).
(12) P. D. Jeffrey and J. H. Coates, *Biochemistry*, **5**, 489 (1966).
(13) J. C. Nichol, *J. Biol. Chem.*, **243**, 4065 (1968).
(14) D. A. Albright and J. W. Williams, *Biochemistry*, **7**, 67 (1968).

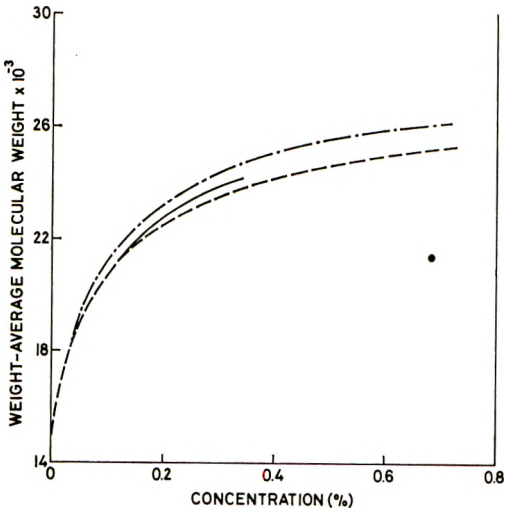

Figure 2. Plots of weight-average molecular weight *vs.* total concentration for the system described in Figure 1: ω = 1500 radians/sec (—); ω = 2500 radians/sec (-·-). The curve (---) is included for comparison and was calculated with $\partial\rho/\partial c_A = \partial\rho/\partial c_C = 0.27$ (*i.e.*, $\Delta V = 0$).

been offered to explain such effects observed experimentally. These factors may well contribute to the nonoverlap observed with certain systems, but it is now established that possible pressure effects must also be considered. This is particularly pertinent to the study of associating protein systems involving large molar volume changes on reaction and studied by the meniscus depletion method of Yphantis,[15] which utilizes relatively high values of ω and measurements near the base of the cell. It has been pointed out by one of our reviewers that Kegeles, Kaplan, and Rhodes[16] have independently reached similar conclusions.

Finally, it is possible to extend the treatment to encompass chemically interacting systems of the type $mA + nB \rightleftarrows C$. In this case, the analog to eq 1 is

$$\Delta V = \frac{mM_A\partial\rho/\partial c_A + nM_B\partial\rho/\partial c_B - M_C\partial\rho/\partial c_C}{\rho} \quad (12)$$

while eq 2, 3, 5, and 6 pertain directly with i denoting A, B, or C. It may be shown in an entirely similar way as used in the development of eq 4 that the condition for sedimentation equilibrium specified in eq 3 is consistent with the requirement of chemical equilibrium as described by eq 2 and 12. Moreover, it is possible to reformulate eq 8 to evaluate the ratio $(Q_C)_{cell}/(Q_A)_{cell}^m \cdot (Q_B)_{cell}^n$ for a known set of parameters. The individual values of $(Q_i)_{cell}$ follow by using the additional simultaneous equations

$$(Q_A)_{total} = (Q_A)_{cell} + (Q_C)_{cell}\frac{mM_A}{mM_A + nM_B} \quad (13a)$$

$$(Q_B)_{total} = (Q_B)_{cell} + (Q_C)_{cell}\frac{nM_B}{mM_A + nM_B} \quad (13b)$$

where $(Q_A)_{total} = \bar{c}_A V_{cell}$ and $(Q_B)_{total} = \bar{c}_B V_{cell}$, $\bar{c}_A$ and $\bar{c}_B$ being the total concentrations of A and B, respectively, in the original mixture. The remaining steps in obtaining a numerical solution or in analyzing an experimental distribution are directly analogous to those described above.

(15) D. A. Yphantis, *Biochemistry*, **3**, 297 (1964).

(16) G. Kegeles, S. Kaplan, and L. Rhodes, *Ann. N. Y. Acad. Sci.*, **164**, 183 (1969).

Low-Temperature Mesomorphism in Terminally Substituted Benzylideneanilines

by J. B. Flannery, Jr.,* and W. Haas

Research Laboratories, Xerox Corporation, Rochester, New York 14603 *(Received May 8, 1970)*

A new series of anils (*p*-*N*-alkoxybenzylidene-*p*-*n*-alkylanilines) has been prepared and examined for mesomorphic behavior. It is characteristic of these materials that mesophase stability is confined to low temperature ranges. As a consequence, a dominant role is indicated for residual lateral attractions in stabilization of the mesophases, particularly the nematic phase. This contrasts to the more commonly observed influence of residual terminal interactions in materials which exhibit nematic mesophases at higher temperatures. Some of these compounds are smectic trimorphic, and one, OCTOBUTA (VII), is a rare example of such trimorphism in a compound which does not also exhibit a nematic phase.

Introduction

The sensitivity of the optical properties of nematic liquid crystals to electric fields makes these materials very interesting for electrooptical applications. A serious drawback is the high temperatures at which the majority of compounds become mesomorphic. Hence, several attempts have been made recently to produce low temperature nematic materials, in binary[1] and single component[2] systems.

The aim of this work was to prepare and characterize pure compounds with low temperature mesomorphic ranges. This has been accomplished with low molecular weight Schiff bases (anils) of the type

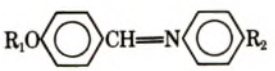

I

wherein R_1 and R_2 are generally alkyl groups in the range C_1–C_8. One of the members of this new series, anisylidene-*p*-*n*-butylaniline (ABUTA[3]), has only recently been reported[2] as a nematogenic material with a low crystallization temperature. Many others related to ABUTA have been examined for their transition temperatures, the morphology of their mesomorphic states, and their electrooptical properties. This paper discusses the relation of the observed transition temperatures to the constitution of these compounds and the textures of their mesophases. Some of the electrooptic phenomena are discussed elsewhere.[3]

Experimental Section

A. Syntheses. The compounds of the series I were prepared by condensation in refluxing ethanol of the respective *p*-*n*-alkoxybenzaldehydes and the appropriate *p*-*n*-alkylaniline, all of which were commercial products. After several hours reflux, solvent was removed by distillation. Crystalline products were purified by multiple recrystallization from methanol and petroleum ether. In cases of low-melting materials, recrystallization had to be carried out at low temperatures.[4] ABUTA was obtained as an opaque yellow liquid by high vacuum distillation [210–230° (0.1 mm)]. Product yields were generally greater than 50%. Elemental analyses (C, H, N, and O by Schwarzkopf Laboratories) were satisfactory for all compounds. Thin layer chromatography was used to confirm total impurity levels to be less than 1%.

B. Transition Temperatures and Mesophase Textures. Samples were studied as thin films between glass cover slips. The mesophases were identified and the transition temperatures measured using a calibrated hot stage on a Leitz Ortholux polarizing microscope. Simultaneously, photomicrographs of the mesophase textures were obtained. Phase transitions were also confirmed by differential thermal analysis (DTA) using a Du Pont 900 differential thermal analyzer equipped with chromel–alumel thermocouples.

Results

A. Materials. The compounds synthesized, their measured transition temperatures, and the nature of the transitions are given in Table I. Where other data are available[2] for comparison, this is included.

Of the fifteen compounds prepared, only two, XI and XV, exhibited no mesomorphic behavior, in spite of the fact that they could be supercooled 30 and 10°, respectively. Of the others, XII and XIII showed monotropic nematic phases only, VIII had a monotropic smectic phase, and another, IX, had a monotropic smectic phase as well as an enantiotropic nematic phase. The remaining nine compounds all exhibited enantio-

* To whom correspondence should be addressed.

(1) D. Demus, *Z. Naturforsch.*, **22a**, 285 (1967).

(2) H. Kelker and B. Scheurle, *Angew. Chem., Intern. Ed. Engl.*, **8**, 884 (1969).

(3) W. Haas, J. Adams, and J. B. Flannery, *Phys. Rev. Lett.*, **24**, 577 (1970).

(4) I. A. Kaye, *J. Chem. Educ.*, **46**, 697 (1969).

Table I: Substituted Schiff Base Transition Temperatures[a,b]

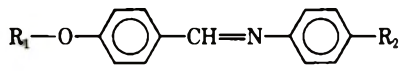

No.	R_1	R_2	Temperature °C of transition to: Smectic III	Smectic II	Smectic I	Nematic	Isotropic
I[c]	CH_3	C_4H_9				17[20]	39.5 [41]
II[d]	C_2H_5	C_4H_9				37 [36]	83 [80]
III[e]	C_4H_9	C_4H_9		7	41	46	75
IV[f]	C_5H_{11}	C_4H_9		24	52	54	71
V[g]	C_6H_{13}	C_4H_9	?	59.5	60.5	70	78
VI[h]	C_7H_{15}	C_4H_9	29	64	66.5	76	77.5
VII[i]	C_8H_{17}	C_4H_9	39.5	66	69.5		83.5
VIII	C_4H_9	H		(20)	22		44
IX[j]	C_4H_9	CH_3			(49)	66	68
X[k]	C_4H_9	C_2H_5			39	48	62.5
XI	CH_3	F					62
XII	CH_3	CH_3				(39) [(38)]	91 [92–3]
XIII	CH_3	C_2H_5				(32) [(28)]	56 [57]
XIV	C_2H_5	C_2H_5				63 [67]	69 [70]
XV	HOC_2H_4	C_2H_5					91

[a] Values in parentheses denote monotropic transitions. [b] Values in brackets from reference 2. [c] ABUTA. [d] EOBUTA. [e] BOBUTA. [f] PENTOBUTA. [g] HEXOBUTA. [h] HEPTOBUTA. [i] OCTOBUTA. [j] BOMETA. [k] BOETHA.

tropic nematic phases and/or smectic polymorphism. In three cases, V, VI, and VII, smectic trimorphism was found. Compound VII, OCTOBUTA, is of particular interest, as it represents a rare example[5] of smectic trimorphism without an accompanying nematic phase. ABUTA (I) is also of interest, because it has the lowest enantiotropic nematic thermal stability yet reported.

With the exception of ABUTA (I), BOBUTA (III), HEXOBUTA (V), and BOETHA (X), all compounds were normally crystalline at room temperature. After melting, however, many remained in a supercooled state at room temperature for periods of months. HEXOBUTA was unique in the series studied, in that it existed only as a waxy smectic fluid, resisting crystallization even at very low temperatures (77°K).

B. Thermal Behavior. The use of DTA to gain information on the energy changes which accompany the phase changes in the present materials was important in assigning the nature of the observed mesophase, and particularly in locating the number and temperatures of transitions. As will be shown below, texture changes accompanying the smectic transitions were often subtle and could easily be missed on optical examination alone. Figure 1 shows representative differential thermograms for HEXOBUTA (V) and HEPTOBUTA (VI) at a heating rate of 10°/min. The temperatures at the beginning of a phase transition endotherm were taken as the characteristic temperatures. These were determined by linear extrapolation of the leading edge of the endotherm to its intersection with the base line, as illustrated for the melting point of HEPTOBUTA in Figure 1b. The location of such transition points was dependent on heating rate, but at the rate chosen,

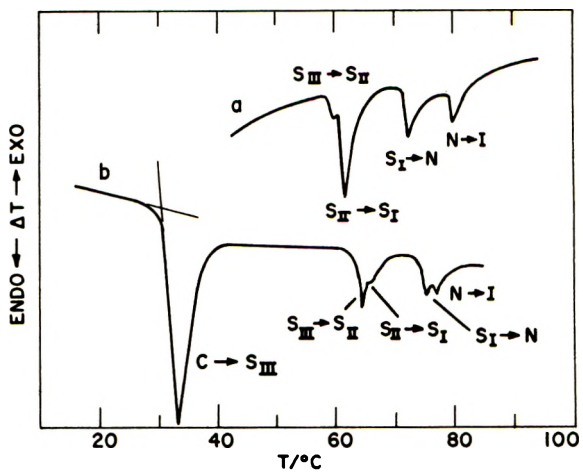

Figure 1. Differential thermograms for (a) HEXOBUTA and (b) HEPTOBUTA. Heating rate 10°/min.; sensitivity 0.1°/in.

agreement with the visually observed transitions was generally within 2°. Usually the DTA result was lower than the visual observation.

While precise calorimetric studies were not carried out on the present materials, several semiquantitative observations were made regarding the enthalpy changes accompanying the transitions. Using DTA endotherm peak areas as an estimate of the various caloric effects, it was seen that the heat of fusion was generally an order of magnitude or more greater than the heats of all smectic phase transitions. Similarly, the nematic–

(5) D. Demus, H. Sackman, G. Kunicke, G. Pelzl, and R. Salffner, *Z. Naturforsch, A*, **23**, 76 (1968); H. Sackman and D. Demus, *Mol. Cryst.*, **2**, 81 (1966).

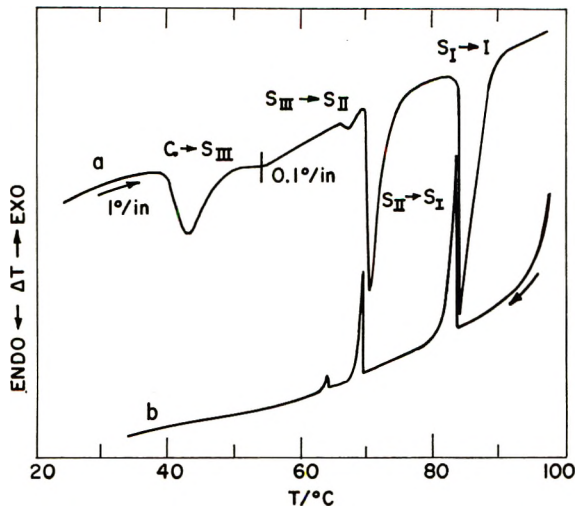

Figure 2. Differential thermograms for OCTOBUTA: (a) heating 10°/min; (b) cooling; note sensitivity change at 54°.

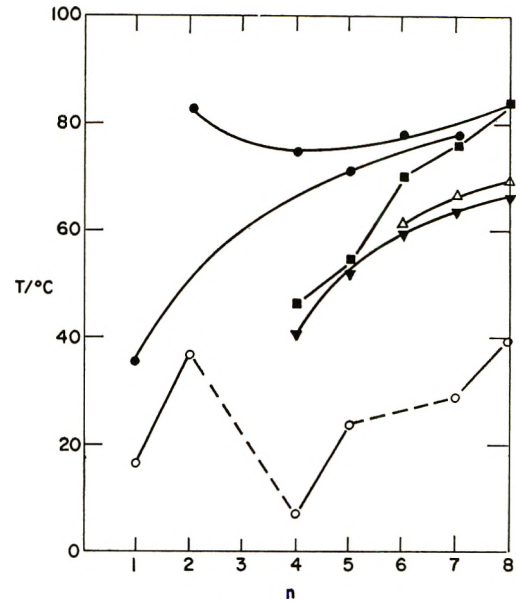

Figure 3. Plot of transition temperatures *vs.* number of carbon atoms in the alkoxy chain R_1O- of

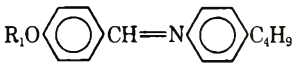

Upper temperature limits for the respective phases are ●, nematic; ■, smectic I; △, smectic II; ▼, smectic III; ○, crystalline-solid.

isotropic transition required only a fraction of the energy associated with the smectic phase changes. Figure 1 for HEXOBUTA and HEPTOBUTA is typical.

Compound VII, OCTOBUTA, as noted above, represents a rare example of trimorphism involving only smectic phases.[5] The thermal behavior of this compound is illustrated in Figure 2. The melting point and three mesomorphic transitions appeared as endotherms on the heating curve a, while only the mesomorphic transitions appeared as exotherms on the cooling curve b. Crystallization of the supercooled liquid was slow at ambient temperatures. Most noteworthy was the observation that the highest temperature mesomorphic–isotropic transition (83.5°) for OCTOBUTA was that with the highest caloric value, rather than the lowest, as has been observed by us and others[6] for nematic–isotropic transitions. An examination given below of the textures of the mesomorphic phases will show that this was a result of smectogenic trimorphism for OCTOBUTA.

The present materials comprise in part several homologous series of varied molecular structure. It is of interest to investigate the relationship of chemical constitution to mesomorphism in these series.

The values for the various transition temperatures *vs.* the length n of the alkyl chain R_1 for the Schiff bases derived from *p*-*n*-butylaniline are plotted in Figure 3. All members of this series were enantiotropic mesomorphic. All the mesomorphic-isotropic transition temperatures for compounds with odd numbers of carbon atoms in the alkoxy chain were monotonically increasing from C_1 to C_7. The same curve for even-number C-atom chains fell from C_2 to C_4, and then increased at a rate similar to that for odd *n*-alkoxy chains. However, the mesomorphic–isotropic transition curve for even-numbered chains was above that for the odd-numbered. Smectic phases first appeared in this series for $n = 4$. The smectic I–nematic transition curve also rose with increasing n (regardless of n odd or even) and merged with the rising nematic–isotropic curve at $n = 8$. For $n > 6$, three enantiotropic smectic phases were observed. The transition temperatures for the lower smectic phases were also found to lie on smooth rising curves. The identity of these phases as indicated by the curves in Figure 3 is based on similarity of textures, as discussed below.

A similar set of curves was found for the lower homologs of the *N*-alkoxybenzylidene-*p*-*n*-alkylanilines, where the alkyl substituent R_2 in the aniline moiety was varied. Examples are given in Figure 4. For the *N*-methoxybenzylidene anils, the nematic–isotropic transition temperatures were on separate *rising* curves, and the curve for the even-numbered carbon chains was below that for the odd C_n compounds (Figure 4a). The same observations held true for the *N*-ethoxybenzylideneanils (Figure 4b), and most likely for the *N*-butoxybenzylidene compounds as well, although in the latter series the data for $n = 3$ are not available (Figure 4c). For this latter group of compounds, smectic mesomorphism (monotropic) appeared for n as low as unity. Enantiotropic smectic dimorphism was obtained for $n = 2$. It is also notable that even *N*-butoxybenzylideneaniline (VIII) was smectogenic.

(6) R. S. Porter, E. M. Barrall, II, and J. F. Johnson, *Accounts Chem. Res.*, **2**, 53 (1969); E. M. Barrall, II, R. S. Porter, and J. F. Johnson, *J. Phys. Chem.*, **68**, 2810 (1964); H. Arnold, *Mol. Cryst.*, **2**, 63 (1966).

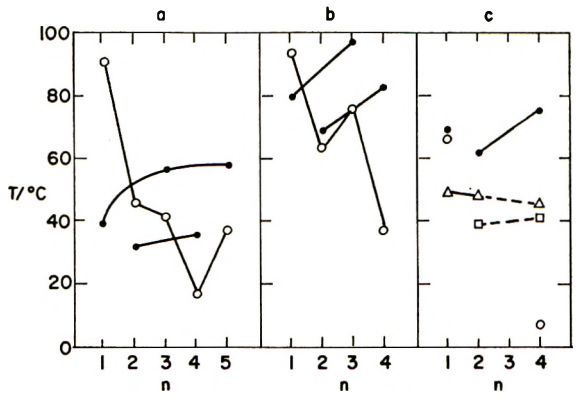

Figure 4. Plots of transition temperatures *vs.* number of carbon atoms in the alkoxy chain R_2 of: (a)

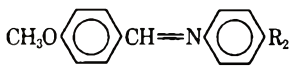

●, nematic–isotropic; ○, solid–nematic. Data for n = 3,5 from ref 2. (b)

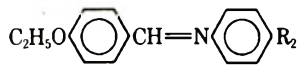

●, nematic–isotropic; ○, solid–nematic. Data for n = 1,3 from ref 2. (c)

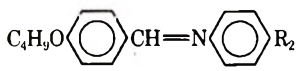

●, nematic–isotropic; △, smectic I–nematic; □, smectic II–smetic I; ○, solid–liquid crystal.

C. Mesophase Textures. A detailed microscopic examination was made of the textures shown by the mesophases. In all cases, definite texture changes corresponding to the phase changes measured by thermal methods were also observed optically. In two cases, however, discontinuous changes in texture were observed optically, but no evidence could be found for a thermal phase change. These latter two were ABUTA (I) and BOMETA (IX).

1. OCTOBUTA and Related Smectogenic Homologs. Photomicrographs (between crossed polarizers) of the texture changes which occur on cooling OCTOBUTA from the isotropic melt are shown sequentially in Figure 5. The onset of liquid optical anisotropy was marked by the initial appearance of smectic batonnets[7] at the isotropic transition temperature (Figure 5a). These coalesced spontaneously to give (Figure 5b) the focal-conic simple fan-shaped texture.[5] This texture persisted unaltered until the $S_{II} \rightleftarrows S_I$ transition (69.5°) was reached. At this point, an abrupt change occurred which appeared as a sudden collapse of the confocal S_I texture. The striated or broken fan-shaped texture in Figure 5c resulted. The range of stability of this latter phase was only ~3°. Thus at 66°, the $S_{III} \rightleftarrows S_{II}$ transition point, another discontinuous but subtle change was observed, the preparation taking on the

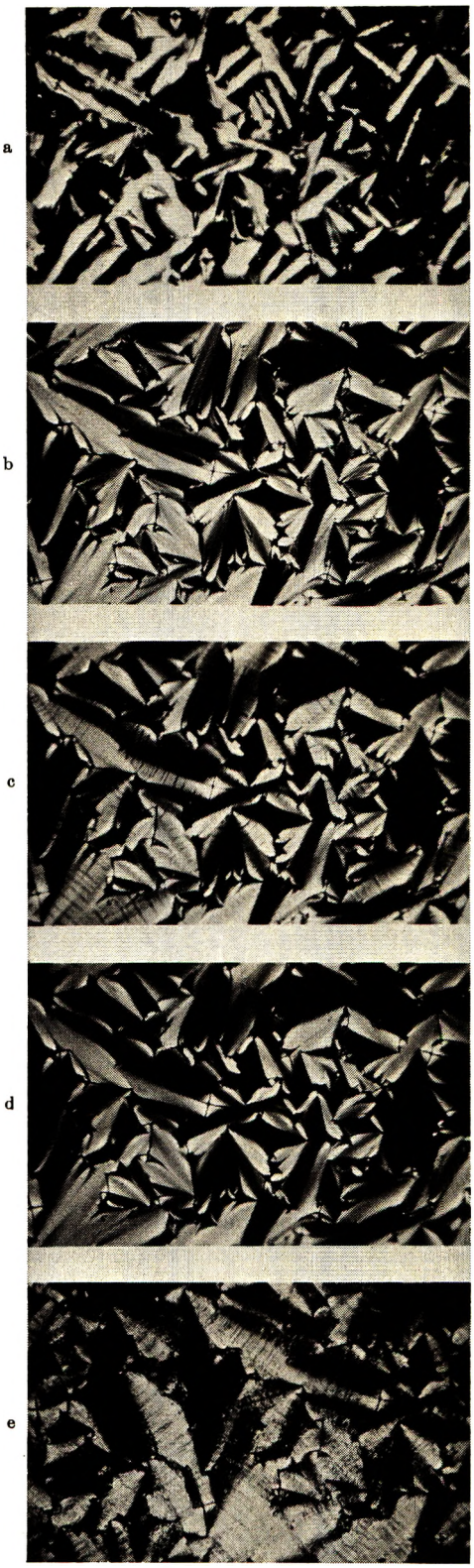

Figure 5. Photomicrographs of OCTOBUTA mesophases. (a) smectic batonnets, 84.0°; (b) smectic I, fan-shaped texture, 84.0°; (c) smectic II, broken fan-shaped texture, 69.0°; (d) smectic III, fan-shaped texture with diminished discontinuities, 68.0°; (e) smectic III, 48.0°.

(7) G. W. Gray, "Molecular Structure and the Properties of Liquid Crystals," Academic Press, New York, N. Y., 1962.

appearance illustrated in Figure 5d, a confocal fan-shaped texture with diminished discontinuities.[5] Further cooling of the sample produced no further optical discontinuities, but rather a gradual change to the polygon texture shown in Figure 5e; crystallization eventually occurred at room temperature. On warming, these changes were reversed, but optical detection of the S_{II} phase was more difficult, since the S_{III} appeared to convert continuously over several degrees to the S_I phase.

For the other smectogenic compounds derived from *p*-*n*-butylaniline, similar observations were made, although all others exhibited a nematic phase with marbled texture[5] as well.• The smectic textures for HEXOBUTA were identical in all respects with those for OCTOBUTA. For HEPTOBUTA, the textures observed were as follows: S_I, fan-shaped confocal; S_{II}, schlieren; S_{III}, mosaic texture. PENTOBUTA and BOBUTA exhibited simple fan-shaped S_I textures, while the S_{II} phase was a mosaic.

2. ABUTA and Nematogenic Homologs. For most materials examined, the nematic state was of the marbled texture and behaved normally[7] with temperature. However, ABUTA and BOMETA were peculiar in the following respect. On warming the marbled nematic phase, a front was observed to pass through the preparation within ~1° of the N → I transition temperature. Passage of this front resulted in formation of the nematic schlieren texture,[5] and was accompanied by a pronounced color (birefringence) change. These changes are illustrated for ABUTA in Figure 6a,b. The micrographs were taken immediately before and after passage of the front, within 0.2° of each other. In neither case did these changes appear reversible, *i.e.*, the schlieren texture was not readily identified on cooling the isotropic liquid. In neither case, also, was any evidence found for a caloric effect in differential thermal analysis.

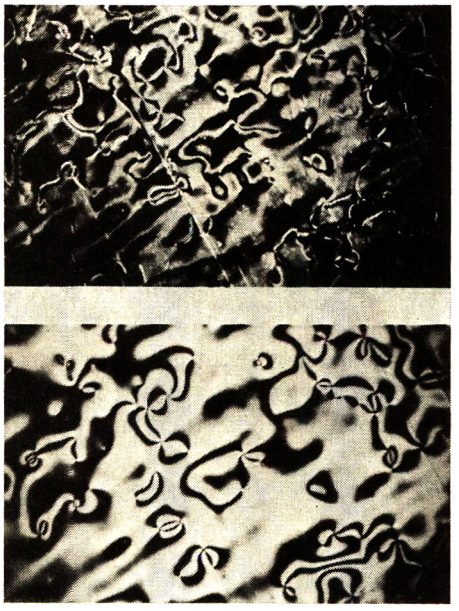

Figure 6. Photomicrographs of nematic textures of ABUTA: (a) marbled texture, 38.0°; (b) schlieren texture, 38.2°.

The nematic phase of BOBUTA was notable in that it showed a high propensity for spontaneous alignment (optic axis normal to substrate) between cover slips at the lower end of its nematic range. Thus, the $S_I \rightarrow N$ transition appeared as one to pseudoisotropy. On further warming nematic birefringence appeared.

Discussion

The aim of this work was the preparation of mesomorphic materials with low nematic–isotropic transition temperatures. The average isotropic transition temperatures for the lower homologs of three of the series prepared, *N*-*p*-methoxy, -ethoxy, and -butoxybenzylidene-*p*-*n*-alkylaniline, indicate the success of the present approach.

	CH_3O–	C_2H_5O–	C_4H_9O–
N → I av temp, °C, for C_2–C_4 anilines	42	83	72

The nematic stability for the methoxy compounds is the lowest yet reported; the relatively low transition temperatures for these compounds as a group are unique. Undoubtedly this is related to the unusual dependence of transition temperatures on constitution noted above, and discussed below.

The absence of mesomorphism in XI is attributed to strong primary attractions favoring crystallization. (Compare XII for which a nematic mesophase appears on supercooling the melt 52°.) The low polarizability of fluorine and its contribution to a permanent long-axis dipole is sufficient to reduce the residual terminal and lateral attractions which might otherwise stabilize a nematic phase.[8]

The melting points of XV and its structural isomer XVI[9] are both 91°. Yet XVI has an enaniotropic

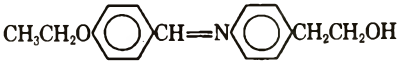

XVI

nematic mesophase,[9] while XV crystallizes at 80° from the supercooled melt without appearance of a mesophase. This contrast can be understood as indicating enhanced long-axis polarizability for XVI relative to XV if the "cogwheel" configuration is adopted by the side chains. On the other hand, primary lateral interactions may be high in XV, because of the spatial disposition of the OH group.[10]

(8) J. A. Castellano, J. E. Goldmacher, L. A. Barton, and J. S. Kane *J. Org. Chem.* **33**, 3501 (1968).

(9) J. E. Goldmacher and M. T. McCaffery, Abstracts, 158th National Meeting of the American Chemical Society, Sept 1969, No. COLL 92.

(10) More recent evidence indicates that the zigzag conformation may be the important one. If so, the spatial arrangement of end groups would be considered to dominate terminal interactions.[11]

(11) G. W. Gray, *Mol. Cryst.* **1**, 333 (1966).

Extensive studies have been made[6-9,11,12] of the relationship between molecular structure and mesomorphism in organics, particularly substituted Schiff bases. The present results in Figure 4 coincide in part with those obtained earlier, *viz.*, short alkyl or alkoxy chains are associated with nonmesomorphic or nematic behavior, while increasing chain length gives rise to smectic mesomorphism, and parallels an increase in smectic stability. Generally, the nematic–isotropic transition curve decreases with growing chain length because of diminishing residual terminal cohesive forces.[11] The present series shows the usual[11] odd–even alternation of N → I transition temperatures, but is exceptional on at least two points. (a) The curve for even members decreases for n = 2–4, and then reverses slope, for $n > 4$. (b) The curve for odd members rises monotonically with increasing n. A similar reversal in slope has been observed[7,8] for even members of two other series of *N*-alkoxybenzylideneanilines. On the other hand, the anomalous monotonic rise of the odd-member curve has only been reported[12] for *p*-*N*-alkoxybenzylidene-*p*-*n*-alkoxyanilines. It appears in those, and in the present compounds, that the stability of the nematic phase, particularly with the lower temperature materials, depends strongly on enhanced residual lateral cohesive forces with increasing chain length. It is not clear as to the causes underlying the differences between the even and odd series, although possible reasons have been suggested elsewhere.[11,12] That the residual lateral cohesions resulting from increasing polarizability as chain length increases are important in these materials for nematic stability is evidenced by the approximately parallel slopes of the N → I and S_I → N temperature curves. In fact, beyond n = 7, primary lateral cohesions become dominant and the nematic phase is replaced by the smectic I.

Even more striking examples of the unique behavior of the present series are seen in Figure 4, particularly for the methoxy and ethoxy derivatives, neither of which exhibits smectogenic behavior. The N → I transition curves both rise with increasing n (length of alkyl chain in aniline moiety). Residual terminal cohesive forces are not particularly strong in these compounds (witness the low nematic thermal stabilities). Hence, increasing residual lateral interactions strongly reinforce terminal cohesions and the nematic stability is enhanced. These are the only materials so far known in which this influence manifests itself at such low (n = 1) alkyl chain lengths.

It appears from Figure 4 that the butoxy group is required for smectogenic behavior in these anils. No smectic phases were observed for $n < 4$ in R_1, in any series. (Even with $R_1 = C_2H_5$, $R_2 = C_5H_{11}$ no smectic phase is observed.[2]) It thus appears that lengthening R_2 does not provide the same salutary effect in terms of increasing residual lateral cohesion as does lengthening R_1, at least for the lower members of these series.

The examination of textural changes accompanying phase transitions in these anils allows classification of the mesophases.[5] Thus, for OCTOBUTA (Figure 5) the sequence of transitions is seen to be

$$\text{smectic B} \rightleftharpoons \text{smectic C} \rightleftharpoons \text{smectic A} \rightleftharpoons \text{isotropic}$$

This information is particularly useful in that it now presents a further example of this relatively uninvestigated group in the scheme of polymorphism of liquid crystals by Sackman and Demus.[5] For HEXOBUTA and HEPTOBUTA, the same sequence of smectic phases was observed, based on textural manifestations. In these latter two, of course, the nematic phase separated the isotropic from smectic A. The lower homologs PENTO- and BOBUTA showed textures corresponding to smectic A and smectic B. It is on the basis of this common B texture that the low temperature smectic phases in Figure 4 are shown on the same curve for all homologs. It appears, therefore, that the smectic C phase is an intermediate one, existing only for the higher homologs.

There have been very few studies of the thermal changes accompanying transitions involving smectic phases. Arnold[6] made a calorimetric study of two mesomorphic compounds with dimorphic smectic phases. One was of the group

$$\text{smectic B} \rightleftharpoons \text{smectic A} \rightleftharpoons \text{isotropic}$$

and the other

$$\text{smectic C} \rightleftharpoons \text{smectic A} \rightleftharpoons \text{isotropic}$$

The difference in enthalpy between the smectic modifications C and A (100 joules/mol) for one compound was much smaller than the difference between B and A (2100 joules/mol) for the other. The interpretation was that differences in molecular order between C and A are much smaller than between B and A. One can conclude then that the difference between B and C is similarly large, and that in trimorphic smectic systems with the succession B → C → A with rising temperature that the largest caloric effect would occur at the lowest temperature B → C transition; that for the C → A change would be small.[13] Reference to Figures 1 and 2 shows that for HEXOBUTA and OCTOBUTA the reverse is true! The enthalpy changes accompanying the B → C transition are clearly the lowest of those involving smectic phases. For HEPTOBUTA a judgment cannot be made without precise calorimetric data. However, it is clear from at least two of the present three cases that an understanding of the molecular

(12) J. S. Dave and P. R. Patel, *Mol. Cryst.* **2**, 103 (1966); *ibid.* **2**, 115 (1966).

(13) Further evidence for this contention is found in the X-ray results of Herrmann.[14] No differences in diffraction patterns were found for adjacent A and C phases. The low temperature B phase was more highly ordered relative to the A phase.

(14) K. Herrmann, *Z. Kristallogr. Mineral. Petrogr., Abt. A*, **92**, 49 (1935).

order and phase transitions of smectic phases will require attention to the energies of such transitions, as well as correlation of same with textural phenomena observed optically.

ABUTA and BOMETA are particularly intriguing in that the passage of an additional front across the samples below the isotropic transition temperature was reminiscent of a phase change. The absence of an enthalpic effect, however, suggests the change is not a first-order transition, or at best, one with very low latent heat change. It is likely that the effects observed are pretransition,[6] representing discontinuities in other physical properties as well. An anomalous break in the specific heat *vs.* temperature curve was observed by others[15] for *p*-azoxyanisole just below the clarification point.

Some electrooptic effects have been observed in these new compounds. For example, dynamic scattering[16] is common to all those materials which exhibit nematic phases. Another example, an ac field-induced alignment in cholesteric-nematic (ABUTA) mixtures, was reported recently.[3]

The present work has made possible several new correlations of optical and thermal data on phase transformations in mesomorphics. The differences between present observations on the heats of thermal phase changes and reports by others[6] on the same transitions for related materials emphasize the need for additional studies using complementary techniques, to generate a firmer understanding of mesophase order. Furthermore, it is indicated that the role of residual lateral *vs.* residual terminal interactions in determining nematic stabilities may be more readily understood by the study of liquid crystals with low isotropic transition temperatures, as in this work.

Acknowledgment. The assistance of Joel Pollack in obtaining photomicrographs of phase textures and helpful discussions with James Adams are gratefully acknowledged.

(15) E. M. Barrall, II, R. S. Porter, and J. F. Johnson, *J. Phys. Chem.*, **71**, 895 (1967).

(16) G. H. Heilmeier, L. A. Zanoni, and L. A. Barton, *Appl. Phys. Lett.*, **13**, 46 (1968).

Solvation Effects and Ion Association in Solvent Extraction Systems. II. The Thermodynamics of Perchloric Acid in the Water–Methyl Isobutyl Ketone System[1a]

by H. Michael Widmer[1b]

Chemistry Department, Brookhaven National Laboratory, Upton, New York 11973 *(Received February 27, 1970)*

The distribution of perchloric acid between water and methyl isobutyl ketone has been studied. The solvent extraction behavior is determined by ion associates formed in the organic phase at concentrations above 10^{-4} M. Below this concentration the dissociated acid is the predominant species in the organic phase. The apparent ion association constant, (ion associates)/$(H^+)_{org}(ClO_4^-)_{org}$($K_A{}'^{org} = 1.61 \times 10^3\ M^{-1}$), describes the ion association equilibrium of the acid and includes the formation of ion pairs (H^+–ClO_4^-) as well as triple ions (ClO_4^-–H^+–ClO_4^-). The ion pair formation constant $K_A{}^{org} = (H^+ClO_4^-)_{org}/(H^+)_{org}(ClO_4^-)_{org}$ is $1.12 \times 10^3\ M^{-1}$ at 25°. Several different hydrated and solvated acidic species exist in the organic phase. At 25° and at moderate and higher acid concentrations the ion paired complex $HClO_4 \cdot 9H_2O \cdot 1MIBK$ is the major species in the organic phase. The values of the distribution constants $(H^+)_{org}(ClO_4^-)_{org}/(H^+)_{aq}(ClO_4^-)_{aq}$ and $(H^+ClO_4^-)_{org}/(H^+)_{aq} \cdot (ClO_4^-)_{aq}$ are $K_{D1} = 1.21 \times 10^{-4}$ and $K_{D2} = 1.35 \times 10^{-1}\ M^{-1}$, respectively, at 25°. An attempt is made to explain the observed differences in the solution, solvent extraction, and ion association properties of perchloric and hydrochloric acids in terms of known anion hydration models.

Introduction

The thermodynamics and solvent extraction properties of perchloric acid have been studied on many occasions. The results of different investigations are often contradictory. In solvent extraction studies, in particular, poor agreement is frequently obtained between different investigators working on the same extraction system. This may be explained in part by the variety of perchloric acid species, characterized by different hydration and solvation numbers, which exist in equilibrium with each other in the two liquid phases. In addition to the changes that occur in the primary hydration and solvation shells of the ionic species when the activity of the solvents is altered, ion association processes may also take place. These processes complicate the interpretation of the perchloric acid system. Unfortunately the study of the solvation effects has been of minor interest to the authors of several papers. Therefore, the understanding of hydration and ion association processes is incomplete even for aqueous solutions, and the thermodynamics of perchloric acid is full of controversy.

The perchlorate anion is generally considered to be inert. Not only is it supposed to lack a pronounced metal-complexing ability but its hydration is also often claimed to be weak. This argument is used to explain the observed structure-breaking properties of perchlorates in solution.[2–4] Nevertheless a number of investigators have found that perchloric acid is highly hydrated, perhaps even more than most of the other strong mineral acids.[5–9]

Probably the most thoroughly studied solvent extraction system involving $HClO_4$ is the water–$HClO_4$–tri-*n*-butyl phosphate system. It is mentioned as an example of the apparent inconsistency of published results on the properties of perchloric acid. At least five different ionic and associated species are formed in the organic phase.[10–15] The water–acid mole ratio of the extracted complexes varies from 0:1 to 8:1[10–13] and the TBP–acid mole ratio changes within the limits of 1:1

(1) (a) Research performed under the auspices of the U. S. Atomic Energy Commission; (b) address inquiries to H. M. Widmer, Department of Chemistry, University of Massachusetts, Boston, Boston, Mass. 02116.

(2) C. S. Rao, *Indian J. Phys.*, **11**, 143 (1937).

(3) H. S. Frank and W.-Y. Wen, *Discuss. Faraday Soc.*, **24**, 133 (1957).

(4) E. R. Nightingale, *J. Phys. Chem.*, **63**, 742 (1959).

(5) J. N. Pearce and A. F. Nelson, *J. Amer. Chem. Soc.*, **55**, 3075 (1933).

(6) M. A. Klochko and M. Sh. Kurbanov, *Chem. Abstr.*, **52**, 5949*b* (1958).

(7) L. Genov, *ibid.*, **51**, 17351*e* (1957); *ibid.*, **53**, 8775*i* (1959).

(8) D. P. Semchenko, I. I. Appenin, and K. L. Ushakova, *ibid.*, **53**, 12797*d* (1959).

(9) E. Högfeldt, *Acta Chem. Scand.*, **14**, 1597 1627, (1960); **17**, 785 (1963).

(10) D. G. Tuck and R. M. Diamond, *Proc. Chem. Soc.*, 236 (1958).

(11) E. Hesford and H. A. C. McKay, *J. Inorg. Nucl. Chem.*, **13**, 156 (1960).

(12) A. S. Kertes and V. Kertes, *J. Appl. Chem.*, **10**, 287 (1960).

(13) D. G. Tuck and R. M. Diamond, *J. Phys. Chem.*, **65**, 193 (1961).

(14) F. D. Shevchenko, *Chem. Abstr.*, **61**, 2535*d* (1964).

(15) V. S. Smelov, Yu. I. Vereshchagin, and A. A. Pushkov, *ibid.*, **62**, 11128*g* (1965).

and 4:1[10-15] depending on the temperature and acid concentration of the phases. The high amount of water coextracted with the acid indicates that under certain circumstances (high water activity and appropriate choice of the organic solvent) the perchlorate ion is capable of retaining part or even its entire aqueous phase hydration shell in the organic phase.

Perchloric acid generally extracts much more readily into organic solvents than does hydrochloric acid, and perchloric acid seems to be a stronger electrolyte in organic phases than most of the other mineral acids. The existence of the ion paired acid in the organic layer is often confirmed by conductance measurements and a decreasing equivalent conductance is observed with the increase of the acid concentration. But there are exceptions worth mentioning. In water-free acetic acid the equivalent conductance of perchloric acid decreases regularly with increasing acid concentration but after passing a minimum at about 10^{-2} M it increases again.[16-18] Similar observations have been made on water–dioxane mixtures.[19] According to the theory of Bjerrum[20] and of Fuoss and Kraus[21] on ion association this behavior can be explained by the formation of nonconducting ion pairs at lower acid concentrations and the formation of conducting triple ions at higher concentrations.

There are only a limited number of publications available on the extraction of perchloric acid by methyl isobutyl ketone (MIBK). Tribalat[22] and Vinarov and Byk[23] observed an increase in the distribution coefficient with increasing initial aqueous perchloric acid concentration, indicating an ion association process in the organic phase. Vinarov and Byk also claim an increase in the water content of the organic phase that parallels the acid extraction. Tribalat[24] estimated a distribution constant ($K_{D2}' = 0.17\ M^{-1}$) and derived an association constant ($K_A'^{org} = 3.3 \times 10^3\ M^{-1}$) from conductance measurements.

Experimental Section

The preparation of the organic solvent and the experimental procedure have been described elsewhere.[25] Perchloric acid (70–72%) (Baker Analyzed Reagent) was used to prepare stock solutions with triply distilled water. All solutions were kept in quartz bottles and standardized by potentiometric titration with carbonate-free sodium hydroxide.

The phase analyses were conducted so that the final acid concentration in the aqueous phase was 0.5 ± 0.1 M. In this concentration range the molar volume of $HClO_4$ varies only slightly and has a value of 44.55 ml.[26] This value was used for the volume corrections.

Results and Discussion

The symbols and terms used have been previously described.[25] The additional symbols are explained in Appendix I, where some additional equations are also derived. In order to avoid confusion the equations used in this article are numbered consecutively with the first paper of this series.

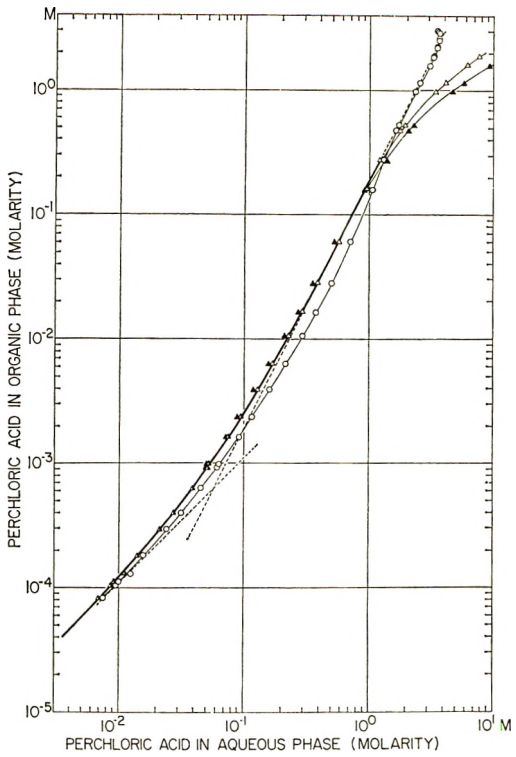

Figure 1. Distribution of perchloric acid between water and MIBK at 25° (on molar scale): ○, $C_{HClO_4}^{org}$ *vs.* C_{HClO_4}; △, $C_{HClO_4}^{org}$ *vs.* a_{HClO_4}; the activities were calculated from data published by Robinson and Stokes[28-30] and Haase, Dücker, and Küppers;[32] ▲, $C_{HClO_4}^{org}$ *vs.* a_{HClO_4}; the activities were calculated from data published by Pearce and Nelson;[5] ▲ $C_{HClO_4}^{org}$ *vs.* a_{HClO_4}; the activities were calculated from data published by Covington and Prue.[31]

Solvent Extraction Equilibria. The distribution of perchloric acid between water and MIBK at 25° is shown in Figure 1. The logarithmic plot of the organic-phase concentration *vs.* the aqueous phase acid activity

(16) I. M. Kolthoff and A. Willman, *J. Amer. Chem. Soc.*, **56**, 1007 (1934).

(17) G. Maass and G. Jander, *Fortschr. Chem. Forsch.*, **2**, 619 (1953).

(18) A. M. Shkodin, *Russ. J. Phys. Chem.*, **34**, 775 (1960).

(19) P. A. Zagorets and T. I. Yurasova, *Russ. J. Inorg. Chem.*, **10**, 1387 (1965).

(20) N. Bjerrum, *Kgl. Dan. Vidensk. Selsk., Mat.-Fys. Medd.*, **7** [9] (1926).

(21) R. M. Fuoss and C. A. Kraus, *J. Amer. Chem. Soc.*, **55**, 21, 476, 1019, 2387, 3614 (1933); *ibid.*, **79**, 3301 (1957); *ibid.*, **80**, 5059 (1958).

(22) S. Tribalat, *Ann. Chim. (Paris)*, **8**, 642 (1953).

(23) I. V. Vinarov and G. I. Byk, *Ukr. Khim. Zh.*, **29**, 929 (1963); *cf.* "Gmelins Handbuch der Anorganischen Chemie," 8th ed, Suppl. [B] "Cl," 1969, p 470.

(24) Tribalat's definitions of the equilibrium constants differ from our definitions; the values from reference 34 are converted to our approach for reasons of comparison.

(25) H. M. Widmer, *J. Phys. Chem.*, **74**, 3251 (1970).

(26) H. E. Wirth and F. N. Collier, *J. Amer. Chem. Soc.*, **72**, 5292 (1950).

is characterized by the change of slope from 1 to 2 when the acid concentration is increased. This indicates the presence of the free single ions in the organic phase at low concentrations, and the formation of ion associates beyond an organic acid concentration of 8×10^{-4} M. The observed change of slope may be caused by ion pairs or other species of the same association order. This means that the number of aqueous solute particles involved in the distribution equilibrium is twice the number of the equilibrium species in the organic phase. To a first approximation the extraction behavior can be expressed in terms of the distribution constant K_{D1} and an apparent distribution constant K_{D2}' which yield an apparent association constant $K_A'^{org}$, defined by eq 29 and 30.

$$C_{HClO_4}^{org} = K_{D1}^{1/2} a_{HClO_4} + K_{D2}' a_{HClO_4}^2 \quad (29)$$

$$K_A'^{org} = \frac{K_{D2}'}{K_{D1}} \quad (30)$$

In Appendix II it is shown that eq 29 fits reasonably well the distribution data at low and high concentrations, that is, the concentration range where the single ions and the ion associates are the predominant species, respectively. But eq 29 predicts too high values of the organic-phase concentration in the intermediate concentration range, where ion associates beyond the ion pair but of the same association order exist in the organic phase. Triple ions of the form $H(ClO_4)_2^-$ as conjugate anions of the hydrogen ions (or $H_2ClO_4^+$ as conjugate cations of the perchlorate ion) possess the same association order as the acid ion pair $H^+ClO_4^-$. Because of the common ion effect of the hydrogen or perchlorate ion, the change of slope is different for these triple ions. Using eq 29 the calculated value differs from the true organic-phase concentration by a maximum error of 49.3% if it is assumed that in the association process only triple ions but no ion pairs are formed. Smaller deviations are obtained as the ratio K_{D2}/K_{D3} increases. The extraction data plotted in Figure 1 reveal a maximum deviation of about 18%, which is well beyond the expected experimental error, indicating the formation of a triple ion in addition to the ion pair. This finding is confirmed by conductance measurements performed on organic phases. These measurements reveal the formation of a nonconducting ion pair (H^+-ClO_4^-) and a conducting triple ion ($H(ClO_4)_2^-$).[27]

In order to calculate the distribution constants of the different organic species, the activity coefficients of perchloric acid in aqueous solutions must be known. There are four different sets of activity coefficients derived by three different methods published in the literature.[5,28-32] It is not known to what power the water activity enters the distribution equilibria. The evaluation of the distribution constants and association constants is thus limited to the concentration range where the water activity remains practically unchanged at unity. This is the case for aqueous solutions below about 0.3 M. Higher concentrations would also introduce an increasing error due to changes in the activity coefficients of the organic-phase solute particles. Within this limited concentration range the published activity coefficients of aqueous perchloric acid agree to within 7% with each other, but at higher concentrations the published activities no longer agree.

Introducing the triple ion formation constant (log $K_T^{org} = 1.69$), derived by conductometric methods,[27] the true distribution constants K_{D1}, K_{D2} and the true association constant K_A^{org} can be derived in addition to the apparent constants K_{D2}' and $K_A'^{org}$. At 25° the following values are obtained by a computational best fit method.

$$K_{D1} = (1.21 \pm 0.03) \times 10^{-4}$$

$$K_{D2} = (1.35 \pm 0.04) \times 10^{-1}\ M^{-1}$$

$$K_{D2}' = (1.92 \pm 0.06) \times 10^{-1}\ M^{-1}$$

$$K_{D3} = (9.01 \pm 0.25) \times 10^{-4}\ M^{-2}$$

$$K_A^{org} = (1.12 \pm 0.03) \times 10^{3}\ M^{-1}$$

$$K_A'^{org} = (1.61 \pm 0.04) \times 10^{3}\ M^{-1}$$

$K_A'^{org}$ and K_{D2}' may be compared with the values published by Tribalat,[22] who estimated the association and distribution constants[24] to be 3.3×10^3 M^{-1} and 1.7×10^{-1} M^{-1}, respectively.

The Solvation of Perchloric Acid in the Organic Phase. The right-hand side of the binodal curves in the ternary diagram (Figure 2) can be represented over a wide range by a straight line intercepting the H_2O–MIBK base line at 100 mol % MIBK and the H_2O–$HClO_4$ base line at 10 mol % $HClO_4$. This indicates that any change of the acid concentration in the organic phase is simultaneously accompanied by a change in the water concentration in the stoichiometric mole ratio $H_2O:HClO_4$ equal to 9. This is evidence for the existence of an aquo complex $HClO_4 \cdot 9H_2O$ in the organic phase. The high hydration number of 9 is equally observed at 0, 25, and 35° (Figure 3).

Whereas at the two latter temperatures the hydration number of 9 is preserved up to the concentration of the critical point in the ternary diagram, at 0° the hydration number assumes lower values at concentrations close to the critical point resulting in a concave part of

(27) (a) H. M. Widmer, Abstracts, 158th National Meeting of the American Chemical Society, New York, N. Y., Sept 1969, No. PHYS 84; (b) H. M. Widmer, part IV of this series, in preparation.

(28) R. A. Robinson and O. J. Baker, *Trans. Proc. Roy. Soc. New Zealand*, **76**, 250 (1946).

(29) R. A. Robinson and R. H. Stokes, *Trans. Faraday Soc.*, **45**, 612 (1949).

(30) R. A. Robinson and R. H. Stokes, "Electrolyte Solutions," Academic Press, New York N. Y., and Butterworths Scientific Publications, London, 1955, pp 476, 489.

(31) A. K. Covington and J. E. Prue, *J. Chem. Soc.*, 1567 (1957).

(32) R. Haase, K. H. Dücker, and H. A. Küppers, *Ber. Bunsenges. Phys. Chem.*, **69**, 97 (1965).

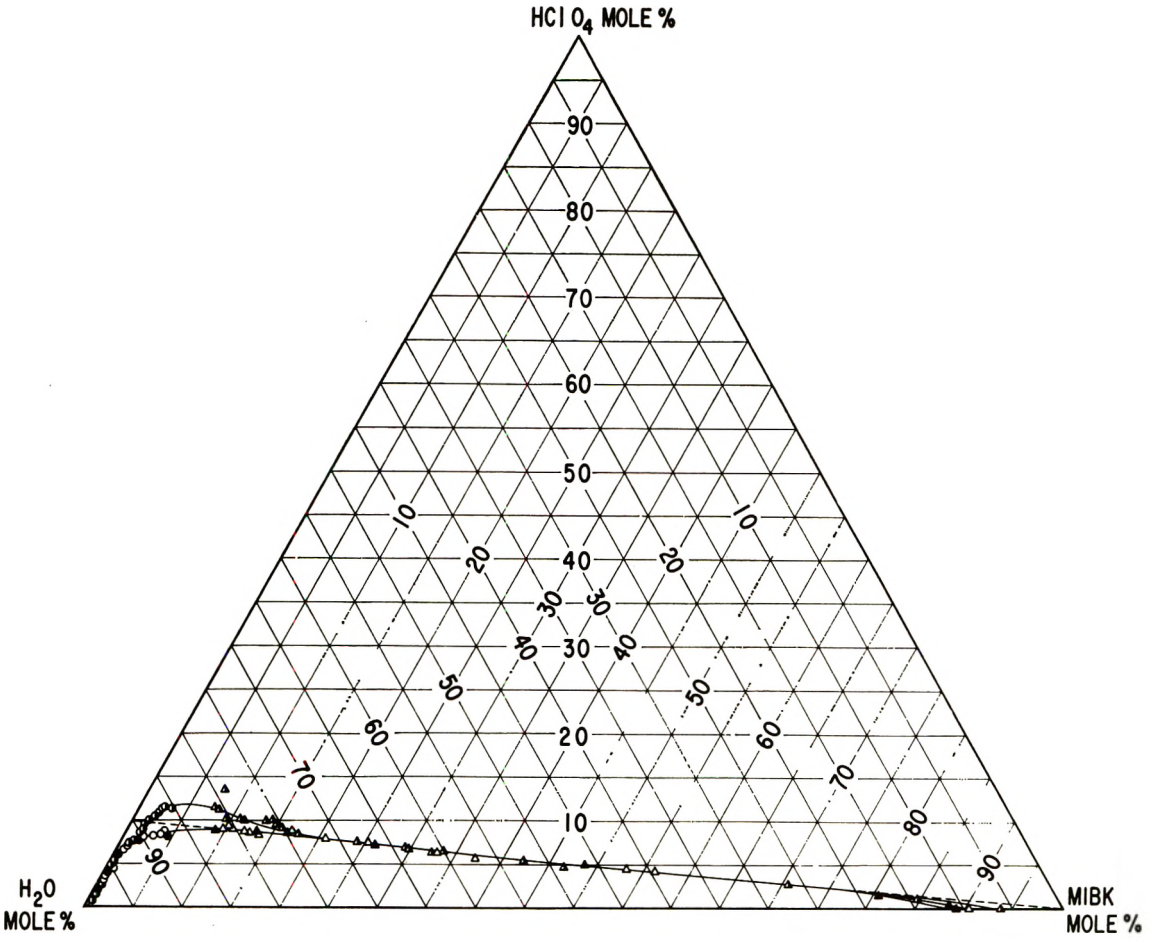

Figure 2. Ternary diagram for the H_2O–$HClO_4$–MIBK system in mole %. Circles denote aqueous phase, triangles denote organic phase: ○, △, data at 25°; ●, ▲, data at 35°; ◑, ◭, data at 0°.

the binodal curve. It is shown in studies of the H_2O–HCl–MIBK and H_2O–$HFeCl_4$–MIBK systems[25,33] that the water uptake in the organic phase with increased electrolyte concentration is due to the existence of aquo complexes in the organic phase rather than to an increased water solubility resulting from the medium changes.

The phase analysis of the organic phase reveals that at high organic concentrations the MIBK–$HClO_4$ mole ratio drops well below the limiting value of 3 observed for HCl. For concentrated organic phases a limiting value of 1.1 ± 0.1 is observed for perchloric acid at 25 and 35° and even lower results are obtained at 0° (Figure 4). The extracted species is thus $HClO_4 \cdot 9H_2O \cdot$ 1MIBK at high acid concentrations at 25 and 35°.

The hydration and solvation of the free hydrogen ion in the organic phase has been discussed previously.[25] There is no doubt that the hydronium ion is solvated by 3 water and 3 organic solvent molecules to form $H_9O_4 \cdot$ $3MIBK^+$ in the MIBK phase. The lower solvation number found for the ion pair indicates the release of solvating molecules in the ion association process.

This model assigns at least five water molecules to the hydration shell of the perchlorate ion. The phase analysis discloses that the predominant species (the ion pair) is solvated by at most one MIBK molecule. The species is therefore not simply a contact ion pair that forms without any major changes in the solvation sphere of the ions. This observation is in contrast to the results obtained with the hydrochloric acid system, and some basic difference in the hydration shell of the anions must cause this effect.

Since two MIBK molecules are removed from the hydronium ion in the process of ion pair formation, it is likely that one water molecule is shared by the anion and hydrogen ion in the ion associate. It is therefore very probable that the perchlorate ion is hydrated by six water molecules. The reduced number of solvating MIBK molecules observed for the acid ion pair might well be the result of steric hindrance caused by the bulky hydrated anion situated in close contact with the hydronium ion.

The Solvation of Perchloric Acid in the Aqueous Phase and the Solvent Extraction Mechanism. The phase analysis of the perchloric acid extraction system reveals only a slight coextraction of MIBK into the aqueous

(33) H. M. Widmer, part III of this series, in preparation.

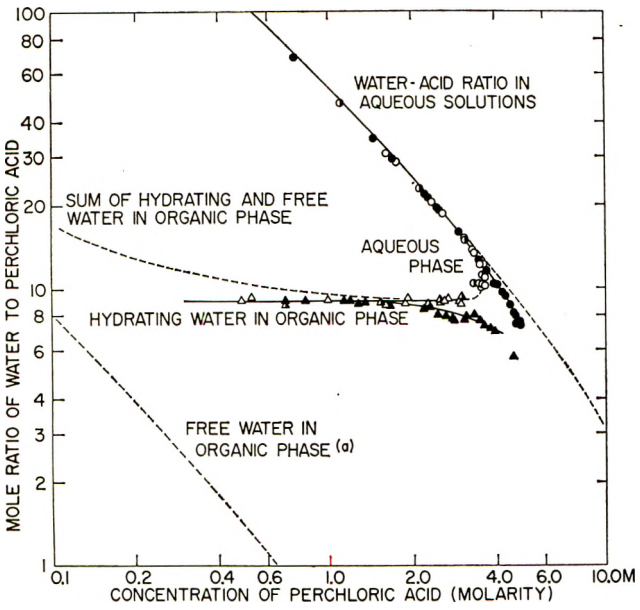

Figure 3. Mole ratio of complexed and free water to $HClO_4$ in the organic and aqueous phases as a function of the acid concentration: O, values from analysis of the aqueous phase; Δ, values from analysis of the organic phase (corrected for the solubility of MIBK in pure H_2O, as indicated by dashed line); O, Δ, data at 25°; ◑, ◭, data at 35°; ●, ▲, data at 0°; (a) solubility of MIBK in bulk water at different temperature (corrected for volume occupied by the acid complex).

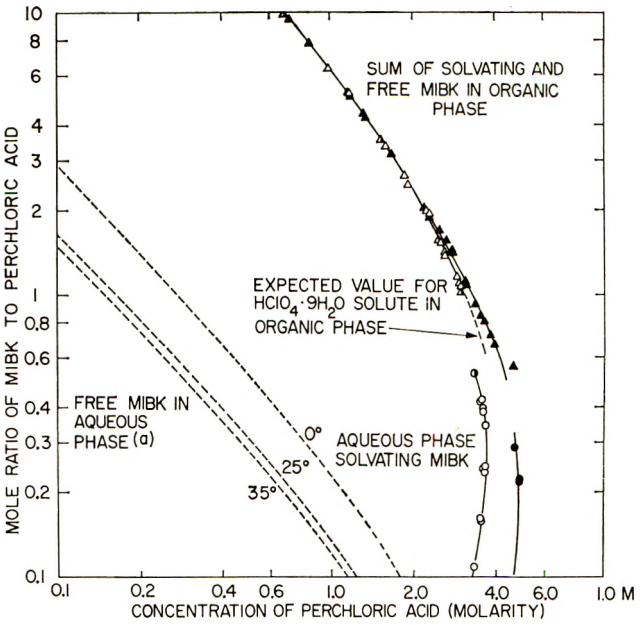

Figure 4. Mole ratio of complexed and free MIBK to $HClO_4$ in the organic and aqueous phases as a function of the acid concentration: O, values from analysis of the aqueous phase; Δ, values from analysis of the organic phase (corrected for the solubility of water in pure MIBK, as indicated by the dashed lines); O, Δ, data at 25°; ◑, ◭, data at 35°; ●, ▲, data at 0°; (a) solubility of water in bulk MIBK (corrected for the volume occupied by the acid complex).

phase (Figure 4). The mole ratio MIBK:$HClO_4$ reaches the maximum limiting value of about one only at concentrations close to the critical point in a ternary diagram. The solvation of perchloric acid beyond the hydration is therefore of minor interest, although it indicates the need for an additional solvation when the H_2O:$HClO_4$ mole ratio drops below 11:1. This may be an indication that a primary hydration number of about 10 is effective in aqueous solutions. Evidence for the existence of perchloric acid hydrated by ten water molecules in aqueous solutions was reported by both Klochko and Kurbanov[6] and Semchenko, Appenin, and Ushakova,[8] who observed a maximum of the specific conductivity in solutions with 9.2–10 mol % $HClO_4$.

Perchloric acid differs from hydrochloric acid not only in its solvent extraction behavior but also in the properties of its aqueous solutions. The perchlorate ion is known to be a structure-breaker but the chloride ion has rather structure-forming properties. These differences can be explained by two different anion hydration models, proposed by a number of investigators. The two models are represented in Figure 5. Structure A, suggested by Bernal and Fowler[34] and accepted in theoretical considerations by Eley and Evans,[35] Verwey,[36] Haggis, Hasted, and Buchanan,[37] and Muirhead-Gould and Laidler,[38] represents the interaction of atomic groups (hydrogen bonds and interactions of charges located on particular atoms). Structure B, suggested by Buckingham,[39] and Azzam,[40,41] represents the ion-dipole interaction. Everett and Coulson[42] showed that the potential energy of an isolated system in which the water molecule rotates around

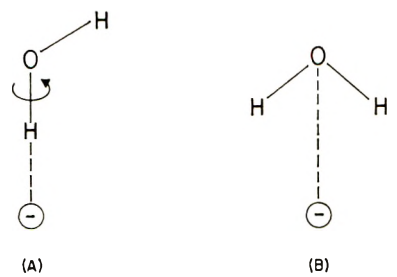

Figure 5. Orientation of water molecules in the anion hydration shell. Structure A suggested by Bernal and Fowler.[34] Structure B suggested by Buckingham[39] and Azzam.[40,41]

(34) J. D. Bernal and R. H. Fowler, *J. Chem. Phys.*, 1, 515 (1933).
(35) D. D. Eley and M. G. Evans, *Trans. Faraday Soc.*, 34, 1093 (1938).
(36) E. J. W. Verwey, *Recl. Trav. Chim. Pays-Bas*, 61, 127 (1942).
(37) G. H. Haggis, J. B. Hasted, and T. J. Buchanan, *J. Chem. Phys.*, 20, 1452 (1952).
(38) J. S. Muirhead-Gould and K. J. Laidler, *Trans. Faraday Soc.*, 63, 944 (1967).
(39) A. D. Buckingham, *Discuss. Faraday Soc.*, 24, 151 (1957).
(40) A. M. Azzam, *Z. Elektrochem.*, 58, 889 (1954).
(41) A. M. Azzam, *Can. J. Chem.*, 38, 2203 (1960).
(42) D. H. Everett and C. A. Coulson, *Trans. Faraday Soc.*, 36, 633 (1940).

its axis perpendicular to the molecular plane passes through two minima corresponding to the position represented by structure A and its mirror image. The minima are separated by a potential hill at a position represented in structure B. However the energy difference between structures A and B is small. This consideration is not complete as stated by the authors and other effects must be included in a thorough theoretical treatment. For structure A the rotational freedom around the H–O bond of the water molecule is conserved and the linkage to the bulk water structure is achieved *via* the free hydrogen atom and the electron pairs of the oxygen atom. This arrangement provides structure-forming electrolyte properties and accounts for the properties of aqueous chloride solutions. In structure B a rotation around the H–O bond is no longer possible and the linkage to the bulk water structure is achieved only *via* the electron pairs of the oxygen atom. This hydrate structure hardly fits into the structure of the bulk water and must provide structure-breaking properties.

It has been shown theoretically that structure B is unfavorable for small, simple anions and for large, complex anions some additional stabilizing effects are needed. In complex ions with strong electronegative groups, such as the perchlorate ion, a stabilization might be achieved by hydrogen bonds between a hydrating water molecule and two oxygen atoms of the anion.

These hydration models explain not only the structure-forming and structure-breaking properties of different electrolytes, but also the large differences in the solvent extraction behavior and ion association properties observed for hydrochloric and perchloric acids. Perchloric acid extracts much better than hydrochloric acid into MIBK. Its distribution constant K_{D1} is about 10^6 and K_{D2} about 10^3 times as large as for hydrochloric acid, but the ion pair formation constant is about 10^3 times as small for perchloric as for hydrochloric acid.

If a structure-forming electrolyte, such as hydrochloric acid, is extracted from an aqueous solution, several water bonds have to be broken in order to transfer the anion into the organic phase. In this process some of the water molecules situated in the primary hydration shell are released, so that the species in the organic phase carries only part of its aqueous-phase hydration shell. The species extracted into the organic phase is not a major component in the dilute aqueous phase and therefore a poor extraction ratio results. But as soon as the water activity drops, due to an increase of the electrolyte concentration, the hydration equilibrium in the aqueous phase is shifted toward the species with smaller hydration numbers and the extractable species becomes an increasingly important constituent in the aqueous phase thus increasing the extraction ratio.

If a structure-breaking electrolyte, such as perchloric acid, is extracted from an aqueous solution, only weak bonds between the primary hydration shell of the anion and the bulk water must be broken in order to transfer the anion into the organic phase. Therefore the anion is able to retain its entire or almost complete aqueous-phase hydration shell in organic solvents like MIBK. The species extracted into the organic phase resembles closely a major component in the dilute aqueous phase and a relatively high extraction ratio is observed. The water activity cannot drop too low because the well-extracted species forms a one-phase system before this happens. Only at lower temperatures, where the bulk water structure is more rigid, is the primary hydration shell of the anion weakened by the rupture and less hydrated species are observed in the organic phase. The relatively weak hydration bonds in the perchlorate ion are often broken by other effects and a number of solvents used for extraction studies are known to extract the perchlorate ion without the hydration shell.[10–15] In these systems the relative difference in the extractability of perchloric and hydrochloric acids is smaller than that observed in MIBK.

Because of its pronounced hydration in the organic phase the perchlorate anion is much more stable than the weakly hydrated chloride ion. This relative instability of the two anions is the major driving force for the ion pair formation and is expressed in the difference of the association constant K_A^{org} of the two acids.

Acknowledgments. The author wishes to express his thanks to Dr. N. Sutin for many helpful comments and suggestions. During part of this study the author held a Swiss fellowship (Stiftung für Stipendien auf dem Gebiete der Chemie).

Appendix I

To describe the thermodynamic consequences of the presence of triple ions in the organic phase a number of terms and equations must be introduced in addition to the definitions previously given:[25] $c_{H(ClO_4)_2^{-org}}$ denotes the concentration of the triple ion in the organic phase.

The total acid concentration in the organic phase can be described to a first approximation by eq 29, but for an exact description more rigorous eq 31 and 37 are needed.

$$C_{HClO_4}^{org} = c_{H^+}^{org} + c_{H^+ClO_4^-}^{org} + c_{H(ClO_4)_2^-}^{org} = c_{ClO_4^-}^{org} + c_{H^+ClO_4^-}^{org} + 2c_{H(ClO_4)_2^-}^{org} \quad (31)$$

where

$$c_{H^+}^{org} = c_{ClO_4^-}^{org} + c_{H(ClO_4)_2^-}^{org} \quad (32)$$

K_{D3} is the distribution constant of the triple ion in the organic phase

$$K_{D3} = \frac{c_{H^+}^{org} c_{H(ClO_4)_2^-}^{org}}{c_{H^+}{}^2 c_{ClO_4^-}{}^2 y_\pm{}^4} = \frac{c_{H^+}^{org} c_{H(ClO_4)_2^-}^{org}}{a_{HClO_4}{}^4} \quad (33)$$

K_T^{org} is the formation constant of the triple ion in the organic phase

$$K_T^{org} = \frac{c_{H(ClO_4)_2}^{org}}{c_{H^+ClO_4^-}^{org} c_{ClO_4^-}^{org}} \quad (34)$$

By combination of eq 5, 6, and 34 it follows that

$$K_T^{org} = \frac{K_{D3}}{K_{D1}K_{D2}} \quad (35)$$

The hydrogen ion concentration and the total acid concentration in the organic phase are given by eq 36 and 37. They are derived by the combination of eq 5, 34, and 32

$$c_{H^+}^{org} = (K_{D1}a_{HClO_4}^2 + K_{D3}a_{HClO_4}^4)^{1/2} \quad (36)$$

$$C_{HClO_4}^{org} = (K_{D1}a_{HClO_4}^2 + K_{D3}a_{HClO_4}^4)^{1/2} + K_{D2}a_{HClO_4}^2 + \frac{K_{D3}a_{HClO_4}^4}{(K_{D1}a_{HClO_4}^2 + K_{D3}a_{HClO_4}^4)^{1/2}} \quad (37)$$

The slope of a plot of log $C_{HClO_4}^{org}$ *vs.* log a_{HClO_4} is given by eq 38. It is apparent that a change of slope from 1 to 2 results when a_{HClO_4} is increased

$$\frac{d(\log C_{HClO_4}^{org})}{d(\log a_{HClO_4})} = \frac{A^2 + 2[3AC + 2C^2 + B(A + C)^{1/2}]}{A^2 + [3AC + 2C^2 + B(A + C)^{1/2}]} \quad (38)$$

where $A = K_{D1}$; $B = K_{D2}a_{HClO_4}$; and $C = K_{D3} \cdot a_{HClO_4}^2$. Expression 38 reduces to (8) if K_{D3} equals zero, that is, if no triple ions are formed.

Appendix II

To a first approximation eq 37 can be replaced by the much simpler expression 29, which also predicts a change of slope from 1 to 2 with increasing acid concentration. Here $K_{D2}'a_{HClO_4}^2$ represents the ion associate term. For the two limiting cases, where $K_{D1}^{1/2} \gg K_{D2}'a_{HClO_4}$ and $K_{D1}^{1/2} \ll K_{D2}'a_{HClO_4}$, both equations yield identical values if

$$K_{D2}' = K_{D2} + 2K_{D3}^{1/2} \quad (39)$$

where $c_{H^+}^{org} = c_{ClO_4^-}^{org}$ if $K_{D1}^{1/2} \gg K_{D2}'a_{HClO_4}$; and $c_{H^+}^{org} = c_{H(ClO_4)_2}^{org}$ if $K_{D1}^{1/2} \ll K_{D2}'a_{HClO_4}$.

In the intermediate concentration range a difference $\Delta C_{HClO_4}^{org}$ results, which has a maximum value of 49.3% of the value calculated by eq 37 when K_{D2} is equal to zero. It generally assumes smaller values depending on the relative magnitude of K_{D2} and $K_{D3}^{1/2}$.

$$\Delta C_{HClO_4}^{org} = K_{D1}^{1/2}a_{HClO_4} + 2K_{D3}^{1/2}a_{HClO_4}^2 - \frac{(K_{D1}a_{HClO_4}^2 + 2K_{D3}a_{HClO_4}^4)}{(K_{D1}a_{HClO_4}^2 + K_{D3}a_{HClO_4}^4)^{1/2}} \quad (40)$$

Determination of the Acid Dissociation Constant for Diethyldithiocarbamic Acid. The Primary and Secondary Salt Effects in the Decomposition of Diethyldithiocarbamic Acid

by Keijo I. Aspila, Serge J. Joris,[1] and Chuni L. Chakrabarti*

Department of Chemistry, Carleton University, Ottawa 1, Ontario, Canada

A primary and a secondary salt effect has been observed at low and high pH values, respectively, for the decomposition of diethyldithiocarbamic acid (Et_2DTCH). The acid dissociation constant for Et_2DTCH has been investigated in solutions of various ionic strength (μ) in order to evaluate the influence of μ on the acid dissociation constant K_c. This apparent constant, K_c, has been calculated from the ionic strength parameters and the apparent and limiting rate constants for the decomposition of the dithiocarbamic acid. A value of $(4.2 \pm 0.4) \times 10^{-4}$ has been obtained for the true acid dissociation constant K_a by extrapolation of K_c to an ionic strength equal to zero.

Introduction

A survey of the literature[2,3] on dithiocarbamic acids indicates that the acid dissociation constants (K_c) reported for these compounds are not consistent. The following investigations were made on the influence of ionic strength (μ) on the K_c value of diethyldithiocarbamic acid in order to determine if the differences in these reported values are due to variations in experimental conditions such as ionic strength. The structure of Et_2DTCH is shown below.

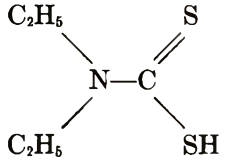

Because of the unstable nature[2b,4-6] of many dithiocarbamic acids, direct techniques[7] such as titrimetry and spectrophotometry are not very suitable for determining the K_c values; so indirect methods are required. One such method is based on the study of the decomposition rates since there is a direct relationship between the rate of decomposition and the ratio of the protonated and nonprotonated forms of the dithiocarbamate in aqueous solutions. In fact, extensive studies[4] have shown that the decomposition occurs only when the dithiocarbamate is in the protonated form. A rate equation for the decomposition process has been established by these studies. In addition to the rate constants and the proton concentration, this rate expression contains the acid dissociation constant K_c for the dithiocarbamic acid. By studying the variation of all the parameters in this equation as a function of ionic strength (μ) it should be possible to evaluate the acid dissociation constant K_c (expressed in terms of concentrations). Furthermore, the results obtained by this method can be extrapolated to zero ionic strength to obtain K_a (dissociation constant in terms of activities). A comparison with the results obtained from Debye–Hückel theory should also be possible.

Experimental Section

Reagents. The diethyldithiocarbamic acid used was obtained commercially as the trihydrated sodium salt. The percentage dithiocarbamate was determined by amperometric titration. The acid form of the dithiocarbamate was generated by addition of the sodium salt to the aqueous buffer solutions. The buffer solution corresponding to pH equal to 5.00 and of a specific ionic strength was prepared by the method of Bates.[8] The solution corresponding to pH 1.0 was prepared to various ionic strengths by the addition of appropriate amounts of KCl. Reagent grade KCl was used for all solutions to obtain a desired ionic strength.

Apparatus. A modified Bausch and Lomb Spectronic 505 recording spectrophotometer was used to study the kinetics of decomposition. Matched silica cells of 10-mm path length were used and maintained at a constant temperature of 25.0 ± 0.1°. All pH measurements were made with a Fisher Accumet pH

* To whom all correspondence should be addressed.

(1) Postdoctoral Fellow.

(2) (a) I. M. Bhatt, K. P. Soni, and A. M. Trivedi, *J. Indian Chem. Soc.*, **45**, 354 (1968); (b) A. Hulanicki, *Talanta*, **14** 1371 (1967).

(3) D. M. Miller and R. A. Latimer, *Can. J. Chem.*, **40**, 246 (1962).

(4) S. J. Joris, K. I. Aspila, and C. L. Chakrabarti, *Anal. Chem.*, **41**, 1441 (1969).

(5) D. J. Halls, *Mikrochim. Acta*, 62 (1969).

(6) H. Bode, *Fresenius Z. Anal. Chem.*, **142**, 414 (1954).

(7) A. Albert and E. P. Serjeant, "Ionization Constants of Acids and Bases," Methuen and Co., Ltd., London, 1962.

(8) N. G. Bates, "Electrometric pH Determinations," Wiley, New York, N. Y., 1954.

meter, Model 210. Standardization of this pH meter with several buffer solutions near pH 5.00 assured that the solutions of various ionic strength were accurate to within ±0.05 pH unit.

Procedure. For the kinetic studies, solutions of 10^{-3} to 10^{-4} *M* Et_2DTCH were prepared by adding a measured amount of a solution of unbuffered dithiocarbamate salt to the various buffer solutions kept in the silica cells at constant temperature. Mixing of these solutions of buffered dithiocarbamate was done with a Teflon (Du Pont) stirrer or a pipet bubbler and was completed within an average time of 6 sec before absorbance measurements were recorded. The pH values were checked before the addition of the dithiocarbamate and at the conclusion of the experiment in order to check for constancy (±0.05 pH unit).

The initial concentration for the decomposition studies ranged from 10^{-3} to 10^{-4} *M* DTC acid. The plot of the log concentration *vs.* time was found to be linear at pH 1.0 and 5.0 and at all ionic strengths. The rate constants were evaluated to an accuracy of ±2%. Absorbance measurements were made at the wavelength of maximum absorbance (about 280 nm). A small shift (5 to 10 nm) in the absorption maximum was found when the pH of the solution was changed from 5 to 1. This confirmed the findings of other workers.[3]

Theory

The stability of dithiocarbamic acids in aqueous solutions has been described in the literature.[2b,4-6] The decomposition of these acids follows a pseudo first-order rate law that is shown by

$$V = \frac{k_1[H^+]}{[H^+] + K_c}[DTC]_t = k_{app}[DTC]_t \qquad (1)$$

where V = rate of decomposition; k_1 = limiting rate constant; K_c = acid dissociation constant (based on concentration); $[DTC]_t$ = total dithiocarbamate concentration; $[H^+]$ = hydrogen ion concentration; k_{app} = apparent rate constant.

The overall rate profile[4,9] for the decomposition of the dithiocarbamic acid as a function of pH reveals a limiting rate constant at low pH (*e.g.*, pH 3). Indeed, at these pH values the above rate equation can be reduced in such a manner that k_1 equals k_{app} since the value of K_c is almost negligible compared to the hydrogen ion concentration. Study of the variation of this limiting rate constant as a function of ionic strength at these low pH values then gives the magnitude of the primary salt effect[10] on the limiting decomposition rate constant. On the other hand, at high pH values (*e.g.*, pH 5.00), the apparent rate constant (which is the measured rate constant) becomes a linear function of the hydrogen ion concentration. When $[H^+] \ll K_c$ the apparent rate constant can be written as follows

$$k_{app} = \frac{k_1[H^+]}{[H^+] + K_c} \doteq \frac{k_1[H^+]}{K_c} \qquad (2)$$

This equation implies that a secondary salt effect[10] should be observed when the apparent rate constant, k_{app}, is measured at pH 5.00 as a function of ionic strength. This is apparent from eq 2 since the rate constant is proportional to the acid dissociation constant, which is a function of the ionic strength. The following equations describe how the value of K_c can be evaluated from the above rate constants when all the parameters are known as a function of the ionic strength.

The acid dissociation constant is related to the thermodynamic acid dissociation constant K_a (expressed in terms of activities) by the relationship

$$K_c = \frac{[H^+][DTC^-]}{[DTCH]} = K_a \frac{\gamma_{DTCH}}{\gamma_{H^+}\gamma_{DTC^-}} \qquad (3)$$

where γ are molar activity coefficients and [] stands for molar concentrations.

Rearrangement of eq 2 gives the dissociation constant K_c in terms of the decomposition rate constants and the hydrogen ion concentration. This equation is

$$K_c = \frac{k_1 - k_{app}}{k_{app}}[H^+] \qquad (4)$$

However, before eq 4 can be applied to evaluate K_c, it is necessary to convert the pH meter readings of hydrogen ion activities (a_{H^+}) to hydrogen ion concentrations. Strictly speaking, such a conversion would require the use of single ion activity coefficients (γ_{m^+}) for the hydrogen ion. However, such values are difficult to obtain,[11] and in view of the errors associated with the measurement of pH and rate constants, it seems appropriate to use, as a first approximation, the mean activity coefficients ($\gamma_{m\pm}$) of HCl. Furthermore, it must be recognized that the variation of the ionic strength must not effect the junction potentials in the measurement of the pH. The use[11] of saturated KCl in the reference electrode normally gives a fairly constant junction potential for solutions of ionic strength 0.01 to 1.0. This prevents the pH from deviating more than 0.04 unit in the ionic strength range required for these kinetic studies. The conversion[12] of hydrogen ion activities to hydrogen ion concentrations is done by the use of the equation

$$\gamma_{c\pm} = \gamma_{m\pm} d_0 m/c \qquad (5)$$

where $\gamma_{c\pm}$ = mean molar activity coefficient; $\gamma_{m\pm}$ = mean molal activity coefficient; m = molality of HCl; d_0 = density of pure water; and c = molar concentration of HCl. Equation 5 relates the molal and the

(9) K. I. Aspila, V. S. Sastri, and C. L. Chakrabarti, *Talanta*, **16**, 1099 (1969).

(10) G. Pannetier and P. Souchay, "Chemical Kinetics," Elsevier, New York, N. Y., 1969, Chapter 7.

(11) I. Feldman, *Anal. Chem.*, **28**, 1859 (1956).

(12) R. A. Robinson and R. H. Stokes, "Electrolytic Solutions," Butterworths, London, 1959.

molar activity coefficients to the hydrogen ion concentration. The evaluation of the ratio m/c can be made through the approximation[12]

$$m/c = \frac{1}{d - (0.001)(c)(w_b)} \doteq \frac{1}{d} \quad (6)$$

where d = density of the solution at an ionic strength μ (obtained from reference 13); w_b = molecular weight of HCl; c = molar concentration of HCl. The above approximation[12] is valid when the concentration of HCl is low. Equations 5 and 6 may now be combined to give the following

$$\gamma_{c\pm} = \gamma_{m\pm} d_0/d \quad (7)$$

This mean molar activity coefficient ($\gamma_{c\pm}$) for the hydrogen ion may now be used to calculate the actual hydrogen ion concentration at the various ionic strengths.

$$c = [H^+] = \frac{a_{H^+} d}{\gamma_{m\pm} d_0} \quad (8)$$

The value of $\gamma_{m\pm}$ at various concentrations of KCl has been established by Harned and Owen.[14] The interpolated values from this reference have been shown in Table I. Finally, by combining eq 4 and 8, it is

Table I

Ionic strength, μ	Density[a] of solution, d	Molality of KCl, m	Mean molal activity[b] coefficient of HCl $\gamma_{m\pm}$
0.03	1.0006	0.0300	0.837
0.05	1.0010	0.0500	0.816
0.07	1.0020	0.0700	0.800
0.09	1.0027	0.0900	0.787
0.10	1.0032	0.1004	0.782
0.20	1.0075	0.2015	0.747
0.30	1.0122	0.3031	0.726
0.40	1.0172	0.4051	0.713
0.50	1.0217	0.5079	0.706
0.60	1.0262	0.6113	0.706
0.70	1.0307	0.7154	0.708
0.80	1.0355	0.8197	0.712
0.90	1.0400	0.9250	0.716
1.00	1.0445	1.0309	0.721

[a] Reference 13. [b] Interpolated from Table 14-2-1A, of ref 14.

possible to obtain an expression that relates the acid dissociation constant K_c to the decomposition rate constants at various ionic strengths. This relationship is given below by eq 9.

$$K_c = \frac{a_{H^+} d(k_1 - k_{app})}{(\gamma_{m\pm}) d_0 k_{spp}} \quad (9)$$

Results and Discussion

The variation of the limiting rate constant (k_1) and the apparent rate constant (k_{app}) as a function of ionic strength is illustrated in Figures 1 and 2, respectively.

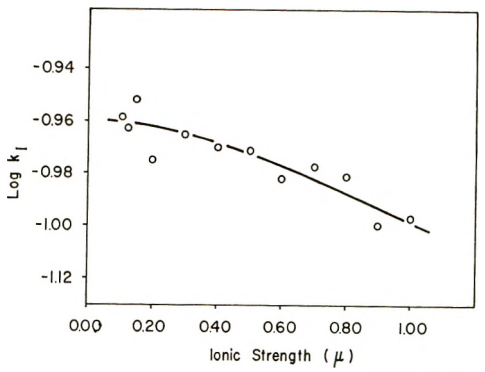

Figure 1. Variation of the limiting rate constant k_1 (sec^{-1}) for the decomposition of Et_2DTCH as a function of ionic strength (pH 1.00, 25.0 ± 0.1°): O, experimental data; —, best curve from a second-order least-squares analysis.

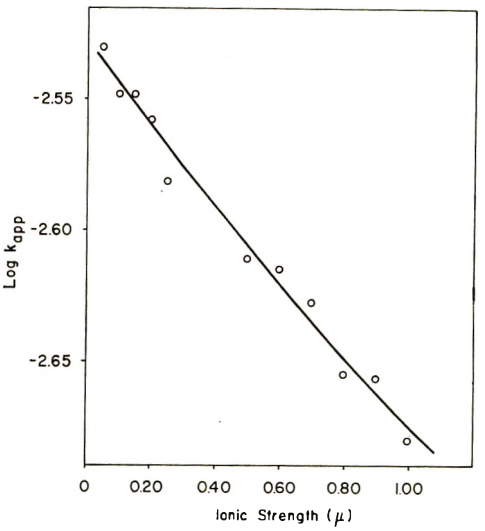

Figure 2. Variation of the apparent rate constant k_{app} (sec^{-1}) for the decomposition of Et_2DTCH as a function of ionic strength (pH 5.00, 25.0 ± 0.1°): O, experimental data; —, best curve from a second-order least-squares analysis.

In both cases (pH 1 and 5), the first-order rate constants are reduced by an increase in the ionic strength but the magnitude of the salt effect is the largest at the higher pH.

Before an interpretation of the variation in k_1 (at pH 1) can be made, it must be realized that the dithiocarbamic acid at this pH is entirely in the protonated form[4] and undergoes no further protonation or reaction before it decomposes to diethylamine and carbon disulfide. Consequently, the interpretation of the primary salt effect for this monomolecular decomposition should not involve the collision theory characteristics for a bimolecular reaction. Instead, in this case of the decomposition rate constants at pH 1 as a function

(13) "Handbook of Chemistry and Physics," 47th ed, The Chemical Rubber Co.

(14) H. S. Harned and B. B. Owen, "The Physical Chemistry of Electrolytic Solutions," 3rd ed, Reinhold, New York, N. Y., 1958.

of ionic strength, one should consider the effects of the added electrolyte (KCl) on the polarization of the solvent molecules that solvate all the species in solution. The addition of salt to water decreases the bulk dielectric constant[15] by reducing the ability of the water molecules in the hydration sphere of the ions to orientate on the application of an external electric field. Furthermore, the water molecules in the vicinity of the ions will be more polarized and will have a higher dipole moment.[15,16] Such an effect would affect the hydration of the dithiocarbamic acid at high ionic strengths. In fact, extensive studies[17] have shown that the stability of dithiocarbamic acids is dependent on the solvation of the fractional charges in the acid molecules. This solvation is directly related to the dipole moment of the solvent. Thus, when the ionic strength is increased, a higher stability is expected because of the more efficient solvation by the water molecules. Such an increase in the stability of the dithiocarbamic acid is indeed observed as can be seen in Figure 1. In addition, it should be noted that due to the dipolar character of the dithiocarbamic acid, the observed magnitude of the primary salt effect is much lower than for most bimolecular ionic processes.[18]

The variation in the apparent rate constant (k_{app}) as a function of ionic strength at the higher pH (see Figure 2) is predominantly a secondary salt effect since the decomposition process is influenced by changes in the acid dissociation constant K_c. The magnitude of K_c has been calculated from the apparent rate constant and the limiting rate constant, which have been determined at the same ionic strength μ. The additional factors necessary to calculate K_c (see eq 9) have been obtained from Table I.

Regarding Figure 3 it should be noted that there are three values (closed circles) that have been determined

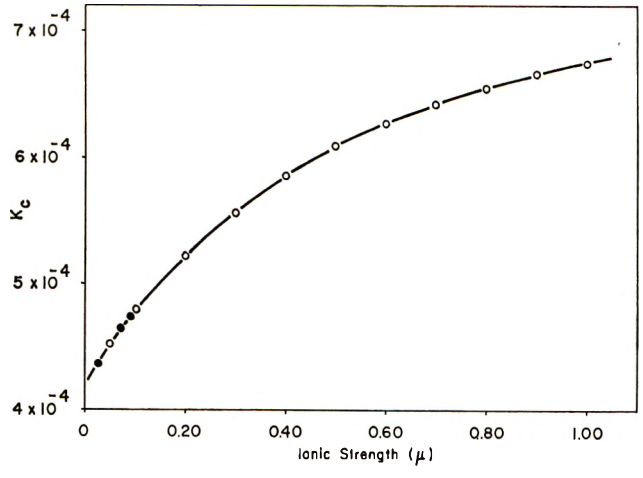

Figure 3. Variation of the acid dissociation constant K_c for Et_2DTCH as a function of the ionic strength μ: O, K_c values calculated from the least-squares curve shown in Figures 1 and 2; ●, extrapolated values using the data from Figures 1 and 2.

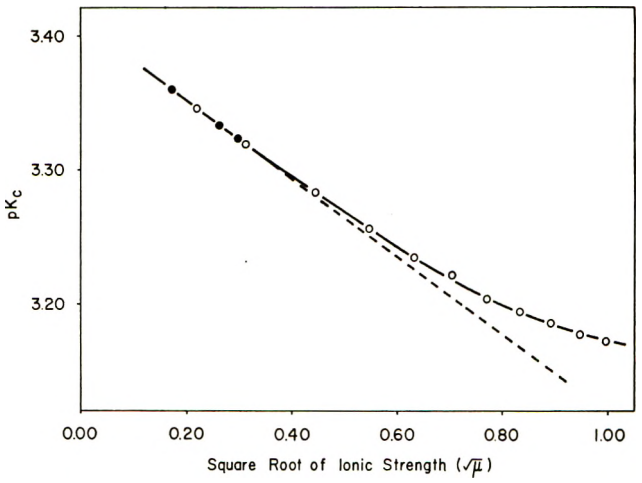

Figure 4. Variation of pK_c as a function of the square root of the ionic strength.

by extrapolation of the second-order least-squares curve shown in Figures 1 and 2. By extrapolation of the curve in Figure 3, K_a is found to be $(4.2 \pm 0.4) \times 10^{-4}$. The uncertainty in this value is due to the possible errors in the determination of the pH and the evaluation of the rate constants (k_1 and k_{app}). Although this value of K_a is comparable to the reported values,[2,3] a critical comparison is not possible since these reported values[2,3] were determined at unspecified ionic strengths.

A plot of log K_c *vs.* the square root of the ionic strength was made (see Figure 4) to determine to what extent the acid dissociation constant for Et_2DTCH agrees with the Debye–Hückel theory. Figure 4 shows that pK_c is a linear function of $\sqrt{\mu}$ only for low values of μ, which is apparently consistent with the Debye–Hückel limiting law. However, this linear relationship is observed up to $\sqrt{\mu}$ about 0.2, even though the Debye–Hückel limiting law is not normally valid at these high μ values.

To rationalize this extension of the linear relationship in Figure 4, the following three factors could be considered: (1) the size of the dithiocarbamate anion, (2) the proximity of the nitrogen and sulfur atoms, and (3) some possible change in the electronic resonance in the dithiocarbamate anion, the consequence being a change in the activity for the dithiocarbamate anion. The first two of these considerations have been dealt with by Neuberger[19,20] in the studies of the ionic strength effects

(15) G. Kortum, "Treatise on Electrochemistry," 2nd ed, Elsevier, New York, N. Y., 1965.

(16) J. E. Prue in "Chemical Physics of Ionic Solutions," B. E. Conway and R. G. Barradas, Ed., Wiley, New York, N. Y., 1966, p 166.

(17) S. J. Joris, K. I. Aspila, and C. L. Chakrabarti, *J. Phys. Chem.*, **74**, 860 (1970).

(18) S. W. Benson, "The Foundations of Chemical Kinetics," McGraw-Hill, New York, N. Y., 1960.

(19) A. Neuberger, *Biochem. J.*, **30**, 2085 (1936).

(20) A. Neuberger, *Proc. Roy. Soc., A*, **158**, 68 (1937).

on the acid dissociation constants of several amino acids which are similar to the dithiocarbamic acids but have a zwitterion character. These studies[19,20] on the amino acids indicate that the separation between the charges in the zwitterion has a definite influence on the variation of pK with ionic strength. In order to substantiate the above interpretations further work on several other dithiocarbamates is in progress.

Acknowledgment. The authors are grateful to the National Research Council of Canada for research grants. This paper will constitute part of the Ph.D. thesis of K. I. Aspila.

The Structure of the Aluminate Ion in Solutions at High pH

by R. J. Moolenaar,* J. C. Evans, and L. D. McKeever

The Dow Chemical Company, Midland, Michigan 48640 *(Received December 2, 1969)*

Infrared and Raman spectra of sodium aluminate dissolved in H_2O and D_2O and ^{23}Na and ^{27}Al nmr spectra of sodium aluminate dissolved in H_2O have been obtained in the concentration range 0.5 to 6 M. At aluminum concentrations below 1.5 M, four vibrational bands were observed in H_2O, two of them infrared active at ~950 and 725 cm^{-1}, and three Raman active at 725, 625, and 325 cm^{-1}. The ^{27}Al nmr showed a narrow resonance line. These data are consistent with the existence of the tetrahedral $Al(OH)_4^-$ as the predominant aluminum-bearing species in solution. At aluminum concentrations of about 1.5 M and above, new vibrational bands appeared at 900 (ir), 705, and 540 cm^{-1} (R). The ^{27}Al nmr resonance was considerably broadened, but no change in chemical shift was noted. These observations are interpreted in terms of the condensation of $Al(OH)_4^-$ with increasing concentration to form $Al_2O(OH)_6^{2-}$, such that in 6 M solution the two forms coexist.

Introduction

The nature of cationic aluminum species in acid solution and in mixed solvents has recently been elucidated by the use of nuclear magnetic resonance measurements. In studying ^{17}O-enriched acidified aqueous solutions of $AlCl_3$, Connick and Fiat[1] concluded that the aluminum ion was octahedrally coordinated. Similar results have been obtained for Al^{III} in aqueous mixtures of various solvents using proton magnetic resonance.[2,3] The nature of the aluminum species during the process of neutralization has been inferred from crystallographic studies of various basic salts. For example, Johansson[4] described the structure of the $[Al_{13}O_4(OH)_{24}(H_2O)_{12}]^{7+}$ ion existing in certain basic aluminum salts as having the aluminum octahedrally surrounded by oxygens, some of which form oxo bridges to other Al^{III} ions. It was inferred that the $Al(H_2O)_6^{3+}$ ion in solution undergoes hydrolysis and polymerization as the solution pH is raised, but still retains octahedral coordination. Recent potentiometric measurements on Al^{III} solutions around pH 3 have supported this conclusion.[5]

The dissolution of $Al(OH)_3$ in aqueous NaOH is well known, and serves as a key step in the extractive metallurgy of aluminum. However, the nature of the Al-bearing ion in basic solution continues to be a subject of considerable controversy. In early studies of the nature of alkaline aluminate solutions[6-8] it was concluded that discrete, nonpolymeric, nonhydrolyzed anionic species were present. However, later studies[9,10] led some workers to postulate the existence of polymeric ions such as $Al_2(OH)_{10}^{4-}$, $Al_2O_2(OH)_8^{6-}$, etc. Recently, polyvalent ions such as $Al(OH)_5^{2-}$ and $AlO(OH)_3^{2-}$ have been suggested.[11]

Raman studies by Lippincott and coworkers[12] were

* To whom correspondence should be addressed.

(1) R. E. Connick and D. N. Fiat, *J. Chem. Phys.*, **39**, 1349 (1963).

(2) A. Fratiello, R. E. Lee, V. M. Nishida, and R. E. Schuster, *ibid.*, **47**, 4951 (1967).

(3) L. D. Supran and N. Sheppard, *Chem. Commun.*, 832 (1967).

(4) G. Johansson, *Acta Chem. Scand.*, **14**, 771 (1960).

(5) E. Grunwald and D. W. Fong, *J. Phys. Chem.*, **73**, 650 (1969).

(6) T. G. Pearson, "The Chemical Background of the Aluminum Industry," The Royal Institute of Chemistry, 1955.

(7) S. I. Kuznetsov, "Production of Aluminum," Metallurgy Publishing House, Sverdlovsk, 1956.

(8) S. I. Kuznetsov and V. A. Dereogankin, "Physical Chemistry of Aluminum Production by the Bayer Method," Metallurgy Publishing House, Moscow, 1964.

(9) H. Brintzinger, *Z. Anorg. Allg. Chem.*, **256**, 98 (1948).

(10) K. F. Jahr and H. Plaetschke, *Naturwissenschaften*, **38**, 302 (1951).

(11) I. Maksimova, V. P. Mashovets, and V. Yushkevich, *Zh. Prikl. Khim.*, **40**, 2717 (1967); *J Appl. Chem. USSR*, **40**, 2594 (1967).

(12) E. R. Lippincott, J. A. Psellos, and M. C. Tobin, *J. Chem. Phys.*, **20**, 536 (1952).

interpreted in terms of a tetrahedrally coordinated $Al(OH)_4^-$ ion. Later, Plumb, and coworkers,[13] using both Raman and infrared data, concluded that two aluminate species exist; one, predominant in the pH range 8–12, whose vibrational spectrum was interpreted to indicate either a square-planar $Al(OH)_4^-$ or a polymeric six-cooordinate aluminate ion, and another, predominant in more strongly alkaline solutions, was indicated to be the linear AlO_2^- ion. The lower pH species was studied in a metastable region highly supersaturated in aluminum, and apparently is the only reported spectroscopic work in this pH range. Attempts to prepare solutions with an appreciable aluminum concentration in this pH range were unsuccessful in the present investigation.

In a detailed study of the vapor pressure of aqueous sodium aluminate solutions,[14] formation of $Al(OH)_4^-$ at low alumina concentrations, followed by gradual dehydration to AlO_2^- as the alumina concentration increased, was reported. Mal'tsev and coworkers[15] found a correlation between the proton chemical shift in aqueous aluminate solutions of varying concentration and the corresponding vapor pressure changes. This observation was interpreted as added support for the dehydration of the aluminate ion at high concentration. Furthermore, increasing the Al_2O_3 concentration caused a slight increase in ^{23}Na nuclear magnetic resonance line width, but no chemical shift was observed. Similar results had been reported on the concentration dependence of the ^{23}Na line width in aqueous NaOH.[16,17] On the basis of this similarity, Mal'tsev and coworkers reasoned that ion pairing in concentrated sodium aluminate solutions occurred as it is believed to in concentrated aqueous NaOH.

A study of the ^{27}Al nuclear magnetic resonance line widths of a variety of aluminum-containing species led O'Reilly and later Haraguchi and Fujiwara[18] to conclude that the aluminate ion has cubic symmetry. The large negative chemical shift of the ^{27}Al in basic solution, as compared to that for octahedral Al^{III} in acid solution, suggests a coordination number less than 6 for the aluminate ion. These observations are best interpreted in terms of the tetrahedral $Al(OH)_4^-$ as the predominant aluminum-bearing species in alkaline solution.

A recent review by Glastonbury[19] summarizes much of the remaining work on the structure of dissolved aluminates.

The need for the present spectroscopic study (Raman, infrared, and nmr) of the aluminate ion in highly basic aqueous solutions became apparent when solubility studies of $Al(OH)_3$ in such solutions containing other salts required interpretation;[20] although there appears to be general agreement that the predominant species is $Al(OH)_4^-$, the discordant conclusion that linear AlO_2^- is the predominant anion was reached from a Raman study which is likely the most direct method of studying the problem.

Experimental Section

Reagent grade NaOH and $Al(OH)_3$ were used in all experiments. Solution concentrations were determined using standard volumetric methods. Deuterated solutions of sodium aluminate were prepared by dissolution of metallic sodium and aluminum wire in D_2O. The 6 *M* Al solution was prepared at 200°, cooled rapidly to 52°, and filtered quickly through a medium sintered glass frit. The resulting supersaturated solution remained clear at room temperature for ~1 week. No aging effects were noted in the spectra of any of these high pH solutions. Prior to recording Raman spectra, the solutions were again filtered through an ultrafine sintered glass frit.

Potassium aluminate, $K_2[Al_2O(OH)_6]$, was prepared following Johansson's procedure,[21] and the X-ray powder diffraction pattern of the product confirmed that the same phase was obtained.[22] The deuterium substituted salt was prepared by exchange with D_2O.

Raman spectra were recorded photoelectrically, initially with a Perkin-Elmer LRI instrument and later with a Spex Ramalog instrument, using for excitation in both cases a Spectra-Physics 125 helium–neon laser emitting approximately 70 mW at 6328 Å; most recently, an argon–krypton laser (Coherent Radiation Lab) emitting approximately 200 mW at 4880 Å was used. The polarized output of the laser and an analyzer between sample and spectrometer ensured that spectra proportional to $(45\alpha^2 + 4\beta^2)$ and to $3\beta^2$ were obtained using the two standard orientations of the analyzer; α^2 and β^2 are, respectively, the isotropic and anisotropic parts of the derived polarizability tensor.

Only semiquantitative intensity measurements were made when it was found that the spectra were concentration dependent. Since the primary interest was in the lower concentration solutions, which contain one aluminate species, detailed quantitative intensity studies using internal standards were not employed to elucidate the higher concentration equilibria.

Infrared absorption spectra of thin films of solution between silver chloride plates were recorded using Herscher prism-grating instruments and a Beckman IR9 instrument. The region of interest is largely

(13) L. A. Carreira, V. A. Maroni, J. W. Swaine, and R. C. Plumb, *J. Chem. Phys.*, **45**, 2216 (1966).

(14) I. A. Dibrov, G. Z. Mal'tsev, and V. P. Mashovets, *Zh. Prikl. Khim.*, **37**, 1920 (1964).

(15) G. Z. Mal'tsev, G. V. Malinin, and V. P. Mashovets, *Zh. Strukt. Khim.*, **6**, 378 (1965); *J. Struct. Chem.* (*USSR*), **6**, 359 (1965).

(16) O. Jardelzky and J. E. Wertz, *J. Amer. Chem. Soc.*, **82**, 318 (1960).

(17) G. Z. Mal'tsev, G. V. Malinin, V. P. Mashovets, and V. A. Shcherbakov, *Zh. Strukt. Khim.*, **6**, 371 (1965); *J. Struct. Chem. USSR*, **6**, 353 (1967).

(18) (a) D. E. O'Reilly, *J. Chem. Phys.*, **32**, 1007 (1960); (b) H. Haraguchi and S. Fujiwara, *J. Phys. Chem.*, **73**, 3467 (1969).

(19) J. R. Glastonbury, *Chem. Ind.* (*London*), 121 (1969).

(20) Unpublished work.

(21) G. Johansson, *Acta Chem. Scand.*, **20**, 505 (1966).

(22) We are grateful to Mr. H. W. Rinn for this determination.

overlapped by the broad absorption band of water, which is assigned to the liquid's librational modes, but good spectra were obtained with the more concentrated solutions and with solutions in D_2O for which the librational modes appear at a lower wave number. Solvent–absorption compensation was used in attempting to improve the spectra of the dilute solutions in H_2O.

^{27}Al nmr measurements were made at 15.63 MHz on the spectrometer described by Baker and Burd.[23] Spectra were recorded in the absorption mode and were characterized by well defined Lorentzian lines. A 3 *M* $AlCl_3$ solution was used as an external reference. Chemical shifts are precise to ±0.2 ppm and line widths to ±0.004 G. Owing to improved instrumentation, these measurements are taken to be substantially more accurate and precise than previously reported values.[18] ^{23}Na spectra were run at 15.87 MHz in the absorption mode. Chemical shifts are precise to ±0.05 ppm and line widths to ±0.001 G. A 1 *M* NaCl solution was used as an external reference.

Results

Typical infrared and Raman spectra of the solutions are illustrated in Figures 1–4. Spectra are concentration dependent, the intensity changes being consistent with the presence of a single aluminate species at lower concentration (approximately 1 *M*), and the formation of a new species as the concentration of aluminate is increased. The addition of more NaOH to solutions containing the new species enhanced its concentration, but attempts to observe the effects of other added salts (perchlorate, nitrate, and chloride) were frustrated by overlapping perchlorate bands and limited solubility of the nitrates and chlorides.

Wave number data for the lower and higher concentration solutions with the estimated uncertainties arising largely from the broad nature or the low intensities are listed separately in Table I. Considerable uncertainty is associated with a broad band (definitely absent in D_2O solution) which is centered near 950 cm^{-1} in the infrared spectra of dilute solutions of aluminate in H_2O; at higher concentrations, another sharper band arises near 900 cm^{-1} and obscures this region. The ambiguity arises because the band is broad and the solvent absorption not only rapidly changes with wave number in this region but also is, solute dependent. Previous studies have established, and exploratory spectra obtained here have confirmed, that solutes influence the position and intensity of the water librational bands. Compensated spectra obtained by using films of water or of sodium hydroxide solutions in the reference beam of the instrument showed a broad absorption but with a large uncertainty in its shape; 950 cm^{-1} is an estimate of its band center.

Another region of uncertainty is near 540 cm^{-1} where an impurity infrared-absorption band induced in the silver chloride plates by concentrated NaOH solutions arose during the spectral scans.

Band intensities are low in the Raman but it was possible, with the use of the 4880-Å line under high amplifier gain conditions, to demonstrate the Raman activity of the 725-cm^{-1} band (745 cm^{-1} in D_2O) in the $3\beta^2$ spectrum where the relatively more intense isotropic scattering of the adjacent 625 cm^{-1} is absent. Spectra e of Figure 3 and c of Figure 4 show that the anisotropic scatterings of the 625- and 725-cm^{-1} bands are approximately the same while the 745-cm^{-1} band is about twice as intense as the 605-cm^{-1} band. These measurements were made on dilute solutions which did not show the

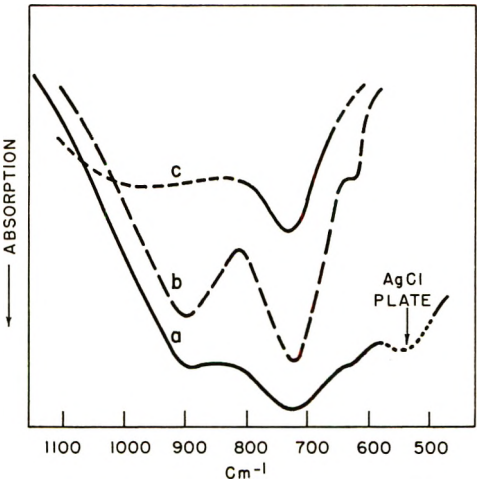

Figure 1. Infrared absorption spectra of thin films of H_2O solutions of sodium aluminate between AgCl plates: (a) uncompensated spectrum of 6 *M* Al (2.3 *M* excess NaOH); (b) spectrum a corrected for solvent absorption using 6 *M* NaOH as reference; (c) 1.28 *M* Al (1.34 *M* excess NaOH) compensated with film of H_2O in reference beam.

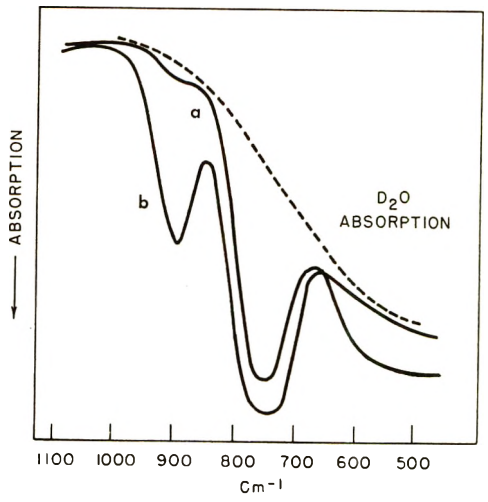

Figure 2. Uncompensated infrared absorption spectra of thin films of D_2O solutions of sodium aluminate between AgCl plates: (a) 1.5 *M* Al (~1.5 *M* excess NaOD); (b) 6 *M* Al (3.15 *M* excess NaOD).

(23) E. B. Baker and L. W. Burd, *Rev. Sci. Instrum.*, **28**, 313 (1958); **34**, 238 (1963).

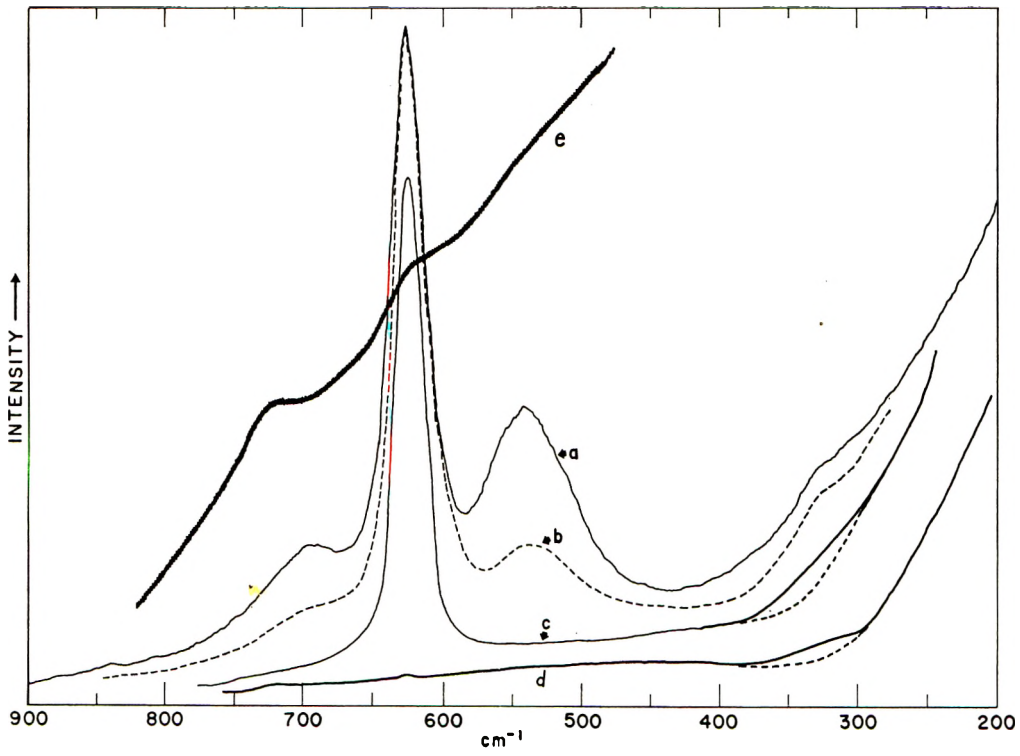

Figure 3. Raman spectra of sodium aluminate solutions in excess NaOH: (a) 5.3 M Al (2.5 M excess NaOH); (b) 2.6 M Al (1.3 M excess NaOH); (c) 0.5 M Al (0.75 M excess NaOH); (d) 1 M Al (1 M excess NaOH); (e) 1 M Al (1 M excess NaOH). Slit widths were approximately 8 cm^{-1}. Spectra a, b, and c are proportional to $45\alpha^2 + 4\beta^2$ while spectra d and e are proportional to $3\beta^2$. Spectrum e obtained under high gain illustrates the weak band near 725 cm^{-1} and the dotted lines drawn in the 300–400-cm^{-1} region under spectra c and d demonstrate the presence of a weak band occurring there in dilute solutions.

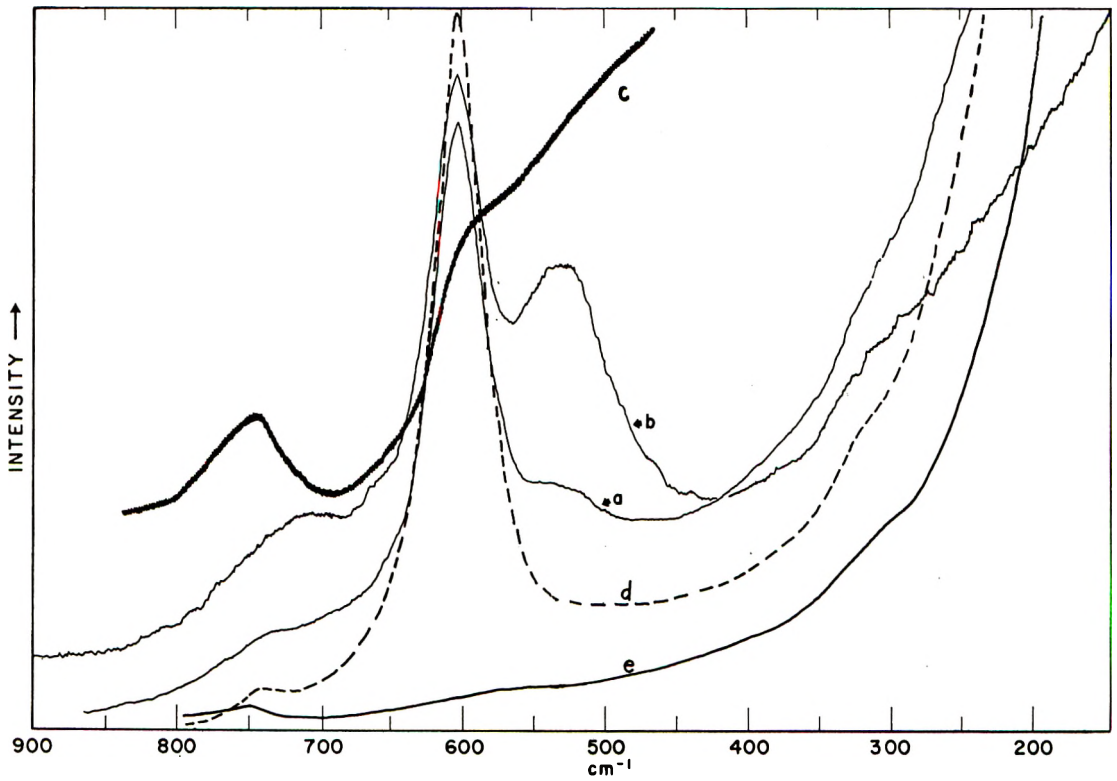

Figure 4. Raman spectra of sodium aluminate solutions in excess NaOD: (a) 1.5 M Al (1.5 M excess NaOD); (b) 6 M Al (3.2 M excess NaOD); (c), (d), and (e) 0.9 M Al (0.9 M excess NaOD). Spectra a, b, and d are proportional to $45\alpha^2 + 4\beta^2$ while c and e are proportional to $3\beta^2$; c obtained under high gain illustrates the band at 745 cm^{-1}.

Table I: Raman and Infrared Data for Sodium Aluminate Solutions[a]

Raman		Infrared	
H_2O	D_2O	H_2O	D_2O
(a) 1 *M* in Al (~1 *M* in NaOH)			
		~950 ?	
725 ± 5, vw, dp	745 ± 5, vw, dp	725 ± 5, s	745 ± 5, s
625 ± 2, s, p	605 ± 2, s, p		
~325 ± 10, vw, dp	~320 ± 10, vw, dp		
(b) 6 *M* in Al (~2.3 *M* in NaOH)			
		900 ± 5, s	895 ± 5, s
705 ± 10, m, p	725 ± 10, m, p		
		725 ± 5, s	745 ± 5, s
625 ± 2, s, p	605 ± 2, s, p	625 ± 3, vw	
540 ± 5, m, p	534 ± 5, m, p	Obscured by AgCl plate absorption	
330 ± 10, w, dp	316 ± 10, w, dp		

[a] s = strong; w = weak; p = polarized; dp = depolarized.

bands of the new species present at higher concentration.

The depolarization ratio, ρ, of the 625-cm^{-1} band in dilute solution (1 *M*, Al) was also obtained more precisely using the argon laser line at 4880 Å. In H_2O, $\rho = 0.007 \pm 0.003$ and in D_2O $\rho(605\ cm^{-1}) < 0.005$. At higher concentrations, *e.g.*, at 5 *M* in Al, ρ was still small, 0.10, and overlapping by the adjacent, less polarized bands of the new species probably contributes much to this value.

Infrared and Raman spectra of potassium aluminate obtained for comparison purposes are shown in Figures 5 and 6.

Summarized in Table II are ^{27}Al and ^{23}Na nmr data. Line widths increase with increasing concentration in the expected manner. The change in $\delta^{23}Na$ with concentration contrasts previously reported data.[15] The relatively high precision of the present measurements, however, permits detection of small chemical

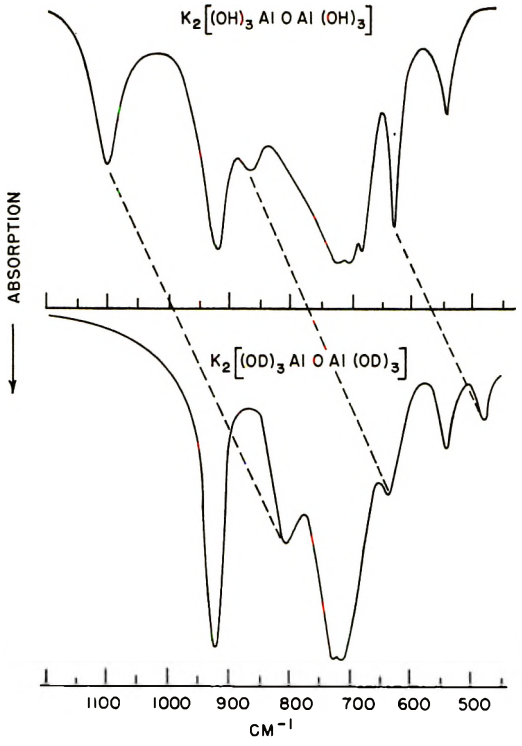

Figure 5. Infrared absorption spectra of Nujol mulls of the salt $K_2[(OH)_3AlOAl(OH)_3]$ and its deuterated analog. The dashed lines connect bands which are assigned to AlOH and AlOD bending modes.

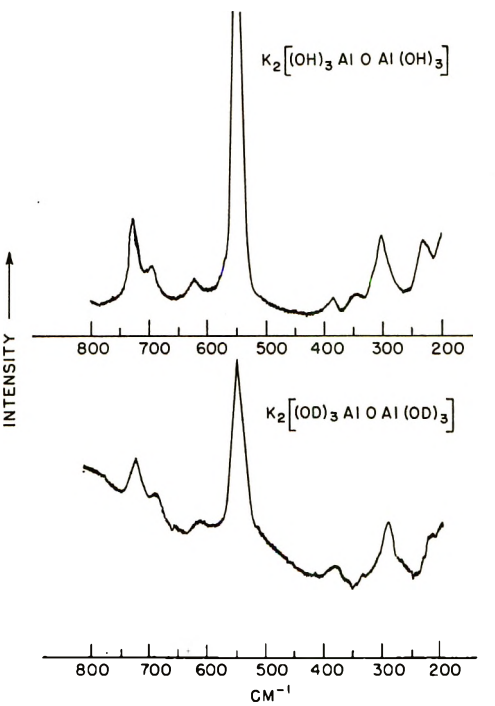

Figure 6. Raman spectra of solid samples of $K_2[(OH)_3AlOAl(OH)_3]$ and $K_2[(OD)_3AlOAl(OD)_3]$. The salts are weak scatterers and show some background due to fluorescent impurities, particularly the D compound. No bands were observed above 800 cm^{-1}.

Table II

Sample	Concn, *M* Al	Concn, *M* NaOH	Temp, °C	$\delta_{AlCl_3}{}^{27}Al$, ppm	Width, G	$\delta_{NaCl}{}^{23}Na$, ppm	Width, G
$AlCl_3$	3		27	0	0.054		
$Al(OH)_3$	0.5	0.75	27	−79.8	0.021	−0.45	0.008
$Al(OH)_3$	1.28	1.34	27	−80.0	0.041	−1.10	0.012
$Al(OH)_3$	6.0	2.0	80[a]	−79.5	> 0.2		

[a] Resonance line was too broad to observe at 27°. Substantial narrowing with increasing temperature was observed.

shift changes. In both tables, the NaOH concentrations are the quantities in excess of that necessary to form $NaAl(OH)_4$ from $Al(OH)_3$ and NaOH.

Discussion

Lower Concentration Solutions. The tetrahedral structure, $Al(OH)_4^-$, was proposed to accommodate the data obtained from the initial Raman study by Lippincott and coworkers[12] of high pH sodium aluminate solutions. The aluminate concentration was not specified. A strong band near 615 cm^{-1} and a weaker band near 310 cm^{-1} were observed. In a more recent study by Plumb and coworkers,[13] high aluminum concentrations, reportedly 4 *M*, were used in the pH range 8–13. Only the strong band at 628 cm^{-1} in both H_2O and D_2O solutions was observed. These findings prompted a reassignment; the strong, highly polarized, solvent insensitive Raman band was assigned to the totally symmetric stretching mode of a linear AlO_2^- ($D_{\infty h}$). No infrared data were reported by either worker.

In this study, stable solutions containing appreciable amounts of aluminum at pH below 13 could not be prepared; so, only those solutions of immediate practical interest with pH above 13 were examined. Comparison with Plumb and coworkers' data can thus be made only for the high pH spectra, and here there are some points of disagreement. The spectra illustrated in Figure 3 show the 628-cm^{-1} band, but it is significantly shifted (20 cm^{-1}) between H_2O and D_2O. Additionally, the spectra show a number of other bands which must be assigned to a new species favored by high aluminum and hydroxide concentrations. This species will be discussed in the next section. These discrepancies may be explained in part by the use of a much more powerful light source for the Raman measurements in this work.

The data for the dilute solution species above pH 13 show that: (1) a prominent Raman band at 625 cm^{-1} is highly polarized with a ρ value barely distinguishable from zero and is also distinctly solvent isotope dependent; (2) two other depolarized Raman bands occur near 320 and near 725 cm^{-1} which are also shifted in D_2O; (3) a strong infrared band coincides with the 725-cm^{-1} (745 cm^{-1} in D_2O) Raman band; (4) a second, broad infrared band near 950 cm^{-1} in H_2O is absent in D_2O solution, but its expected new location, near 700 cm^{-1}, is obscured by the strong 745-cm^{-1} band; (5) the ^{27}Al resonance is narrow and the chemical shift is in accord with a tetracoordinate species.[18]

These observations require an aluminate ion with approximately cubic symmetry and strongly bound hydroxy groups. Linear AlO_2^-, bent AlO_2^-, or any solvated form of AlO_2^- which retains the O–Al–O unit as the central structural feature are extremely improbable, if not conclusively eliminated, from consideration. On the other hand, no model accommodates the data as well as tetrahedral $Al(OH)_4^-$. Although the AlO_4 unit is tetrahedral, the hydrogen atoms reduce the overall symmetry, and this explains the very small departure from zero observed for the depolarization ratio of the totally symmetric stretching motion; this mode's isotope dependence is also reasonable. The prominent infrared band at 725 cm^{-1} is approximately described as the AlO_4 antisymmetric stretching mode but its upward shift to 745 cm^{-1} in D_2O shows that mixing with OH bending motions occurs to different extents in the light and heavy species. An assignment of the observed bands to the modes of this model is given in Table III.

An additional indication that $Al(OH)_4^-$ predominates in dilute solution is provided by the structure derived in the following section for the aluminate species which forms in more concentrated solutions.

Higher Concentration Solutions. In this study, the solutions of primary interest were in the lower concentration range, and the detailed Raman intensity measurements required to determine the concentration de-

Table III: An Assignment of the Raman and Infrared Bands Observed in Dilute Sodium Aluminate Solutions[a,b]

Cm^{-1}	Approximate description
~325	AlO_4 antisymmetric bending
625	AlO_4 symmetric stretching
725	AlO_4 antisymmetric stretching
~950	Al–O–H bending

[a] Descriptions are approximate only, solvent dependence shows that so-called AlO_4 modes include OH motions. [b] Lippincott, *et al.*,[12] observed the two lower wave number bands and calculated a value of 725 cm^{-1} for the AlO_4 antisymmetrical stretch using these and the tetrahedral model.

Table IV: Bands Characteristic of the Higher-Concentration Aluminate Species[a]

In H_2O, cm^{-1}	In D_2O, cm^{-1}	Spectrum
900 ± 10	895 ± 5	Infrared
705 ± 10	725 ± 10	Raman, polarized
540 ± 5	534 ± 5	Raman, polarized

[a] Bands of this species may also occur in regions overlapped by bands of $Al(OH)_4^-$, *i.e.*, near 330, 620 cm^{-1} (Raman) and 725 cm^{-1} (infrared).

pendence of the new species which was apparent in the spectra of solutions of concentrations greater than ~1.5 *M* were not made. It was, however, qualitatively established that the new species was characterized by the bands listed in Table IV, and that, although the addition of base enhanced the concentration of the new species, the degree of enhancement was not sufficient to be consistent with a proton abstraction process leading to $OAl(OH)_3^{2-}$ formation.[11]

Another process, ion-pair formation between the $Al(OH)_4^-$ and the solvated sodium ion, undoubtedly occurs, is enhanced by increasing concentrations of aluminate and sodium hydroxide, and must influence the spectra to some degree. However, this perturbation should, in itself, not influence the aluminate ion to the extent observed. It may, however, facilitate the abstraction of water from a single $Al(OH)_4^-$ ion to yield $OAl(OH)_2^-$ [14] or from a pair of $Al(OH)_4^-$ ions to yield the divalent, single-bridged species $(HO)_3AlOAl(OH)_3^{2-}$.

Monovalent, monomeric species are apparently favored for the interpretation of vapor pressure data, osmotic and other properties of the higher concentration aluminate solutions, as well as the lower concentration solutions;[6,19] and, on this basis, the dehydration process yielding $OAl(OH)_2^-$ at the first step would appear to be the more probable interpretation. The $OAl(OH)_2^-$ ion presumably has a planar or nearly planar AlO_3 skeleton but, in either case, it possesses three skeletal stretching modes which may be described approximately as Al–O stretching, $Al(OH)_2$ antisymmetric stretching, and $Al(OH)_2$ symmetric stretching. The three bands in Table IV at 900, 705, and 540 cm^{-1} may be reasonably assigned to these three modes, respectively. Analogous structures have been postulated, *e.g.*, in solutions of arsenious acid treated with base.[24]

However, in spite of this apparently satisfactory rationalization of the spectra, we prefer the alternative interpretation for the spectral changes observed in the higher concentration solutions, *i.e.*, condensation of two $Al(OH)_4^-$ ions to form the divalent $[(HO)_3AlOAl(OH)_3]^{2-}$ ion. The evidence is more direct and does not require major assumptions comparable to those necessarily made concerning water activities in interpreting osmotic and related data for concentrated solutions. The evidence rests upon a direct comparison of the solution spectra and the solid state spectra of the dimeric ion (Figures 5 and 6). Johansson[21] recently determined the structure of solid potassium aluminate *via* single crystal X-ray work, and demonstrated the presence of discrete $[(HO)_3AlOAl(OH)_3]^{2-}$ ions built up from two AlO_4 tetrahedra which share an oxygen; the bridge AlOAl angle is 132°. Comparison of Figures 1 to 6, with due account being taken of the relatively small differences attributed to the phase difference (solution–solid), shows that all the bands of the higher concentration species appear in the solid spectra and that the additional bands in the solid phase spectra, which are shown by deuterium substitution to be Al–O modes of the dimer, occur in regions obscured in the aqueous solution by the strong bands of the monomer or by the solvent. Also prominent in the solid spectra, but understandably difficult to discern in the solution spectra from the solvent absorption, are the AlOH and AlOD bending modes; the wave number ratios, 1105/805 = 1.37, 870/640 = 1.36, and 630/480 = 1.31, are those expected for the bending modes of OH groups involved in hydrogen bonding but not in appreciable interaction with other skeletal modes. The three corresponding O–H stretching modes are also well defined. The simplest interpretation is that the three OH groups at each end of the ion form, in the solid phase, hydrogen bonds of different strengths and that each of these vibrates essentially independently of the others. In aqueous solution, of course, this is no longer the case and a broad absorption band near 950 cm^{-1} which encompasses the bending vibrations of all the OH groups is a reasonable expectation. Table V summarizes the data for the solids and an approximate vibrational assignment which is based on the C_s model[21] for the $O_3AlOAlO_3$ skeleton. The three main features observed in the solution spectra (Table IV) are assigned by comparison with Table V to the Al–O stretching modes: ~900 cm^{-1} (two AlO_3 modes), ~700 cm^{-1} (four AlO_3 modes), and 545 cm^{-1} (one AlOAl mode).

The nmr data are also consistent with a dimeric aluminate species in concentrated solution. The chemical shift of $(HO)_3AlOAl(OH)_3^{2-}$ would not be expected to be appreciably different from $Al(OH)_4^-$ as observed. If the dehydrated species, $OAl(OH)_2^-$, were formed, no ^{27}Al resonance is expected because of substantial line broadening owing to an asymmetrical electrical field gradient about the aluminum nucleus.

In accord with the expected increase in contact ion pair formation in these concentrated solutions, both the ^{27}Al and ^{23}Na resonances broaden. This observation is consistent with previously reported studies of line broadening in the sodium resonance of aqueous salts.[15,17,25]

(24) T. M. Loehr and R. A. Plane, *Inorg. Chem.*, **7**, 1708 (1968).
(25) V. S. Griffiths and G. Socrates, *J. Mol. Spectrosc.*, **27**, 358 (1968).

Table V: Vibrational Spectra and Assignments for $[(OH)_3AlOAl(OH)_3]^{2-}$ and Its Deuterated Analog

$[(OH)_3AlOAl(OH)_3]^{2-}$		$[(OD)_3AlOAl(OD)_3]^{2-}$		
Infrared	Raman	Infrared	Raman	Assignment[a]
3540 m		2620 m		O′–H(D) stretch
3370 m		2510 m		O″–H(D) stretch
3275 m		2440 m		O‴–H(D) stretch
1105 m		805 m		O‴–H(D) bend
920 ms		920 ms		$\nu(AlO_3)$ A′(2)
870 mw		640 mw		O″–H(D) bend
725 s	725 mw	730 s	~725 w	$\nu(AlO_3)$ (4) A′ and A″, overlapping
700 s		710 s		
	695 w		~690 vw	
685 s				
628 m		480 mw		O′–H(D) bend
	625 w	~620 w		$\nu_{antisymmetric}$(AlOAl) A′
545 m	546 s	546 m	546 s	$\nu_{symmetric}$ (AlOAl) A′
385 sh	~385 w	380 m		Bending modes of skeleton
374 m		360 m		
344 m	~340 w	337 w		
325 m		310 m		
	302 mw	290 vw	~290 w	
270 m		265 m		
226 w	~226 w	225 vw		

[a] These descriptions are approximate labels only since all skeletal modes will involve Al–OAl and Al–OH motions.

The evidence presented here for the existence of dimeric aluminate species in concentrated solutions also lends support to the arguments given earlier for tetrahedral $Al(OH)_4^-$ at lower concentrations. If four-coordinate aluminum is present in solutions of high ionic strength, dilution would almost certainly not be expected to produce the dehydrated AlO_2^- ion. An additional interesting observation made in this study was that the spectrum of a 2 *M* aluminate solution containing both aluminate species did not change at temperatures up to 150°. Apparently, the equilibrium is not highly temperature dependent.

Acknowledgments. We thank Miss G. Y.-S. Lo and Mr. F. F. Stec for their assistance in making the vibrational spectroscopic measurements, and Mr. R. J. Hamilton and Mr. J. A. Rogers for their assistance in the experimental work.

Application of Differential Refractometry to the Measurement of Association Constants for Molecular Complex Formation[1]

by Allan K. Colter and Ernest Grunwald

Contribution from the Department of Chemistry, Brandeis University, Waltham, Massachusetts 02154
(Received May 15, 1970)

It is shown that differential refractometry can be used to investigate molecular complex formation in liquid solution. The method yields the association constant, K, and the standard volume change, $\Delta\bar{V}^0$. Aqueous solutions of potassium 3,5-dinitrobenzoate (π acceptor) and 1-naphthol (π donor) were examined by differential refractometry at 25°. Association proceeds with 1:1 stoichiometry; $K = 15 \pm 3$ l. mol^{-1} (in good agreement with an independent potentiometric determination), and $\Delta\bar{V}^0 = 10.2 \pm 0.5$ cm^3. The large positive value for $\Delta\bar{V}^0$ is discussed in terms of known properties of aqueous solutions of organic solutes.

Recently, a refractometric method for studying chemical equilibria was described and used to measure K_A and $\Delta\bar{V}^0$ for the acid dissociation of trifluoroacetic acid in water.[2] A similar method is now described for measuring the association constant, K, and standard volume change, $\Delta\bar{V}^0$, for molecular complex formation between potassium 3,5-dinitrobenzoate (K^+DNB^-) and 1-naphthol (N) in aqueous solution. There were several reasons for this study and choice of system. (1) It seemed desirable to investigate the application of the refractometric method to molecular complex formation, especially in view of recurrent questions concerning the accuracy of the spectrophotometric method[3] and of the 1:1 stoichiometry usually assumed for molecular complex formation.[4] (2) The particular system was chosen because K has been measured independently by a potentiometric method,[5] and because refractometry in water is uncommonly precise owing to the small temperature coefficient of the refractive index. (3) There is considerable interest in the measurement of $\Delta\bar{V}^0$ because of the information it might yield concerning the structure and solvation of the molecular complexes.[6]

It is clear, from the appearance of characteristic charge-transfer interaction absorption and other qualitative experiments,[5] that 3,5-dinitrobenzoate ion associates with 1-naphthol in aqueous solution. In treating our data, we assumed the formation of a single complex with 1:1 stoichiometry

$$DNB^- + N \rightleftharpoons N\cdot DNB^-$$

and were thus able to fit an extensive series of data easily within the experimental error. Although the presence of higher complexes cannot be ruled out entirely, the fact that refractometric and potentiometric[5] data, covering rather different concentration ranges, lead to 1:1 association constants in good agreement is reassuring.

While the refractometric method is more laborious than other methods if the object is solely the measurement of K, it is relatively convenient for the measurement of $\Delta\bar{V}^0$, especially if the required value of K is already available by an independent method.

In the present case, $\Delta\bar{V}^0$ has the surprisingly large value of $+10.2$ cm^3. Approximations inherent in the method (see below) are such that this value may be a lower limit. We interpret the positive sign of $\Delta\bar{V}^0$ to mean that complex formation releases water molecules from tightly-packed solvation shells around the donor and acceptor molecules into the more loosely-packed state characteristic of bulk water. The effect is too large to be ascribed entirely to release of electrostriction produced by the negative charge.

Measurement of Association Constant by Differential Refractometry. The equilibrium of interest is

$$D + A \overset{K}{\rightleftharpoons} D\cdot A$$

where D is the donor, A the acceptor, and D·A the 1:1 molecular complex. Equation 6 of reference 2, when applied to the present system, yields eq 1, where the c's are molar concentrations, and ϕ and ϕ_0 are the refractions per cm^3 of solution and solvent, respectively; $\phi = (n^2 - 1)/(n^2 + 2)$; $\phi_0 = (n_0^2 - 1)/(n_0^2 + 2)$, and n and n_0 are the corresponding refractive indices.

$$10^3(\phi - \phi_0) = 6000(n - n_0)n_0/(n_0^2 + 2)^2 = \Omega_D c_D + \Omega_A c_A + \Omega_{DA} c_{DA} \quad (1)$$

(1) Work supported in part by the National Science Foundation and the Petroleum Research Fund of the American Chemical Society. Grateful acknowledgment is made to that foundation and to the donors of that fund.

(2) E. Grunwald and J. F. Haley, Jr., *J. Phys. Chem.*, **72**, 1944 (1968).

(3) P. H. Emslie, R. Foster, C. A. Fyfe, and I. Horman, *Tetrahedron*, **21**, 2843 (1964).

(4) (a) N. B. Jurinski and P. A. D. de Maine, *J. Amer. Chem. Soc.*, **86**, 3217 (1964); (b) G. D. Johnson and R. E. Bowen, *ibid.*, **87**, 1655 (1965).

(5) D. Buben, unpublished results.

(6) A. H. Ewald, *Trans. Faraday Soc.*, **64**, 733 (1968).

The quantity Ω_J for the Jth solute is defined by eq 2, where R_J is the apparent molar refraction and V_J the apparent molar volume of the Jth solute. On introducing the stoichiometric concentrations, c_D^0 and c_A^0, of donor and acceptor into eq 1, we obtain eq 3 and 4.

$$\Omega_J = R_J - V_J\phi_0 \quad (2)$$

$$10^3(\phi - \phi_0) = \Omega_D c_D^0 + \Omega_A c_A^0 + \Delta\Omega c_{DA} \quad (3)$$

$$\Delta\Omega = \Omega_{DA} - \Omega_D - \Omega_A \quad (4)$$

In our actual experiments, the refraction ϕ_A of a solution containing A (0.01 − 0.3 M) was compared to the refraction ϕ of the same solution to which a small amount (3–5 × 10^{-3} M) of D had been added. In interpreting the difference of the two refractions, it is convenient to choose the solution containing only A as the reference solution. Because $10^3(\phi_A - \phi_0) = \Omega_A c_A^0$ substitution of $(\phi_A - 10^{-3}\Omega_A c_A^0)$ for ϕ_0 in eq 3 yields eq 5, where n_A is the refractive index of the solution containing only A.

$$10^3(\phi - \phi_A) = 6000(n - n_A)n_A/(n_A^2 + 2)^2 = \Omega_D c_D^0 + \Delta\Omega c_{DA} \quad (5)$$

To calculate K, the values of $(\phi - \phi_A)$ were treated in two ways. The first treatment, which follows, is well suited for use with a digital computer. The second treatment makes use of the more conventional reciprocal plot.[7]

Because c_D^0 is small and c_A^0 is constant, $(\phi - \phi_A)/c_D^0$ is a good experimental approximation of the partial derivative $(\partial\phi/\partial c_D^0)_{c_A^0}$. Partial differentiation of eq 5 accordingly yields expression 6.

$$10^3\left(\frac{\phi - \phi_A}{c_D^0}\right)_{c_A^0} \doteq 10^3\left(\frac{\partial\phi}{\partial c_D^0}\right)_{c_A^0} = \Omega_D + \Delta\Omega\left(\frac{\partial c_{DA}}{\partial c_D^0}\right)_{c_A^0} \quad (6)$$

On introducing the equilibrium expression 7 and performing the required partial differentiation, we obtain expression 8. To evaluate $\partial c_{DA}/\partial c_D^0$ in expression 8, we calculate c_{DA} from expression 9, which is an explicit solution of expression 7.

$$K = \frac{c_{DA}}{(c_D^0 - c_{DA})(c_A^0 - c_{DA})} \quad (7)$$

$$\left(\frac{\partial c_{DA}}{\partial c_D^0}\right)_{c_A^0} = \frac{(c_A^0 - c_{DA})}{(c_A^0 + c_D^0 + K^{-1} - 2c_{DA})} \quad (8)$$

$$c_{DA} = (1 + Kc_D^0 + Kc_A^0)/2K + [(1 + Kc_D^0 + Kc_A^0)^2 - 4K^2c_D^0c_A^0]^{1/2}/2K \quad (9)$$

K is obtained from the data by trial and error, as follows: A specific value is assumed for K. $\partial c_{DA}/\partial c_D^0$ is calculated for each experimental point according to expression 8, and the results of that calculation are tested for linear correlation with the experimental values of $(\phi - \phi_A)/c_D^0$, as required by expression 6. The calculation and test for linear correlation are repeated for various trial values of K until optimum linear fit is obtained.

The more conventional reciprocal plot[7] of eq 7, when applied to differential refractometry, takes the form of eq 10.

$$\frac{c_D^0}{10^3(\phi - \phi_A) - \Omega_D c_D^0} = \frac{1}{\Delta\Omega K}\frac{1}{c_A} + \frac{1}{\Delta\Omega} \quad (10)$$

The required value of Ω_D is obtained from measurements with solutions of D alone. $\Delta\Omega$ and K are derived from the slope and intercept of the plot required by eq 10: $\Delta\Omega$ = (intercept)$^{-1}$; K = intercept/slope. It is convenient to treat the data by successive approximations. In first approximation $c_A \doteq c_A^0$, since $c_D^0 \ll c_A^0$. The resulting estimate of K is then used to calculate c_A more precisely, and the treatment of the data is repeated until successive values of K converge.

If the calculation is made by objective statistical methods, then the assignment of appropriate statistical weights to the experimental points becomes important. In our experiments the least accurate quantity was $[10^3(\phi - \phi_A) - \Omega_D c_D^0]$, which appears on the left-hand side of eq 10. On defining X according to expression 11, the left-hand side of eq 10 becomes X^{-1}, its standard

$$X = [10^3(\phi - \phi_A)/c_D^0] - \Omega_D \quad (11)$$

deviation becomes σ_X/X^2, and the statistical weight for each point becomes X^2/σ_X. In our experiments σ_X was approximately constant, and the statistical weight for each point was taken as proportional to X^2.

Measurement of $\Delta\bar{V}^0$. Equations 6 and 10 involve two parameters: $\Delta\Omega$ and K. $\Delta\bar{V}^0$ must be obtained from $\Delta\Omega$. The basic equation, eq 12, can be derived immediately from eq 2 and 4. Because of our assumption

$$\Delta\Omega = \Delta R - \Delta V\phi_0 \quad (12)$$

of dilute-solution behavior, ΔV may be identified with $\Delta\bar{V}^0$.

Given $\Delta\Omega$, to derive $\Delta\bar{V}^0$ we need values for ϕ_0 and ΔR. ϕ_0, the specific refraction of the pure solvent, is probably known or can be measured easily. ΔR presents more of a problem.

We believe that for molecular complex formation, $\Delta R \doteq 0$. Hence $\Delta\bar{V}^0$ is given by eq 13.

$$\Delta\bar{V}^0 = -\Delta\Omega/\phi_0, \text{ with an error of } \Delta R/\phi_0 \quad (13)$$

The molar refraction R is one of the more reliable additive-constitutive properties of molecules and is well known to be quite insensitive to external conditions

(7) H. A. Benesi and J. H. Hildebrand, *J. Amer. Chem. Soc.*, **71**, 2703 (1949); R. M. Keefer and L. J. Andrews, *ibid.*, **72**, 4677 (1950).

such as temperature, pressure, and the solvent medium. The formation of a weak molecular complex produces a perturbation similar to, and only slightly greater than, that produced by a change of solvent. We therefore expect that ΔR is quite small. For the formation of charge-transfer complexes, we expect, moreover, that ΔR is small and *positive*, because at least one occupied molecular orbital becomes more delocalized owing to intermolecular charge transfer. Thus the error term $\Delta R/\phi_0$ in eq 13, if significant at all, will be positive. That is to say, the value obtained for $\Delta\bar{V}^0$ may be too small (in the algebraic sense).

Experimental Section

Materials. Potassium 3,5-dinitrobenzoate was prepared from Eastman Kodak White Label 3,5-dinitrobenzoic acid, as follows. A 50.0-g (0.236 mol) quantity of acid was dissolved by warming in a solution of 23.6 g (0.236 mol) of reagent grade potassium bicarbonate in 1 l. of distilled water. The solution was filtered while hot and evaporated to 200 ml under vacuum. On standing at room temperature, 49.8 g (84.4%) of product separated. The product was recrystallized twice from distilled water to yield yellow crystals which were dried for 8 hr at 100° and 0.1 mm over P_2O_5 before use. 1-Naphthol (Fisher Certified Reagent) was steam distilled and recrystallized twice from 65–110° petroleum ether; mp 95.0–96.5°. Distilled water was redistilled over potassium permanganate in a system protected from atmospheric carbon dioxide.

Densities and Apparent Molal Volumes. Densities of aqueous solutions of potassium 3,5-dinitrobenzoate (K^+DNB^-), prepared gravimetrically, were obtained at 25° by direct weighing in a calibrated 25-ml volumetric flask. Results are listed in Table I, and are reproduced within their experimental error by eq 14, where m is the molality.

$$\rho = 0.99709 + 0.1172m \qquad (14)$$

Equation 14 was used to convert concentrations of K^+DNB^- from molality to molarity. The apparent molal volume of K^+DNB^- is calculated from eq 14 to be 133.0 ml.

Owing to the low solubility of 1-naphthol (N) in water, it was not feasible to derive the apparent molal volume $\bar{V}_N$ from density measurements. Instead, an indirect approach was used, based on refractive index measurements and eq 2. In the following, all optical data are for λ 5775 Å. Ω was measured for N in water at 25° and found to be 21.96 ± 0.05 cm³ mol⁻¹. R for 1-naphthol, measured[8] for the pure liquid at 99.3°, is 46.33 cm³ mol⁻¹. (By comparison, R for 2-naphthol, measured[8] at 18.6°, is 46.37 cm³ mol⁻¹.) ϕ_0 for water at 25° is 0.20562. Hence $\bar{V}_N = (46.33 - 21.96)/0.20562$, or 118.5 ml, in water at 25°. The determinate error of $\bar{V}_N$ is essentially that of R/ϕ_0, and should be within 1 cm³ mol⁻¹. However, high accuracy is not required for our purposes: error analysis indicates that an error of as much as 10 cm³ mol⁻¹ would have little effect on K and $\Delta\bar{V}^0$ inferred for molecular complex formation.

Interferometry. Refractive index differences δn were measured at 25° with a Rayleigh interferometer,[9] as described by Grunwald and Haley,[2] except that measurements were taken only at wavelengths of 5461, 5775, and 6342 Å. δn at 5775 Å was then calculated by a least-squares analysis of the three readings, assuming the relationship[10] $\delta n = a\lambda^{-2} + b$. Differences between the values of δn (5775 Å) so obtained and those measured directly appeared to be random and were generally less than $\pm 1 \times 10^{-7}$, suggesting that any contribution to the refraction from charge-transfer absorption is probably negligible at these wavelengths. At 4358 Å, there was difficulty in obtaining reproducible readings for the more concentrated solutions of K^+DNB^- and for the K^+DNB^-–N mixtures, owing to optical absorption. The temperature during the measurements was maintained at 25.00 ± 0.02°, with temperature fluctuations of ±0.001° or less. It was found that the reproducibility of the readings could be improved noticeably by placing layers of aluminum foil along the sides of the cell in order to make it fit in the cell holder as snugly as possible.

Refractometric Comparisons. Refractive index differences were measured for three sets of solutions: (a) pairs of K^+DNB^- solutions of concentration c and $c + \delta c$; (b) solutions of N *vs.* pure water; (c) solutions of K^+DNB^- with N *vs.* the same solutions without N.

(a) The refractive index of aqueous K^+DNB^- was needed as a function of concentration for two reasons: to calculate ϕ_A (eq 5), since DNB^- is the acceptor molecule in complex formation; and in series c, to correct δn for the small differences in K^+DNB^- concentration that arise necessarily when a small amount of N is added to the given solution of K^+DNB^-.

To measure $\delta n_A/\delta c_A$, seven aqueous K^+DNB^- solutions covering the concentration range 0.05 m to 0.3 m were prepared gravimetrically. To weighed portions of each solution were then added weighed quantities of

Table I: Densities of Aqueous Solutions of Potassium 3,5-Dinitrobenzoate at 25.0°

Molal concentration	ρ, g/ml
0	0.99704
0.0486	1.0027
0.0989	1.0088
0.2043	1.0210
0.3097	1.0334

(8) F. Krollpfeiffer, *Justus Liebigs Ann. Chem.*, **430**, 161 (1923).

(9) E. Grunwald and B. J. Berkowitz, *Anal. Chem.*, **29**, 124 (1957).

(10) N. Bauer and S. Z. Lewin in "Technique of Organic Chemistry," Volume I, Part II, 3rd Ed., A. Weissberger, Ed., Interscience, New York, N. Y., 1960, p 1151.

water to obtain slightly more dilute solutions for refractometric comparison. Concentrations were converted from molality to molarity using eq 14. Differences in concentration, δc, ranged from about 2.5×10^{-3} to 4.3×10^{-3} M and were accurate to $\pm 0.02\%$. Results for $\delta n_A/\delta c_A$ at 25° and 5775 Å varied with concentration and are described, within their experimental precision of 0.3%, by eq 15. Integration of eq 15, and introduction of n_0 for pure water at 25° and 5775 Å, leads

$$\delta n_A/\delta c_A = 4.509 \times 10^{-2} - 4.506 \times 10^{-3} c_A - 1.240 \times 10^{-2} c_A^2 \quad (15)$$

$$n_A = 1.332874 + 4.509 \times 10^{-2} c_A - 2.253 \times 10^{-3} c_A^2 - 4.133 \times 10^{-3} c_A^3 \quad (16)$$

to eq 16. The curvature described by eq 15 is experimentally significant and merits further investigation.

(b) Four aqueous solutions of 1-naphthol, covering the concentration range 0.002 to 0.004 m, were prepared gravimetrically and compared refractometrically with pure water. Concentrations were converted from molality to molarity using the density of pure water and the value of $\bar{V}_N$ reported above. The concentrations are accurate to about 0.2%, the limitation being the accuracy to which 1-naphthol could be weighed. Results are listed in Table II.

(c) To obtain $10^3(\phi - \phi_A)/c_D^0$ at constant c_A^0, we proceeded as follows. Thirteen aqueous solutions of K^+DNB^-, covering the concentration range 0.011 to 0.3 m, were prepared gravimetrically. To a weighed portion of each solution was added a weighed amount of 1-naphthol, such that the concentration of N was in the range 0.002 to 0.005 m. Concentrations were converted from molality to molarity using the density data for aqueous K^+DNB^- reported above and (in the final calculations) representing the apparent molal volume N by the equation $\bar{V}_N = (118.5 + 10.5\alpha)$ ml, where α is the fraction of N that is associated with DNB^-. The term 10.5α accounts for the volume change owing to molecular complex formation and was obtained in an early cycle of calculations. It is slightly different from the final "best value." Similarly, α is calculated on the slightly erroneous assumption that $K = 14$. Actually, addition of the term 10.5α has little effect on the final results and was done more for the sake of consistency than of necessity.

δn was measured by comparison of the solution containing $K^+DNB^- + N$ with its mother solution, which contained K^+DNB^- alone. Since the latter solution was slightly more concentrated in K^+DNB^-, δn was corrected on the basis of eq 15 so that the data used in the investigation of molecular complex formation would represent identical concentrations of K^+DNB^-. The corrections ranged from 0.1% to 4%, increasing with the concentration of K^+DNB^-. Values of $(\phi - \phi_A)/c_D^0$ derived from the corrected values of δn were quite reproducible: of eleven duplicate measurements reported in Table II, ten differ by less than 0.3%.

Table II: Results of Differential Refractometry for Aqueous Solutions of Potassium 3,5-Dinitrobenzoate and 1-Naphthol at 25° and 5775 Å

K^+DNB^- c_A^0, mM[a]	N c_D^0, mM[b]	$10^3(\phi - \phi_A)/c_D^0$ (c_A^0 = constant)[c]
		21.89
		22.04
		21.94
		21.98
10.86	3.648	21.76
10.86	3.652	21.76
20.24	5.496	21.61
20.24	3.662	21.58
29.81	4.699	21.46
29.81	3.644	21.39
31.58	2.077	21.29
39.83	4.459	21.22
39.83	4.257	21.28
45.48	3.033	21.13
49.85	4.017	21.13
49.85	3.954	21.12
60.09	4.827	20.94
60.09	5.079	20.93
74.57	4.732	20.95
74.57	3.857	20.89
98.99	4.470	20.86
99.00	4.087	20.73
141.8	3.874	20.64
141.8	3.143	20.58
177.2	5.005	20.44
177.2	3.706	20.44
286.7	3.313	20.32
286.7	2.453	20.32

[a] Experimental error less than 0.1%. [b] Experimental error 0.1–0.3%. [c] Corrected for dilution of the reference K^+DNB^- solution by the addition of N, on the basis of eq 15. See text. Experimental error 0.1–0.3%.

Results

Refractometric results for aqueous solutions of 1-naphthol at a series of 3,5-dinitrobenzoate concentrations are compiled in Table II. The measurements are so extensive because we had decided to secure as much information as possible by refractometry alone, and the effect of complex formation was relatively small: $\Delta\Omega$ was only about 10% of Ω_D. The data are plotted in Figure 1. The plot shows clearly that as c_A^0 becomes large, $10^3(\phi - \phi_A)c_D^0$ approaches a constant limit, which implies with high probability that association does not involve an infinite series of steps but stops after a single step. If that be granted, then the absence of systematic curvature in Figure 2 shows that the association complex that is formed is a 1:1 complex.

Unfortunately, the calculation of K for 1:1 complex formation from the data entails considerable loss of

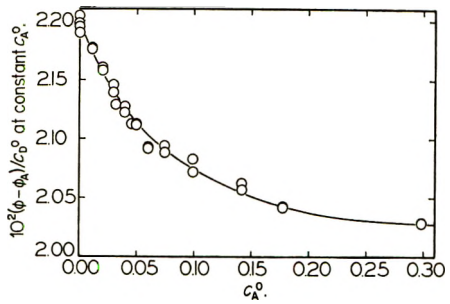

Figure 1. Results of differential refractometry for aqueous solutions of potassium 3,5-dinitrobenzoate and 1-naphthol at 25° and 5775 Å. Values of $(\phi - \phi_A)$ have been corrected for small differences in c_A in the actual refractometric comparisons.

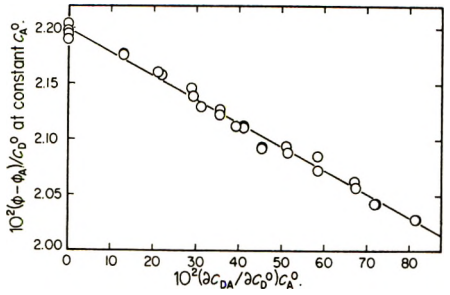

Figure 2. Plot of data in Table II according to eq 6–8 (K = 15).

accuracy. The results of our statistical analysis are presented in Table III. Somewhere between K = 14 and K = 16, the correlation coefficient goes through a maximum and the standard error of fit goes through a minimum. In that region the correlation coefficient is satisfactorily high and the standard error of fit is consistent with the experimental precision. Outside that region the fit deteriorates noticeably. We conclude that K is defined by the data as 15 + 3(M^{-1}) with a relative error of ±20%. Correspondingly, $\Delta\Omega$ is defined as −2.10 ± 0.10,

Table III: Interpretation of Refractometric Data on the Basis of 1:1 Molecular Complex Formation

K (assumed)	$\Omega\Delta$, cm³	r[a]	σ,[b] %
	Calculations Based on Eq 6, 7, and 8		
12.0	−2.21 ± .05	0.9868	0.28
14.0	−2.13 ± .04	0.9893	0.26
14.5	−2.11 ± .04	0.9895	0.25
15.0	−2.10 ± .04	0.9896	0.25
15.5	−2.08 ± .04	0.9896	0.25
16.0	−2.07 ± .04	0.9895	0.25
18.0	−2.01 ± .04	0.9878	0.27
	Results of Reciprocal Plot (Eq 10)		
14 ± 1	−2.17 ± .11	"Best values"	

[a] Correlation coefficient for fit of data in Table II to eq 6, 7, and 8. [b] Standard error of fit for *the same data*.

with a relative error of ±5%. On applying eq 13, we then find that $\Delta\bar{V}^0$ = 10.2 cm³, with a precision of ±0.5 cm³ and an additional determinate error, $\Delta R/\phi_0$, that we expect to be comparatively small. The most direct evidence that ΔR is negligible at 5775 Å is our observation, described in the Experimental Section, that δn at 5461, 5775, and 6342 Å closely follows a two-parameter Cauchy relationship[10] for all pairs of solutions compared, showing that the increased absorption near 4000 Å caused by molecular complex formation is too weak to exert an effect. This charge-transfer absorption appears only as an enhancement at the long-wavelength end of the K^+DNB^- absorption spectrum and has its band maximum below 4000 Å.

An independent potentiometric study of complex formation between 3,5-dinitrobenzoate ion and 1-naphthol in water[5] leads to K = 16.3 ± 0.6(M^{-1}) at 30°. That study was carried out using 0.0015 M 1-naphthol–0.0005 M potassium naphthoxide buffer, 0.045 M to 0.1 M K^+DNB^-, and enough potassium chloride to make a total ionic strength of 0.1 M. Since the magnitude of $\Delta\bar{H}^0$ for molecular complex formation is usually quite small, we may neglect the 5° difference in temperature and conclude that the potentiometric and refractometric values for K are in good agreement.

Discussion

An interesting result of the present study is the substantial positive value found for $\Delta\bar{V}^0$. This result is strikingly different from the values of −2 to −12 cm³ that were found by Ewald[6] for $\Delta\bar{V}^0$ of complex formation between a series of aromatic hydrocarbon donors and a group of π acceptors in methylcyclohexane and methylene chloride. We wish to consider two possible reasons for the difference: the fact that our acceptor is an ion while Ewald's are nonelectrolytes, and the fact that our studies were carried out in aqueous solution.

A positive $\Delta\bar{V}^0$ could result from release of electrostriction around the carboxylate group of 3,5-dinitrobenzoate ion on molecular complex formation. An estimate of the maximum contribution to $\Delta\bar{V}^0$ by this mechanism can be made as follows. The apparent molar volumes of acetic acid[11] (54.0 cm³) and hydrogen ion[12] (−5.4 cm³) together with $\Delta\bar{V}^0$ for acid dissociation of acetic acid[11] (−9.2 cm³) lead to −50.2 cm³ for the apparent molar volume of acetate ion, all data being for aqueous solutions at 25°. Assuming that $\bar{V}_{OAc^-} \doteq \bar{V}_{HOAc}$ in the absence of electrostriction, we obtain an estimate of 50.2 − 54.0 = −3.8 cm³ for $\Delta\bar{V}$ resulting from electrostriction of water by the carboxylate group in the acetate ion. The volume decrease resulting from electrostriction by the more weakly basic DNB^- anion should be somewhat smaller,[13] and it does not seem rea-

(11) B. B. Owen and S. R. Brinkley, *Chem. Rev.*, **29**, 461 (1941).
(12) R. Zana and E. Yeager, *J. Phys. Chem.*, **71**, 521 (1967).
(13) W. Kauzmann, A. Bodanszky, and J. Rasper, *J. Amer. Chem. Soc.*, **84**, 1777 (1962).

sonable that complex formation with 1-naphthol should reduce this amount by more than half. Consequently, we estimate that release of electrostriction can contribute no more than 1–2 cm^3 to the observed 10.2 cm^3 for $\Delta\bar{V}^0$ of complex formation.

Most of the volume increase appears to result from the peculiar properties of organic solutes in aqueous solution. There is much evidence to suggest that the partial molal volumes of organic solutes with "hydrophobic" exposed groups are substantially smaller in dilute aqueous solution than in dilute solution in nonpolar solvents, or than the molar volumes of the pure liquid solutes.[14-16] For example, the apparent molar volume of benzene in dilute aqueous solution is 6.4 cm^3 less than the molar volume of pure liquid benzene at 25°.[16] The corresponding volume loss for toluene is 8.57 cm^3.[17] The extent of the contraction appears to increase with increasing size of the nonpolar portion of the molecule.[15,18] Evidently the water molecules are packed more tightly near the nonpolar surfaces of organic solute molecules than in the bulk water region. To explain the positive value of $\Delta\bar{V}^0$, we then need to postulate only that complex formation between 1-naphthol and 3,5-dinitrobenzoate ion reduces the total nonpolar surface area per mole of complex and thus displaces some water molecules into the more loosely packed state characteristic of the bulk water region. The experimental value of $\Delta\bar{V}^0$, after allowing for release of electrostriction, is quite similar to the volume change when toluene is transferred from dilute aqueous solution to pure liquid toluene, and hence of a plausible magnitude.

(14) F. Franks and D. J. G. Ives, *Quart. Rev., Chem. Soc.*, **20**, 1 (1966), and references cited.

(15) F. Franks in "Physico-Chemical Processes in Mixed Aqueous Solvents," F. Franks, Ed., Heineman Ltd., London, 1967, p 61.

(16) W. L. Masterton, *J. Chem. Phys.*, **22**, 1830 (1954).

(17) J. E. Desnoyers and F. M. Ichhaporia, *Can. J. Chem.*, **47**, 4639 (1969).

(18) F. Franks and J. M. Quickenden, *Chem. Commun.*, 388 (1968).

Electron Impact Studies. II. Stannous Bromide and Stannic Bromide

by D. J. Knowles,*

Department of Physical Chemistry, University of Melbourne, Parkville, Victoria, Australia 3052

A. J. C. Nicholson, and D. L. Swingler

Division of Chemical Physics, CSIRO, Chemical Research Laboratories, Clayton, Victoria, Australia 3168
(Received April 7, 1970)

Ionization efficiency curves are given for the ions produced by electron impact on stannous bromide and stannic bromide. Ionization potentials are given for the parent molecules and derived for some of the radical fragments. Ionization potentials for the group IV halides and subhalides are discussed.

Introduction

As part of a study of the vapor-phase reactions of the metal halides, ionization potentials (I.P.) and fragment appearance potentials (A.P.) were needed. A previous paper[1] gives data for tin chlorides and this paper gives similar data for tin bromides. Ionization efficiency (I.E.) curves were measured for the ionization of $SnBr_2$ and $SnBr_4$ by electrons. A discussion of the available IP of the group IV halides MX_{1-4} is given.

Experimental Section

The quadrupole mass spectrometer and Knudsen cell assembly used have been described previously.[1,2] The experimental procedure employed for the electron impact (E.I.) measurements was identical with that used in the previous study of chlorides.[1] It has been our experience with E.I. studies of the vapors over heated inorganic halides that the apparent electron energy as measured by the circuit voltmeter increased slowly with time. This most likely reflects a gradual build up of a salt layer on the ion source during experimentation which results in changes in contact and surface potentials. For this reason the I.E. curve of the reference gas was measured frequently during the exper-

* All correspondence should be directed to D. J. Knowles, Preston Institute of Technology, St. Georges Road, Preston, Victoria, Australia 3072.

(1) A. S. Buchanan, D. J. Knowles, and D. L. Swingler, *J. Phys. Chem.*, **73**, 4394 (1969).

(2) J. W. Hastie and D. L. Swingler, *High Temp. Sci.*, **1**, 46 (1969).

iments and the ion source was electropolished after any one set of measurements.

$SnBr_2$ (Alfa Inorganics) was contained in a silica-lined Knudsen cell and heated under dynamic vacuum at *ca.* 200° for 12 hr prior to taking measurements. $SnBr_4$ (Hopkins & Williams) was admitted *via* a gas leak. The mass spectra of these compounds showed no impurity ions and the isotope patterns agreed with those calculated from the known abundance ratios of tin and bromine. The Knudsen cell was held, to ±1°K, at temperatures suitable to give adequate ion currents (575°K for $SnBr_2$, room temperature for $SnBr_4$). The ion source temperature was 410°K.

Results

I.E. curves are shown in Figure 1 and the results assembled in Table I. The reactions postulated are numbered in the table and referred to in the text by these numbers. A.P. values were calculated exactly as in ref 1 assuming that all ions are formed in their ground states and carry no excess kinetic energy. The calculations establish that the postulated reactions are reasonable ones. It is recognized that the methods used for determining I.P. and A.P. (semilog plot and "initial break") can give erroneous values but such values are almost always too high. Knowledge of the upper bound of an A.P. is still useful in disentangling reaction mechanisms, particularly in determining whether products are formed by ion–molecule or molecule–molecule reactions.

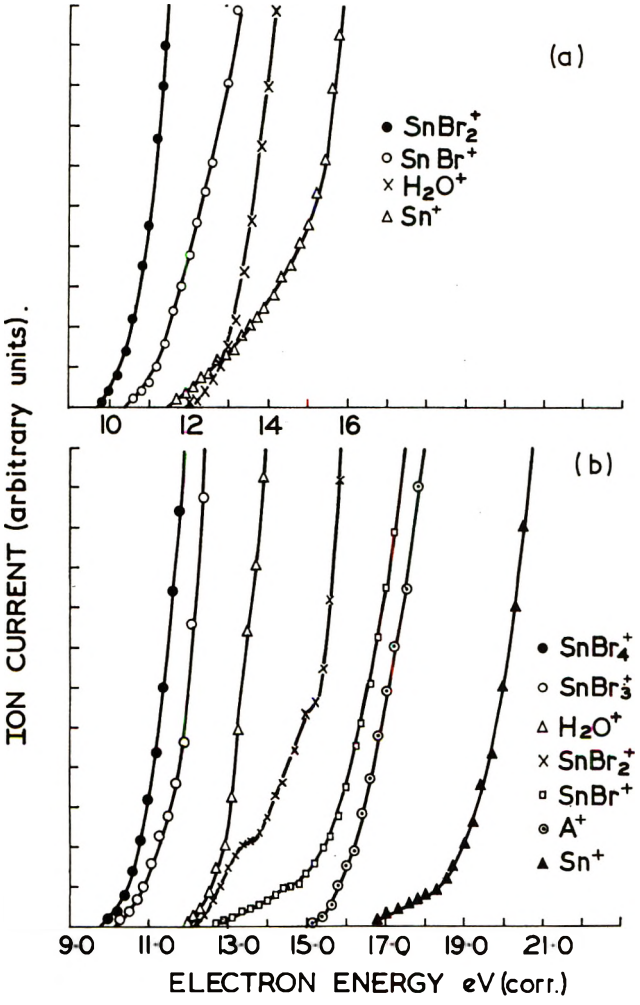

Figure 1. Ionization efficiency curves: (a) stannous bromide; (b) stannic bromide.

$SnBr^+(SnBr_2)$. The A.P. of the $SnBr^+$ fragment from $SnBr_2$, A.P.[$SnBr^+(SnBr_2)$], is related to the bond dissociation energy in the molecule, D(BrSn–Br), and the I.P. of the radical SnBr by

$$\text{A.P.}[SnBr^+(SnBr)] \geq \text{I.P.}(SnBr) + D(\text{BrSn–Br}) \quad (1)$$

D(BrSn–Br) is equal to the heat of atomization, $\Delta H_{at}°$, of $SnBr_2$, less D(Sn–Br). $\Delta H_{at}°(SnBr_2)$ = 6.8 eV.[3] D(Sn–Br) is not known accurately, Feber[4] gives 3.2 eV and Gaydon[5] favors 2.0 ± 1.0 eV. The higher value gives a minimum D(BrSn–Br) = 3.6 eV; substituting this value and the upper limit of A.P.[$SnBr^+(SnBr_2)$] from Table I gives I.P.(SnBr) < 7.8 eV.

$Sn^+(SnBr_2)$. This is the least abundant ion from $SnBr_2$ and gives rather featureless I.E. curves. Figure 1 shows a representative example and all curves for this ion showed changes in slope at 14.5 and 12.8 eV. These are interpreted as due to the onset of reactions 3 and 4 and the signal below 12.8 eV assumed to be due to the ion-pair process 5.

$SnBr_3^+(SnBr_4)$. $D(Br_3Sn–Br)$ is not known but estimating it as half the difference between $\Delta H_{at}°$ ($SnBr_4$) and $\Delta H_{at}°(SnBr_2)$, 2.2 eV, should not cause a large error. The A.P. for reaction 7 and the equivalent equation to 1 give I.P.($SnBr_3$) < 9.5 eV.

$SnBr_2^+(SnBr_4)$. The major reaction producing this ion has its onset around 15.2 eV and corresponds to reaction 8. At lower voltages 9 and 10 contribute and the steeper step-shape of the lowest portion of this curve supports the view that reaction 10 produces an ion pair.

$SnBr^+(SnBr_4)$. The I.E. curve for this ion does not show well defined break-points. It seems probable that the onset around 15.0 eV is due to reaction 11.

$Sn^+(SnBr_4)$. This I.E. curve has a relatively small "foot" (≃2 eV) compared to that for the same ion from $SnCl_4$ (≃7 eV).[1] Reaction 14 seems to be the only one occurring and there was no evidence for reaction 15 or an ion-pair process equivalent to that occurring in the $SnCl_4$ case.

Discussion

The experimental I.P. values of the molecules and radicals MX_{1-4} (M = group IV metal, X = halogen

(3) T. L. Cottrell, "The Strengths of Chemical Bonds," 2nd ed, Butterworths, London, 1958.

(4) R. C. Feber, "Heats of Dissociation of Gaseous Halides," LA-3164, TID-4500, UC-4 Chem., 1965.

(5) A. G. Gaydon, "Dissociation Energies and Spectra of Diatomic Molecules," 2nd ed, Chapman and Hall, London, 1953.

Table I: Appearance Potentials for Ions from $SnBr_4$ and $SnBr_2$

Ion	Parent molecule	Postulated reaction (neglecting electrons)	A.P., eV, measd	A.P., eV, calcd[a]
$SnBr_2^+$	$SnBr_2$	(1) $SnBr_2 \rightarrow SnBr_2^+$	10.0 ± 0.4[b]	
$SnBr^+$	$SnBr_2$	(2) $SnBr_2 \rightarrow SnBr^+ + Br$	11.0 ± 0.4[b]	
Sn^+	$SnBr_2$	(3) $SnBr_2 \rightarrow Sn^+ + 2Br$	14.5 ± 1.0	14.1
		(4) $SnBr_2 \rightarrow Sn^+ + Br_2$	12.8 ± 1.0	12.1
		(5) $SnBr_2 \rightarrow Sn^+ + Br^- + Br$		10.7
$SnBr_4^+$	$SnBr_4$	(6) $SnBr_4 \rightarrow SnBr_4^+$	10.6 ± 0.4[b]	
$SnBr_3^+$	$SnBr_4$	(7) $SnBr_4 \rightarrow SnBr_3^+ + Br$	11.3 ± 0.4[b]	
$SnBr_2^+$	$SnBr_4$	(8) $SnBr_4 \rightarrow SnBr_2^+ + 2Br$	15.2 ± 1.0	14.5
		(9) $SnBr_4 \rightarrow SnBr_2^+ + Br_2$	13.6 ± 1.0	12.5
		(10) $SnBr_4 \rightarrow SnBr_2^+ + Br^- + Br$	12.0 ± 1.0	11.1
$SnBr^+$	$SnBr_4$	(11) $SnBr_4 \rightarrow SnBr^+ + 3Br$	15.0 ± 1.0	15.5
		(12) $SnBr_4 \rightarrow SnBr^+ + Br_2 + Br$	13.7 ± 1.0	13.5
		(13) $SnBr_4 \rightarrow SnBr^+ + Br^- + 2Br$		12.1
Sn^+	$SnBr_4$	(14) $SnBr_4 \rightarrow Sn^+ + 4Br$	18.5 ± 1.0	18.6
		(15) $SnBr_4 \rightarrow Sn^+ + Br_2 + 2Br$		16.6

[a] Using values I.P.(Sn) = 7.3 eV, C. E. Moore, "Atomic Energy Levels," National Bureau of Standards Circular 467, U. S. Government Printing Office, Washington, D. C., 1958. E.A.(Br) = 3.4 eV, H. B. Gray, "Electrons and Chemical Bonding," W. A. Benjamin, New York, N. Y., 1965, p 34. $D(Br_2)$ = 2.0 eV,[5] D(Sn–Br) = 3.2 eV,[4] $\Delta H_{at}°(SnBr_4)$ = 11.3 eV,[3] $\Delta H_{at}°(SnBr_2)$ = 6.8 eV,[3] and I.P. ($SnBr_2$) and (SnBr) from this work. [b] Semilog treatment.

except iodide) can be divided into three groups with fairly well separated IP.

1. MX_4 Molecules. Values for these I.P., all ≥ 10.6 eV, are given in Table II together with the values of the halogen molecules. The I.P. of any particular halide is very close to that of the corresponding halogen, of a mixed halide to that of the halogen with the lowest I.P. This is a clear indication that the electron removed on ionization comes from a lone pair orbital on the halogen. To a good approximation the energy of this orbital can be regarded as unaffected by the largely covalent bond between the halogen and the valency saturated metal. This is also true for organic halides,[6] group III halides, $InCl_3$,[7] $SbCl_3$,[6] $AsCl_3$,[6] boron halides,[8] but not for group I halides.[9]

2. MX_2 Molecules and MX_3 Radicals. Here the I.P. (Table III) lie between 9 and 10.5 eV and the distinction between halogens has almost disappeared. These I.P. are well above those for the metal atom. The bond angles employed (determined and estimated) for various calculations on some of these species by Margrave, *et al.*,[10,11] suggest that the central atom is sp^3 hybridized. Hence the ionized electron comes from a nonbonding hybrid orbital which would be expected to be lower in energy (have a higher I.P.) than the atomic orbital of

Table II: I.P. for MX_4 (M = Group IV Element, X = Halogen or Hydrogen + Halogen)

Molecule	I.P. exptl,[a] eV	Molecule	I.P. exptl, eV	Molecule	I.P. exptl,[a] eV
CF_4	<15.0	$SiCl_4$	12.06	F_2	15.7
CCl_4	11.47	$GeCl_4$	11.6,[b]	Cl_2	11.48
CCl_3F	11.77		11.9[a]	Br_2	10.55
CH_2ClBr	10.75	$GeBr_4$	10.8[b]		
SiF_4	15.4	$SnCl_4$	11.5[c]		
		$SnBr_4$	10.6[d]		

[a] Reference 6. [b] Reference 11. [c] Reference 1. [d] This work.

Table III: I.P. for MX_3 and MX_2 (M = Group IV Element, X = Halogen)

Molecule	I.P., exptl, eV	Molecule	I.P., exptl, eV
CF_3	10.1[a]	$GeCl_2$	10.4[d]
CCl_3	8.78[a]	$GeBr_2$	9.5[d]
$GeCl_3$	9.3[b]	$SnCl_2$	10.2[c]
$GeBr_3$	8.8[b]	$SnBr_2$	10.0[c]
$SnCl_3$	9.5[c]	$PbCl_2$	10.3[e]
$SnBr_3$	9.1[c]	$PbBr_2$	10.2[e]

[a] Reference 6. [b] These values were calculated using the data in reference 11 in the same way as calculated for $SnCl_3$, reference 1, and $SnBr_3$, this work. [c] This work. [d] Reference 11. [e] J. W. Hastie, H. Bloom, and J. D. Morrison, *J. Chem. Phys.*, **47**, 1580 (1967).

(6) (a) R. W. Kiser, "Introduction to Mass Spectrometry and Its Applications," Prentice-Hall, Englewood Cliffs, N. J., 1965; (b) J. L. Franklin, J. G. Dillard, H. M. Rosenstock, J. T. Herron, K. Draxl, and F. H. Field, "Ionization Potentials, Appearance Potentials, and Heats of Formation of Gaseous Positive Ions," *Nat. Stand. Ref. Data Ser., Nat. Bur. Stand.* (*U. S.*), **26** (1969).

(7) D. J. Knowles and D. L. Swingler, unpublished work.

(8) R. J. Boyd and D. C. Frost, *Chem. Phys. Lett.*, **1**, 649 (1968).

(9) J. W. Hastie and J. L. Margrave, *Fluorine Chem. Rev.*, **2**, 77 (1968).

(10) J. W. Hastie and J. L. Margrave, *J. Phys. Chem.*, **73**, 1105 (1969).

(11) O. Manuel Uy., D. W. Muenow, and J. L. Margrave, *Trans. Faraday Soc.*, **65**, 1296 (1969).

Table IV: Some Energies Associated with the Group IV Subhalides

Molecule	I.P., exptl,[a] eV	I.P., calcd, eV (b)	I.P., calcd, eV (c)	I.P.(M),[d] eV	I.P., calcd,[b] − I.P., exptl	I.P.(M), − I.P., exptl
CF	8.9	11.55	8.9	11.25	2.65	1.35
SiF	7.3, 7.5	6.1	7.49	8.15	−1.2, −1.4	0.65, 0.85
SiCl		(7.6)[e]	7.36			
GeF	7.3, 7.8	6.5	7.56	7.88	−0.8, −1.3	0.58, 0.08
GeCl	7.2	7.6	7.28		0.4	0.68
GeBr	7.3	7.9			0.6	0.58
SnF	7.0, 7.8	6.8		7.34	−0.2, 1.0	−0.46, 0.34
SnCl	6.4, 6.8	7.7, 7.3			1.3, 0.5	0.96, 0.54
SnBr	7.4	7.2			−0.2	−0.06
PbF	7.4	7.5		7.42	0.1	−0.06
PbCl	7.5	8.1			0.6	−0.08
PbBr	7.8	8.3			0.5	−0.38

[a] CF, SiF, GeF, SnF, PbF, PbCl, and PbBr from reference *e*, Table III. GeCl and GeBr calculated from data in reference 8; SnCl and SnBr this work. [b] Reference 9. [c] Reference 10. [d] Reference 6. [e] Estimated in ref 9.

the metal. The I.P. of the radicals are about 1 eV lower than those of the molecules which presumably represents the difference between removing an electron from a half-filled and a filled orbital.

3. MX Radicals. I.P. for MX are given in Table IV which is an updated version of Hastie and Margrave's Table 5[9] with "estimated" values removed. Values are largely below 8 eV and again there is little difference between the halogens. Columns 3 and 4 give the I.P. calculated by the method used by Hastie and Margrave,[9] which is based on the postulate that the radical has a 100% ionic structure, M^+X^-, which proved adequate for group I halide molecules. Column 6 gives the deviations of the calculated from the experimental values and it can be seen that they are both large and random in sign. It would seem more profitable to compare the radical I.P. with the I.P. of the metal. Column 7 gives the difference I.P.(M) − I.P.(MX) and this varies as M goes down the periodic table from an appreciable positive deviation to an almost negligible negative value. Clearly the ionized electron comes from a molecular orbital constructed mainly from an atomic orbital of the metal and the radical structure is largely covalent. Hastie and Margrave's method[9] is not therefore suitable for the monohalides of this group.

Acknowledgment. D. J. K. wishes to thank Dr. A. L. G. Rees for the hospitality extended to him at the Laboratories of the Division of Chemical Physics, CSIRO.

A Field Emission Study of the Decomposition of Acetylene and Ethylene on Tungsten[1]

by Robert S. Hansen* and Nelson C. Gardner

Institute for Atomic Research and Department of Chemistry, Iowa State University, Ames, Iowa 50010
(Received May 22, 1970)

The adsorption, surface diffusion, and decomposition of acetylene and ethylene on tungsten were studied by field electron emission microscopy (FEEM). Surface diffusion characteristics provided evidence that the (110) and (211) planes are planes of high site density for acetylene adsorption and that the (211) and (111) planes are planes of high site density for ethylene adsorption. These findings are in good accord with known tungsten pair densities if both species are assumed associatively diadsorbed by σ bonding. Work function–temperature plots give features indicating a single dehydrogenation step for acetylene, and dehydrogenation of ethylene in two steps *via* an acetylene intermediate, in good agreement with flash desorption results. Both work function–temperature plots and emission patterns provide evidence of carbon migration above 700°K (after complete dehydrogenation). A carbon predose accelerates the first dehydrogenation of ethylene but markedly inhibits the dehydrogenation of acetylene (whether dosed *per se* or formed from ethylene). A simple approximate method for estimating activation energies and their coverage dependence is presented and applied to the acetylene dehydrogenation reaction.

Introduction

"No problems in surface chemistry have been more hotly debated than the adsorption and hydrogenation mechanisms for ethylene, and few debates have resulted in such meager conclusions." This 1962 view of Selwood[2] was restated in the 1964 review of Bond and Wells.[3] By far the majority of catalytic hydrogenation studies have involved the inference of surface reactions from observations of changes in the gaseous environment of the surface. The existing uncertainty in ethylene chemisorption and hydrogenation mechanisms makes these problems particularly attractive for investigation by techniques such as low energy electron diffraction, surface infrared spectroscopy, field electron emission microscopy, and field ion emission microscopy permitting direct observation of properties of surface structures.

The field emission electron microscope (FEEM) was invented by Müller in 1937[4] and good general discussions of its properties are to be found in reviews by Good and Müller[5] and Hansen and Gardner[6] and a book by Gomer.[7] It resembles a small television tube; electrons emitted from a tiny cathode impact a phosphor screen to provide an image which can be photographed and a current which can be measured. It offers a number of attractive possibilities for surface chemical research, including the following. (1) It is easily adapted to ultrahigh vacuum techniques permitting ambient partial pressure control at the 10^{-10} Torr level or better. (2) Metal emitter tips are generally obtained in single crystal form, crystal faces can be indexed from emission pattern symmetries, and in favorable cases processes assigned to crystal faces. (3) The tube can be operated immersed in liquid helium. In this mode all materials except hydrogen desorbed from the tip are instantly condensed on the walls. While the tube walls are at 4°K the tip can be heated electrically to any desired temperature. (4) The tip can be dosed to provide coverage on one side only, and surface migration on heating can be directly observed. (5) The emission current i is related to the tube voltage V and metal work function φ by the Fowler–Nordheim equation[5]

$$i = AV^2 \exp\{(-B\varphi^{3/2})/V\} \qquad (1)$$

where A and B are known functions. Hence, work functions can be obtained from the slope of a plot of ln (i/V^2) against $1/V$ (a Fowler–Nordheim plot). Changes in work function resulting from adsorption or

* To whom correspondence should be addressed.

(1) Work was performed in the Ames Laboratory of the Atomic Energy Commission. Contribution No. 2728. Based in part on a dissertation submitted by Nelson C. Gardner to the Graduate College of Iowa State University in partial fulfillment of the requirements for the degree of Doctor of Philosophy, 1966.

(2) P. W. Selwood, "Adsorption and Collective Paramagnetism," Academic Press, New York, N. Y., 1962, p 147.

(3) G. C. Bond and P. G. Wells, *Advan. Catal. Relat. Subj.*, **15**, 91 (1964).

(4) E. W. Müller, *Z. Physik*, **106**, 541 (1937).

(5) R. H. Good and E. W. Müller in "Handbuch der Physik," Vol. XXI, 1956, p 176.

(6) R. S. Hansen and N. C. Gardner in "Experimental Methods in Catalytic Research," R. B. Anderson, Ed., Academic Press, New York, N. Y., 1968, pp 169–216.

(7) R. Gomer, "Field Emission and Field Ionization," Harvard University Press, Cambridge, Mass., 1961.

surface reactions can be obtained from slope ratios, thus

$$\varphi_{ad} = (S_{ad}/S_0)^{2/3}\varphi_0 \quad (2)$$

They may also be obtained much more quickly but less accurately by comparing voltages required for a fixed current, *e.g.*, 5×10^{-8} A; thus

$$\varphi_{ad} = (V_{ad}/V_0)^{2/3}\varphi_0 \quad (3)$$

This is the "single point" method. Since the tip displays many crystal faces it is evident that work functions derived from total current measurements will be average work functions, and it is easily shown that the average weights heavily the faces of lowest work function. According to the simplest model the change in work function resulting from addition of a set of species to a metal surface is

$$\Delta\varphi = 4\pi\sum_i n_i M_i \quad (4)$$

where n_i and M_i are the number of molecules per cm^2 and normal component of the dipole moment for species i. This permits inference of changes in surface species from work function changes.

FEEM studies of surface reactions have been almost limited to mono- and diatomic adsorbates. This laboratory has previously reported FEEM studies of the decomposition of ethylene and acetylene on iridium[8,9] and of ammonia on tungsten.[10] The present work is similar in concept.

Experimental Section

The field emission tube and associated electronic equipment have been previously described.[6,10] The tube was first processed on an auxiliary ultra-high vacuum system, after which the desired hydrocarbon was admitted and condensed on the inner cold finger by adding liquid nitrogen to the outer Dewar flask. The tubing connecting the microscope to the pumps was then collapsed and the tube immersed in a liquid helium cryostat. Thus immersed, partial pressures of species other than helium, hydrogen, and neon cannot exceed 10^{-14} Torr and maximum surface contamination possible from such species over the data-taking period (3–8 hr) cannot exceed 10^{-3} monolayer.

Phillips Research Grade ethylene, specified 99.98% (mol) pure, was used without further purification. Matheson acetylene (impurities 0.5% methane, 0.5% ethylene and ethane, 0.5% nitrogen, traces of oxygen, argon, and carbon monoxide) was purified by repeated distillations from a cold finger cooled by an *n*-pentane slush (143°K).

The tip was cleaned by flashing its supporting filament to ~3000°K for 5 sec. It was then allowed to cool to 4°K and dosed from one side by heating the dosing finger; molecules missing the tip condensed on the wall and a multilayer deposit was formed on the side of the tip facing the dosing finger. This dose could be caused to spread over the tip by warming it. The spreading process itself was observed to characterize surface diffusion. For the study of surface reactions the initial dose was made sufficient to permit spreading over the entire tip on warming.

All photomicrographs and work function measurements were made at 4°K to avoid field-induced reactions. In the study of surface reactions, the tip was flashed for 20 sec to T°K, quenched, and photographed, and the work function measured. The process was then repeated at successively higher values of T. Fowler–Nordheim work functions were obtained from current–voltage data extending over two decades in current.

Results and Discussion

A. Surface Diffusion. With both ethylene and acetylene doses, Type 1 diffusion[11] occurs at a rate convenient for observation when the tip is heated to 85°K. This process is characterized by immobility of the first layer of molecules presumed chemisorbed; boundary motion results from diffusion of molecules in higher adsorbed layers until they reach the edge of the deposit, whereupon they spill over the edge, are themselves chemisorbed, and extend the deposit. The sharpness of the diffusion boundary in both cases indicates spacing

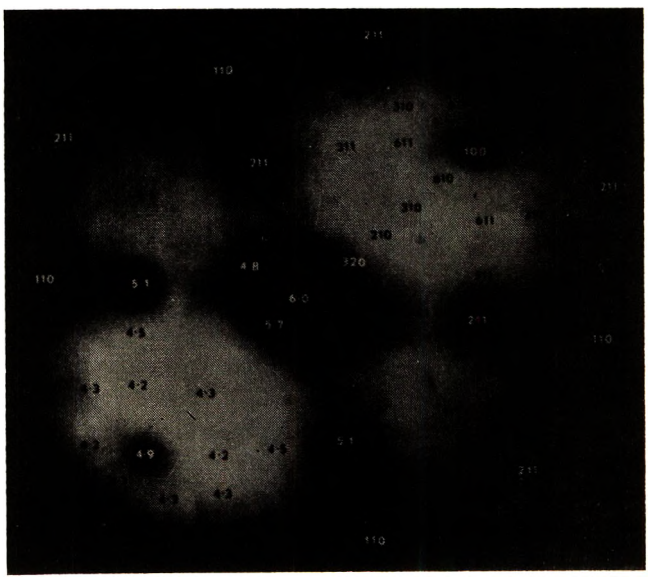

Figure 1. Indexed field electron emission photomicrograph of clean tungsten. Crystal plane locations are shown in the upper portion of the micrograph, and corresponding work functions (eV) are designated on their mirror images on the bottom portion.

(8) J. R. Arthur, Jr., and R. S. Hansen, *J. Chem. Phys.*, **36**, 2062 (1962).

(9) J. R. Arthur, Jr., and R. S. Hansen, *Ann. N. Y. Acad. Sci.*, **101**, 756 (1963).

(10) P. T. Dawson and R. S. Hansen, *J. Chem. Phys.*, **48**, 623 (1968).

(11) R. Gomer, R. Wortman, and R. Lundy, *ibid.*, **26**, 1147 (1957).

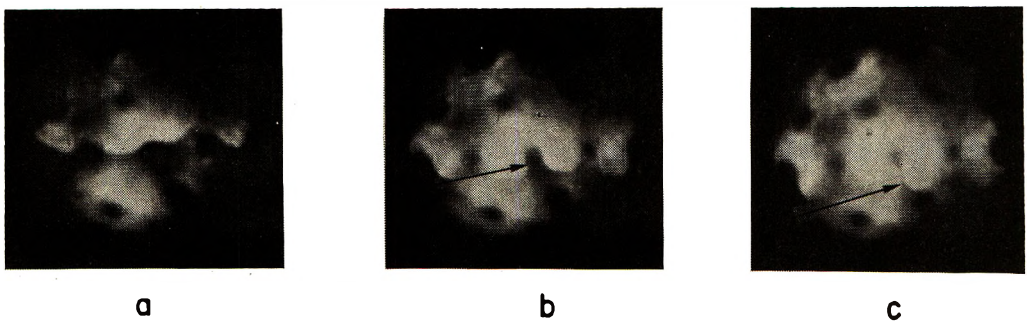

Figure 2. Diffusion of acetylene on tungsten at 85°K. The upper portion of the tip has received a multilayer dose initially, and the sequence (a), (b), (c) shows the motion of the boundary between dosed and undosed portions from top toward bottom. The arrows draw attention to the uneven motion about the (110) plane, including the backfilling below it.

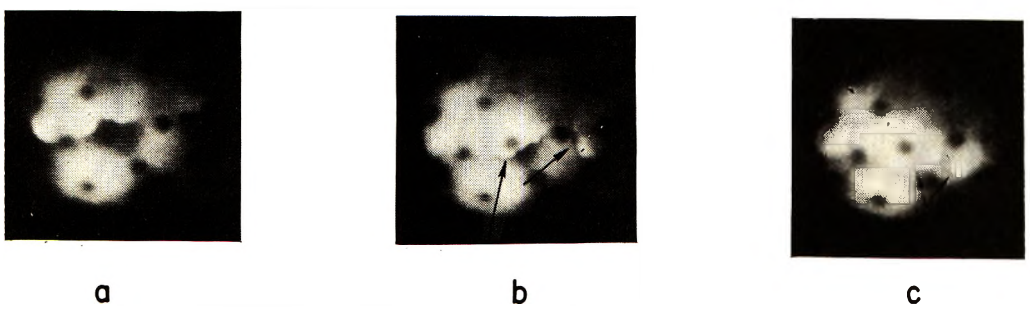

Figure 3. Diffusion of ethylene on tungsten at 85°K. The upper portion of the tip has received a multilayer dose initially, and the sequence (a), (b), (c) shows the motion of the boundary between dosed and undosed portions from top toward bottom. The arrows draw attention to the absence of backfilling below the (110) plane and the irregular motion with backfilling about the (211) plane.

between adsorption sites small compared to the microscope resolution limit (~20 Å).

Figure 1 is a FEEM photomicrograph of clean tungsten indexed to show crystal plane locations (upper portion) and corresponding work functions in eV (lower portion). Figures 2 and 3 are selected photomicrographs illustrating the principal features of diffusion of acetylene and ethylene, respectively, on tungsten at 85°K. The acetylene boundary motion is not uniform, and it is particularly evident that a layer of physically adsorbed acetylene moves around the central (110) plane and that the plane is partly filled from the back side. Boundary deflection occurs to a lesser extent around the (211) planes. A similar phenomenon occurs in ethylene diffusion at 85°K, except that in this case irregular motion and backfilling occurs about the (211) plane (and to a less evident extent about the (111) plane); the motion about the (110) plane appears to be uniform or even accelerated.

The irregular motion about certain crystal planes does not involve motion of chemisorbed ethylene or acetylene. In both cases it is easily possible to dose the tip in such a way that the multilayer is insufficient to spread a monolayer over the entire tip, so that a boundary between chemisorbed monolayer and bare tip remains. This boundary is immobile at least to 600°K and pattern changes indicative of lability of carbon-to-metal bonds do not occur at appreciable rate below 725°K.

The irregular motion of acetylene about the (110) and (211) planes and of ethylene about the (211) and (111) planes cannot be due to a repulsion of adsorbate by these planes, for at 85°K the van der Waals forces should suffice for at least a strong physical adsorption. The irregular motion and backfilling would also result if the plane involved had an unusually *high* site density for the adsorbate. In this case the plane would act as an adsorbate sink, depleting the multilayer in its immediate neighborhood. This explanation can be attractively rationalized in terms of surface structures. Infrared spectroscopy has provided good support for a σ-bonded structure, symbolically MCH=CHM, for acetylene chemisorbed on a number of metals.[12] Figure 4 shows atom arrangements and spacings on tungsten crystal planes involved in the present discussion. Pairs of atoms spaced 2.74 and 3.16 Å apart are most dense on the (110) plane, and the CCM bond angles for these spacings are 109° and 114°, respectively (see reference 13). The (211) plane has a high density of 2.74 and 4.47 Å spacings. The principal pair spacing on the (111) plane is 4.47 Å. The surface diffusion ex-

(12) L. H. Little, N. Shepard, and D. J. C. Yates, *Proc. Roy. Soc. (London)*, **A259**, 242 (1960).

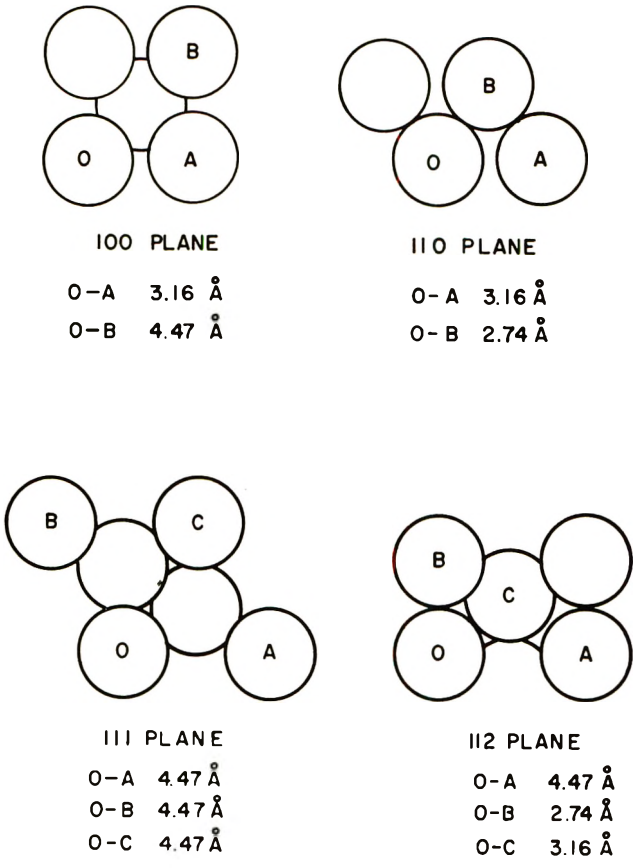

Figure 4. Diagrams of prominent planes in tungsten field emission patterns, with atom spacings indicated.

periments are best rationalized by supposing that acetylene chemisorbs preferentially on 2.74 Å spacings, and ethylene on 4.47 Å spacings. This latter spacing can readily be spanned by chemisorbed ethylene, symbolically MCH_2–CH_2M, in the trans configuration shown in Figure 5; this structure places two hydrogen atoms in the trough between tungsten atoms separated by 4.47 Å, and would appear impossible for steric reasons for any olefin not having at least one hydrogen atom on each side of the double bond.

Figure 5. Trans diadsorbed ethylene (cork ball model).

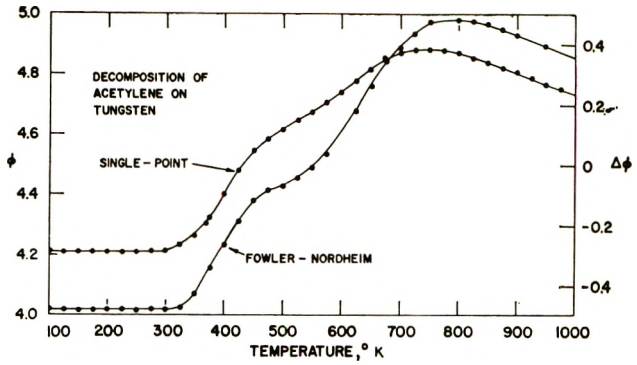

Figure 6. Work function, evaluated by Fowler–Nordheim and single point techniques, *vs.* heating temperature for an acetylene covered tungsten emitter. The emitter was held at each temperature for 20 sec. The work function of clean tungsten is 4.51 V.

The apparent prevalence of π-bonded structures in olefin and acetylene transition metal complexes[13] has led to use of such structures in discussing chemisorption of olefins and acetylenes.[3] The strong association of high site density with high densities of *pairs* of atoms appropriately spaced for σ-bonded adsorbates makes a σ-bonded model more attractive than a π-bonded model for interpretation of the present work.

B. Surface Reactions. Work function shifts resulting from flashing acetylene-dosed tungsten to T°K for 20 sec are shown in Figure 6. Curves obtained by Fowler–Nordheim and single point techniques, based on eq 2 and 3, respectively, differ in magnitude but show the same qualitative features; for this system the values can be correlated linearly by $\Delta_{\varphi F.N.} = 1.05\Delta_{\varphi S.P.} - 0.17$ for $-0.5 < \Delta_{\varphi F.N.} < 0.15$. The work function remains constant over the range 100°K $< T <$ 325°K, and this is most simply ascribed to an unchanging surface composition, presumably associatively chemisorbed acetylene. From 325°K to 750°K the Fowler–Nordheim work function increases nearly a volt; the work function against temperature plot in this temperature range can be considered to consist of two parallel straight line segments connected by a transition curve over the range 450–550°K. Parallel flash desorption experiments of Rye and Hansen[14] have shown that hydrogen is evolved over the temperature range 325°K $< T <$ 750°K and have strongly indicated that acetylene dehydrogenation (not hydrogen desorption) is rate-limiting in this process. The work function increase over this temperature range must therefore be associated with the dehydrogenation of acetylene. As the flash temperature increases above 750°K the work function gradually decreases.

Figure 7 presents a series of photomicrographs showing representative patterns obtained when an acet-

(13) R. G. Guy and B. L. Shaw, *Advan. Inorg. Chem. Radiochem.*, **4**, 78 (1962).

(14) R. R. Rye and R. S. Hansen, *J. Chem. Phys.*, **50**, 3585 (1969)

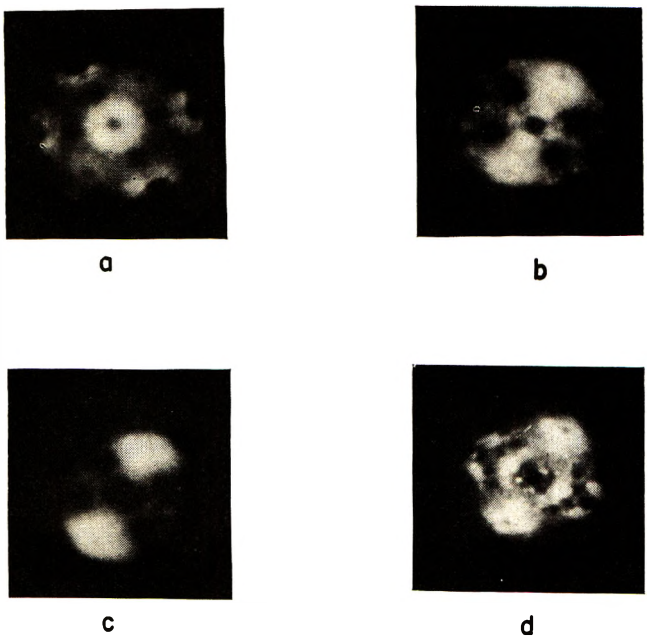

Figure 7. Field emission photomicrographs showing patterns resulting when acetylene is dosed on tungsten at 75°K and the emitter tip heated 20 sec to (a) 300°K, (b) 425°K, (c) 525°K, and (d) 1000°K.

ylene-dosed field emitter is heated. In light of the dependence of work function on temperature illustrated in Figure 6, it should be expected that tip regions of highest acetylene density should show relatively the greatest increase in emission intensity (because acetylene lowers the work function); decomposition of acetylene on heating leads to a work function increase so tip areas of highest acetylene density should darken relative to their neighbors on heating. Figure 6 shows no significant variation in work function with temperature below 300°K, and emission patterns in this temperature range are very similar. Figure 7a is characteristic; brightest emission comes from a doughnut-shaped region around the 110 plane (note that 5 such planes appear in the figure; although the "doughnut" is clearly imaged only for the central plane portions of it are imaged on the other 4 as well). Figures 7b and 7c show the transition in pattern associated with the marked work function increase as flash temperature is increased above 325°K. The regions around the (100) planes are now much brighter relative to those about the (110) and 211 planes, or alternately phrased, the regions about the (110) and 211 planes are darkening relative to their surroundings; in Figure 7c they are scarcely visible. The patterns are therefore consistent with the model inferred from the surface diffusion experiments, according to which the 2.74 Å spacings common on (110) and (211) planes (and also on planes near them) are preferred sites for acetylene chemisorption. Figure 7d shows crystallites resulting from carbon migration; such crystallites are increasingly evident as flash temperature increases above 700°K.

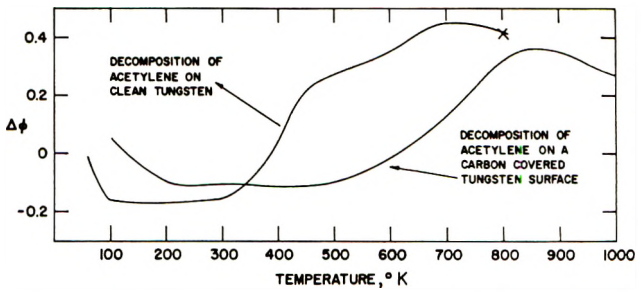

Figure 8. Comparison of decompositions of acetylene on clean and carbon-covered tungsten surfaces as reflected by single-point work function measurements. The carbon-covered surface was prepared by heating an acetylene-dosed emitter to 800°K; the tip was then cooled to 50°K and redosed.

A carbon-dosed tungsten surface was prepared by dosing the emitter tip with acetylene, heating it to 800°K to dehydrogenate the acetylene, cooling to50 °K, and again dosing with acetylene. The decomposition of acetylene on the carbon-dosed surface was also studied by flashing the tip for 20 sec to successively higher temperatures with intermittent cooling to 4°K for pattern photograph and work function measurement (in this case, by single-point method). Emission patterns all resembled strongly the clean tungsten pattern (Figure 1) except for a slight graininess at low temperatures and a very pronounced graininess for flash temperatures of 850°K or higher. Figure 8 compares work function shift *vs.* flash temperature curves reflecting the decomposition of acetylene on clean and carbon-dosed tungsten surfaces; the latter curve somewhat resembles the former in shape but its main features occur at temperatures higher by about 150°K. The latter curve also shows no feature similar to the hump at 450°K in the former but there was also no shift in sets of emitting planes during decomposition of acetylene on the carbon-dosed surface such as occurred near 450°K in the decomposition of acetylene on clean tungsten. The decomposition of acetylene on carbon-predosed tungsten is hence most simply characterized as molecular dissociation (possibly dehydrogenation) of acetylene over the range $500°K < T < 800°K$, and agglomeration of the carbon residue above 800°K. In contrast to the decomposition on clean surfaces, photomicrographs of patterns associated with heating acetylene dosed on carbon-predosed surfaces showed little change in character for heating temperatures below 800°K.

Work function changes resulting from heating ethylene-dosed tungsten to T°K for 20 sec are shown in Figure 9. Comparing the Fowler–Nordheim work function curves in Figures 6 and 9, it is evident that the initial steady work function representing the associatively adsorbed species on tungsten is about 0.2 V higher for ethylene than for acetylene, and that decomposition achieves an appreciable rate at about 225°K in the case of ethylene, 325°K in the case of acetylene.

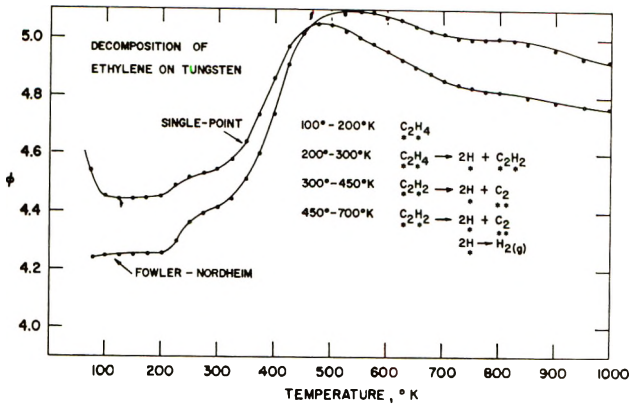

Figure 9. Work function, evaluated by Fowler–Nordheim and single-point techniques, *vs.* heating temperature for an ethylene covered tungsten emitter. The emitter was held at each temperature for 20 sec.

Thereafter each curve passes through a maximum with increasing temperature; the maximum is 5.1 V at 550°K for ethylene, 5.0 V at 800°K for acetylene. It should be noted that the two curves are substantially identical above 800°K.

Figure 10 shows representative photomicrographs obtained on flashing an ethylene-dosed tip. Figure 10a is characteristic of patterns obtained with flash temperatures of 225°K or below (where the dependence of work function on flash temperature suggests that no reaction occurs). It is less structured than the corresponding pattern for an acetylene-dosed tip, and in fact rather resembles the clean tungsten pattern, except that the area around the (100) face is dark. As the tip is heated

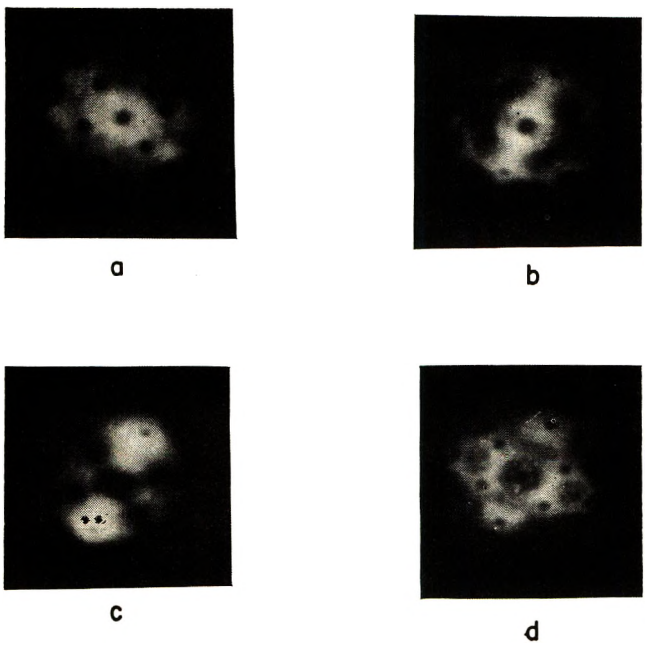

Figure 10. Field emission photomicrographs showing patterns resulting when ethylene is dosed on tungsten at 75°K and the emitter tip heated for 20 sec to (a) 225°K, (b) 375°K, (c) 500°K, and (d) 750°K.

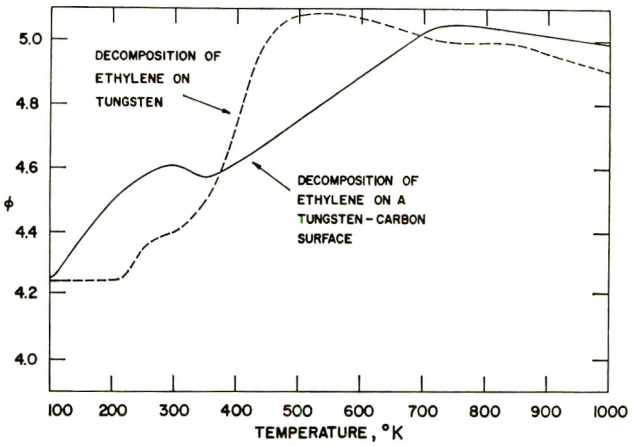

Figure 11. Comparison of decompositions of ethylene on clean and carbon-covered tungsten surfaces as reflected by single-point work function measurements. The carbon-covered surface was prepared by heating an ethylene-dosed emitter to 800°K; the tip was then cooled to 50°K and redosed.

the areas around the 111 and 211 planes evidently darken, and those around the 100 plane evidently brighten relative to the whole pattern. This development is shown in Figures 10b and 10c. Figure 10d shows the pattern development as carbon migration proceeds. The sequence of patterns is well in accord with an ethylene preference for 4.47 Å spacings, as suggested by the diffusion experiments, insofar as the areas about the (111) and (211) planes, expected to be active, are concerned. The patterns suggest no adsorption in the areas about the (100) plane, and this is not in accord with the model nor do we have at present a model to account for it.

Figure 11 compares single-point work function *vs.* temperature plots resulting from decomposition of ethylene on clean and carbon-predosed tungsten surfaces, the latter being obtained by decomposing an ethylene predose by heating the emitter to 800°K. The initial increase in work function begins at 100°K on the carbon-predosed surface rather than at 225°K as on the clean surface but the work function maximum occurs about 200° higher in the carbon-predosed case. The carbon predose hence appears to have catalyzed the dehydrogenation of ethylene to acetylene, but to have decelerated the dehydrogenation of the acetylene produced (as it also decelerated the dehydrogenation of an initial acetylene dose).

Rye and Hansen[14] found that flash decomposition of ethylene dosed on carbon-predosed tungsten was characterized by a very broad unstructured hydrogen flash-off extending from 400°K to at least 800°K. First appearance of hydrogen hence occurred well above the temperature of the β_1 peak for ethylene decomposition on clean tungsten (300°K) and close to the β_2 peak maximum (450°K). The surface reaction leading to the work function increase at 100°K for ethylene dosed on carbon-predosed tungsten cannot, therefore, be a de-

hydrogenation of ethylene yielding gaseous hydrogen, and the work of Rye and Hansen makes a dehydrogenation with hydrogen adsorbed on tungsten sites very improbable as well. Loss of physically adsorbed ethylene would result in a decrease, not an increase, in single-point work function (the true work function would be unchanged in first order).[6] The reaction beginning at 100°K is hence most probably a dehydrogenation of ethylene to acetylene with hydrogen taken up by carbon atoms of the predose.

Work function–temperature plots such as Figure 6 can provide kinetic information if certain assumptions are valid (eq 8, 5). For example, if the work function shift is linear in each surface species density as indicated in eq 4 the surface fraction θ of undecomposed acetylene in the reaction

$$\underset{**}{C_2H_2} \longrightarrow \underset{**}{C_2} + H_2 \qquad (5)$$

can be calculated from

$$\theta = \frac{\varphi_{C_2} - \varphi}{\varphi_{C_2} - \varphi_{C_2H_2}} \qquad (6)$$

where φ is the work function observed following a flash to temperature T, $\varphi_{C_2H_2}$ the work function of the surface fully dosed with associatively chemisorbed acetylene (4.02 V in Figure 6), and φ_{C_2} the work function of the surface when this dose has been completely dehydrogenated but not agglomerated (4.98 V in Figure 6). If the rate expression is of the form

$$-\frac{d\theta}{dt} = \nu_n\theta^n \exp\left(-\frac{\Delta H^{\pm}}{RT}\right) \qquad (7)$$

and the activation energy varies linearly with coverage

$$\Delta H^{\pm} = \Delta H^{\circ} - \alpha\theta \qquad (8)$$

for $n = 1$, and $\Delta H_{\pm}$ given by eq 8, eq 7 can be integrated to give

$$\nu t \exp\left[-\frac{\Delta H^{c}}{RT}\right] = E_1\left(\frac{\alpha\theta}{RT}\right) - E_1\left(\frac{\alpha\theta_0}{RT}\right) \qquad (9)$$

where

$$E_1(x) = \int_x^{\infty} \frac{e^{-y}}{y}\,dy = f(x)e^{-x}/x \qquad (10)$$

is the tabulated exponential integral function. Further, approximate formulas for $f(x)$ suitable for computer use are known[15] and for $2 < x < \infty$, $0.72 < f(x) < 1$. An approximate form useful for analyzing data in the present work is obtained by setting $f(\alpha\theta/RT) \approx 1, E_1(\alpha\theta_0/RT) \approx 0$ to obtain

$$\ln\left[\frac{\alpha\theta}{RT}\nu t\right] = \frac{\Delta H^{\circ}}{RT} - \frac{\alpha\theta}{RT} \qquad (11)$$

Evaluation of parameters ΔH° and α is relatively insensitive to approximations made within the logarithm term; taking $\nu \approx 10^{13}$, $\alpha\theta/RT \approx 5$, $t = 20$ sec in that term there results

$$T = \frac{\Delta H^{\circ}}{34.5R} - \frac{\alpha\theta}{34.5R} \qquad (n = 1) \qquad (12)$$

A similar treatment of eq 7 for $n = 2$, using $\nu = (\sigma\pi kT/m)^{1/2}$ and with similar approximations, leads to

$$T = \frac{\Delta H^{\circ}}{32.5R} - \frac{\alpha\theta}{32.5R} \qquad (n = 2) \qquad (13)$$

To the extent that approximations made in deriving eq 12 and 13 are valid it is obvious that they furnish no basis for resolving between first- and second-order kinetics in the absence of further information. In either case portions of work function–temperature plots corresponding to a given surface reaction should generate *linear* temperature–surface coverage plots, with surface coverage calculated from relations such as eq 6.

This analysis was applied to portions of work function–temperature curves attributed to acetylene dehydrogenation, using eq 12. For curves characterized by transition sections, *e.g.*, Figure 6, the segment nearest the maximum was used for analysis and the minimum work function used was corrected for segment shift by estimation. Results are shown in Table I.

Table I: First-Order Kinetic Parameters for Decomposition of Acetylene on Tungsten

Acetylene source	Predose	ΔH°, kcal/mol	α, kcal/mol monolayer
Acetylene	None	47	15
Ethylene	None	31	7
Acetylene	Carbon	58	19
Ethylene	Carbon	51	15

The absorption model advanced, according to which the planes of high site density should differ for ethylene and acetylene, would imply a probable difference in decomposition characteristics between acetylene dosed *per se* and acetylene formed from decomposition of chemisorbed ethylene. The difference indicated in Table I is greater than would be expected from the work of Rye and Hansen,[14] who found the flash desorption patterns from acetylene dosed *per se* or formed from ethylene to be almost indistinguishable. It is very likely that the difference in parameters obtained results in part from the ambiguity in data treatment caused by the "hump" in the work function–temperature plot particularly evident from acetylene dosed as such on clean tungsten, in part because of differences in emission anisotropy in the two cases leading to a different weighting of crystal faces in the two analyses. The

(15) C. Hastings, "Approximations for Digital Computers," Princeton University Press, Princeton, N. J., 1955, pp 188–190.

carbon predose should tend to mask the differences between tungsten crystal faces, and the emission patterns resulting from acetylene on carbon-predosed tungsten are relatively much less dependent on whether the acetylene was dosed as such or formed from ethylene. It is therefore not surprising that activation energies and their coverage dependencies are quite similar in these two cases.

Overall, the field emission microscopic study of the decomposition of acetylene and ethylene on tungsten has confirmed and extended results obtained by flash filament desorption spectroscopy. The hydrogen-producing reactions detected by the latter method were indicated by distinctive features in work function–temperature plots obtained by the former. In addition, FEEM has provided clear evidence, both through surface diffusion and decomposition residue patterns, of anisotropic adsorption both of acetylene and ethylene and of the surface migration of carbon above the dehydrogenation temperature.

Intermediates in Ethylene Hydrogenation over Zinc Oxide

by A. L. Dent and R. J. Kokes*

Department of Chemistry, The Johns Hopkins University, Baltimore, Maryland 21218 *(Received June 22, 1970)*

Isosteric heats of adsorption for ethane and ethylene were determined from isotherms at 0 and 20°. The heats for initial adsorption (5 kcal for ethane and 14 kcal for ethylene) suggest ethane is physically adsorbed, whereas ethylene is (in part) chemically adsorbed. The infrared spectrum of the chemically adsorbed ethylene yields bands corresponding roughly to fundamentals for gaseous ethylene and includes several bands forbidden in the ir of the latter species. One of such bands is the C=C stretch. Details of the spectrum suggest adsorbed ethylene is olefinic in character and bound to the surface by interaction of the π electrons. Studies of the spectrum in a flow system show that in the presence of a hydrogen–ethylene stream during hydrogenation, a new adsorbed species is formed; this aliphatic hydrocarbon species, X, is rapidly removed by hydrogen alone. The initial rate of removal of X by hydrogen is comparable to the steady state hydrogenation rate; hence, X behaves as an intermediate. Similar experiments with D_2–C_2H_4 and H_2–C_2D_4 as reacting streams were also carried out. It is concluded that the resulting data are consistent with an assignment of the spectrum of X to an alkyl intermediate attached to the zinc half of the zinc–oxygen active site.

Introduction

Hydrogenation of ethylene over metals presumably occurs *via* the following steps

$$C_2H_4(\text{ads.}) + H \rightleftharpoons CH_2{-}CH_3 \quad (1)$$

$$CH_2{-}CH_3 + H \longrightarrow C_2H_6(\text{gas}) + 2^* \quad (2)$$

where * represents a surface atom. The following observations[1] are consistent with this scheme.[1] (1) Active catalysts for ethylene hydrogenation also catalyze H_2–D_2 equilibration, which suggests, as indicated above, that hydrogen is adsorbed as atoms. (2) Reaction of light ethylene with deuterium leads to a distribution of ethanes of the form $C_2H_{6-x}D_x$ ($0 \leq x \leq 6$), which suggests, as indicated above, that the first step is reversible. (3) Double-bond isomerization of olefins requires hydrogen as a cocatalyst as would be expected if the "alkyl reversal" of step 1 is the primary isomerization pathway.[2] Finer details of isomerization, hydrogenation, and related exchange studies reveal defects in the above picture;[3,4] nevertheless, this picture remains the best simple approximation to the truth.

A number of researchers have utilized infrared techniques in an attempt to provide evidence more direct than mechanistic inference for the above-mentioned surface species and intermediates.[4-6] These studies, however, have demonstrated, primarily, that adsorption

* To whom correspondence should be addressed.

(1) G. C. Bond, "Catalysis by Metals," Academic Press, New York, N. Y., 1962, pp 229–279; G. C. Bond and P. B. Wells, *Advan. Catal. Relat. Subj.*, **15**, 257 (1964).

(2) J. Bartek, Ph.D. Thesis, 1970, The Johns Hopkins University.

(3) W. M. Hamilton and R. L. Burwell, Jr., *Actes Congr. Int. Catal.*, 2e, 1960, **1**, 987 (1961).

(4) R. P. Eischens and W. A. Pliskin, *Advan. Catal. Relat. Subj.*, **10**, 1 (1958).

(5) N. Sheppard, *Pure Appl. Chem.*, **4**, 71 (1962).

(6) L. H. Little, "Infrared Spectra of Adsorbed Species," Academic Press, New York, N. Y., 1966.

of olefins on metals is complex; for example, as many as five surface species appear to form when ethylene is adsorbed on nickel.[6] Such complexity is also indicated by simple adsorption studies inasmuch as they show that surface reactions such as self-hydrogenation and dimerization accompany ethylene adsorption on metals.[7-10] The variety of surface species makes it difficult to sort out which bands are due to which species and what their role is in the hydrogenation reaction. Therefore, it is not surprising that ir studies provide only limited support for the picture put forward on mechanistic grounds. This disappointing result is a consequence of the occurrence of side reactions that play a minor role in hydrogenation catalysis but a major role in determining the surface species present. It has been suggested that these side reactions arise from processes akin to alkyl reversal.[10]

In recent years hydrogenation over oxides has been studied by a number of groups.[11-18] It appears that the reaction pathway still involves the steps depicted in eq 1 and 2 but the first step is now irreversible. The following observations are consistent with this modified scheme. (1) Active catalysts for ethylene hydrogenation also catalyze H_2–D_2 equilibration, which suggests, as indicated above, that hydrogen is adsorbed as atoms.[11,17] (2) Reaction of light ethylene with deuterium yields $C_2H_4D_2$,[11-14] which suggests the first step is *not* reversible. (3) Double-bond isomerization of olefins does *not* require hydrogen as a cocatalyst; hence, alkyl reversal is *not* an important pathway for isomerization.[11] It has also been shown (at least on zinc oxide) that ethylene adsorption is less complex than on metals; ethylene adsorption is weak, readily reversible, and not accompanied by surface reactions such as self-hydrogenation and dimerization.[18]

The relative simplicity of hydrogenation and adsorption of ethylene on zinc oxide indicates that ir studies aimed at providing evidence for surface species and intermediates may be more successful than such studies over metals. A number of other properties of zinc oxide make this an attractive system for such studies. (1) Strong bands due to adsorbed hydrogen assignable to ZnH and OH species are readily observable[19] even during hydrogenation.[18] (2) The mechanism depicted in eq 1 and 2 (without alkyl reversal) suggests the amount of alkyl intermediate should increase with ethylene pressure. Furthermore, when deuterium rather than hydrogen is used, any C–D band due to an adsorbed species should be due to the intermediate. (Ethylene does not exchange with deuterium as it does over metals.) (3) The transmission properties of zinc oxide are excellent from about 4000 to 1150 cm^{-1}; hence, the spectrum of adsorbed hydrocarbons can be examined over a wide range of frequencies. All of these features of zinc oxide favor the view that it might be possible to examine the ir spectrum of each reactant surface species, to determine their behavior under reaction conditions, and to characterize the reaction intermediate. In this paper we report on attempts to do the above. A brief communication dealing with this work has already appeared.[20]

Experimental Section

Materials. Tank hydrogen, deuterium, and helium were purified by passage through degassed charcoal at liquid nitrogen temperatures. Tank ethylene was purified by passage through a series of traps containing Ascarite, calcium sulfate, and a trap maintained at −78°. Perdeuterioethylene, obtained from Merck Sharp and Dohme, was purified by passage through Ascarite followed by alternate condensation, vaporization, and pumping cycles. Mass spectroscopic analysis indicated 95.0% C_2D_4 with the remainder partially deuterated ethylene. Tank ethane was purified by the procedure described for perdeuterioethylene.

The zinc oxide used for these studies was Kadox-25 supplied by the New Jersey Zinc Company.

Adsorption Studies. Adsorption studies were carried out on 10.0 g of zinc oxide that had been pressed into disks at 25,000 psi and broken into smalller pieces. The activation procedure paralleled that employed for the ir studies, detailed later. Adsorption measurements were conducted in a conventional BET apparatus connected to the catalyst chamber (which was part of a circulation loop). Adsorption isotherms for both ethylene and ethane were determined at 0 and 20°.

Infrared Studies. Samples of zinc oxide weighing 0.7 to 0.9 g were pressed into circular disks 20 mm in diameter under a pressure of 25,000 psi in a stainless steel plug. This disk was centered in a cylindrical cell with NaCl end windows. Heating coils around the central portions of the cell permitted heating the sample to 500° while the windows were watercooled by copper coils. A measure of the sample temperature was provided by two thermocouples; one of these formed a pressure contact with the disk; the other made contact with the outer wall of the cell at the position of the sample holder. Tubulations, with stopcocks, con-

(7) D. W. McKee, *J. Amer. Chem. Soc.*, **84**, 1109 (1962).
(8) G. I. Jenkins and E. K. Rideal, *J. Chem. Soc.*, 2490 (1955).
(9) S. J. Stephens, *J. Phys. Chem.*, **62**, 714 (1958).
(10) R. J. Kokes, *J. Catal.*, **14**, 83 (1969).
(11) R. L. Burwell, Jr., G. L. Haller, K. C. Taylor, and J. F. Read, *Advan. Catal. Relat. Subj.*, **20**, 1 (1969).
(12) W. C. Conner, R. A. Innes, and R. J. Kokes, *J. Amer. Chem. Soc.*, **90**, 6858 (1968).
(13) A. Ozaki, private communication, see ref 12.
(14) Y. Amenomiya, *J. Catal.*, **12**, 198 (1969).
(15) D. L. Harrison, D. Nichols, and H. Steiner, *ibid.*, **7**, 359 (1967).
(16) F. Bozon-Verduraz and S. J. Teichner, *ibid.*, **11**, 7 (1968).
(17) W. C. Conner and R. J. Kokes, *J. Phys. Chem.*, **73**, 2436 (1969).
(18) A. L. Dent and R. J. Kokes, *ibid.*, **73**, 3772, 3781 (1969).
(19) R. P. Eischens, W. A. Pliskin, and M. S. D. Low, *J. Catal.*, **1**, 180 (1962).
(20) A. L. Dent and R. J. Kokes, *J. Amer. Chem. Soc.*, **91**, 7207 (1969).

nected to either side of the sample, permitted gases to be circulated over the catalyst when the cell was attached to the vacuum system *via* ball joints.

Activation was as follows. First, the sample was degassed 1 hr at 100°; degassing was continued while the temperature was slowly raised to 500° and held for 2 hr at that temperature. At this point oxygen at 160 mm was circulated over the catalyst for 2 hr with a trap at −195° in the circulation loop; then, the sample was cooled in oxygen to room temperature and degassed for about 30 min. This activation procedure yielded a sample with excellent transmission properties (*e.g.*, 55% transmission at 1250 cm^{-1}) with the same activity as a sample pretreated by degassing at high temperature.[18]

The flow system consisted of three separate purification trains for hydrogen, helium, and ethylene similar to those described above; at the end of each train there was a 20-g sample of degassed zinc oxide for further purification. After purging the lines an appropriate blend of the three gas streams was passed *via* a mercury blow-off (to assure a total pressure of 1 atm) through the sample cell and the matched reference cell which were mounted in series in the ir spectrometer. The flow of each gas could be controlled independently and the total effluent from the reference cell was monitored with a wet test meter.

Infrared spectra were recorded with a Perkin-Elmer Model 521 grating double beam spectrometer with a spectral slit width varying from 5 cm^{-1} at 3600 cm^{-1} to 2 cm^{-1} at 1200 cm^{-1}. All spectra were recorded with the sample at ambient temperatures, nominally 25°, but probably somewhat higher due to heating by the ir beam. A series of calibrated screens was positioned in the reference beam to offset transmission losses due to the catalyst in various regions of the spectrum. In each case prior to adsorption a background scan for degassed zinc oxide was recorded and is shown in the reported spectra as a dashed line.

In experiments involving perdeuterioethylene equal pressures of C_2D_4 and hydrogen were equilibrated in a 500-cc 5-m Pyrex coil. This mixture was forced through the cells by hydrogen flowing at a low rate. Plug-like flow was assumed to occur.

A typical sequence in a run with the flow system is outlined below. (1) The background spectrum was recorded in a helium flow of 260 cc/min. (2) The stable spectrum was recorded for a blended flow containing 150 cc/min of helium and 120 cc/min of ethylene. This corresponds to an ethylene partial pressure of 340 mm. (3) The system was then purged with helium. The spectrum due to adsorbed ethylene disappeared in less than 1 min in a helium flow of 1 l./min, but the purging time was extended for at least 10 min. The stable spectrum was then recorded in a blended flow containing 120 cc/min of helium and 150 cc/min of hydrogen. This corresponds to a hydrogen partial pressure of 420 mm. (4) The stable spectrum was recorded for a blended flow of 120 cc/min of ethylene and 150 cc/min of hydrogen. This corresponds to a hydrogen and ethylene partial pressure of 420 and 340 mm, respectively. Hydrogenation of ethylene occurs under these conditions and in some cases the effluent was sampled for analysis. The rates of hydrogenation agreed within 10 to 20% with those estimated from the kinetic data reported earlier.[18] (5) After about 1 hr on stream as depicted in 4, the ethylene flow was replaced by helium. This yielded a stream in which the partial pressure of hydrogen was 420 mm. The rapidly changing spectrum was repeatedly scanned to determine the changes as a function of time. The above procedure was chosen so that we could study the spectrum of ethylene alone (2), hydrogen alone (3), hydrogen and ethylene together (4), and the decay of the spectrum in hydrogen (5). Insofar as possible the pressures of reacting gases were kept comparable from one step to another. It should be noted that this system is not limited to studies in which the total pressure of reactants is 1 atm. If in step 4 helium is added as a diluent, the partial pressures of hydrogen and ethylene can be varied over a wide range; for example, runs were made with ethylene partial pressures as low as 8 mm and hydrogen pressures as low as 120 mm. The ir bands in these runs at lower pressures were much weaker but the results were consistent with the runs reported herein at higher pressures.

Results

Adsorption Studies. Adsorption of ethylene on zinc oxide at room temperature is rapid and the adsorbed ethylene can be removed by a few minutes evacuation at room temperature. Analysis of the recovered adsorbed ethylene, even after a 24-hr exposure to the solid, reveals that the ethylene is quantitatively recovered unchanged; in other words, there is no evidence for the dimerization or self-hydrogenation found for adsorption of ethylene on metals.

The boiling point of ethylene is −104° and the critical temperature is 10°.[21] These data suggest that the amount of adsorption at room temperature[18] is too much to be accounted for by physical adsorption alone, but the amount of adsorption is not as good a criterion for chemical adsorption *vs.* physical adsorption as the heat of adsorption. Accordingly, we determined isotherms for ethylene at 0 and 20° and computed isosteric heats therefrom. To have some bases for comparison we have obtained like data for ethane. Ethane (with a boiling point of −89° and a critical temperature of 32°[22]) would be expected to show more extensive physical adsorption than the lower-boiling

(21) N. A. Lange, "Handbook of Chemistry," Handbook Publishers Inc., Sandusky, Ohio, 1952.

(22) J. L. Carter, D. J. C. Yates, P. J. Lucchesi, J. J. Elliott, and V. Kevorkian, *J. Phys. Chem.*, **70**, 1126 (1966).

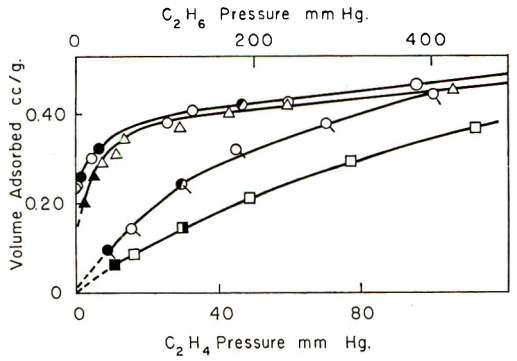

Figure 1. Adsorption isotherms for ethylene and ethane: O, C_2H_4 at 0°; △, C_2H_4 at 20°C; Q, C_2H_6 at 0°; □, C_2H_6 at 20°. (Filled symbols are desorption points.)

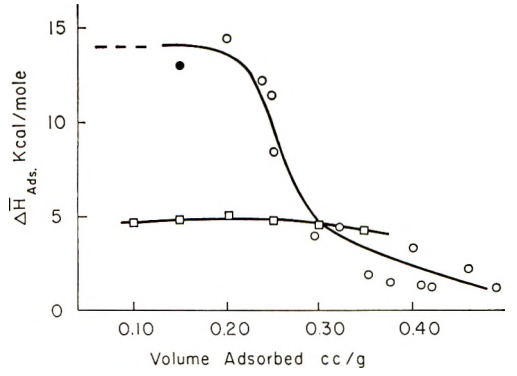

Figure 2. Heats of adsorption of ethane and ethylene: O, C_2H_4; □, C_2H_6. (The filled symbol is a determination on a different sample.)

ethylene. These data are given in Figures 1 and 2.

The data for ethane are what one would expect for physical adsorption. The isotherm at 20° shows only slight departure from linearity with little evidence for saturation. The heat values of about 5 kcal are only slightly greater than the heat of liquefaction (3.5 kcal at the boiling point but much less this near to the critical point). The data for ethylene compared to ethane show clear evidence that chemisorption is occurring. Ethylene adsorption at 1 mm and 0° is about two orders of magnitude greater than the extrapolated value for ethane and the isotherm shows strong evidence for saturation. In addition to this the initial heat of adsorption is about four times the heat of liquefaction of ethylene (3.2 kcal/mol). This high value for the isosteric heat applies up to about 0.20 cc/g and does not reach values consistent with physical adsorption until about 0.30 cc/g. It should be recalled, however, that the isosteric heats are related to differential heats; hence, the integral heats remain high even at higher coverages. Thus, while the ethylene adsorption at higher pressures has heats compatible with physical adsorption, the first portion of the ethylene adsorbed, *i.e.*, up to about 0.3 cc/g, must be classified as chemical adsorption.

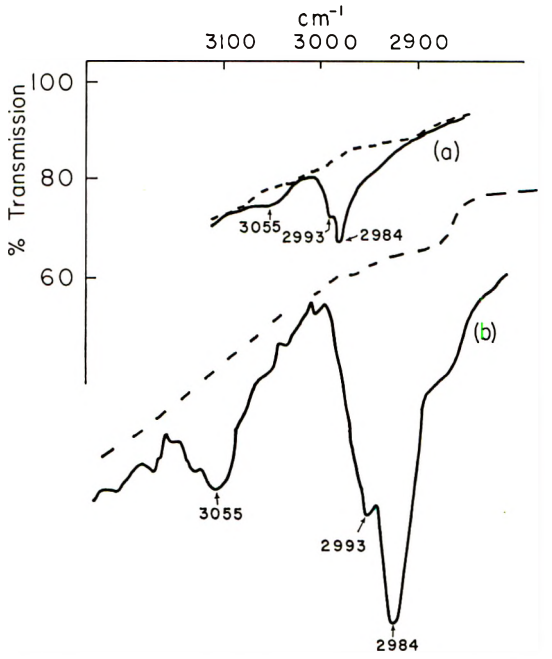

Figure 3. Infrared spectrum of adsorbed ethylene at 100 mm: (a) normal scale spectrum; (b) expanded scale spectrum (see text).

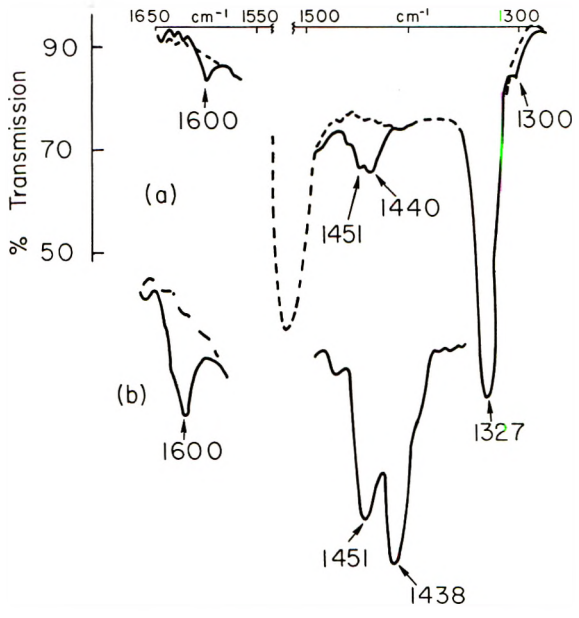

Figure 4. Infrared spectrum of adsorbed ethylene at 100 mm: (a) normal scale spectrum; (b) expanded scale spectrum (see text).

Infrared Spectrum of Adsorbed Ethylene. Figures 3 and 4 show the spectrum of adsorbed ethylene at a pressure of 100 mm in the C–H stretching and deformation regions, respectively. (No bands were observed in the ZnH or OH region; hence, unlike propylene[23] ethylene adsorbs without appreciable dissociation.) In each figure the upper curve gives the spectrum without

(23) A. L. Dent and R. J. Kokes, *J. Amer. Chem. Soc.*, **92**, 1092 (1970).

amplification; the lower figure was run with a fivefold ordinate expansion and a twofold expansion in the wavelength scale. In the stretching region (Figure 3) the strongest band is at 2984 cm^{-1}; progressively weaker bands are found at 2993, 3055, and 3125 cm^{-1}. (The latter band is not shown in Figure 3.) In the deformation region (Figure 4) there are two strong bands at 1521 and 1327 cm^{-1} due to the zinc oxide itself. The weak band at 1300 cm^{-1} seems to be caused by perturbation of the surface by adsorbed molecules. It is observed at the same place for perdeuterioethylene and also for differently labeled deuterio isomers of chemisorbed propylene.[23,24] The band at 1600 cm^{-1} is assigned to the >C=C< stretch of chemisorbed ethylene; the bands at 1451 and 1438 cm^{-1} are assigned to CH deformations. Support for this assignment is supplied by the spectrum of perdeuterioethylene, which shows only one band in this region at 1495 cm^{-1}. This shift is comparable to the shift in the C=C frequency that occurs on deuteration of gaseous ethylene, *i.e.*, from 1623 to 1515 cm^{-1}.[25] Shifts on deuteration for carbon–hydrogen deformation bands are much larger, of the order of 400 cm^{-1}; hence, as expected, we see no bands corresponding to the 1451- and 1438-cm^{-1} bands. With adsorbed perdeuterioethylene we, of course, also see bands in the CD stretching region (near 2200 cm^{-1}) corresponding to those for adsorbed ethylene in the CH stretching region.

The data in Figures 1 and 2 suggest that both chemical and physical adsorption of ethylene occur. By analogy with the behavior of ethane we would expect the physically adsorbed ethylene to be roughly proportional to pressure whereas chemisorption would be nearly independent of pressure above about 25 mm. Except for a relatively small intercept the bands at about 3130 and 3060 cm^{-1} are roughly proportional to pressure between 22 and 240 mm, whereas the bands at 1451, 1438, 1600, and 2984 cm^{-1} are insensitive to pressure in this region. (The band at 2993 cm^{-1} seems to behave similarly to the bands above 3000 cm^{-1}, but its overlap with the band at 2984 cm^{-1} makes analysis difficult.) Thus, the bands above 3000 cm^{-1} (and perhaps the band at 2993 cm^{-1}) are in part due to physically adsorbed ethylene; nevertheless, the fact that they are apparent even at low pressures and shift in position with increasing amounts of physical adsorption leads us to believe that weak bands due to chemisorbed ethylene also occur at these positions but that they overlap stronger bands due to physically adsorbed ethylene. This association of these bands with chemisorbed ethylene is not as clear cut, however, as it is for the bands below 2984 cm^{-1}.

The band in the C=C region due to chemisorbed ethylene shows the ethylene is olefinic in character. The occurrence of C–H stretching bands above 3000 cm^{-1} supports this view. Interaction of an *olefin* with a surface with appreciable heat suggests there must be some π bonding involved. Powell and Sheppard[26] have noted that the spectra of olefins in π-bonded transition metal complexes appear to involve fundamentals similar to those found for the free olefin. Two striking differences occur. First, infrared forbidden bands for the free olefin become allowed for the lower symmetry complex; second, the fundamentals of ethylene corresponding to ν_2 and ν_3 shift much more than the other fundamentals. In Table I we compare the fundamentals observed for liquid ethylene[27] and a π complex[28] to those observed for chemisorbed ethylene. (We choose liquid ethylene rather than gaseous ethylene to offset, in part, the shifts in frequencies that occur when one passes from the gas phase to a condensed phase.) Two points are clear from Table I. First, many bands forbidden in the ir for gaseous ethylene are observed for chemisorbed ethylene; second, the ν_3 band is shifted more than the corresponding band for the π complex whereas the ν_2 band is shifted less. This comparison suggests it is valid to view chemisorbed ethylene as "π-bonded" to the surface.

Table I: Observed Bands for Chemisorbed Ethylene and Related Systems

Type[a] of vibration	C_2H_4(l),[b] cm^{-1}	π complex,[c] cm^{-1}	Adsorbed ethylene[d]
9	3105 (I)	3094	3140[e](3122)
5	3075 (R)	3079	3055 (3078)
1	3008 (R)	3013	2993 (3000)
11	2980 (I)	2988	2984
2	1621 (R)	1518	1600
12	1435 (I)	1426	1438
3	1342 (R)	1419	1451

[a] Numbering is the same as in ref 25. [b] For gaseous ethylene bands labeled I and R are infrared and Raman active, respectively. See ref 27 for liquid ethylene. [c] For the salt $KPtCl_3(C_2H_4)$.[28] [d] Some of these bands shift as a function of pressure. The numbers listed are for the lowest pressures of ethylene (22 mm); the numbers in parentheses are the positions at the highest ethylene pressures (240 mm). In part these bands are due to physically adsorbed ethylene. [e] This band is broad and weak. The position is uncertain to ± 10 cm^{-1}.

The shift in the C=C frequency, ν_2, for adsorbed ethylene relative to that in the gas phase is 23 cm^{-1}. This is much greater than the 2-cm^{-1} shift that is observed on liquefaction but is less than that found for complexes of silver salts[29] (about 40 cm^{-1}) or platinum

(24) A. L. Dent and R. J. Kokes, *J. Amer. Chem. Soc.*, in press.

(25) J. Herzberg, "Molecular Spectra and Molecular Structure: II. Infrared and Raman Spectra of Polyatomic Molecules," D. Van Nostrand Co. Inc., Princeton, N. J., 1945, p 326.

(26) D. B. Powell and N. Sheppard, *Spectrochim. Acta*, **13**, 69 (1958).

(27) B. P. Stoicheff, *J. Chem. Phys.*, **21**, 755 (1956).

(28) J. Pradilla-Sorzana and J. P. Facker, Jr., *J. Mol. Spectrosc.*, **22**, 180 (1967); see also J. Hiraishi, *Spectrochim. Acta, Part A*, **25**, 749 (1969).

(29) H. W. Quinn and D. N. Glev, *Can. J. Chem.*, **40**, 1103 (1962).

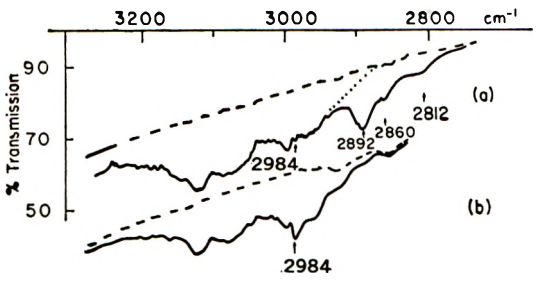

Figure 5. Spectrum of ethylene in the presence and absence of hydrogen: (a) P_{H_2} = 420 mm, $P_{C_2H_4}$ = 340 mm; (b) C_2H_4 at 240 mm (displaced ordinate).

complexes[28] (105 cm^{-1}). A number of investigators[22,29] have noted a correlation of the enthalpy of formation of complexes of ethylene to the frequency shift. If we use the correlation that has been observed between heat of adsorption of ethylene on various molecular sieves and the frequency shift, we find that a shift of 23 cm^{-1} should correspond to a heat of adsorption of 13.8 kcal. This value is in excellent agreement with the value of 14 kcal obtained for isosteric heats at low coverage.

Infrared Spectrum under Reaction Conditions. Figure 5b shows the C–H stretching region of the spectrum of adsorbed ethylene (at 240 mm) in a flow system with helium as a diluent. The reference cell does cancel the strong absorption due to gaseous ethylene between 2975 and 3140 cm^{-1} but at pressures above 150 to 200 mm the energy loss in both beams is sufficiently great that there is limited instrument response in this region. Nevertheless, we see once again prominent bands at roughly the same positions listed in Table I for the better defined spectrum at lower pressures (Figure 3).

Figure 5a shows the spectrum of adsorbed species[30] on an active catalyst in a hydrogen–ethylene stream. This spectrum appears and stabilizes within minutes after hydrogen is blended into the ethylene stream. It is immediately apparent that three new bands appear in the presence of hydrogen at 2892, 2860, and 2812 cm^{-1}. The appearance and location of these bands were verified by expanded scale spectra. Experiments at lower ethylene pressures reveal that there is an additional band at about 2940 cm^{-1} partially obscured in Figure 5 by overlap of the ethylene spectrum.

One sequence of runs was initiated on a catalyst later found to be poisoned. This catalyst yielded the typical spectrum for adsorbed ethylene but in the presence of hydrogen alone did not yield ZnH and OH bonds. When this catalyst was exposed to a hydrogen–ethylene stream, only the spectrum of adsorbed ethylene was observed; bands at 2940, 2892, 2860, and 2812 cm^{-1} did *not* appear. The cause of poisoning was not established but when this catalyst was again subjected to standard pretreatment, it was active and the bands corresponding to those in Figure 5a were observed. Thus, the new bands did not appear on this poisoned catalyst; they appear to be characteristic of a reacting catalyst.

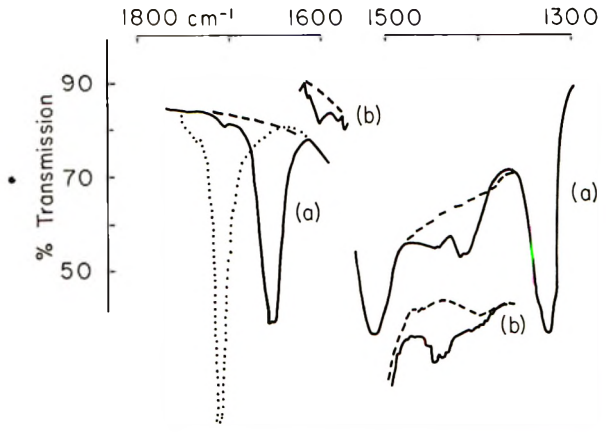

Figure 6. Spectrum of ethylene in the presence and absence of hydrogen: (a) P_{H_2} = 420 mm, $P_{C_2H_4}$ = 340 mm (the dotted curve is for H_2 in helium with P_{H_2} = 420 mm); (b) $P_{C_2H_4}$ = 240 mm (displaced ordinate).

Figure 6 shows the spectrum for the deformation region in an ethylene–helium stream and an ethylene–hydrogen stream. In the deformation region the two bands at 1451 and 1438 cm^{-1} due to ethylene alone appear to weaken and shift slightly and a new band (or perhaps two) appears at about 1415 cm^{-1}. Figure 6 also shows that under reaction conditions the ZnH band is shifted from 1709 cm^{-1} to 1655 cm^{-1}; the corresponding shift in the OH band is from 3490 to 3510 cm^{-1}.

The changes that occur in a reacting system are not limited to the appearance of new bands. Close scrutiny of the data in Figures 5 and 6 reveals that the bands definitely associated with chemisorbed ethylene are weakened. The bands at 2984 and 1600 cm^{-1} are no longer evident; hence, it seems that a major portion of the chemisorbed ethylene is converted to the new species under reaction conditions. In view of this we believe the bands centered at about 1440 cm^{-1} under reaction conditions (which is weaker than that due to ethylene alone) are not due primarily to ethylene but rather to the species formed under reaction conditions. The bands ascribable to the species formed under reaction conditions (hereafter referred to as X) are listed in Table II.

Similar studies to the above have been carried out with C_2H_4–D_2 as the reactant. These results are consistent with studies of the C_2H_4–H_2 mixture insofar as they suggest that a large portion of the chemisorbed ethylene is converted to a new species. A strong band occurs at about 2905 cm^{-1} with a somewhat weaker band at 2860 cm^{-1}; in addition a broad band seems to appear at 2955 cm^{-1}, but since runs at lower ethylene pressures were not carried out, this band is uncertain. Bands in the deformation region are found at 1445 and 1415 cm^{-1}

(30) The configuration of the flow system is such that the amount of product ethane in the reference beam would be greater than that in the sample cell; hence, ethane should contribute only negative peaks to the spectrum. At the low conversions encountered here, of the order of 0.1%, the contribution of ethane to the spectrum is trivial.

Table II: Frequencies of Species Formed under Reaction Conditions

Bands from[a] C_2H_4–H_2, cm^{-1}	Bands from[a,c] C_2H_4–D_2, cm^{-1}	Bands from[a] C_2D_4–H_2, cm^{-1}
(2940)[b] m br	(2955)[b] m	
2892 s	2910 s	2890 w
2860 m	2860 m	2100–2160 w br
2812 w	2150 m	
1440 s br	1445 s br	
1415 s br	1415 s br	1289 w

[a] The strongest band is labeled s and progressively weaker bands are labeled m and w, respectively. Bands labeled br are broad and may consist of two or more overlapping bands. [b] Centers of these bands are uncertain due to overlap with bands due to adsorbed ethylene. [c] There may be a band at 2812 cm^{-1} in this spectrum, but if it is present, it is weaker and less stable than the band of this position in the C_2H_4–H_2 reactant stream.

and both of these are somewhat sharper than those found in the C_2H_4–H_2 reaction mix. It is most significant that only a *single* band appears in the C–D stretching region at 2150 cm^{-1} which suggests that a monodeuterio species is formed.[31] All bands associated with this species are listed in Table II.

Similar studies to the above, but more abbreviated, were also carried out with C_2D_4–H_2 as a reactant mixture. The species formed under reaction conditions yields a *single* weak band at 2890 cm^{-1} which suggests a monohydrido species. There are also several very weak bands between 2100 and 2160 cm^{-1} and a weak band at 1289 cm^{-1}. The observed bands for the species formed under reaction conditions are listed in Table II.

Reaction of Surface Species with Hydrogen. Figure 7a and b shows the spectrum of X in the region of its strongest bands under steady state reaction conditions in a C_2H_4–H_2 stream; the spectrum, which forms immediately, is clearly stable for a prolonged period of time. Immediately after the spectrum in Figure 7b was obtained, helium was substituted for ethylene in the reacting stream; the decay of the dominant 2890-cm^{-1} band in the He–H_2 stream is shown in Figure 7c through Figure 7j.

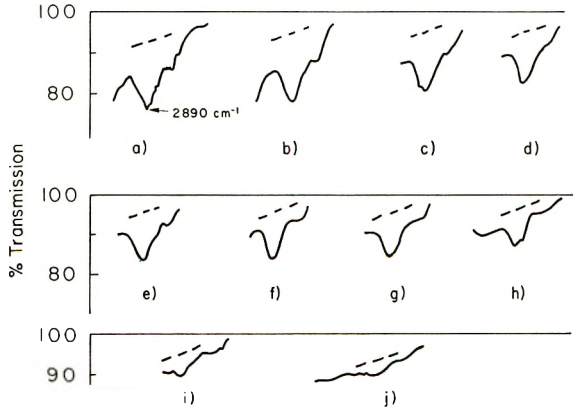

Figure 7. Changes in 2890-cm^{-1} band with time: (a–b) steady state (P_{H_2} = 420 mm; $P_{C_2H_4}$ = 340 mm); (a) 20 min on stream; (b) 65 min on stream. (c–j) In H_2–He stream (P_{H_2} = 420 mm, P_{He} = 340 mm); (c) 0.4 min; (d) 1.5 min, (e) 2.8 min, (f) 4.4 min, (g) 6.9 min, (h) 13.5 min, (i) 29.5 min, (j) 35.5 min.

Figure 8 is a plot of the optical density of the 2890-cm^{-1} band center *vs.* time for the spectra shown in Figure 7. At the point labeled A on this graph, the H_2–C_2H_4 stream was changed to a H_2–He stream. The decrease in intensity of the spectrum due to X is rapid initially but becomes slower as time proceeds. Based on the *first two points* the initial rate of fall-off is such that if this rate were maintained (dashed line) it would take about 2 min in pure hydrogen to remove all of X from the surface. Similar conclusions are reached if the integrated intensity in the 2925–2825-cm^{-1} region is plotted as a function of time.

These results are best interpreted in terms of the mechanism suggested earlier.[18] Hydrogenation of ethylene is believed to occur on a limited number of zinc–oxygen pair sites capable of adsorbing hydrogen to form Zn–H and OH. The proposed bottleneck in the reaction is the two-step irreversible sequence

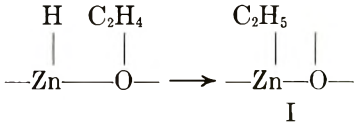

(3)

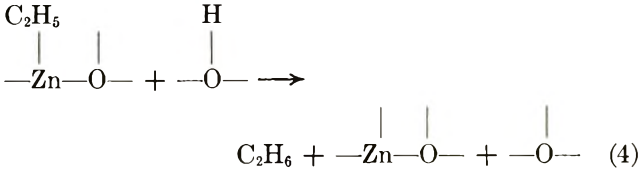

(4)

wherein -O- represents a hydrogen atom adsorbed on the oxide layer between the pair sites. The rate of the reaction, given the steady state, is the rate of *either* step 3 or 4. Accordingly, during steady state reaction, the concentration of the intermediate I should be constant; if the ethylene is suddenly removed but hydrogen is still present, the concentration of I should decrease and *the initial rate of decrease of I should be equal to the steady state conversion to ethane.* We have already noted that the initial rate of decline of X in Figure 1 is such that if the rate were maintained, X would be gone in about 2 min. Earlier it was noted that most of the

(31) The behavior of the OD bands under reaction conditions was striking inasmuch as the OD band split into two bands. In the absence of reaction the OD band occurred at 2584 cm^{-1}; under reaction conditions the two bands occurred at 2605 and 2624 cm^{-1}. When the ethylene flow was turned off but the deuterium flow was maintained, the two OD bands merged into one which returned to its initial position. Earlier reports from this laboratory reported the shift but not the splitting of the OD bands. In this current study, however, the ethylene pressure is higher than in the earlier study; hence, the differences may be more apparent than real.

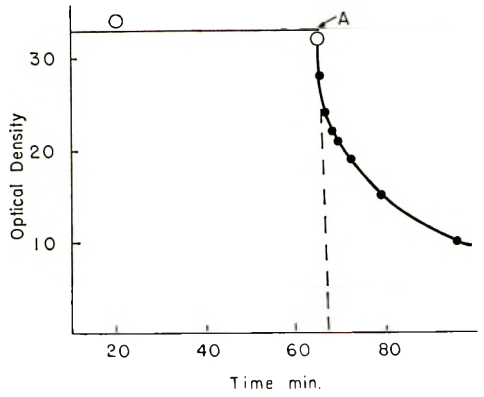

Figure 8. Optical density (in arbitrary units) of 2890-cm^{-1} band as a function of time. Open symbols are for steady state conversion (P_{H_2} = 420 mm, $P_{C_2H_4}$ = 340 mm). At point A the ethylene was removed from the stream but the hydrogen flow was continued. The dashed line represents the initial rate.

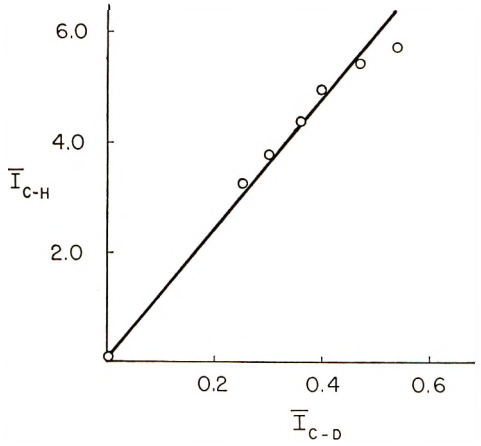

Figure 10. Intensity of the 2910-cm^{-1} band *vs.* the 2150-cm^{-1} band during the decay in deuterium. Conditions are the same as for Figure 9.

strongly held ethylene seemed to be converted to X during reaction. If we assume the amount of X on the surface is roughly comparable to the amount of strongly held ethylene (0.3cc/g) this means the initial rate of removal of X at point A of Figure 8 is 6.7 × 10^{16} molecules/sec/g. The measured rate of conversion to ethane in the steady state is 7.9 × 10^{16} molecules/sec/g. Within the rather large experimental error, these rates are identical.

[If indeed all sites to which X was attached were identical, we would expect the decay in Figure 8 to follow first-order kinetics. It does not; instead, the rate falls off faster than one would expect for first-order kinetics. This implies there is a distribution of sites and the more weakly bound X reacts first. If X and I were equivalent, this would imply hydrogenation occurs on a heterogeneous set of sites and the bulk of the reaction occurs *via* the sites on which I is most labile.]

Experiments similar to those depicted in Figure 7 were carried out with a C_2H_4–D_2 reaction mixture. Figure 9 is a plot of the decay of the integrated intensity of the single C–D stretching band at 2150 cm^{-1}. The

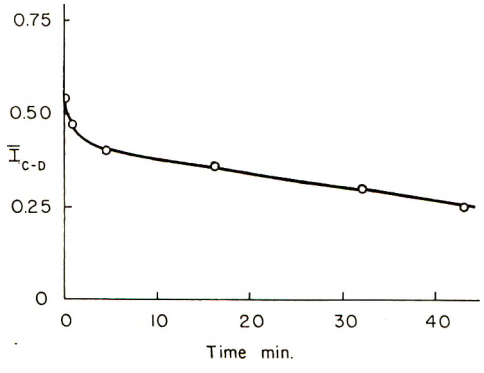

Figure 9. Integrated intensity of 2150-cm^{-1} band as a function of time. Before t = 0 the catalyst was effecting steady state conversion in a stream containing 445 mm of C_2H_4 and 315 mm of deuterium. At t = 0 helium was substituted for the ethylene.

estimated initial rate of decay corresponds to 4.5 × 10^{16} molecules/sec/g *vs.* a measured steady state conversion of 3.3 × 10^{16} molecules/sec/g. The slower rate in deuterium compared to hydrogen is roughly consistent with the isotope effect reported earlier.[18]

Figure 10 shows a plot of the decaying C–D stretch intensity *vs.* the intensity of the decaying C–H stretch intensity for this run. The fact that these data can be represented by a straight line through the origin indicates that a single species gives use to both the C–H and C–D bands.

The estimate of the rate of decay of X in hydrogen depends critically on the estimate of the amount of X on the surface. Although justifiable by the ir data, the assumption that the initial amount of X is comparable to the amount of chemisorbed ethylene in the absence of hydrogen seems like an overestimate. Accordingly, a few attempts were made to estimate the amount of intermediate by a series of experiments in which the steady state hydrogenation of ethylene was interrupted, the system was purged briefly, and the surface species were removed by a stream of hydrogen or deuterium. The amount of C_2H_6 or C_2H_5D found in the effluent provides a rough estimate of the amount of complex on the surface. The results were somewhat ambiguous but suggest the amount of intermediate on the surface was about 0.1 cc/g. Combination of this estimate with that made earlier suggests the amount of X is 0.2 ± 0.1 cc/g. Revised estimates of the initial decay rate of X then become 55 ± 27% and 90 ± 45% of the steady state rate for C_2H_4–H_2 and C_2H_4–D_2, respectively. The fact that the measured rate of decay of X may be lower than the steady state hydrogenation rate is not greatly disturbing; in fact, two factors make this reasonable. (1) The estimate of the initial rate of decay based on the initial two points is clearly an underestimate of the initial rate. (2) The expected identity of the initial decay rate is based on the idealization that ethylene is removed instantaneously at t = 0. Ethylene is

removed very rapidly but not instantaneously. Since reaction of this retained ethylene will replace some of the complex removed by hydrogen, the rate of removal of intermediate as judged by ir would be expected to be somewhat less than the rate of steady state hydrogenation. In sum, then, the data strongly suggest X is an intermediate.

The bands assigned to X near 1415 cm^{-1} also decay rapidly in a $He-H_2$ stream. Cursory measurements suggest their decay is somewhat faster than the decay of bands in the C–H stretching region; but this conclusion may be an artifact: the bands are relatively broad and the sloping background makes intensity measurements difficult.

Discussion

It has been suggested[18] that activated zinc oxide contains a limited number of noninteracting active sites. These sites, formed by surface reconstruction, were visualized as zinc ions systematically distributed in trigonal holes of a closely packed layer of oxide ions. If we approximate the ions by spheres, the plane tangent to the surface of the oxide ions would be 0.53 Å above the surface of the sphere corresponding to the zinc ion;[18] hence, it was concluded that for steric reasons the "π-bonded" adsorbed ethylene was more likely to be bound to oxide ions surrounding the imbedded zinc than the imbedded zinc ion itself. It was suggested, however, that once an alkyl radical was formed, the more directed σ bond might be attached to the imbedded zinc ion. Clearly, nonbonded interactions with the hydrogens on this alkyl group would be quite great.

Infrared and heat data support the view that about 0.3 cc/g of ethylene is chemisorbed *via* a π bond to the zinc oxide surface. This amount is roughly twice as great as the amount of hydrogen adsorption on the active sites[18] but it should be remembered that the number of oxide ions is three times as great as the number of imbedded zinc ions which are part of the site for hydrogen adsorption. Thus, in the main, the data for ethylene presented here are consistent with the earlier picture.

The species X has all the characteristics of an intermediate. The amount of this intermediate is much greater than we implicitly assumed earlier[18] in our discussions of kinetics. This means that the explanation of the rate dependence of ethylene is based on assumptions more approximate than we thought earlier. Table III lists the bands observed for X and compares them to bands observed for diethylmercury, a compound with a spectrum typical of metal alkyls including diethylzinc.[32] The band at 2812 cm^{-1} for X is too low to be a CH stretching fundamental and must be a reasonably strong overtone or combination. The three bands at 2860, 2892, and 2940 cm^{-1} suggest we are dealing with a species which is paraffinic and contains at least three hydrogens. The occurrence of these bands in the $C_2H_4-D_2$ reaction mixture together with a single band at 2150 cm^{-1}, the paraffinic C–D region, suggests that X is a species with at least four hydrogen atoms. If we admit to the possibility that the 2940-cm^{-1} band, which is broad, may be more than one band, the assignment given for these three bands in Table III follows.

Table III: Assignments for Intermediate and Diethylmercury

Bands of diethylmercury,[a] cm^{-1}	Assignment[a]	Intermediate bands, cm^{-1}
2975 vs	CH_3 anti	(2940) br
2930 vs	CH_2 anti	
2900 vs	CH_3 sym	2892 s
2850 sh	CH_2 sym	2860 m
2750 m	2δ CH_3	2812 w
1468 1460 ssh	CH_3 anti def	1440 s br
1430 s 1375 s	CH_2 scissor CH_3 sym def	1415 s br

[a] These data were taken from Kaesz and Stone.[32] Above 2800 cm^{-1} we accepted their assignment; below 2800 cm^{-1} we used the more explicit assignments of Green.[33] Only those bands were listed above 1300 cm^{-1} that were listed as m or stronger.

The infrared spectra of all metal alkyls studied by Kaesz and Stone[32] show a band at about 2750 cm^{-1} assignable to an overtone of the symmetric methyl deformation vibration. If we assign the band at 2812 cm^{-1} to this overtone, that places the symmetric methyl deformation frequency in the region near the broad band observed at 1415 cm^{-1}. If we make this assignment and take account of the fact that a band also occurs here for $Zn-CH_2-CH_2D$, we must conclude that this broad band also includes the scissor-like vibration of the CH_2 group attached to the zinc. This leaves the band at 1440 cm^{-1} for the antisymmetric methyl deformation vibration. This band would be expected to persist for the species $Zn-CH_2-CH_2D$ since monodeuteration effectively removes the degeneracy of the antisymmetric deformation of methyl and gives rise to one band nearly unchanged in position and another at much lower frequencies.[34] On the other hand, one would expect that for $Zn-CH_2-CH_2D$ the band, due to an overtone of the symmetric methyl deformation (2810 cm^{-1}), would be missing;[34] this seems to be the case.

The above assignments can be criticized on two grounds. (1) The relative intensities of the CH

(32) H. D. Kaesz and L. G. A. Stone, *Spectrochim. Acta*, **15**, 360 (1959).

(33) J. H. S. Green, *ibid.*, *Part A*, **24**, 863 (1968).

(34) J. R. Riter, Jr., and D. F. Eggers, Jr., *J. Chem. Phys.*, **44**, 745 (1966).

stretching bands are not those expected for ethyl groups. (2) The symmetric methyl deformation is generally extremely stable in position at about 1380 cm^{-1} when the methyl group is attached to a carbon atom. The assignment of a band above 1400 cm^{-1} to this vibration seems unlikely.

We believe the first objection poses no great difficulties. Usually, it is true, the antisymmetric stretching band of the methyl is more intense than the symmetric stretching band. It is possible, however, that steric effects of the surface split the degenerate antisymmetric stretching band. When this occurs, as it may in some methyl aromatics,[35,36] the antisymmetric methyl stretch is not always the strongest band in the aliphatic C–H stretching region. It is also possible that the strong band at 2890 cm^{-1} is a band enhanced by overlap of CH_3 symmetric stretch with the antisymmetric CH_2 stretch as has been suggested by Weedlein and Krieg[37] for diethylaluminum flouride. In any case when one encounters behavior like that encountered for ethylene adsorbed on molecular sieves,[22] for which the deformation bands are quite strong but the stretching frequencies are not observed, it seems overly scrupulous to reject assignments for adsorbed species on the basis of relative intensities alone.

The second objection, *i.e.*, the position of the symmetric methyl deformation, we regard as a difficult one to answer. This frequency has been discussed in some detail recently by Bellamy.[38] He points out that a major factor contributing to the position of the band when a methyl group is bound to other than carbon atoms are the nonbonding interactions. This is particularly evident in Urey–Bradley calculations for the methyl halides.[39] For these molecules the rather high value for the methyl symmetric deformation in CH_3F is almost entirely due to these nonbonding interactions.[40] [It is noteworthy that the symmetric deformation, which involves motion of all methyl hydrogens toward the other bond, is the deformation–vibration most sensitive to the neighboring group. In methylmercury compounds[33] the asymmetric deformation is shifted about 30 cm^{-1}; the symmetric deformation is shifted 180 cm^{-1}.] It is these nonbonded effects that are probably operative in CH_3CF_3;[38] for this compound even though the methyl group is bonded to a carbon, the symmetric deformation occurs at 1409 cm^{-1}. In view of our model for the bound ethyl and the close approach of methyl hydrogen to oxide ions that it entails, it does not seem too contrived to assume similar interactions combine to shift the symmetric deformation frequency to higher than usual values. Some support for the view that a methyl group is present is afforded by the appearance of a band at 1289 cm^{-1} for the species Zn–CD_2–CHD_2. This band, clearly due to a deformation of the lone C–H bond, is near the range attributable to the CH bending vibration (1301–1309 cm^{-1}) in CD_3–CD_2H.[41]

Finally, we wish to note that we considered alternative assignments for X. The only possibilities seemed to be polymeric paraffinic species. A careful search was made for polymers in the effluent of the reaction of hydrogen with X. No such polymers were found. Accordingly, we conclude that X is an intermediate of the form S–CH_2–CH_3 and the occurrence of the overtone at 2812 cm^{-1} is strong evidence that S is a zinc ion. The lack of detailed agreement of the assignment with that expected on the basis of model compounds can be viewed as evidence that such arguments by analogy are of limited value when surface species are involved.

Acknowledgment. Acknowledgment is made to the donors of the Petroleum Research Fund, administered by the American Chemical Society, for support of this research.

(35) N. Fuson and M. L. Josien, *J. Amer. Chem. Soc.*, **78**, 3049 (1956).

(36) G. M. Badger and A. G. Moritz, *Spectrochim. Acta*, **15**, 672 (1959).

(37) J. Weedlein and V. Krieg, *J. Organometal Chem.*, **11**, 9 (1968).

(38) L. J. Bellamy, "Advances in Infrared Group Frequencies," Methuen & Co. Ltd., London, 1968, pp 9–13; L. J. Bellamy, "Proceeding of the Xth Colloquium Spectroscopicum Internationale," E. R. Lippincott and M. Margoules, Ed., Spartan Books, Washington, D. C., 1963, p 487.

(39) J. Overend and J. R. Scherer, *J. Chem. Phys.*, **33**, 446 (1960).

(40) W. T. King and B. Crawford,Jr ., *J. Mol. Spectrosc.*, **5**, 421 (1960).

(41) R. Van Riet, *Ann. Soc. Sci. Bruxelles*, **71**, 102 (1957).

Involvement of Hydrated Electrons in Electrode Processes

by B. E. Conway* and D. J. MacKinnon

Department of Chemistry, University of Ottawa, Ottawa, Canada *(Received September 4, 1969)*

Recently, pathways in cathodic hydrogen evolution have been proposed which involve the initial production of hydrated electrons. Attention is directed to some kinetic and, under certain conditions, thermodynamic difficulties which arise with this type of mechanism. Problems of microscopic reversibility, electrochemical adsorption of H, role of the electrode metal, and the standard potential of the hydrated electron are considered, as well as the chemical basis for distinction between the hydrated electron and atomic H when reduction reactions at catalytic electrode surfaces are involved. Electrode reductions involving direct electron transfer (in distinction to electrochemical hydrogenations) are possible with the electrode surface acting as the nucleophile in Sn2-type reactions.

1. Introduction and Statement of Problems

The hydrated electron is well known[1] as a transient intermediate in radiolysis of water and photolysis of certain aqueous solutions and the kinetics and mechanisms of its reactions have been extensively studied and reviewed.[1] More recently, a number of suggestions have been made[2-7] (and discussed in relation to various experiments[2,3,7]) that hydrated electrons are the primary entities involved in cathodic hydrogen evolution and metal dissolution on open-circuit (corrosion processes). From an electrochemical kinetic and thermodynamic point of view, however, there are several serious difficulties which arise in these suggestions. It is the purpose of this paper to examine these problems in terms of the electrochemical principles involved, since the mechanisms of the hydrogen evolution reaction (h.e.r.) involving the hydrated electron which have been proposed differ radically from pathways previously considered (until about 1965) in a large body of work published since Tafel's early contributions. In some of these papers, particularly those published in recent years, is to be found certain critical evidence indicating involvement of protons directly discharged at the metal.

That hydrated electrons are the precursors of cathodically evolved hydrogen in electrochemical hydrogen production and metal dissolution in aqueous solutions seems to have been first discussed by Pyle and Roberts[5] and by Walker,[2] who proposed this mechanism as a general basis for cathodic hydrogen evolution. Experimental indications of this view were obtained[2] by him under certain conditions (see below) by means of an ingenious multiple reflectance light absorption experiment, and by chemical experiments involving the use of scavengers.[2] Photoelectrochemical emission of electrons at mercury electrodes was studied earlier by Barker[8] and in related work by Delahay[9] but under these conditions of photoexcitation the difficulties associated with the suggestions of ref 2–6 are not involved. Yurkov's observation[7] of deposition of Cu *between* an anode and cathode of Cu was attributed to neutralization of copper ions by electrons in solution but this explanation and also one that could be based on diffusion of H atoms from the cathode[10] seems unlikely owing to the macroscopic distances involved.[7] Possibly disproportionation of Cu^+ ions is involved. The deduction of a mechanism of e_{aq}^- formation from the kinetic studies of Hills and Kinnibrugh[3] on the hydrogen evolution reaction at high pressures is of interest but the evaluated negative volume of activation $\Delta V^{\pm}$, which led to their conclusions, becomes a (normal) positive value when the data are corrected[4] for pressure effects on the H_2 reversible electrode potential.

We shall now enumerate some of the difficulties and return to several general matters subsequently.

(a) The first is a quasithermodynamic one: the standard potential for the hydrated electron e_{aq}^- on the hydrogen scale has been calculated from kinetic data to

* To whom correspondence should be addressed.

(1) Various papers in "Solvated Electrons," Advances in Chemistry Series, No. 50, American Chemical Society, Washington, D. C., 1965. (See also: E. G. Hart, *Science*, **146**, 19 (1964); M. Anbar, *Quart. Rev., Chem. Soc.*, **22**, 579 (1968); and U. Schindewolf, *Angew. Chem., Int. Ed. Engl.*, **7**, 190 (1968)).

(2) D. C. Walker, *Can. J. Chem.*, **44**, 2226 (1966); E. A. Shaede and D. C. Walker, *Chem. Soc., Spec. Publ.*, **22**, 277 (1967); D. C. Walker, *Can. J. Chem.*, **45**, 807 (1967); *Anal. Chem.*, **39**, 896 (1967); see also G. Hughes and R. J. Roach, *Chem. Commun.*, 600 (1965).

(3) G. J. Hills and D. R. Kinnibrugh, *J. Electrochem. Soc.*, **113**, 1111 (1966).

(4) B. E. Conway in "Chemical Physics of Ionic Solutions," B. E. Conway and R. G. Barradas, Ed., Wiley, New York, N. Y., 1966, p 577; and for later discussions of this point, see L. I. Kristalik, *J. Electrochem. Soc.*, **113**, 1117 (1966); R. Parsons, *ibid.*, **113**, 1118 (1966); B. E. Conway, *ibid.*, **113**, 1120 (1966).

(5) T. Pyle and C. Roberts, *J. Electrochem. Soc.*, **115**, 247 (1968).

(6) F. S. Dainton, *Endeavour*, **26**, 115 (1967).

(7) V. A. Yurkov, *Sov. Electrochem.*, Symposium 1959, **II**, 85 (1961).

(8) G. C. Barker and A. W. Gardner, *Proc. C.I.T.C.E. Meeting, Moscow, 1963;* see also P. J. Hillson and E. K. Rideal, *Proc. Roy. Soc., Ser. A*, **199**, 295 (1949); and G. C. Barker, *Electrochim. Acta*, **13**, 1221 (1968).

(9) P. Delahay and V. S. Srinivasan, *J. Phys. Chem.*, **70**, 420 (1966).

(10) R. C. Krutenat and H. H. Uhlig, *Electrochim. Acta*, **11**, 469 (1966); *cf.* N. Kobosow and V. Nekrassov, *Z. Elektrochem.*, **36**, 529 (1930).

be *ca.* -2.67 V[11,12] yet hydrogen is easily evolved on the more catalytic metals at appreciable rates ($>10^{-4}$ A cm^{-2}) already at 0.1–0.2 V cathodic to the reversible H_2 potential E_H (even in alkaline solutions, *e.g.*, 10^{-4} A cm^{-2} in 0.1 *N* NaOH at 20° at Ni[13]). If the cathodic process were, *cf.*[2]

$$M(e) + H_2O \longrightarrow e_{aq}^- (\longrightarrow H \longrightarrow {}^1/_2H_2) \quad (I)$$

rather than direct discharge of a proton out of H_2O or H_3O^+, it would be necessary to suppose that the e_{aq}^- intermediate was produced at these potentials in a quasiequilibrium[14] concentration C of the order of 10^{-40} g electron/l. (10^{-20} actual electron/cm^2). Since diffusion effects operate,[2,5] this will be an upper limit. It seems kinetically impossible to envisage hydrogen evolution occurring as it does at 10^{-5} to 10^{-3} A cm^{-2} at the catalytic metals (Ni, Pt) at an overpotential $\eta = -0.2$ V, say, by such a mechanism. Even at dissolving amalgams, where $\eta = ca. -1.5$ V, C would be unrealistically small.

As pH is changed from acid to alkaline values, the mechanism of the h.e.r. remains basically the same[13] but H_2O rather than H_3O^+ becomes the proton source[13] giving a zero order in "pH." The essential point is that adsorbed H and molecular H_2 can be extensively produced at any significant overpotential from alkaline or acid solutions since such potentials are (by definition) negative with respect to E_H. The opposite is the case with e_{aq}^-; it must be produced at potentials very positive to its standard potential $E^\circ_{e_{aq}^-}$ yet at a rate equal to twice the overall Faradaic rate of H_2 evolution. In kinetic terms, this would imply an impossibly high exchange current for the process $M(e) \rightleftharpoons e_{aq}^-$, occurring at $E^\circ_{e_{aq}^-}$ ($= -2.67$ V). This difficulty is not very much diminished if it is recognized that a more realistic potential for this calculation should perhaps be $2.67 - 0.06 \times 6 \doteqdot 2.31$ V, *i.e.*, the potential corresponding to the presumed concentration limit for detection of e_{aq}^-, *ca.* 10^{-6} *M* by absorption spectrophotometry.

(b) A related problem arises when microscopic reversibility is considered. At the reversible potential (but not necessarily at other potentials where the electrochemical reaction is not at equilibrium, and kinetic pathways may not be identical[15] with those at equilibrium when $\eta = 0$), the h.e.r. may be regarded as proceeding either by

$$H^+ + e + M \longrightarrow MH \quad (II)$$

with

$$2MH \longrightarrow H_2 \quad (III)$$

or with other desorption steps giving H_2. With the e_{aq}^- path, the reversible process would have to be written (*cf.*[6,11]), for example, as

$$M(e) + H_2O \rightleftharpoons M + e_{aq}^- \quad (IV)$$

$$e_{aq}^- + H_2O \rightleftharpoons H + OH^- \quad (V)$$

$$H \rightleftharpoons {}^1/_2H_2 \quad (III)$$

Pyle and Roberts[5] also considered $e_{aq}^- + e_{aq}^- \rightarrow H_2 + 2OH^-$.

The back reaction pathway would therefore have to be envisaged as H giving e_{aq}^- spontaneously, with the latter entity being the one in charge-transfer equilibrium with the electrode. Similar processes should presumably occur in metal deposition (*cf.* the calomel half-cell reaction discussed by Dainton:[6] $Hg_2^{2+} + 2Cl^- + 2e_{aq}^- \rightarrow 2Hg + 2Cl_{aq}^-$) if this type of mechanism applied. Again it seems difficult to envisage spontaneous e_{aq}^- formation (which would have to occur with very low concentrations of e_{aq}^-) as a basis for reactions, including the h.e.r., which can proceed at quite high, non-diffusion-controlled exchange current densities of 10^{-3} to 10^{-1} A cm^{-2} at certain metals.[16]

(c) In anodic electrolysis very near the reversible potential (so that the process is subject to the requirements of microscopic reversibility) of a metal, *i.e.*, in the back reaction of metal deposition, *e.g.*, $Hg + 2Cl_{aq}^- \rightarrow Hg_2Cl_2 + 2e_{Hg}$ or $Na/Hg \rightarrow Na_{aq}^+ + e_{Hg}$, electrons must pass along the metal electrode and conducting wires. It seems intuitively unlikely that they should first be produced anodically in solution as considered for example by Pyle and Roberts[5] then return to the metal, *viz.*

$$M \rightleftharpoons M^+ + e_{aq}^- \quad (VI)$$

$$e_{aq}^- + M \rightleftharpoons M(e) \quad (VII)$$

e.g., in anodic amalgam dissolution near the reversible potential for Na/Hg. In the final process VII, the electron in the metal M(e) must pass down the external circuit.

Similar difficulties would seem to arise in the interesting suggestion[4] that the absolute potential of the calomel half-cell reaction, written[6] as

$$2Hg + 2Cl^- \rightleftharpoons Hg_2Cl_2 + 2e_{aq}^- \quad (VIII)$$

can be calculated if the hydration energy of e_{aq}^- is known. If estimates of the calomel half-cell absolute potential are to be made (but *cf.* ref 17 for other diffi-

(11) J. H. Baxendale, *Rad. Res.*, **23**, Suppl. 4, 139 (1964).

(12) M. S. Matheson in ref 1, p 45; for the value of $E^\circ_{e^-}$ for NH_3 see H. A. Laitinen and C. J. Nyman, *J. Amer. Chem. Soc.*, **70**, 2241 (1948).

(13) J. O'M. Bockris and E. C. Potter, *J. Chem. Phys.*, **20**, 614 (1952).

(14) The question of the extent of departure from equilibrium conditions, which necessarily arises on account of e_{aq}^- annihilation processes, is considered below.

(15) K. J. Laidler, *Trans. Faraday Soc.*, **62**, 2754 (1966).

(16) *E.g.*, see J. O'M. Bockris, "Modern Aspects of Electrochemistry," Vol. I, 1954, Chapter IV, Butterworths Scientific Publications, London.

(17) W. M. Latimer, K. S. Pitzer, and C. M. Slansky, *J. Chem. Phys.*, **7**, 108 (1939); see also A. N. Frumkin, *ibid.*, **7**, 552 (1939).

culties involved), it seems necessary[18] to consider the electron in a state at the Fermi level of the metal Hg rather than in a solvated condition in the aqueous solution, so that the work function of the metal, rather than the solvation energy of e^-, is involved in determining the potential. In fact, direct electron transfer between anions or cations and metal surfaces can occur[19] with quite low (5–7 kcal mol^{-1}) activation energies, as observed experimentally.[20] Moreover, formation or reduction of surface phases such as Hg_2Cl_2 or AgCl are Faradaically quantitative so that formation of e_{aq}^-, which could lead to secondary H_2 evolution, is not indicated.

(d) A further argument that makes it difficult to accept, in general, a mechanism[5] of metal dissolution producing e_{aq}^- is that the kinetic characteristics of corrosion processes at metals (the steady-state corrosion current and the mixed potential) can be very well accounted for by means of polarization diagrams involving the individual cathodic and anodic reactions proceeding under appreciable polarizations at nonnegligible currents; under such circumstances the arguments in (a) and (c) above apply, so that a mechanism of corrosion based on a primary process of e_{aq}^- production ($M \rightarrow M^{z+} + ze_{aq}^-$) with the associated cathodic process $H^+ + e_{aq}^- \rightarrow {}^1/_2H_2$ raises obvious difficulties.

(e) Finally, at the noble metals Pt, Rh, Ir, electrochemically adsorbed H can be quantitatively and reproducibly determined[21,22] by electrochemical procedures and the potential dependence of its coverage follows relations that can be derived for an electrochemical quasiequilibrium of the type $H_2O + M(e) \rightleftharpoons MH_{ads} + OH^-$ and a corresponding process for acid solutions. Such behavior can, in fact, be studied sufficiently exactly that coadsorption of other chemisorbed blocking species can be determined quantitatively. It seems unlikely therefore that the observed behavior[21,22] could arise if the processes of formation and removal of adsorbed H were

$$M(e) + H_2O \longrightarrow e_{aq}^- \qquad (I)$$

$$e_{aq}^- + H_2O \longrightarrow H + OH^- \qquad (IX)$$

in solution with adventitious readsorption of H from the solution by the process (*cf.* ref 5)

$$H_{(\text{from solution})} + M \longrightarrow MH_{ads} \qquad (X)$$

together with the corresponding back reactions, since the process of electrochemical adsorption of H (prior to H_2 evolution at slightly more cathodic potentials) is highly reversible,[22] so all the steps indicated above would have to be (a) reversible and (b) capable of proceeding at appreciable rates if the e_{aq}^- pathway for H adsorption (and hence H_2 evolution) were accepted. In this connection, it is important to note here that the electrochemisorption behavior of H at Pt, Rh, and Ir is almost the same[23] in acid as in alkaline or neutral solution, so it is unlikely to arise from H homogeneously produced from e_{aq}^-; the latter is irreversibly converted[24] to H much faster in acid than in alkaline or neutral media so that homogeneous recombination of H to H_2 would be favored over adsorption under the latter conditions of pH.

The potentiodynamic behavior for electrochemisorption of H corresponds to a *direct* discharge process. Thus, the charge associated with adsorbed H production is almost independent[22] of potential sweep rate, and the pseudo-capacitance charging currents at the peak maxima are proportional to sweep rate so that only a direct surface discharge, and not a diffusion-controlled[25] process, can be involved.

A closely related question is the interpretation of the fundamental kinetic coefficient b ($= dV/d \ln i$) in Tafel's equation[16] characterizing the dependence of rate of the electrochemical reaction on potential V. For certain metals, *e.g.*, Pd[26] and Pt,[27] and some alloys,[26] $b = RT/(1 + \beta)F$ or $RT/2F$ where β is the usual electrochemical Brønsted factor[28] ($\doteq 0.5$). Such values of b are well characterized over an appreciable range of potentials and can be explained[16] on the satisfactory and quantitative basis that the coverage θ_H by *adsorbed* atomic hydrogen is appreciable and potential dependent according to a relation of the form[29]

$$\frac{\theta_H}{1 - \theta_H} = K \exp -VF/RT \exp -r\theta \qquad (1)$$

for the quasiequilibrium, potential-dependent reaction

$$H^+ + e + M \rightleftharpoons MH_{ads}$$

with a rate-determining desorption process characterizing the kinetics (and in particular b) in the following step such as

(18) J. A. V. Butler, "Electrocapillarity," Methuen, London, 1940, p 42.

(19) B. E. Conway and J. O'M. Bockris, *Electrochim. Acta*, **3**, 340 (1961).

(20) J. E. B. Randles and K. W. Somerton, *Trans. Faraday Soc.*, **48**, 937, 951 (1952); J. O'M. Bockris and E. C. Potter, *J. Electrochem. Soc.*, **99**, 169 (1952); *J. Chem. Phys.*, **20**, 614 (1952).

(21) A. N. Frumkin and A. Slygin, *Acta Physicochim. U.R.S.S.*, **3**, 719 (1935); **4**, 991 (1936); **5**, 819 (1936).

(22) F. Will and C. A. Knorr, *Z. Elektrochem.*, **64**, 258 (1960); D. Gilroy and B. E. Conway, *Can. J. Chem.*, **46**, 875 (1968).

(23) M. W. Breiter, *Ann. N. Y. Acad. Sci.*, **101**, 709 (1963).

(24) J. Rabani in ref 1, p 242.

(25) P. Delahay and G. Perkins, *J. Phys. Coll. Chem.*, **55**, 586, 1146 (1951).

(26) J. P. Hoare and S. Schuldiner, *J. Electrochem. Soc.*, **99**, 488 (1952); **102**, 178 (1955); **104**, 564 (1957); see also S. Schuldiner and J. P. Hoare, *J. Phys. Chem.*, **61**, 705 (1957); **62**, 229 (1958); **62**, 504 (1958).

(27) J. O'M. Bockris and A. M. Azzam, *Trans. Faraday Soc.*, **48**, 145 (1952).

(28) A. N. Frumkin, *Z. Phys. Chem.*, **160**, 116 (1932); *cf.* B. E. Conway, *Discuss. Faraday Soc.*, **39**, 47 (1964); and in "Progress in Reaction Kinetics," G. Porter, Ed., Pergamon Press, London, 1967, Chapter 4.

(29) *E.g.*, see A. Eucken and B. Weblus, *Z. Elektrochem.*, **55**, 114 (1951); B. E. Conway and E. Gileadi, *Trans. Faraday Soc.*, **58**, 2493 (1962).

$$MH_{ads} + H^+ + e \longrightarrow H_2 \qquad b = RT/(1 + \beta)F$$

or

$$MH_{ads} + MH_{ads} \longrightarrow H_2 \qquad b = RT/2F$$

Electrochemical production of solvated electrons at various distances in the solution, followed by homogeneous reaction to give H_2, could not give values of $b < RT/\beta F$ such as are observed in the kinetics of the h.e.r. at a number of metals including platinum studied by Walker[2] in regard to N_2O reduction. If the e_{aq}^- path were involved, $b = RT/\beta F$ would be found for all metals, corresponding to the electron tunneling process of Gurney.[30] Similarly, the kinetics of the h.e.r. are highly specific to the cathode material,[31] an effect which has been attributed to the role of chemisorbed H. Electron emission into solution with homogeneous hydrogen production could not give the observed specificities with regard to values of i_o and b.

From the above remarks, it will be seen that there are substantial difficulties of a basic electrochemical kind if the view is taken that cathodic reactions, and *inter alia* the kinetics at the reversible potential, proceed *via* the primary production of e_{aq}^-. It must be stressed, however, that if cathodic potentials relative to the hydrogen electrode are sufficiently high, say >1.9–2.0 V, it would be kinetically feasible to envisage the e_{aq}^- path operating *at* such potentials; this may be the explanation of Walker's observations at amalgams. Such a path cannot, however, be expected to be a general mechanism for cathodic processes as has been implied.

Most of the above conclusions based on electrochemical arguments depend on the value of the standard redox potential[11,12] being approximately correct. It is of course a calculated value based on rate constants but the revised value[12] quoted cannot, it seems, be excessively in error. For e_{aq}^- involvement to be appreciable in the h.e.r. occurring up to say -0.5 V E_H, it seems that the E° value would have to be in error by at least 2 V. An error of such magnitude would be unlikely[32] since it would require revision of one of the rate constants by many powers of ten.

A final matter concerns electrochemical reductions of organic compounds at the mercury cathode which are stereoselective, *e.g.*, in the electrolysis of diphenylcyclopropyl bromides,[33] dimethylmaleic and -fumaric acids,[34] and 2-chloro,2-phenylpropionic acid.[35] The stereoselectivity must arise by direct electron transfer from the cathode to an adsorbed molecule, preferentially oriented in one direction at the electrode interface. The kinetics are usually also specific to the metal, *e.g.*, in reduction of ketones and alkyl halides.[36] If such reductions occurred homogeneously by an SN2 type of mechanism through solvated electrons (*cf.* the reaction of chloroacetic acid with e_{aq}^- [37]) it is difficult to see how the observed stereoselectivity could arise. These difficulties are avoided if the view hitherto held in electrode kinetics is retained, namely that cathodic reduction occurs by a suitable thermal reorganization of the oxidant molecule and/or its solvation shell in the activation step and this condition allows radiationless electron transfer directly *from the metal.*[19,30] This is the general mechanism of electroreduction and there is no reason why it may not occur just as well with electron scavengers such as N_2O or $ClCH_2COOH$ which, in homogeneous processes, are specific for e_{aq}^- (in distinction to H) as it does in other cathodic processes. For example, at Hg or amalgam cathodes there is no question electrochemically of organic reductions occurring by an atomic hydrogen mechanism. Direct transfer of an electron to the thermally reorganized transition state of a reactant must be distinguished from the e_{aq}^- pathway where e_{aq}^- is a true intermediate having an appreciable lifetime in comparison with that of a kinetic transition state in the electrode double layer.

The general conclusions made above for most electrode reactions proceeding at low potentials are, we believe, not invalidated by the interesting positive identification by Bennett, *et al.*,[38] of the hydrated electron produced from Na or K atoms at 77°K on ice. Here a sufficiently small flux of Na or K atoms was condensed on a rotating layer of ice that, as the authors state, atoms adjacent to one another were rare. Under these conditions, the Na or K will be appreciably more reactive and "base" to an extent determined approximately by the free energy of sublimation. Taking this quantity as approximately 26 kcal mol^{-1}, it is seen that Na or K atoms will be, from a thermodynamic point of view, appreciably more reactive than bulk metallic sodium and would have hypothetically an electrode potential some 1.1 V more negative than that of sodium in its normal state. Under these conditions, e_{aq}^- production in the ice is easy to understand.

2. Standard Potential for e_{aq}^- and the Nonequilibrium Situation

It is clear that the thermodynamic objections (but not, however, the kinetic ones based on observed Tafel

(30) R. W. Gurney, *Proc. Roy. Soc., Ser. A*, **134**, 137 (1931).

(31) B. E. Conway and J. O'M. Bockris, *J. Chem. Phys.*, **26**, 532 (1957).

(32) For comparison, the polarographically determined value of the standard potential for electrons in liquid NH_3 is -1.95 ± 0.1 V E_H (calculated for 25°)[12] and for this case the uncertainties are small.

(33) R. Annino, R. Erickson, J. Michaelovich, and B. MacKay, *J. Amer. Chem. Soc.*, **88**, 4424 (1966).

(34) I. Rosenthal, J. R. Hayes, A. J. Martin, and P. J. Elving, *ibid.*, **80**, 3050 (1958).

(35) Z. R. Grabowski, B. Czochralska, A. Vincenz-Chodkowska, and M. Balasiewicz, *Discuss. Faraday Soc.*, **45**, 145 (1968).

(36) E. Muller, *Z. Elektrochem.*, **33**, 253 (1927); T. Sekine, A. Yamura, and K. Sugino, *J. Electrochem. Soc.*, **112**, 439 (1965); see also B. E. Conway and E. R. Rudd, *Trans. Faraday Soc.*, in press.

(37) E. Hayon and A. O. Allen, *J. Phys. Chem.*, **65**, 2181 (1961).

(38) J. E. Bennett, B. Mile, and A. Thomas, *J. Chem. Soc.*, 1393 (1967); see also *Nature*, **201**, 919 (1964).

slopes and electrochemisorption behavior of H) may be diminished if the calculated reversible potential were substantially in error (but see above) and/or if the "equilibrium" potential were inapplicable. That the latter situation should receive further consideration[39] is indicated by the conditions imposed by the short lifetime of the electron in acid media. Electrons may be ejected under suitable conditions of potential and/or irradiation[8,9] but may not exist long enough for the reversible equilibrium I to be kinetically established. Under these conditions, this is equivalent to requiring that in the following equality of rates

$$\vec{v}_{\mathrm{I}} = k_{\mathrm{I}} \exp -\beta VF/RT = \overleftarrow{v}_{\mathrm{I}} = k_{-\mathrm{I}} C_{e_{aq}^-} \exp(1-\beta)VF/RT \quad (2)$$

written for equilibrium conditions, the $\overleftarrow{v}_{\mathrm{I}}$ term is actually appreciably less than the first term. In fact, a steady-state condition for production and annihilation of e_{aq}^- by IX at a given potential V should be written and an approximate form of such a relation is shown below

$$\frac{d\bar{C}_{e_{aq}^-}}{dt} = k_{\mathrm{I}} \exp(-\beta VF/RT) - k_{-\mathrm{I}} \bar{C}_{e_{aq}^-} \exp(1-\beta)VF/RT - k_{\mathrm{IX}} \bar{C}_{e_{aq}^-} = 0 \quad (3)$$

where $\bar{C}_{e_{aq}^-}$, for the approximation, expresses a mean concentration of solvated electrons near the surface and the rate constants refer to the reactions designated by I and IX earlier. The difference between the first two terms in eq 3 is the net cathodic current. Then

$$\bar{C}_{e_{aq}^-} = \frac{k_{\mathrm{I}} \exp[-VF/2RT]}{k_{-\mathrm{I}} \exp[VF/2RT] + k_{\mathrm{IX}}} \quad (4)$$

for $\beta = 0.5$. If e_{aq}^- could be produced under true equilibrium conditions, the same concentration $\bar{C}_{e_{aq}^-}$ would be attained when the potential was equal to the reversible, but not the standard, value V^* given by

$$\bar{C}_{e_{aq}^-} = K_{\mathrm{I}} \exp[-V^*F/RT] \quad (5)$$

The potential V required for reaching any given concentration in the steady state and that V^* for attainment of the same concentration under quasiequilibrium conditions therefore differ according to the relation

$$\exp[-(V - V^*)F/RT] = 1 + K_{\mathrm{I}} \frac{k_{\mathrm{IX}}}{k_{\mathrm{I}}} \exp[-VF/2RT] \quad (6)$$

Since the right-hand side is always >1, $V - V^*$ is negative and since we have been considering throughout negative potentials for the cathodic process, V is a more cathodic potential than V^*. This is as expected on general kinetic principles for an irreversible electrode process such as the sequence I, IX.

Alternatively, we can enquire whether the concentration $\bar{C}_{e_{aq}^-}{}^*$ that would be produced under hypothetical equilibrium conditions will be greater or less than the concentration $\bar{C}_{e_{aq}^-}$ for steady-state conditions for any given potential V. The two concentrations are given by eq 5 and 4, respectively, now taking the same V in each expression. The expressions for concentration are then

$$\bar{C}_{e_{aq}^-}{}^* = K_{\mathrm{I}} \exp(-VF/RT)$$

$$\bar{C}_{e_{aq}^-} = \frac{K_{\mathrm{I}} \exp(-VF/RT)}{1 + \frac{k_{\mathrm{IX}}}{k_{-1}} \exp(-VF/2RT)} \quad (7)$$

where eq 4 has been rearranged appropriately to have the same numerator as the right-hand side of the expression for $\bar{C}_{e_{aq}^-}{}^*$. Then, since under all conditions $1 + (k_{\mathrm{IX}}/k_{-1}) \exp(-VF/2RT) > 1$, $C_{e_{aq}^-} < C_{e_{aq}^-}{}^*$, a result which is consistent with the foregoing analysis in terms of V and V^*. The conclusion from this calculation is that the estimates of limiting concentration of e_{aq}^- made in terms of a quasi-thermodynamic equation will be an *upper* rather than a lower limit so that the conclusions made in section 1a are not invalidated by the fact that nonequilibrium conditions generally obtain.

It is useful to examine this question further in energetic terms related to the probability of electron tunneling in reaction I. Radiationless electron transfer to form the hydrated electron must obey Gurney's condition[30] that the so-called "neutralization energy" U is greater than or equal to $\phi - eV$ where ϕ is the work function of the cathode. For reaction I, no ionization potential or electron affinity is involved as in the case with cations or anions and only the solvation energy S_{e^-} of e^- determines U. That is, the condition for formation of e_{aq}^- by tunneling to solvation sites is simply

$$\phi - eV \leqslant |S_{e^-}| \quad (8)$$

S_{e^-} is *ca.* 1.74 eV,[11] so that e_{aq}^- will tend to be formed only when $\phi - eV < 1.74$ eV. ϕ for Ag is *ca.* 4.5 and for Pt *ca.* 5.2 eV, so that the absolute potential difference (pd) at the electrode interface must be at least *ca.* −2.76 V for Ag and *ca.* −3.46 V for Pt for any electron emission to occur forming e_{aq}^-. Conversion of such absolute pd's to figures relative to a practical scale of measurement, *e.g.*, with respect to the reversible hydrogen electrode, raises the usual and old problem of the absolute pd[17] at the interface of a hydrogen electrode at, *e.g.*, Pt or Ag (since the absolute *single* pd will depend on the metal) and in particular the influence of the χ potential.

(39) We are indebted to Dr. D. C. Walker for discussions, in correspondence, on this latter matter as a possible way out of the "thermodynamic" difficulties arising from the published E° value for e_{aq}^-. It is shown here, however, that some other difficulties of an energetic nature still remain.

Recent estimates of the latter quantity indicate that it may be smaller[40,41] than hitherto assumed[42] so that together with the recent reliable estimate[43] of the hydration energy of the proton, *viz.*, -261 ± 2.5 kcal mol^{-1}, and the known ionization potential of H and dissociation energy of $^1/_2H_2$, the single pd at, *e.g.*, the standard $H_2|Pt$ electrode can hardly be numerically in excess of -0.7 ± 0.3 V. Thus the condition in (8) is only realized for Pt when the potential is at least $-3.46 - (0.9)$ V, *i.e.*, *ca.* -2.5 V referred to the reversible hydrogen scale. This result seems at least not inconsistent with the thermodynamic argument based on the supposed standard potential of the electron of -2.67 V.

It is of interest to note that the corresponding "neutralization energies"[30] for Na^+ and K^+ would be -10.8 and -15.8 kcal mol^{-1} based on the ionization potentials and free energies of solvation.[43] These figures are substantially smaller than the "neutralization energy" of -40 kcal mol^{-1} for e_{aq}^- formation. The difference arises of course mainly because in the case of e_{aq}^- formation there is no gain of any energy corresponding to the negative of the ionization energy or the electron affinity in the case of anions. It is evident that these considerations, based on Gurney's conditions for tunneling, lead to the conclusion that formation of e_{aq}^- will be as, or *more*, difficult than neutralization of hydrated Na^+ or K^+ ions.

3. Photoemission and Reflectance Effects

The apparent direct spectroscopic observation by Walker[2] of e_{aq}^- (from absorption at one wavelength, 6330 Å) in the cathodic cycle of ac electrolysis at Ag is an important and interesting result that requires further consideration. Here the magnitude of the cathodic potential swing might have been sufficient (maximum potentials referred to a *reference electrode* were, however, apparently not measured) for e_{aq}^- to be generated, though at Ag it is known[44] that H_2 will be cathodically evolved at extremely high rates (see below) at any potentials sufficiently close to $E^\circ_{e_{aq}^-}$ (*ca.* -2.67 V) for it to be feasible for a detectable concentration (say 10^{-6} *M*) of e_{aq}^- to be generated in the "steady state." In fact, for such a concentration to be achieved in the electrode boundary layer,[5] the hydrogen overpotential would have to be at least (see below) *ca.* 2.3 V at which potential hydrogen would normally be evolved at *ca.* 10^{16} A cm^2! ($i_{o,Ag} = 10^{-8}$ A cm^{-2}, $b = 0.09$ V for the h.e.r. at Ag[44]).

Under conditions of illumination at an electrode, photoelectrochemical generation of e_{aq}^- becomes possible for, in effect, the reversible potential for e_{aq}^- production is then lowered by 300 $h\nu/e$ V where ν is the excitation frequency and e the electronic charge. In this connection, it is interesting to speculate that the reason why Walker[2] was able apparently[45] to detect e_{aq}^- spectrophotometrically was because of his laser illumination of the silver electrode surface at 6330 A. This supplies already an energy equivalent to *ca.* 1.96 V for excitation of electrons in the surface of the metal above the Fermi level, so that only a small extra potential is required to reach the e_{aq}^- "reversible potential" and liberate electrons to an appreciable extent. Expressed in another way, an applied potential V raises the Fermi level by an energy VF. The photoelectric threshold potential $h\nu_0$ corresponding to a critical frequency ν_c is then lowered by VF. It seems then that Walker's result could arise because of electrochemical assistance to the photoelectric effect[8,9] at the metal–solution interface. Effects of this kind have, in fact, been described by Heyrovsky.[48] The result of Walker, interesting as it is, does not therefore seem to provide an adequate proof of production of solvated electrons in cathodic processes in *general*, and the technique used would seem to render complicated any direct interpretation of the results in terms of involvement of solvated electrons in the h.e.r. in the absence of irradiation.

If the local intensity in the narrow laser beam were sufficiently high, this explanation may form a basis for rationalization of the effects observed in the light of the difficulties which have been pointed out in (a) to (e) above.

4. Standard Potential and the Suggested[11] Absolute e_{aq}^- Scale

A final matter related to the question of electrode potentials arises from the suggestion of Baxendale[11] (also discussed by Walker[49]) that an absolute scale of oxidation–reduction potentials could usefully be set up for so-called[11] "real reactions" of the type

$$M^{z+} + e_{aq}^- \longrightarrow M^{(z-1)+} \qquad \text{(XI)}$$

instead of arbitrarily assuming zero standard potential for the hydrogen electrode process corresponding to (II)

(40) J. O'M. Bockris and S. D. Argade, *J. Chem. Phys.*, **49**, 5133 (1968).

(41) J. O'M. Bockris, M. A. V. Devanathan, and K. Müller, *Proc. Roy. Soc., Ser. A*, **274**, 55 (1963).

(42) *E.g.*, see A. N. Frumkin, *Electrochim. Acta*, **2**, 351 (1960); *J. Chem. Phys.*, **1**, 552 (1939).

(43) H. F. Halliwell and S. C. Nyberg, *Trans. Faraday Soc.*, **59**, 1126 (1963); *cf.* B. E. Conway and M. Salomon, "Chemical Physics of Ionic Solutions," B. E. Conway and R. G. Barradas, Ed., Wiley, New York, N. Y., 1966, Chapter 24.

(44) J. O'M. Bockris and B. E. Conway, *Trans. Faraday Soc.*, **48**, 724 (1952).

(45) Since the submission of this paper, Schindewolf has reported[46] that when the experiment of Walker is repeated, but with scanning at *various* wave lengths, it is not the absorption spectrum of e_{aq}^- that is observed but rather the reflectance spectrum[47] of the Ag metal.

(46) U. Schindewolf, Institüt für Kernverfahrenstechnik, Karlsruhe, private communication to R. Haynes and B. E. Conway, "Modern Aspects of Electrochemistry," Vol. VII, in preparation.

(47) *E.g.*, see W. N. Hansen, *Surface Sci.*, **16**, 205 (1969); E. Feinleib, *Chem. Phys. Lett.*, **16**, 1200 (1966).

(48) M. Heyrovsky, *Nature*, **206**, 1356 (1964); see also M. Heyrovsky, *Proc. Roy. Soc., Ser. A*, **301**, 411 (1967).

(49) D. C. Walker, Advances in Chemistry Series, No. 81. American Chemical Society, Washington, D. C., 1968, p 49.

and (III). There seems to be no advantage in this suggestion since we have argued that there are difficulties in supposing that most electrode processes in aqueous solution proceed by the e_{aq}^- mechanism and secondly, in any practical measurement of emf of cells, the electrons in the half-cell processes must surely be associated with the metal otherwise emf measurements "by definition" would be neither feasible nor indeed unambiguous and reliable thermodynamically. (XI) is in fact not a "real" electrochemical reaction at all. In any practical measurement in electrochemical thermodynamics there is of course never any question of the absolute state of the electrons involved: the half-reactions for the cell must be written so as to add up to an overall chemical reaction with no net electrons left over, *e.g.*, $Fe_{aq}^{3+} + e_{Pt} \rightleftharpoons Fe_{aq}^{2+}$ coupled with $H_{aq}^+ + e_{Pt} \rightleftharpoons {}^1/_2H_2$ is equivalent to $Fe_{aq}^{3+} + {}^1/_2H_2 \overset{Pt}{\rightleftharpoons} Fe_{aq}^{2+} + H_{aq}^+$. Also it is important to note that it is not the potential for the isolated half-cell reaction $H_{aq}^+ + e_{Pt} \rightleftharpoons {}^1/_2H_2$ that is assumed conventionally to be zero but rather the potential associated with that reaction at a metal M (not necessarily Pt) in combination in a measuring circuit with possibly, but not necessarily, another metal M′ at which some other electrode process is occurring reversibly. Such circuits always involve the contact potential between M and M′ in addition to the metal–solution interfacial pd's at the two electrode metals and it is the algebraic sum of such pd's that is the measured emf. In order to avoid this practical complication, it may, however, be useful to suggest that what can be assumed to be zero on the conventional hydrogen electrode scale is the pd at the interface of a metal M at which the reversible hydrogen electrode process is occurring, when that metal M is chosen to be the same as that at which the other electrode process in the cell is taking place. Contact pd's are thus avoided in the discussion of the emf and in principle (but not always in practice) any metal can be used for establishing the reversible hydrogen electrode reaction (the only practical limiting factor is, of course, whether the reaction has a sufficiently high exchange current to be useful as a reversible electrode and whether side reactions, *e.g.*, metal dissolution, that may be potential determining, are insignificant or not). It has also been claimed[11] that a primary difficulty with the scale of potentials associated with the usual half-cell reaction of hydrogen involving electrons in the metal is the question of the value to be assigned to the work function ϕ of the metal. This again is not, in fact, a practical difficulty since in both of the cases considered above (*i.e.*, where M and M′ are different, or where hypothetically M constitutes also the metal at which the hydrogen electrode reaction is established reversibly) the work functions cancel out: in one case, because the metal at each of the two interfaces is the same; in the second case (metal M and reference electrode process established at M′), because the different work function terms involved at each metal solution interface are almost cancelled by the difference of work functions (and hence the contact potential) at the M/M′ interface in the external circuit. ϕ only enters into *a priori* kinetic calculations.

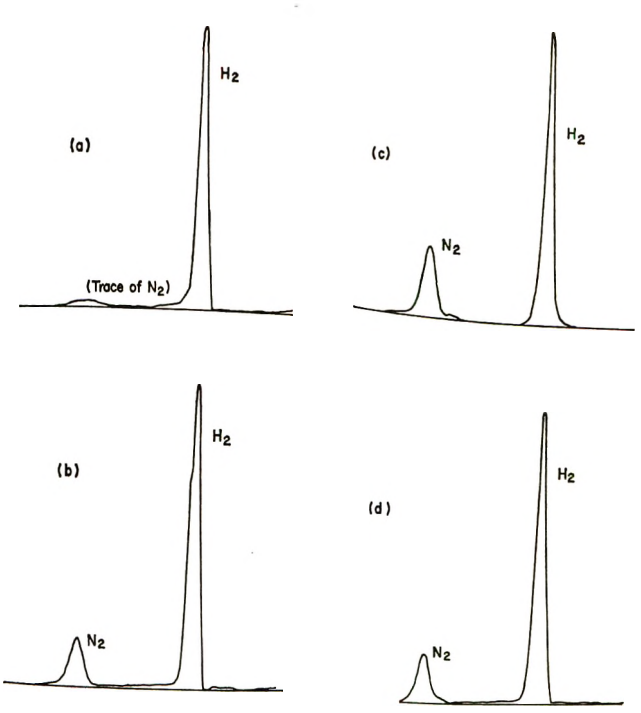

Figure 1. Gas chromatograms of N_2 and H_2 in catalytic reduction of N_2O by H_2 at a platinum catalyst in water on open circuit at 25°: (a) control experiment (no Pt catalyst); (b) and (c) two experiments with N_2O present 30 min in presence of catalyst and 45 min in presence of catalyst; (d) N_2O present +0.5 *M* methanol (30 min).

5. An Experiment on Catalytic Reduction of N_2O by H at Pt

It has been suggested on the basis of reduction of N_2O[24,50–52] that e_{aq}^- is also produced in cathodic electrolysis of aqueous solutions at Pt[2,48] electrodes. We have referred above to the conclusive electrochemical evidence for formation of adsorbed H under such conditions at Pt. It was hence considered of interest to establish if N_2O could be catalytically hydrogenated to N_2 by chemisorbed H atoms at a Pt surface on open-circuit ($E_H \doteqdot 0.0$ V) where e_{aq}^- species could hardly be formed. Experiments with and without methanol as a competitor were carried out.

A gas mixture of $N_2O + H_2$ was made by continuously passing the gases from two flow meters into a mixing tube and thence into a flask containing outgassed, triply distilled water; 0.2 g of reduced platinum dioxide was then added. Control experiments were performed

(50) F. S. Dainton and D. B. Peterson, *Proc. Roy. Soc., Ser. A*, **267**, 443 (1962).

(51) S. Gordon, E. J. Hart, M. S. Matheson, J. Rabani, and J. K. Thomas, *Discuss. Faraday Soc.*, **36**, 193 (1963).

(52) J. P. Keene, *Rad. Res.*, **22**, 1 (1964).

in pure water solutions. After bubbling the gas mixture for 30 min and adding the catalyst, the flask was closed by means of a stopcock and shaken for successive 30-min periods. Gas chromatographic analysis was made of samples of the gas mixture withdrawn into an evacuated bulb; separation was on a column at −80°. The ratio of N_2 to H_2 in the gas mixture progressively increased (Figure 1) with time in the presence of the Pt catalyst while insignificant changes occurred in the control experiment. In the presence of methanol, the rate of reduction of N_2O was somewhat diminished but this probably arises because of competitive chemisorption of radicals (*e.g.*, >C–OH) derived from the methanol.[53] Catalytic hydrogenation was hence indicated unless the extreme and rather unlikely view is taken that catalytic hydrogenations themselves proceed by an e_{aq}^- intermediate, *viz.*

$$Pt + {}^1/_2H_2 \rightleftharpoons PtH$$

$$PtH + H_2O \rightleftharpoons Pt + H^+ + e_{aq}^-$$

$$e_{aq}^- + \text{oxidant} \longrightarrow \text{reduced product}$$

This seems rather improbable since, as in the electrode case, adsorbed H can be detected at the Pt surface, *e.g.*, by infrared absorption, and hydrogenated surface complexes are known. At a cathode passing current, adsorbed atomic H is also present[21,22] and will undoubtedly have similar reducing properties. It is evidently difficult to conclude that N_2O is reduced specifically at Pt by e_{aq}^- or to interpret competitive experiments with methanol when dissociative chemisorption occurs in a heterogeneous system.

6. Conclusions

Difficulties are shown to arise in mechanisms of cathodic hydrogen evolution and for most, but not all, cases of metal dissolution if it is supposed that hydrated electrons are under most conditions the initally formed species at neutral or alkaline pH. Under certain circumstances, *e.g.*, for dissolution of the basest metals in water, *i.e.*, at sufficiently high negative potentials in Na amalgam dissolution or in photoassisted processes, a small steady-state concentration of e_{aq}^- could be established. It seems unlikely, however, that this can be the general mechanism for hydrogen evolution and other cathodic processes, particularly for the more catalytic metals which chemisorb H and at which H_2 evolution can proceed at high rates but at relatively low cathodic potentials near that of the reversible hydrogen electrode.

Acknowledgments. Grateful acknowledgment is made to the National Research Council, Canada, for support of this work and D. J. M. acknowledges the award of a National Research Council Graduate Scholarship. We thank Messrs. J. Esser and P. Schuchmann for performing the gas chromatographic analyses, and Professors G. Stein, U. Schindewolf, and P. Delahay for their comments on this paper prior to its publication.

(53) V. S. Bagotskii and Y. B. Vasilev, *Electrochim. Acta*, **12**, 1323 (1967); **11**, 1439 (1966); see also M. W. Breiter, *Discuss. Faraday Soc.*, **45**, 79 (1968).

On the Oxybromine Radicals

by O. Amichai and A. Treinin

Department of Physical Chemistry, Hebrew University, Jerusalem, Israel *(Received March 31, 1970)*

The pulse radiolysis of BrO_3^- in water and its photolysis in boric acid glass were investigated. Both techniques give rise to three intermediates with λ_{max} at *ca.* 315, 350, and 475 nm. They were identified as BrO_3, BrO, and BrO_2, respectively. BrO results from the decomposition of BrO_3; this reaction appears to proceed by different mechanisms in water and in the rigid matrix.

The flash photolysis of BrO_3^- gives rise to transient absorption in the region 300–500 nm.[1] The band peaking at 475 nm was definitely assigned to BrO_2.[2] The absorption below 400 nm is short-lived and overlapped by the spectrum of BrO^-, which is a permanent product of the photolysis; therefore its analysis is rather difficult. Bridge and Matheson reported[1] an absorption with a double peak in the region 350–390 nm decaying by a first-order process which they assigned to BrO_3. An absorption centered around 360 nm was

(1) N. K. Bridge and M. S. Matheson, *J. Phys. Chem.*, **64**, 1280 (1960).

(2) O. Amichai, G. Czapski, and A. Treinin, *Isr. J. Chem.*, **7**, 351 (1969).

produced by the pulse radiolysis of BrO_3^- and was similarly interpreted.[3] However, no evidence was presented for this assignment.

Our recent flash photolysis work[2,4] has shown that at least two primary processes occur in excited BrO_3^-

$$BrO_3^- \longrightarrow BrO_2 + O^- \text{ (or OH)} \quad (1)$$

$$BrO_3^- \longrightarrow BrO_2^- + O(^3P) \quad (2)$$

Under the conditions employed, the OH radicals react with BrO_3^-

$$OH + BrO_3^- \longrightarrow BrO_3 + OH^- \quad (3)$$

Thus the photolysis is expected to yield BrO_3 radicals. However, the possibility that BrO (λ_{max} 350 nm[5]) is also produced should be carefully considered. The photolysis of IO_3^- yields IO_3, IO_2, and IO; pulse radiolysis[6] and matrix isolation[7] techniques were employed to reach this conclusion. Here we wish to report the results of similar experiments with BrO_3^-.

Experimental Section

The pulse radiolysis setup[6] and the preparation of boric acid glasses[8] were already described. The glasses were irradiated at 2537 Å and their absorption spectra were recorded with a 450 Perkin-Elmer spectrophotometer, using the intensity scale to measure optical densities down to 10^{-3} (reproducible within ±15%). A holder was designed to give good thermal contact with the glass; it was thermostated inside the cell compartment (±1°).

$NaBrO_3$ (Analar grade) was used without further purification. $NaBrO_2$ was supplied to us by the Société d'Etudes Chimiques pour l'Industrie et l'Agriculture, France.

Results

The spectra of the oxybromine anions pertaining to our research are recorded in Figure 1. The absorption of BrO^- is somewhat higher than that previously recorded; unsatisfactory correction for the disproportionation reaction is responsible for the discrepancy.[9]

(1) Pulse Radiolysis. Figure 2 shows some transient spectra produced in air-free 0.1 *M* $KBrO_3$ at pH 4.6. Immediately after the pulse, the spectrum displayed a band peaking at ~315 nm (band A). Its fast decay ($\tau_{1/2} \approx 5$ μsec, independent of the bromate concentration) proceeded in parallel with the growth of another band (B) with λ_{max} ~350 nm; the latter decayed by a second-order process with $2k = (9.0 \pm 0.6) \times 10^6 \epsilon_{360}\, M^{-1}\,\text{sec}^{-1}$ (Figure 3). (ϵ_{360} is the extinction coefficient at 360 nm.) In alkaline solution (pH 12) transient B was observed, but the spectrum of A was overlapped by that of some slowly decaying transient, with λ_{max} below 280 nm; a permanent absorption was finally left, similar to that of a solution containing BrO^- and BrO_2^- in 1:2 mole ratio (Figure 2). Below pH 5, BrO^- could not be detected because of its rapid protonation to

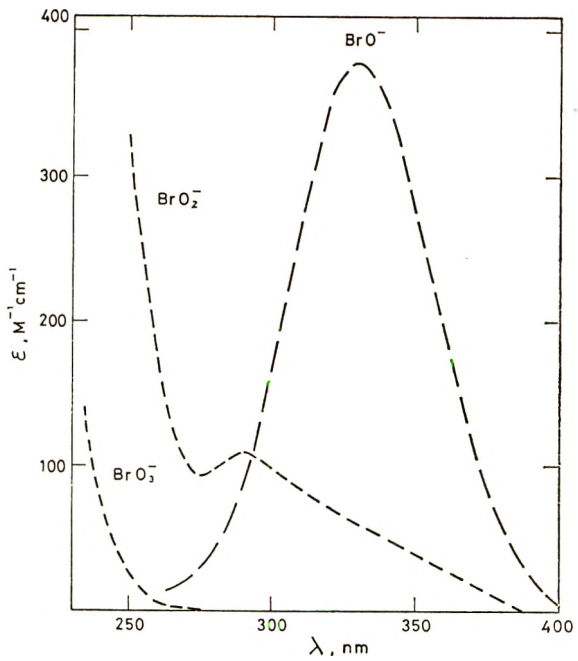

Figure 1. The spectra of BrO^-, BrO_2^-, and BrO_3^- in aqueous solution at pH 13.6.

HBrO, which weakly absorbs above 300 nm;[10] BrO_2^- is unstable under these conditions.[11] Therefore, band B appeared well defined only in acidic solution. Even in neutral solutions the transient absorption revealed a slowly decaying component which could be ascribed to BrO^- reacting with H_3O^+ (probably with some contribution from BrO_2^- below 330 nm).

Above 400 nm the familiar spectrum of BrO_2 peaking at 475 nm[2,5] was observed immediately after the pulse.

A mixture of 0.44 *M* BrO_3^- and 1.6×10^{-4} *M* BrO_2^- (air free) at pH 11.9 was pulsed. (Under these conditions all solvated electrons and most OH radicals should be scavenged by BrO_3^-.[2,12]) The decay of transient B was found to be much faster in this system.

The effect of N_2O was tried with 4×10^{-3} *M* $KBrO_3$ solution, so that most e_{aq}^- were effectively scavenged by N_2O. BrO_2 could hardly be detected but the absorption below 400 nm was enhanced by ~20% compared with the same solution saturated with argon. On the other hand, ethanol did not affect the amount of Br_2O

(3) M. S. Matheson and L. M. Dorfman, *J. Chem. Phys.*, **32**, 1870 (1960).

(4) O. Amichai and A. Treinin, *Chem. Phys. Lett.*, **3**, 611 (1969).

(5) G. V. Buxton and F. S. Dainton, *Proc. Roy. Soc., Ser. A*, **304**, 427 (1968).

(6) O. Amichai and A. Treinin, *J. Phys. Chem.*, **74**, 830 (1970).

(7) O. Amichai and A. Treinin, *J. Chem. Phys.*, **53**, 444 (1970).

(8) A. Gitter and A. Treinin, *ibid.*, **42**, 2019 (1965).

(9) O. Amichai and A. Treinin, to be submitted for publication.

(10) L. Farkas and F. Klein, *J. Chem. Phys.*, **16**, 886 (1948).

(11) J. Breiss, Ing. D. Thesis, University of Strasbourg, Strasbourg, France, 1959.

(12) M. Anbar and P. Neta, *Int. J. Appl. Radiat. Isotop.*, **18**, 493 (1967).

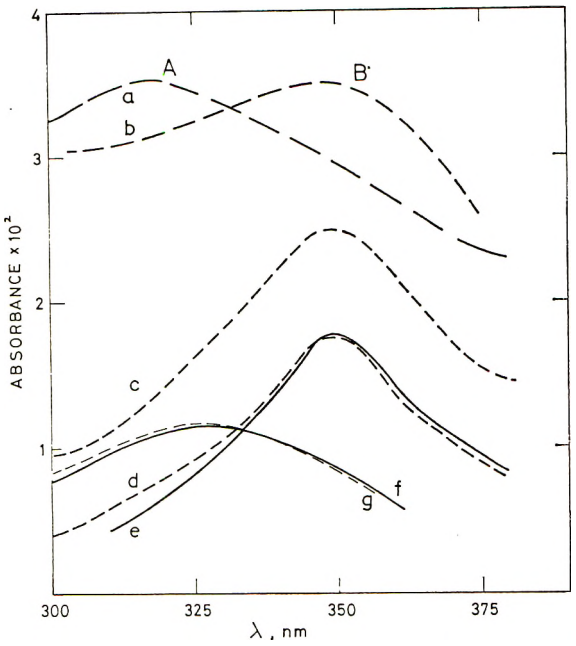

Figure 2. Absorption spectra of the transients produced by pulse radiolysis of 0.1 M BrO_3^- at pH 4.6, 5 μsec (a), 10 μsec (b), 30 μsec (c), and 50 μsec (d) after pulse. Curve e: the spectrum of BrO from pulse radiolysis of 2×10^{-4} M BrO^- at pH 11.6. Curve f: the permanent absorption from pulse radiolysis of 0.1 M BrO_3^- at pH 12.6, 40 msec after pulse. Curve g: the spectrum of $BrO^- + BrO_2^-$ in 1:2 molar ratio.

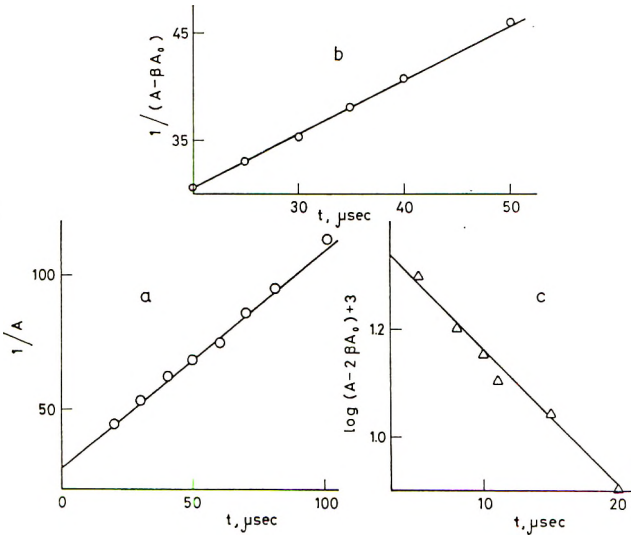

Figure 3. Plots for the decay of BrO under various conditions: (a) second-order decay in 0.1 M BrO_3^- at pH 4.6; (b) second-order decay corrected for the formation of BrO^- in 0.08 M BrO_3^- at pH 13; (c) first-order decay corrected for the formation of BrO^- in 0.44 M BrO_3^- + 1.6×10^{-4} M BrO_2^- at pH 11.9.

(its rate of decay slightly increased) but completely suppressed the absorption at shorter wavelengths. (This result was obtained with 0.1 M BrO_3^- and 2×10^{-3} M ethanol.) This shows that within the limit of error (±10%) the sole source of BrO_2 is the reaction[5]

$$e_{aq}^- + BrO_3^- \xrightarrow{H_2O} BrO_2 + 2OH^-$$

Figure 2 records for comparison the spectrum of BrO which was produced by pulse radiolysis of air-free BrO^- at pH 11.6. BrO^- was prepared by mixing equivalent amounts of ClO^- and Br^-; Cl^- does not interfere since its reaction with OH is much slower.[12] The spectrum of BrO thus produced is very close to that previously reported.[5]

(2) *Matrix Isolation.* The solubility of $NaBrO_3$ in boric acid glass and its extinction coefficient at 2537 Å are rather low; therefore long irradiation times were required to obtain detectable spectral changes. The results are shown in Figure 4. Three bands emerged on irradiation: bands A, B, and C peaking at *ca.* 320, 350, and 470 nm, respectively. Band A could be readily annihilated by moderately warming the glass, bands B and C growing in parallel with its decay. At 41° the decay was found to be first order with $k \approx 7 \times 10^{-5}$ sec^{-1}. At 85°, bands B and C began to fade and a new band (D) grew up, peaking at ~410 nm. Under this treatment the glass was losing its transparency, so complete annihilation of B and C could not be achieved.

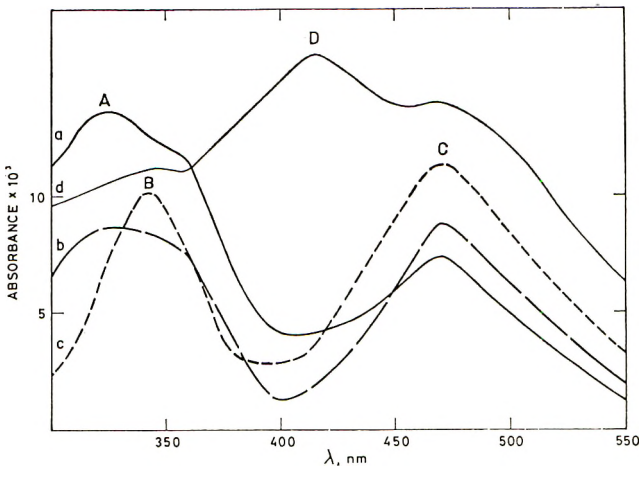

Figure 4. The photolysis of BrO_3^- in boric acid glass at 2537 Å. Absorption curves: (a) after 4.5-hr irradiation; (b and c) after 2 and 19 hr, respectively, at 41°; (d) after 2 min at 85°.

Discussion

Both techniques lead to similar results: in acidic solutions three intermediates are produced by irradiation, but B appears to involve A as its precursor. Band C (Figure 4) is evidently due to BrO_2, with λ_{max} nearly the same as in water. However, contrary to the aqueous system, BrO_2 also results from some thermal process in the glass, which may involve transient A.

The effects of ethanol and N_2O on the pulse radiolysis indicate that OH radicals are the precursors of transients A and B. Ethanol scavenges OH while N_2O converts e_{aq}^- to OH. If all the hydroxyl radicals were reacting with BrO_3^-, then the amounts of A and B should

be doubled in the presence of N_2O (since $G_e \approx G_{OH}$). However, reaction 3 is relatively slow[2] and thus under the conditions employed ($(OH)_0 \approx 10^{-5}$ M and $(BrO_3^-) = 4 \times 10^{-3}$ M; these conditions were chosen to get detectable yields of radicals and to let N_2O effectively scavenge e_{aq}^-) only ~25% of the OH radicals react with BrO_3^-.

The following considerations led us to assign band B to BrO.

(a) In aqueous solution it closely resembles the 350-nm band of BrO (Figure 2). (The discrepancy below 330 nm may be due to BrO_2^- undergoing decomposition.)

(b) The decay of band B at pH 4.6 is somewhat faster than that reported[5] for BrO in the pH range 11–14. This may still be within the limit of error or a genuine pH effect. In order to determine the rate of decay in alkaline solution we had to correct for the absorption of the reaction products. Assuming that BrO decays by the reaction[5]

$$2BrO \longrightarrow BrO^- + BrO_2^- \qquad (4)$$

and ignoring the contribution of BrO_2^- (see Figure 1), we derived the expression

$$\frac{1 - \beta}{A - \beta A_0} = \frac{1}{A_0} + \frac{2k_4 t}{\epsilon_{BrO} l} \qquad (5)$$

l is the optical path; A and A_0 are the optical densities at the given time and zero time, respectively (the latter was found by extrapolation; the short formation period of BrO was ignored); $\beta = \epsilon_{BrO^-}/2\epsilon_{BrO}$, where ϵ_{BrO^-} and ϵ_{BrO} are the extinction coefficients of BrO^- and BrO, respectively. The validity of eq 5 was checked at 360 nm, setting $\epsilon_{BrO} = 900$[5] and $\epsilon_{BrO^-} = 200$ M^{-1} cm^{-1}. A straight line was obtained (Figure 3) from which $2k_4 = (4.8 \pm 0.7) \times 10^9$ M^{-1} sec^{-1} was derived in agreement with previous data.[5]

(c) BrO is known[5] to react with BrO_2^- (in alkaline solution) as in

$$BrO + BrO_2^- \longrightarrow BrO^- + BrO_2 \qquad (6)$$

This explains the effect of BrO_2^- on the decay of B. By correcting for the absorption of BrO^- produced, the expression

$$\ln (A - 2\beta A_0) = \ln (A_0 - 2\beta A_0) - k_6(BrO_2^-)t \qquad (7)$$

was obtained with all the symbols as previously defined. The plot for 360 nm is shown in Figure 3, from which $k_6 = (4.0 \pm 0.5) \times 10^8$ M^{-1} sec^{-1} was obtained. This value agrees (within the limit of error) with previous data.

(d) Above 0.1 M BrO_3^-, reaction 3 should be effectively completed within the pulse duration.[2] Therefore, transient B which still grows after the pulse cannot be due to BrO_3, as previoulsy supposed.[1,3]

Transient A appears to be the precursor of BrO. In boric acid glass the conversion of A to BrO is first order, occurring at relatively low temperatures. This leads us to assign band A to BrO_3 and postulate the reaction

$$BrO_3 \longrightarrow BrO + O_2 \qquad (8)$$

as responsible for the generation of BrO. An analogous reaction occurs with IO_3 in boric acid glass.[7]

In general, boric acid glasses doped with IO_3^- and BrO_3^- show close resemblance. The XO_3 radicals most readily decompose while XO_2 and XO must diffuse for annihilation. All the oxyiodine radicals finally yield iodine.[7] The oxybromine radicals are expected to behave similarly; indeed, band D (Figure 4) is most probably due to Br_2 which has λ_{max} 410 nm in the gas phase.[13] There is one major difference between the two systems: with IO_3^--doped glass IO_2 is produced only by primary photodissociation; there is no thermal generation analogous to that of BrO_2. This thermal reaction does not occur in aqueous solution, where BrO_3 is much less stable than in the rigid system.

There is no evidence that reaction 8 occurs in one stage and that BrO_3 undergoes the same reaction in both fluid and rigid phases. Thus in boric acid glass the decomposition may occur in two stages with BrO_2 being the intermediate. Little is known on the decay of BrO_3 in aqueous solution; the short lifetime and weak absorption made the analysis of its kinetics unreliable. The lack of (BrO_3^-) effect rules out its reaction with bromate. Still, the profound phase effect suggests some basic difference in mechanism, more than a simple cage effect. (In aqueous solution IO_3 undergoes a second-order decay[6] but this process does not generate IO.)

The assignment of band A to BrO_3 is also in keeping with the following regularities:[6] (a) the transition energies of the oxyhalogen radicals increase in the order $XO_3 > XO > XO_2$; (b) $h\nu_{max}$ of XO_n increases almost linearly with the electronegativity of the halogen atom. This strongly supports our analysis of the transient spectra.

By extrapolating the yield of BrO to zero time (ignoring its short period of formation) and taking $G_{BrO} = G_{OH}$, we obtained ϵ_{max}(BrO) 800 M^{-1} cm^{-1} in fair agreement with previous data.[5] $\epsilon_{max}(BrO_3)$ ~1000 M^{-1} cm^{-1} was estimated from the absorption at 315 nm immediately after the pulse.

According to the mechanism proposed, nearly equivalent amounts of BrO and BrO_2 are generated by the pulse (since $G_e \sim G_{OH}$). BrO^- is produced only from the decay of BrO (reaction 4), while BrO_2^- owes its formation to reaction 4 and to the decay of BrO_2[5]

$$2BrO_2 \longrightarrow BrO_2^- + BrO_3^- \qquad (9)$$

This explains the ratio $(BrO_2^-)/(BrO^-) = 2$, obtained in alkaline solution (Figure 2).

From the amount of radicals produced in the glass

(13) A. G. Briggs and R. G. W. Norrish, *Proc. Roy. Soc., Ser. A*, **276**, 51 (1963).

the quantum yield of reaction 1 was estimated as *ca.* 0.1, which is close to that in aqueous solution. Thus for both IO_3^- [6] and BrO_3^- the reaction is not hampered in the rigid matrix by cage recombination. The OH radicals produced by reaction 1 (the matrix is highly acidic[8]) are expected to diffuse fast and react with XO_3^-. The O atoms produced by reaction 2 (there is no analogous reaction with IO_3^- [4]) may behave similarly, but their reaction with BrO_3^- should yield BrO_2^- or BrO_4^- [14] which hardly absorb above 300 nm.

The nature of the slowly decaying transient observed in alkaline solution is still not clear.

(14) E. H. Appelman, *Inorg. Chem.*, **8**, 223 (1969).

NOTES

Activity Coefficients in Equimolal Mixtures of Some Divalent Metal Perchlorates

by Zofia Libuś and Teresa Sadowska

Department of Physical Chemistry of the Institute of Chemical Engineering and Measuring Techniques, Technical University of Gdańsk, Gdańsk, Poland *(Received February 5, 1970)*

Previous work has shown that aqueous solutions of manganese(II), cobalt(II), nickel(II), and zinc(II) perchlorates display the same, in approximation, concentration dependences of their osmotic and activity coefficients in the whole concentration range studied, *i.e.*, up to approximately 3 *m*.[1] In the present paper we report the results obtained for mixtures of some of the divalent metal perchlorates completing, in this way, our study on the osmotic and activity coefficients of the divalent metal perchlorates in aqueous solution.

Experimental Section

Stock solutions of $Co(ClO_4)_2$ and $Ni(ClO_4)_2$ were obtained and analyzed as described in ref 1. Zinc perchlorate, obtained by dissolving reagent grade zinc oxide in aqueous analytical grade perchloric acid, was purified by several recrystallizations, the last operation being performed using conductivity water. The stock solution of $Zn(ClO_4)_2$ was analyzed for zinc by standard EDTA titration as well as gravimetrically by the pyrophosphate method. The results obtained by the two methods were consistent to within 0.01%.

Equimolal solutions of $Co(ClO_4)_2$, $Ni(ClO_4)_2$, and $Zn(ClO_4)_2$ were prepared from the corresponding concentrate stock solutions and were further used in the preparation of mixed solutions having constant total molalities, but different contents of the component salts. Every six equimolal solutions thus obtained (four mixtures and two single salt solutions) were equilibrated in the isopiestic apparatus at 25° and their final concentrations were found from the change in weight. Details of the isopiestic experiments were as described in ref 1.

Results and Discussion

The concentrations of the isopiestic $Co(ClO_4)_2$–$Ni(ClO_4)_2$ and $Zn(ClO_4)_2$–$Ni(ClO_4)_2$ mixed solutions, along with the corresponding water activities as well as the values of Δ, as defined below, are given in Tables I and II. The water activities were determined by reference to the data concerning the corresponding single salt solutions.[1] Inspection of the tables shows that in each case the total concentration of the isopiestic solutions shows but a very small variation with the mole fraction of one of the two metal perchlorates. The variation does not exceed 0.5% in the case of the $Co(ClO_4)_2$–$Ni(ClO_4)_2$ mixtures, and 1.0% in the case of the $Zn(ClO_4)_2$–$Ni(ClO_4)_2$ mixtures. In order to check whether the relation between the total concentration of isopiestic mixtures, on one hand, and the mole fraction of the component salts, on the other, may be approximated by a straight line, the deviation from linearity defined as $\Delta = m - m_1^{\phi}x_1 - m_2^{\phi}x_2$ has been calculated for each experimental point. In this expression m denotes the total concentration of the mixed solution, m_1^{ϕ} and m_2^{ϕ} denote the concentrations of the corresponding isopiestic pure solutions, and x_1 and x_2 are the mole fractions of component salts in the mixture defined as: $x_1 = m_1/m$ and $x_2 = m_2/m$, m_1 and m_2 being the concentrations of salts 1 and 2, respectively. As is seen, the values of Δ are, in general, smaller than 0.2% of m. On this basis we assume that the dependences under consideration are linear, within the experimental error, for each series of the isopiestic solutions studied in this work.

Further conclusions arising from the above results

(1) Z. Libuś and T. Sadowska, *J. Phys. Chem.*, **73**, 3229 (1969).

Table I: Compositions and Total Concentrations of Isopiestic $Co(ClO_4)_2 + Ni(ClO_4)_2$ Solutions in Water at 25°

a_w[a] = 0.9570			a_w = 0.8733		
$x_{Co(ClO_4)_2}$[b]	m	Δ	$x_{Co(ClO_4)_2}$	m	Δ
1.0000	0.6986	0.0000	1.0000	1.5130	0.0000
0.7653	0.6983	−0.0007	0.8018	1.5094	−0.0033
0.6165	0.7003	+0.0010	0.6075	1.5118	−0.0006
0.3999	0.7014	+0.0016	0.4070	1.5102	−0.0020
0.2090	0.7016	+0.0015	0.2205	1.5116	−0.0004
0.0000	0.7005	0.0000	0.0000	1.5117	0.0000
a_w = 0.7425			a_w = 0.6156		
$x_{Co(ClO_4)_2}$	m	Δ	$x_{Co(ClO_4)_2}$	m	Δ
1.0000	2.4038	0.0000	1.0000	3.1445	0.0000
0.7739	2.4009	−0.0004	0.7986	3.1397	−0.0023
0.5614	2.3985	−0.0004	0.6173	3.1347	−0.0051
0.3686	2.3953	−0.0014	0.4772	3.1344	−0.0036
0.1886	2.3948	+0.0001	0.2091	3.1311	−0.0036
0.0000	2.3927	0.0000	0.0000	3.1322	0.0000

[a] Water activity. [b] $x_{Co(ClO_4)_2} = m_{Co(ClO_4)_2}/m$, where m is the the total molality.

Table II: Compositions and Total Concentrations of Isopiestic $Zn(ClO_4)_2 + Ni(ClO_4)_2$ Solutions in Water at 25°

a_w[a] = 0.9446			a_w = 0.8753		
$x_{Zn(ClO_4)_2}$[b]	m	Δ	$x_{Zn(ClO_4)_2}$	m	Δ
1.0000	0.8373	0.0000	1.0000	1.4832	0.0000
0.7999	0.8409	+0.0020	0.7999	1.4854	−0.0008
0.5898	0.8430	+0.0023	0.5898	1.4892	−0.0002
0.4120	0.8444	+0.0021	0.4120	1.4911	−0.0009
0.2032	0.8459	+0.0020	0.2031	1.4956	+0.0005
0.0000	0.8457	0.0000	0.0000	1.4982	0.0000
a_w = 0.7030			a_w = 0.5954		
$x_{Zn(ClO_4)_2}$	m	Δ	$x_{Zn(ClO_4)_2}$	m	Δ
1.0000	2.6176	0.0000	1.0000	3.2211	0.0000
0.7942	2.6210	−0.0007	0.8032	3.2228	−0.0033
0.5559	2.6268	+0.0004	0.6115	3.2292	−0.0017
0.4174	2.6306	+0.0013	0.4087	3.2365	+0.0005
0.2190	2.6353	+0.0021	0.2118	3.2440	+0.0031
0.0000	2.6376	0.0000	0.0000	3.2463	0.0000

[a] Water activity. [b] $x_{Zn(ClO_4)_2} = m_{Zn(ClO_4)_2}/m$, where m is the total molality.

may be obtained using the McKay–Perring relation.[2] The latter, for the purposes of the present work, may be written in the form

$$0.054 \ln \frac{m\gamma_1}{m_1^{\phi}\gamma_1^{\phi}} = \int_0^{\ln a_w} \left\{ -\frac{1}{m^2}\left(\frac{\partial m}{\partial \ln x_2}\right)_{a_w} - \frac{1}{m} + \frac{1}{m_1^{\phi}} \right\} d \ln a_w \quad (1)$$

where γ_1 is the activity coefficient of salt 1 in the mixed solution and γ_1^{ϕ} is the activity coefficient of that salt in its pure solution having the same water activity, a_w, as the mixed one. The integrand in the above equation for any given value of a_w is, in general, a function of x_2, and it is at a given constant value of x_2 that the integration is performed. For the systems under investigation $-(\partial m/\partial x_2)_{a_w} = (\partial m/\partial x_1)_{a_w} \equiv S$ has a constant value, as shown above, for any given series of isopiestic mixtures and, consequently eq 1 may be written in the form

$$0.054 \ln \frac{m\gamma_1}{m_1^{\phi}\gamma_1^{\phi}} = \int_0^{\ln a_w} \frac{S^2 x_2^2}{m^2 m_1^{\phi}} d \ln a_w \quad (2)$$

Approximate numerical values of the integral in this equation were found graphically from the experimental data for different constant values of x_2, as well as for different values of $\ln a_w$, the upper limit of integration. The whole procedure is similar to that used by McCoy and Wallace in their study on aqueous KCl–NaCl mixtures.[3] The results obtained may be summarized in

(2) H. A. C. McKay and J. K. Perring, *Trans. Faraday Soc.*, **49**, 163 (1953).

(3) W. H. McCoy and W. E. Wallace, *J. Amer. Chem. Soc.*, **78**, 1830 (1956).

the statement that the values of the integral are smaller than 3×10^{-6} for the $Co(ClO_4)_2$–$Ni(ClO_4)_2$ mixtures, and smaller than 2×10^{-5} for the $Zn(ClO_4)_2$–$Ni(ClO_4)_2$ mixtures. It follows that in either case the integral may be assumed, with a very good approximation, to be nil at any composition of the mixed solutions, up to considerable concentrations. Hence, the final result of the above considerations is that

$$\gamma_1 = \frac{m_1^{\phi}}{m}\gamma_1^{\phi} \tag{3}$$

Since exactly the same argumentation applies to the other component of the mixture, we shall also have

$$\gamma_2 = \frac{m_2^{\phi}}{m}\gamma_2^{\phi} \tag{4}$$

Taking into account that the variation in m, the total concentration of the isopiestic mixtures for the systems under investigation, always is embraced within very narrow limits, as indicated above, we may assume that $m \cong m_1^{\phi}$, $m \cong m_2^{\phi}$, and $m_1^{\phi} \cong m_2^{\phi}$. It follows that the equalities (5) may be assumed to be valid, in approximation, for equimolal mixtures of the divalent metal perchlorates studied in this paper.

$$\gamma_1 = \gamma_1^{\phi};\ \gamma_2 = \gamma_2^{\phi};\ \gamma_1^{\phi} = \gamma_2^{\phi} \tag{5}$$

It may be noted that eq 5 represent a special case of the well-known Harned rule. However, their validity for the systems under discussion does not seem to be fortuitous. It seems that it should be ascribed to the existence of the corresponding metal ions exclusively in the form of the octahedral hexaaquo complexes, possibly with the second layers of hydrogen-bonded water molecules, as well as to the fact that the interaction potentials of such complex ions are practically independent of the nature of the central metal atoms, as was pointed out in ref 1. It seems very probable that eq 5 will be valid for any two of the divalent metal perchlorates studied in ref 1 in that concentration range in which they show practically the same concentration dependences of the osmotic and activity coefficients. We should like to add, in conclusion, that equimolal mixtures of the divalent metal perchlorates conforming to eq 5 possess the properties of effectively constant ionic media, and as such may be used in studies on coordination equilibria involving the corresponding metal ions.

Journal of Chemical and Engineering Data

July 1970, Vol. 15, No. 3

TABLE OF CONTENTS